ProQuest LLC.
789 East Eisenhower Parkway
P.O. Box 1346
Ann Arbor, MI 48106 – 1346

Laser-Induced Emission Spectrometry for Rapid Elemental Analysis

David Robert Anderson

A thesis submitted in partial fulfilment of the requirements of
Sheffield Hallam University
for the degree of Doctor of Philosophy

October 1994

Collaborating Organisation: Arun Technology Ltd.
Southwater
Horsham
West Sussex
RH13 7UD

This thesis reports investigations into laser-induced emission spectrometry for rapid elemental analysis. An integrated laser and spectrometer system is configured, comprising a Q-switched Nd:YAG laser and an optical multichannel analyser, which enables the discreet monitoring of the laser-induced plasma produced by each laser shot. Novel applications are devised including the survey analysis of polymeric materials and the depth profiling of coated steels.

A survey analysis of polymeric materials for twelve elements (Al, Ba, Ca, Cu, Fe, Mg, Pb, P, Sb, Sn, Ti and Zn) is reported. Results showed that element emission responses are dependent upon operating conditions, selective volatilisation of antimony can occur, and ablation characteristics, such as the rate of material removal and plasma lifetime, are very different compared to metals. With optimised operating conditions of low laser energy and sample positioned at the laser focal point, the limit of detection for antimony is 0.09 % mass/mass with precision of 1.8 (% relative standard deviation) using a carbon signal from the polymer as internal standard. Rapid discrimination between samples of poly (vinyl chloride) is demonstrated with a measurement time of 1 s.

Data for the depth profiling of a range of coated steels using laser-induced plasma emission spectrometry are reported in detail for the first time. Coatings of zinc/nickel, tin, titanium nitride and chromium are examined. Depth profile signatures and crater shape are greatly influenced by operating conditions. Improved depth resolution and signatures are obtained using high laser energy and defocused laser radiation. Correlations are established between coating thickness and output parameters of the technique. Linear calibrations against coating thickness are achieved with good precision for replicate measurements (4 % relative standard deviation). Results showed that the technique can differentiate between tin coated samples with a difference in coating thickness of 0.02 μm, and can detect an ultra-thin chromium coating of 0.020 μm thickness. This performance and measurement times of 50 s indicate the rapid depth profile capability of the technique.

The novel application of an artificial intelligence technique (artificial neural networks) to laser-induced plasma emission spectra is reported for the first time. Studies showed that artificial neural networks can rapidly discriminate between the emission spectra of different materials with a success rate of 100 %, to provide a new means of rapid data processing.

We seemed to tread air rather than crusted snow

We were light of foot, we walked like demigods in joyous serenity

W. H. Murray

Mountaineering In Scotland

To my Mother and the memory of my Father

To Alison and David John

Table of Contents

1.1 Introduction

Atomic emission spectrometry has been used in analytical chemistry for over one hundred years. The history of the technique spans several centuries from early observations by Agricola in the 16th century, through to studies by Bunsen and Kirchoff in the 19th century, to commercial instruments developed over the last 70 years. Modern instrument systems, such as inductively coupled plasma emission spectrometers, are now used world-wide for the rapid and quantitative analysis of many elements.[1]

Atomic emission instruments consist of three main components: an excitation source, a spectrometer and a detector, (Figure 1). The function of the source is to vaporise sample material (depending on the phase of the sample), and to atomise sample components and electronically excite the atoms to produce atomic emission radiation. Ionisation may also occur resulting in ionic emissions. These emissions are in the ultra-violet and visible regions of the electromagnetic spectrum and are characteristic in wavelength for each element. Many different sources have been developed over the years including electrical arcs and sparks, glow discharges, laser-induced plasmas, inductively coupled plasmas, etc.[2]

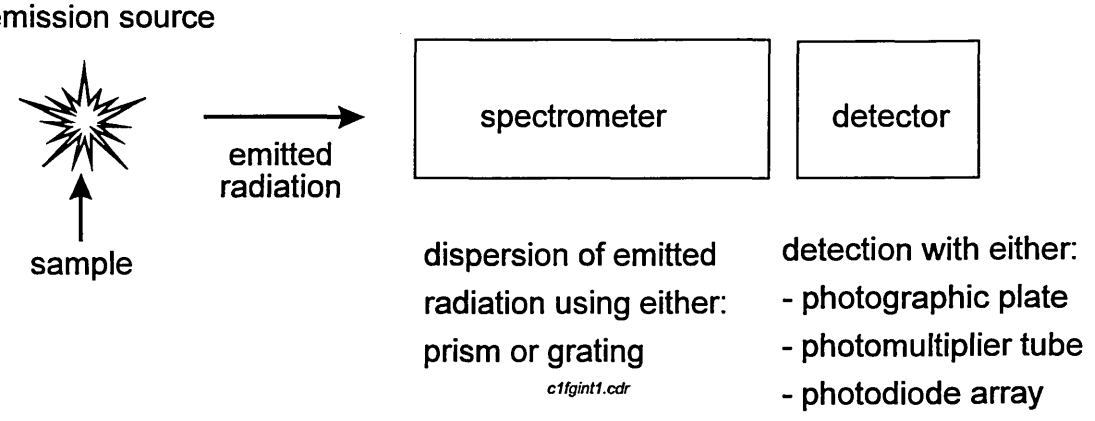

Figure 1 The three main components of an atomic emission spectrometer

The spectrometer disperses the emitted radiation into component wavelengths using either a prism or a diffraction grating to produce a spectrum. Spectrometers can analyse either several wavelengths simultaneously or a single wavelength at a time. The detector records the emission signal of an individual emission wavelength from the spectrum. Detectors are either single-channel and detect a single element response, such as a photomultiplier tube, or are multichannel and can detect several elements simultaneously, such as photographic plates, several photomultiplier tubes and photodiode arrays.

Over the last seventy years, each area of instrumentation has received considerable development. A list of typical instrumentation is given in Table 1.

Emission Source	Instrument and Manufacturer
arc	large quartz spectrograph, Hilger and Watts
	Analoy, Arun Technology
spark	Quantovac, Applied Research Laboratories,
	Polyvac, Hilger and Watts
glow discharge	Leco Instruments
ICP	Applied Research Laboratories
	Thermo Jarrell Ash, Spectro Analytical
	Varian, Perkin Elmer
laser-induced plasma	Laser Microprobe: Carl Zeis
	JEOL
	Jarrell Ash

Note: not all instruments are now available commercially

Table 1 List of atomic emission sources and instruments

In the 1930s, commercial arc emission instruments, such as the Hilger and Watts large quartz spectrograph, became available. The instrument used an arc discharge between a counter electrode and a solid, conducting sample. Material was removed from the sample by the arc through melting, boiling and vaporisation processes. The high temperature of the arc caused atomisation and ionisation and produced atomic/ionic emissions. Radiation from the arc was dispersed in the spectrograph by a prism and a photographic plate recorded the resulting emission spectrum. This sensitive technique allowed the simultaneous detection and semi-quantitative analysis of many elements. The interpretation of the photographic plate is very time-consuming and tedious.

Direct reading spectrometers were developed in the 1950s to meet the demand of the steel industry for a rapid, quantitative analytical technique. A typical instrument was a 'Quantometer' from the company, Applied Research Laboratories.[3] It used a spark discharge for excitation and a polychromator fitted with several photomultiplier tube detectors to measure the light intensity at pre-selected wavelengths. A grating was used in the spectrometer for the dispersion of light. The advance was possible by improvements in the quality of gratings and photomultiplier tubes. The instrument enabled quantitative, multielement analysis to be achieved in approximately 2 to 3 minutes, much less than by the spectrograph, which took about 1 hour. Such direct reading spectrometers are still commercially available and are widely used for the analysis of metals and alloys.

Glow discharge sources such as the Grimm-type lamp have been used for the bulk chemical analysis of solid, conducting materials[2], and more recently, for the depth profiling of conducting coatings on substrates.[4] In the Grimm lamp, a flat sample forms the cathode close to an annular anode in a low pressure argon atmosphere. A high voltage (500-1000 V) between the cathode and

anode produces a glow discharge of high radiant intensity, and sample material is removed through a sputtering process by the bombardment of argon ions. Instruments are available from companies such as Leco Instruments.

Arc, spark and glow discharge sources have been successfully used with solid, conducting materials but have had limited success with the analysis of liquids or non-conducting materials. In the 1960s and 1970s, inductively coupled plasma (ICP) sources were developed to analyse liquid solutions and became widely used for this application.[1] Solutions are generally introduced via a nebuliser which produces an aerosol that is dried, atomised and excited by the plasma. The plasma is sustained by radio-frequency energy from an induction coil. The ICP technique has rapid, simultaneous multielement analysis capabilities. For example, a Thermo Jarrell Ash ICAP9000 can analyse a sample solution for up to 64 elements in under 1 minute. Many systems are available from companies such as Applied Research Laboratories, Spectro Analytical, etc.

The laser was first used as a source for atomic spectrometry in 1962 by Brech and Cross[5] soon after the invention of the laser by Maiman in 1960.[6] In this technique (laser-induced plasma emission spectrometry, LIPS), laser light from a high energy laser is focused onto the sample surface to produce a laser-induced plasma. Sample material is vaporised into the plasma and characteristic atomic/ionic emissions result. Spectrochemical measurement of the laser-induced plasma enables simultaneous, multi-element analysis of the sample. Rapid, in situ micro- and bulk analysis of samples can be achieved, and the technique has a remote sensing capability. The technique has been the subject of development for over thirty years,[7] starting with the laser microprobe with photographic detection used by Brech and Cross[5] to current state of the art optical multi-channel analysers that incorporate computer-controlled photodiode

array detection systems. Some authors refer to the technique as laser induced breakdown spectrometry (LIBS) and refer to the plasma as the 'laser spark'.[8]

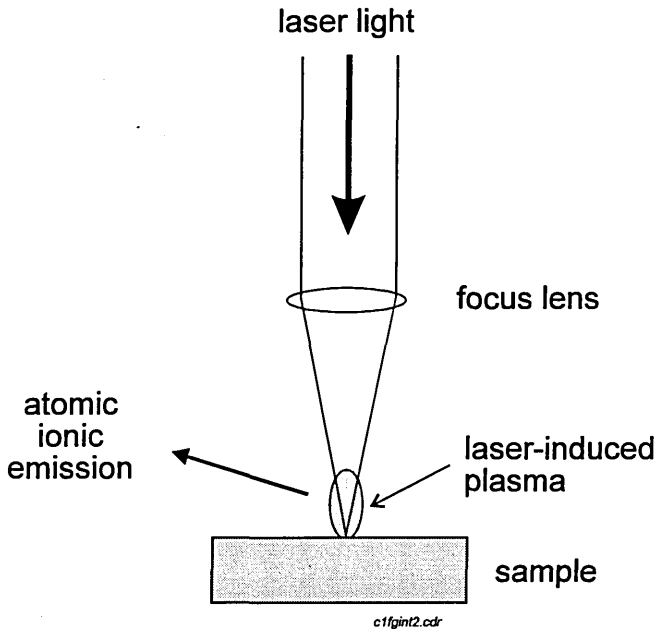

Figure 2 Schematic of laser-induced plasma emission spectrometry

There are, however, some disadvantages associated with the laser-induced plasma technique. Emission spectra are complex and time-dependent because of the high temperature and the transient nature of the plasma, and the plasma is formed with each laser shot and decays away completely between shots. A sophisticated detector system is required to make rapid, time-resolved measurement in order to extract useful analytical data from the laser-induced plasma.[7] Time resolution is important because it enables analyte emission signals to be separated in time from the intense background continuum and provides considerably improved analytical performance .

Laser ablation has also been used as a source for elemental mass spectrometry (laser microprobe mass analysis, LAMMA), and has been coupled

to other techniques such as inductively coupled plasma emission and mass spectrometry's.[7] Here the laser is used only to remove sample material and analysis is achieved with a more powerful excitation source and detector system. Several reviews are published [7,9,10] and laser ablation systems with inductively coupled plasma mass spectrometers are available, e.g. Fisons VG Elemental, Perkin Elmer Sciex, etc. The main advantage of such coupled techniques is improved sensitivity compared to laser-induced plasma emission spectrometry.

There remains, however, considerable interest in laser-induced plasma emission spectrometry because there is a growing need by industry for elemental analysis of materials that is more rapid than currently available. Applications include the monitoring of element compositions in production and process situations so that material composition can be more closely controlled, the rapid sorting of materials, and the rapid, in situ environmental analysis of hazardous materials. Laser-induced plasma emission spectrometry can be used to address these requirements because of the remote sensing, rapid and in situ, simultaneous multielement analysis capabilities. The major disadvantage of laser-induced plasma emission spectrometry is relatively poor sensitivity, which may not present a problem because these industrial applications do not generally require high sensitivity. The work forming the basis of this thesis investigates laser-induced plasma emission spectrometry in order to devise novel applications that will further the understanding and knowledge of the technique.

1.2 Theory of atomic emission spectroscopy

Atomic emission spectra originate from electronic transitions of excited atoms and ions.[11,12] An atom consists of a central nucleus of protons and neutrons, surrounded by electrons arranged in discrete energy levels (orbitals). At low temperatures, such as room temperature, all the electrons are essentially in ground state configurations and are un-excited. Outer valence electrons can be excited to higher orbitals by the high temperature of an atomic emission source such as a chemical flame, inductively coupled plasma (ICP), or laser-induced plasma. The excited atom has a very short lifetime (10^{-8} s) and the excited electron then decays to the ground state, releasing the extra energy as a photon of radiation. The energy of this emitted photon (E_{em}) is governed by the difference in energy levels between the ground state (E_{gs}) and excited state (E_{ex}).

(1) $E_{em} = E_{ex} - E_{gs}$

(2) and $E_{em} = h\nu$

where h = Plank's constant (6.624×10^{-34} Js)

ν = frequency of radiation

(3) $\therefore \quad h\nu = E_{ex} - E_{gs}$

the frequency can be converted to wavelength (λ) from:

(4) $c = \nu\lambda$

where c = velocity of light in vacuum (2.9979×10^{8} ms^{-1})

$\therefore \quad \nu = c / \lambda$

from (3) $h(c / \lambda) = E_{ex} - E_{gs}$

(5) $\therefore \quad \lambda = hc / (E_{ex} - E_{gs})$

As these energy levels are discrete and unique to each element, the emitted photon is characteristic in wavelength of that element and the resultant emission line is narrow and well defined. Depending on the temperature of the

emission source, atoms can be ionised, either singly, doubly, etc., and these ions may also undergo electronic excitation to produce further emission lines.

The probability of a particular electronic transition is given by the Boltzmann Distribution Law:

(6) $$\frac{Nj}{No} = \frac{gj}{go} \exp\left(-\frac{Ej}{kT}\right)$$

where N_j = number of atoms in an excited state

N_o = number of atoms in the ground state

g_j = statistical weight of the excited state

g_o = statistical weight of the ground state

E_j = energy difference between excited state and ground state

k = Boltzmann constant (1.38×10^{-23} J K^{-1})

T = temperature (K)

The emission intensity is proportional to the number of excited species. From (6), the number of excited species and therefore the intensity of emitted radiation is strongly affected by the temperature of the emission source; increasing the temperature increases the intensity of emission lines.

The wavelengths of emission lines are not generally calculated as there are many possible electronic transitions for each element, the number of transitions increasing with atomic number and valancy. For example, in the wavelength range 200 - 800 nm there are more than 200,000 emission lines[2] of neutral atoms and single ions. Emission wavelengths are given in published tables, such as the M. I. T. Wavelength Tables,[13] in which emission lines were obtained from the arc, spark or discharge tube emission spectra of pure elements, and the spectral atlas for an ICP emission source by Fassel et al.[14]

Other types of emission from the source include molecular (or band), and continuous spectra. Band spectra are produced by molecular emission from, for example diatomic molecules, e.g. N_2, CN. Band spectra appear as unresolved broad lines with a low resolution spectrometer, and as a series of fine lines with a high resolution spectrometer. Continuous spectra are not atom or molecule specific and are produced by free electrons in the emission source. These emit continuous, i.e. not wavelength specific, radiation due to Bremsstrahlung and recombination processes. Black body radiation also contributes to the continuum and the intensity increases with temperature.

From the discussions above, the intensity and complexity of emission spectra increase with temperature. Spectra from a laser-induced plasma which has a relatively high temperature (~15 - 30,000 K) will therefore be much more complex and intense than spectra from a lower temperature source, such as a chemical flame (~2000 K) or an inductively coupled plasma source (~6000 K). Spectra will contain intense emissions from atom, and single and multiply charged ionic species, together with intense molecular and continuum signals. The spectra may be additionally complex because the laser-induced plasma is transient, and plasma characteristics, such as temperature and size, change rapidly during the plasma lifetime.

1.3 Theory of laser - material interaction processes

The laser-induced plasma results from a complex series of processes, with many occurring simultaneously. Much has been written about the processes and the many factors that affect them.[7,15-18] A simplified view is presented here and a schematic shown in Figure 3.

When a high power, Q-Switched laser pulse is focused onto the surface of a solid material, the surface in the vicinity of the laser spot is heated very rapidly and several processes occur within a very short period of time, on the ns time scale. The irradiance (power per unit area) is typically 10^9 to 10^{12} W cm^{-2}. Initially, some of the laser light may be reflected depending on the reflectivity and nature of the surface, but this decreases rapidly as the temperature rises. The laser energy is thermally absorbed by the material which causes material to be vaporised. In the case of a conducting material, the conduction band electrons absorb laser photons and the energy is converted to heat through collisions. Heat may be lost from the surface by thermal conduction. Part of the absorbed energy is used to overcome the latent heats of fusion and evaporation to produce phase changes. Vaporisation and heating continues to produce a partially ionised gas above the surface of the material. Other processes also produce electrons and ions. These include multi-photon absorption, where an atom absorbs several photons to gain sufficient energy to cause ionisation, and thermionic emission (desorption) of ions and thermal electrons.

When the electron density of the gas above the sample surface is sufficiently high, heating by inverse Bremsstrahlung processes takes place. Here, electrons gain energy by absorbing photons, and transfer energy to the plasma through collisions with other species in the plasma. The temperature and electron density continues to rise and the plasma expands. An avalanche effect takes place causing rapid heating because the heating rate increases with electron density; as the number of electrons increases, the amount of heating through inverse Bremsstrahlung increases which causes more ionisation and further heating. A rapid expansion of the plasma due to energetic particles occurs with a supersonic velocity (2×10^7 cm s^{-1}), typically at the peak of the laser pulse. The plume develops towards the laser beam. Heating of the

sample continues by the laser and plasma, and material leaves the surface as vapour, droplets, or superheated streams of material. The temperature of the plasma is of the order 10^4 to 10^5 K. As the plasma is very hot and dense, the plasma contains a very high density of energy. This means that the plasma continues to be luminous and expand for a long time after the end of the laser pulse. Depending on many factors, such as the incident laser energy and the density of the ambient gas, the post-pulse lifetime of the plasma may be from 300 ns to 40 μs,[16] to 100 μs.[19] The plasma cools during this time due to expansion and material entering the plasma.

Studies have been made photographically, with streak cameras, and spectroscopically to support this sequence of events.[15,16,20,21] Spectroscopic monitoring[16] of the ablation of steel in air at 0.05 Torr shows that emission from the plasma initially consists of an intense background continuum due to Bremsstrahlung processes and black body radiation. This continues to increase until about 150 ns after the start of the laser pulse. After this, the plasma intensity decreases and emission lines from elements in the sample become apparent. The emission lines can be measured by a suitable spectrometer to gain qualitative and quantitative analytical information about the sample. The emission lines decrease in intensity as the plasma decays to zero over a period of time (100 ns to 100 μs, depending on operating parameters). Improvement in analytical performance can be achieved when analyte emission signals are resolved in time from the intense background continuum.

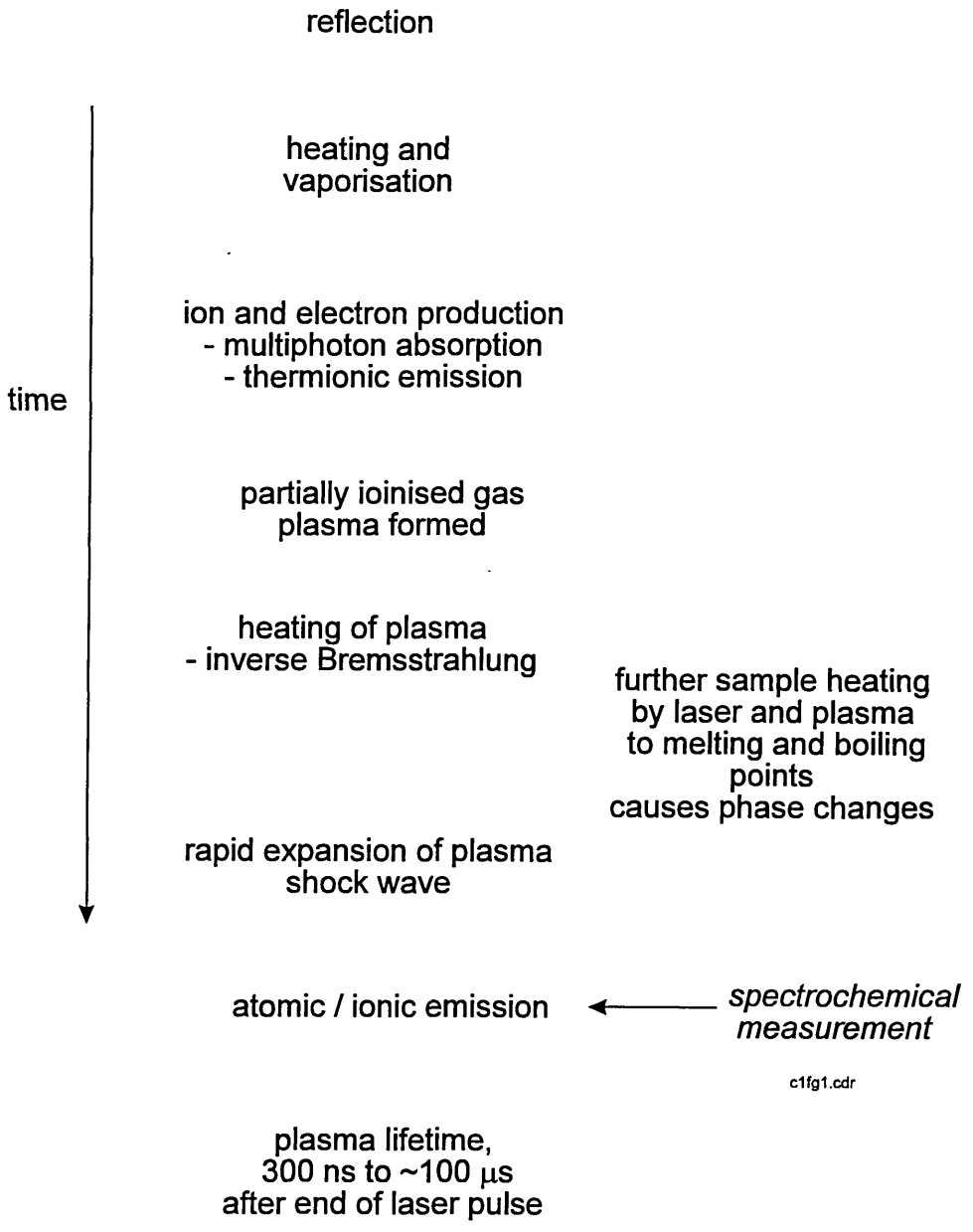

Figure 3 Schematic showing the processes involved in laser-induced plasma spectrometry

1.4 Instrumentation for laser-induced emission spectrometry

The laser was first used as a source for atomic emission spectrometry in 1962 by Brech and Cross[5] who used a laser microprobe. A pulsed ruby laser was focused onto the surface of a sample using a microscope objective lens through which the operator could view the sample for alignment and observation. The laser/laser-induced plasma removed material from the sample, and the laser-induced plasma was supplemented by a conventional electrical spark from a pair of electrodes positioned directly above the sample. This extra excitation is termed cross excitation. Light from the discharge was focused onto the entrance slit of a spectrograph and the dispersed spectrum recorded photographically.

Laser microprobes with cross excitation were for many years the main instruments used in laser-induced emission spectrometry, and commercial instruments were produced in the USA (e.g. Jarrell Ash Mark III), Japan (e.g. JEOL JLM 200), and in the former-East Germany (e.g. Carl Zeis VEB LMA 10). The instruments, developments and applications are described by several authors, notably Moenke-Blankenburg et al[7] , Cremers et al[8] , and Piepmeier et al.[17] A schematic is shown in Figure 4.

Cross excitation improved certain aspects of analytical performance, such as sensitivity, and minimised the effect of the strong background continuum from the laser-induced plasma. The disadvantages of cross-excitation were recognised by many authors,[7,8] and Van Deijck[22] concluded that the technique was not sufficiently reproducible to become fully quantitative. Subsequent studies have concentrated on using the laser-induced plasma as the sole energy source in order to simplify the instrumentation and remove the disadvantages of cross-excitation. Advantages include simpler methodology, because no auxiliary equipment is needed as the laser vaporises and excites

the sample. Also it is possible to make non-invasive measurements as the laser plasma can be produced remotely. Many studies have investigated and used procedures such as internal standardisation, spatial and time resolution to improve analytical performance. Time resolved measurement and modern optical multichannel analysers (OMAs) have compensated for the lack of cross excitation and have brought improved performance. The instrumentation used has generally been modified laser microprobe analysers, or laboratory assembled equipment.

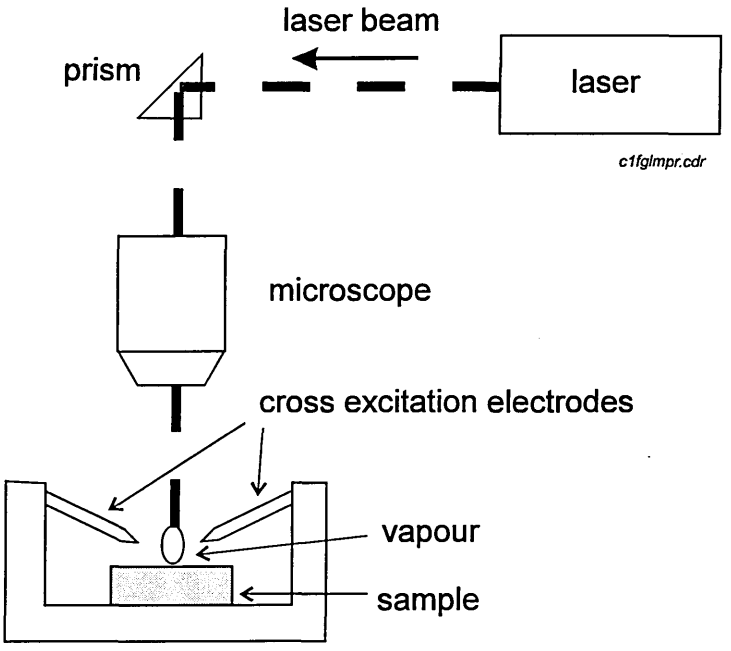

Figure 4 Schematic of a commercial laser microprobe showing the electrodes for cross excitation.[23]

1.4.1 Laser types

The types of laser used in laser-induced plasma emission spectrometry are listed in Table 2 together with output wavelengths. The main difference is the type of active medium used to produce the laser light, and the phase of the medium, either solid or gas.

Laser	Phase of active medium	Wavelength (nm)
Ruby	solid	694
Nd:Glass	solid	1064
Nd:YAG	solid	1064
Nd:YAG (Frequency Doubled)	solid	532
Nd:YAG (Frequency Quadrupled)	solid	266
N_2	gas	337.1
CO_2	gas	10600
Excimer XeCl	gas	308
ArF	gas	193, 248

Table 2 Types of laser used in laser-induced plasma emission spectrometry

The ruby laser found widespread use in the laser microprobe analysers and in early laser induced breakdown spectrometry work, but has generally been superseded by the Nd:YAG laser, (neodymium yttrium aluminium garnet). This laser has been used in most studies since 1980. The advantages of the Nd:YAG are that it is robust and fairly compact, can operate at higher repetition rates than the ruby (15 Hz Vs 4 Hz), and has better repeatability of shot to shot output. The infrared laser output (1064 nm) of the Nd:YAG is absorbed by most

materials making it suitable to ablate a wide range of materials. It is generally used in the Q-Switched mode, in which all the energy of the laser pulse is released within a very short time period, typically a peak width of 10 ns. This is achieved by using either an electro-optically operated Q-Switched laser, or an acousto-optically Q-switched laser.[24] The electro-optically switched is generally used because of the relatively high energy output, 0.5 J pulse^{-1} at 10 Hz. The acousto-optically Q-switched can generate 0.012 J pulse^{-1} up to a repetition rate of 5000 Hz.

A disadvantage of the Nd:YAG is that high energies are required to cause ionisation and plasma formation. Also the smallest spot size that can be achieved by focusing this wavelength is about 100 μm in diameter (the calculations are given in Chapter 2, section 2.2). To obtain higher degrees of ionisation and a smaller spot size, it is necessary to use a shorter laser wavelength. This can be achieved by using a laser with an ultra violet (UV) wavelength, such as a a frequency doubled or quadrupled Nd:YAG laser (Niemax et al[25]), a N_2 laser (Kagawa et al[26,27]), or an excimer laser (Chau et al[28], Hoffman,[29] Lorentzen et al,[30] Petit et al,[31] Sneddon et al [32,33,34] and Weimer et al[35]). The UV wavelengths of these lasers are sufficiently short to cause the photoelectric effect by single or double -photon processes and so the plasma can be generated easily with relatively low threshold energy, (Kagawa[26]). Further advantages of the N_2 laser include high repetition rates, which may improve precision, and short pulse duration (~ 5 ns), which may minimise selective vaporisation effects.

In the following sections, the laser type and wavelength are not generally recorded if a Nd:YAG laser with an output wavelength of 1064 nm has been used. The laser and wavelength are specified if they are different from these.

1.4.2 Detection systems

Different detection systems have been used in laser-induced plasma emission spectrometry and are summarised in Table 3.

Detector	Year of introduction to LIPS
photographic plate	1962
photomultiplier tube	1969
silicon intensified target vidicon	1981
intensified photodiode array	1981
charge coupled device	1990

Table 3 Detectors used in laser-induced plasma emission spectrometry

The photographic plate was generally used in laser-induced emission spectrometry as a detection device for over 25 years because of its unique advantages, (Cremers and Radziemski,[8] 1986). These are, (a) the plate can store permanently the position and intensity of spectral lines, (b) it has a good sensitivity for many elements, (c) it is fairly cheap and easy to operate. This versatility enables not only simultaneous recording of much of the periodic table but also recording of all available lines for each available element. This technique, however, has several disadvantages: the chemical process and the reading of the plate are both time consuming, the latter necessitating the skill of an experienced chemist; it is only semi-quantitative because of inherent errors in the technique, variation in the plate emulsion, chemical processing of the plate and difficulties in reading the plate. The lack of direct access to the analytical data led to the introduction of photoelectric detection systems in 1969 by Beatrice and Glick.[36] Here a polychromator with two photomultiplier tubes

was attached to a Czerny-Turner spectrograph to facilitate the simultaneous measurement of an analytical line and the adjacent background, enabling simultaneous background correction. A system described by Marich et al[37] (1974) contained a six tube vacuum polychromator, in which six elements could be determined simultaneously. In a study with a three channel spectrograph, Moenke-Blankenburg[38] found that it was possible to reduce the limits of detection by an order of magnitude, the precision of the determination of concentration was about 5% (RSD), a factor of two better than the photographic method, and the speed of analysis was very much faster. However the normal disadvantage of a direct reading spectrometer remained, namely only pre-selected elements could be determined and so photographic plates continued in general use for simultaneous analysis. Other elements could only be measured sequentially by adjustment of the channels to other wavelengths, or by using a scan facility.

In order to combine the speed of the direct reader with the versatility of the photographic plate, instrumentation has been developed which use an optoelectronic image device as a multi-channel detector. Initially a silicon-intensified target vidicon (SIT) was used,[7] but this was superseded by a photodiode array device when these became available. Talmi et al[39] (1981) compared both systems and found detection limits for both to be in the range 2-500 ppm.

The silicon-intensified target vidicon tube comprises an image intensifier and a target crystal containing 500 silicon photodiodes, 10 mm high x 25 μm. Each photodiode is storage device. Incident photons neutralise part of this charge, the extent being proportional to the number of photons. Each photodiode is recharged by an electron beam and so the size of the recharging current is proportional to the light intensity between two scans. This signal is passed to a

computer for processing to yield a wavelength spectrum of, for example, 30 nm. In terms of performance, the silicon-intensified target vidicon has similar sensitivity to a photomultiplier tube, but suffers from inferior signal/noise ratio.[8]

A typical photodiode array contains a linear array of 1024 detector elements (diodes, pixels), 2.5 mm high x 25 μm, covering a length of 25.4 mm, i.e. 40 diodes per mm. Each diode, or pixel, stores charge which is again partly neutralised by incident photons. The array is scanned by individual switches attached to each pixel opening in turn and recharging the pixel. These switches are field effect transistors and are part of the integrated circuit containing the array. It is scanned typically every 30 ms, so the integration time is 30 ms, and the data processed by computer to yield wavelength spectra. Depending on the grating utilised in the spectrometer, medium and high dispersions can provide spectral regions of 70 and 17 nm respectively (Talmi[39]). By choosing a suitable region, multi-element analysis can be achieved, and by scanning the grating to other wavelengths, a wide range of elements can be detected. A development has been the addition of an image intensifier located in front of the photodiode array (Radziemski,[40] Figure 5). A microchannel plate image intensifier amplifies the incident light with a gain in the order of 25,000 giving improved sensitivity and allowing shorter integration times to be used.

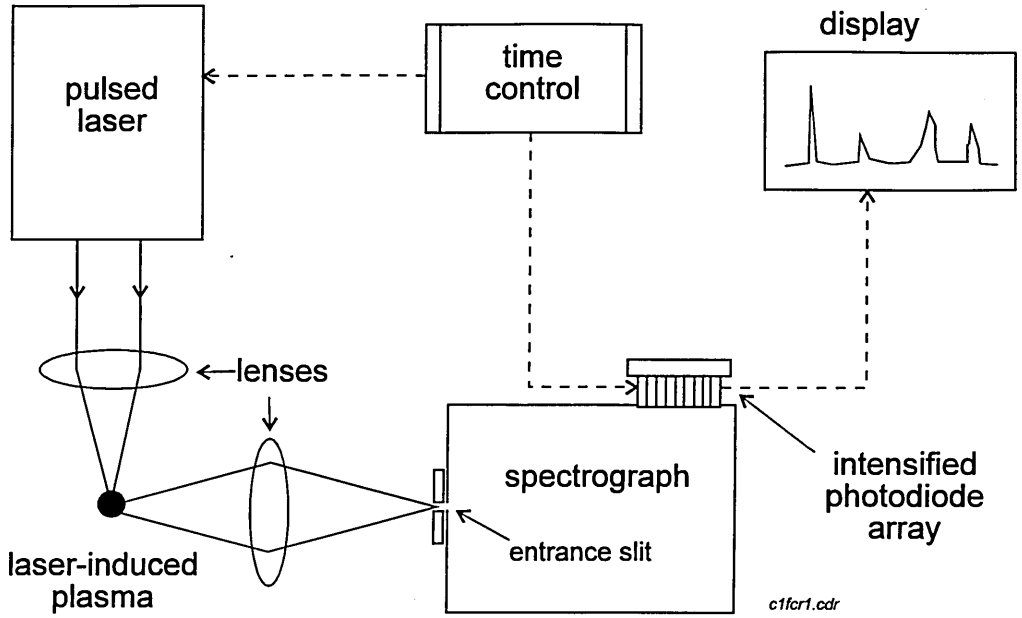

Figure 5 Typical apparatus for laser-induced plasma analysis of a material. The detector is an intensified photodiode array (time-gated). The image of the laser-plasma is focused onto the entrance slit of the spectrometer with a simple lens. (from reference[40])

More recently other measuring devices, such as the charge coupled device (CCD) and the charge injection device (CID) detectors have been developed,[41] and utilised in commercial inductively coupled plasma emission spectrometers. The charge coupled device detector is available as a linear array or as a two dimensional array of measuring elements, typically 512 x 512, and benefits from improved sensitivity and readout noise. The two dimensional array facility was used in an optical imaging spectrometer by Iida[42] (1990) to spectrally map laser-induced plasmas, (discussed in section 1.5.4).

A time resolved measurement capability is advantageous when monitoring the laser-induced plasma in order to separate analyte emission signals from the intense background continuum and improve analytical performance. Various methods were used to achieve this with photographic detection, such as streak photography of the spectrally resolved emission line (Cremers et al[8]), or a system of rotating mirrors synchronised with the laser Q-Switch to sweep the plasma image across a spectrograph entrance slit (Piepmeier et al,[43] 1969). With photomultiplier tube detection, electronic systems were devised to gate and integrate the signal (Marich et al,[44] 1971; Allemand,[45] 1972; Schroeder,[46] 1971). However, this photomultiplier tube technique had the disadvantage of measuring only one element at a time, with no possibility to make simultaneous background measurement unless a second photomultiplier tube channel was fitted. Image-intensified photodiode arrays can be used (Radziemski,[40] 1981) by switching the intensifier on and off to control the exact time period that is observed. This is termed 'gating'. The device has the ability to make simultaneous, multi-element and background measurements, and is thus a most powerful and convenient method to capture time resolved spectra. Studies of laser-induced plasma emission spectrometry since 1981 have either used intensified photodiode arrays, or, to a lesser extent, time-gated photomultiplier tubes.

A recent development (1993) in charge coupled detection (CCD) device technology is a 'masked' CCD, (EG&G OMA 4),[47] which enables time resolved measurement with a CCD. Here, only a single row of the 512 rows available is exposed to radiation, the remaining 511 are masked. After exposure, the charges on the exposed row are shifted down to the next row, which is behind the mask, and exposure of the first row is repeated. After each exposure, the charges are shifted down the array and are stored until readout at the end of the experiment. Time resolution is limited compared to an intensified

photodiode array, however, the minimum delay and integration times are 3 μs for the 'masked' CCD compared to 20 - 100 ns for the intensified photodiode array.

The general method of transferring radiation from the laser-induced plasma to the spectrometer system has been to use a straight optical path with a simple lens to focus the image of the plasma onto the entrance slit (Figure 5). Some studies have used an optical mask to shield part of the plasma in order to make spatial measurements. More recently, an optical fibre has been used to capture and transfer the emitted light to the spectrometer (Figure 6), by researchers such as Campos et al[48] (1992), Cremers et al[49] (1987), Grant et al[50] (1991), Kuzuya et al[51] (1992), and Lorenzen et al[52] (1992). This has the advantage that spectrometer and plasma do not have to be precisely aligned, and remote sensing is more easily achieved. These studies have generally achieved analytical performance that is comparable to that obtained with a straight optical path, despite the losses in light intensity due to fibre optic light transmission. Some studies[48,51,52] have used a lens arrangement to focus emitted radiation onto the entrance of the fibre optic in order to increase the light intensities.

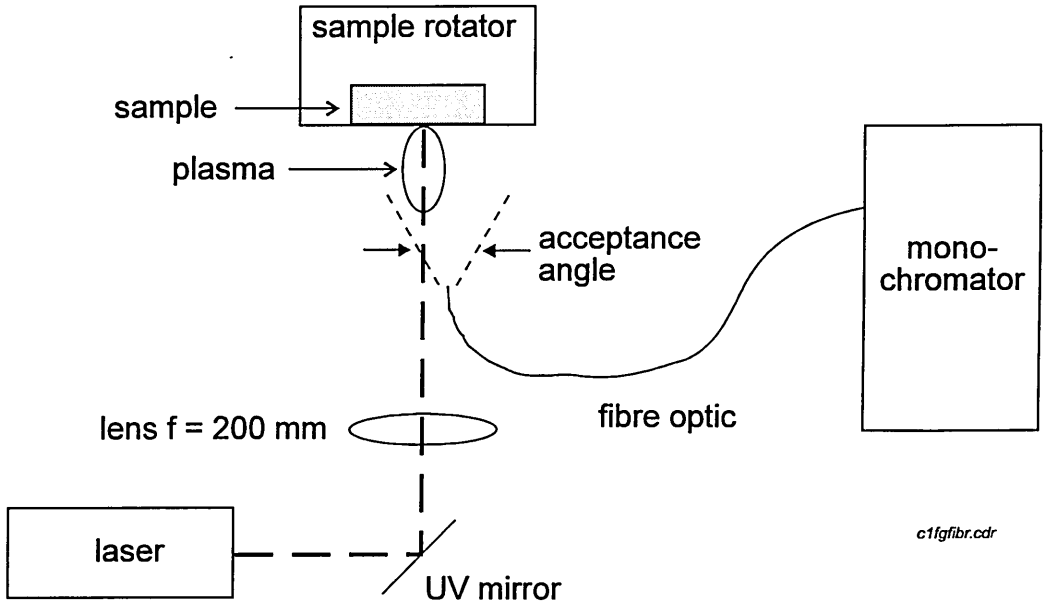

Figure 6 Schematic showing part of the apparatus used by Grant et al[50] to measure laser-induced emission spectra of iron ore. The diagram shows the arrangement used to collect radiation from the plasma with a fibre optic. The end of the fibre optic was positioned 15 mm from the plasma and the acceptance angle was 35°.

1.5 Review of analytical applications

The technique of laser-induced plasma emission spectrometry has been used to determine over 60 elements in a very wide range of samples in the solid, liquid and gas phases. The following sections discuss applications of the technique to the three phases.

1.5.1 Solid phase

A comprehensive review of applications with cross excitation is provided by Moenke-Blankenburg[7] (1989), and with direct spectral analysis, i.e. no cross excitation, by Cremers[8] (1986) up to 1986. Solid samples include minerals, meteorites, metals, alloys, semiconductors, glasses, ceramics, paintings, medical and biological specimens. Absolute detection limits are at the ng level, and relative detection limits about 10^{-3} mass percent, an order of magnitude worse than direct current arc optical emission spectrometry. This section reviews applications that use direct analysis of the laser-induced plasma.

Runge et al[53,54] (1964) demonstrated the quantitative analysis of Ni and Cr in solid and molten iron using a Q-Switched ruby laser. Similar results were obtained for both samples, with linear calibration graphs using chromium/iron and nickel/iron ratios. Scott and Strasheim[20] (1970) compared three modes of laser output for spectrochemical analysis. The two forms of Q-Switched firing generated the highest temperatures, and produced line shifts towards the red in the emission spectrum. They concluded that the analytical capability could be increased by monitoring a selected region of the plasma, and that time resolution was only useful with the Q-Switched laser pulse. Felske et al[55] (1972) analysed steel samples using a device that moved the sample between laser shots so that fresh material was ablated each time. Improved precision

was obtained (relative standard deviation, RSD, 1%), but the sensitivity was an order of magnitude poorer than with cross excitation.

Baldwin[56] (1970) studied the Q-Switched laser sampling of copper-zinc alloys and found that material was removed as vapour and liquid metal. Results suggested there were different volatilisation rates for copper and zinc, which explained the error that occurred when copper was used as an internal standard in this matrix. Allemand[45] (1972) found that the size of crater produced by Q-switched laser ablation depended strongly on the type of material ablated, and better reproducibility was obtained from metals that had been polished. The usefulness of time and spatial resolution was demonstrated.

Rare earth elements were detected in a sodium chloride matrix by Ishizuka[57] (1973) at concentrations down to approximately 5 ppm with calibrations linear over an order of magnitude. A Q-switched ruby laser with single pulse was used. Furuta et al[58] (1993) studied the ablation of sodium chloride and observed that atomic emission lines were broadened in air and some were self-reversed, but self-reversal did not occur if the sample was ablated in a vacuum. The line broadening was due to resonance and Stark effect.

In a series of papers, Marich, Treytl et al[37, 59,60,61,62,63] (1970-1975) described a range of applications and studies. The effects of matrix (bovine albumin and human serum) upon silver and magnesium emissions were investigated.[59] It was observed that the presence of increasing concentrations of matrix decreased the amount of sample vaporised, and that these effects were mainly physical rather than chemical. Attempts were made to intensify the laser absorption by adding methyl blue, but no increase in silver emission was found and at higher concentrations the silver emission decreased. Time resolved

measurements were made of magnesium in aluminium foil and calcium in photographic film.[60] Using a gate width of 5 μs, the delay time for maximum signal to background ratio (S/B) was found to increase with laser energy and was different for each sample. In a study into the effects of atmosphere,[63] it was observed that S/B ratios did not vary systematically with laser energy and atmosphere, but larger values were obtained in vacuum with the lower energy used (1.2 mJ). It was concluded that, in certain samples, the selection of an appropriate atmosphere may improve S/B, but in general, there was no need to change the atmosphere from air. Optimal time parameters and detection limits were determined for a series of elements in an organic matrix (Li, Mg, Ca, Fe, Cu, Zn, Hg, Pb).[50] The time delay varied from 4 to 16 μs, and the integration time from 2 to 15 μs, and detection limits were obtained of the order 10^{-13} to 10^{-15} g. An improved instrumental system was described[37] and used to analyse human tissue. Further work[61] investigated the time differentiated analysis of selected regions of the laser-induced plasma. Twofold increases in response relative to on-axis viewing were obtained for gelatin and liver samples by using spatial differentiation. The optimal lateral displacement from the centre of the plasma varied with element, 0.5-0.75 mm. The optimal vertical distance was about 1 mm above the focal plane. Marich concluded that to optimise analytical sensitivity, advantage could be made of the heterogeneous nature of the laser induced plasma.

Using an intensified photodiode array, Cremers et al[64] (1986) evaluated a range of factors affecting the analysis of steels. These included, the lens to sample distance, the laser energy, and the imaging lens position. The maximum S/B ratios for each element were with the sample positioned at, or close to, the laser focal point. It was observed that as the laser pulse energy was increased, the intensities of ion emission lines increased relative to atomic lines, and it was concluded that the choice of iron line for use as internal

standard should be made carefully. In a further study[65] (1985) laser-induced plasma emission spectrometry was compared with laser ablation - inductively coupled plasma - emission spectrometry for the rapid analysis of solid and molten steels. The ICP method appeared to have superior analytical performance, and the authors thought that this might be easier to incorporate into a steel plant environment.

Using a fibre optic for collection and transmission of emitted light, Cremers[66] (1987) analysed solder and steel alloys with RSDs in the range 4-28 %. The fibre optic was positioned between 0.5 m and 2.4 m from the sample and a 500 mm focal length lens was used to focus the laser light. Radziemski et al[67,68] (1986) analysed beryllium-copper alloys and considered the technique useful for the rapid sorting of these alloys.

The spectral emission of atoms and ions from the laser ablation of super-conducting materials for the deposition of thin films was studied by various authors. Yoo et al[69] (1989), Geyer et al[70] (1989), Weimer et al[35] (1990), and Hoffman[29] (1990) studied species emitted from $YBa_2Cu_3O_{7-x}$, while Deshmukh et al[59] (1988) investigated $Bi_2CaSrCu_2O_9$. The emission data was used to monitor in-situ the deposition of these materials and provide information about possible chemical reactions taking place in the plasma.

The spectroscopy of the plasma was used by Chita et al[72] (1990) to monitor the performance of the laser welding of aluminium sheet, and showed that improved performance was obtained with nitrogen as the shield gas compared to Ar and He. Pramanick et al monitored[73] (1991) emission spectra during the growth of thin films (Ti, TiN and $TiSi_2$) with pulsed laser evaporation. Emission spectra were dominated by atomic and ionic titanium emissions (Ti I, Ti II), but signals for atomic and ionic silicon and ionic nitrogen were also observed.

Grant et al[74] (1991) quantitatively measured various elements (Ca, Si, Mg, Al and Ti) in iron ore, and obtained precision in the range 2-25 % (RSD) with detection limits of the order of 0.01 % m/m. A schematic of the instrumental set-up is depicted in Figure 3. Campos et al[48] (1992) determined the carbon content of steel with a precision of 1.6 % and detection limit of 65 μg/g using a nitrogen buffer gas. Carbon was measured at 193.09 nm with a 1 metre monochromator. In a conference abstract, Petit et al[31] (1992) reported the use of a XeCl excimer laser to measure magnesium in aluminium alloy samples. Precision was 2 % (RSD) when the aluminium of the matrix was used as internal standard.

Sneddon et al[32,33,34,75,76] (1991-92) have made a series of studies using an ArF excimer laser (193 nm). Using metallic targets (Zn, Cu, Ni, and Fe metals), they found that the radiation emission intensity from the plasma increased with laser energy, and that this relationship could be quantified.[75] Spatial measurements of the plasma produced by an ArF excimer laser were made with copper and lead targets.[76] They found that the plasma differed in size with the target used, and different observation positions were needed for both. It was attributed to the differences in thermal conductivity and boiling points of the two materials. Studies of the effect of atmosphere[32] with the ablation of copper showed that the size of the plasma was affected by the type of gas and pressure used for ablation. They concluded that maximum S/B ratio for copper was obtained with argon at reduced pressure and with helium at atmospheric pressure. Space and time resolved studies[34] showed the plasma to have a Gaussian distribution of atoms and ions. The lifetime of the plasma was estimated to be 100 μs. Using spatial resolution of the plasma, Sneddon et al[33] reported the quantitative measurement of chromium in steel with an estimated limit of detection of 0.002 % m/m.

Niemax et al[77] (1992) calculated the spatial electron density in an argon plasma from time-resolved measurement studies. The density was derived from the shift of spectral lines and from Stark broadening. They concluded that the argon plasma had a larger volume than the vapour cloud from the ablated material. Esmiller et al[78] (1992) determined the temperature and electronic density of a plasma induced on aluminium, graphite and silicon carbide targets. Majidi and Xu[79] (1993) studied the use of the laser-induced plasma as a continuum source. They concluded that the continuum emissions generated in the first 150 ns of the plasma lifetime should be used for optimum results.

A series of applications have focused on environmental analysis. Cremers and Radziemski[80] (1985) determined beryllium dust collected on an air filter as part of a health and safety programme. The filter was rotated so that the laser-induced plasma (dimensions 0.1 mm x 4-8 mm) could sample a large area. Enhanced beryllium signal was obtained with increased rate of rotation, up to a maximum of 4.8 rpm, above which the signal levelled off. The limit of detection varied with the particle size, typically 0.45 ng cm^{-1} for 0.5 to 5 μm diameter, with RSD for replicate analysis of 4%. Hardjoutomo et al[81] (1992) reported the use of a compact TEA CO_2 laser for field-based analysis of geological samples, (TEA, transverse excitation atmospheric).[82] Using helium gas at atmospheric pressure, semi-quantitative analysis was undertaken using glass reference materials as calibration standards. Minimum detectable concentrations were estimated to be 60 and 500 μg/g for zinc and fluorine respectively. Wisburn et al[83,84] (1992,1993) evaluated the detection of heavy metals in environmental samples such as soils. They compared the use of two lasers, (Nd:YAG, 1064 nm) and an excimer (XeCl, 308 nm) and found that the use of the UV wavelength was more efficient resulting in lower detection limits for lead in sand, 2 μg/g (308 nm) and 15 μg/g (1064 nm), respectively. They concluded that detection limits were acceptable, and with the minimal sample preparation

required, the technique could be used as a fast screening sensor for environmental analysis. Cremers et al[85] (1992) reported the development of a 'Portable Laser Spark Surface Mass Analyser'. The instrument measures light emitted from the laser-induced plasma to detect elements, and has been applied to environmental analyses in the field, such as lead in paint, chromium in soil, lead and arsenic in industrial plant exhaust.

Laser-induced plasma emission spectrometry has been used for on-line process monitoring applications. Several workers have developed applications for the analysis of molten steel in order to monitor steel production. These include, Runge et al[54] (1966), Cremers et al[65] (1985), Jowitt[86] (1985), Lorentzen et al[52] (1992), and Kim[87] (1992). The technique appears to be well suited to this application even in this harsh environment. Jowitt[86] obtained linear calibrations for chromium and manganese in liquid steel. Kim[87] discussed the feasibility of making quantitative measurement with a single laser shot. The monitoring of elements (S, Si, Zn) in rubber slab production for tyre manufacture was reported by Lorenzen and Carlhoff[52] (1992). A schematic diagram is shown in Figure 7 of the arrangement used to deliver laser light to the sample and transmit emitted radiation to the measuring spectrometer.

In the nuclear industry, the technique has been applied to the on-line monitoring of uranium concentration in liquid[88,89] (1987, 1992) (described below, 1.4.2) Adrain et al[90] (1978) studied silicon emission responses from the ablation of mild steel in order to measure in situ the concentration of silicon in the steel of nuclear reactor vessels. More recently, fundamental studies have investigated the remote laser-sampling and analysis of radioactive materials (Shuttleworth 1994).[91] In the energy industry, studies have applied the technique to the on-line monitoring of elements in coal-gas flows,[92,93,94] (1989, 1991, 1993), (described below, 1.4.3).

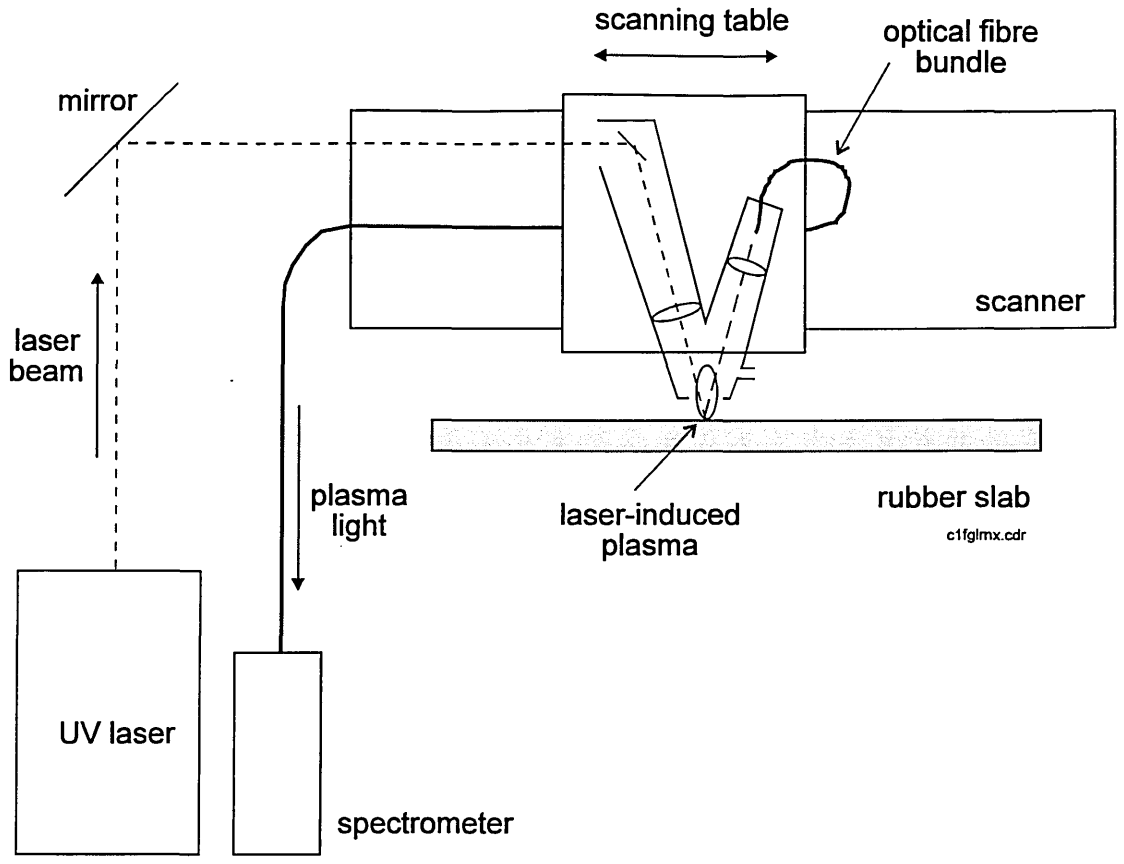

Figure 7 Schematic representation of the system developed by Lorenzen et al[95] of Krupp, Germany, to monitor the elemental composition of rubber for tyre manufacture. The authors refer to the technique as 'remote laser microanalysis' (RELMA).

The application of laser-induced plasma emission spectrometry (LIPS) to the depth profiling of materials and coatings has been limited. Talmi et al[39] (1981) used a laser microprobe (ruby laser and vidicon detector) to obtain a quasi-depth profile of an electrical capacitor by sampling to different depths of the material. This was achieved by changing the size of the laser spot through variation of operating parameters. In discussing surface contamination, Cremers[49] (1987) reported the ablation of aluminium metal coated with a paint film by using the first few laser shots to remove the paint layer. In the same paper, Cremers reported the removal of surface grease from a metallic surface prior to analysis, and the analysis of galvanised steel having removed the zinc coating with the first laser shots. Lorenzen et al[52] (1992)

showed a variation in the thickness of a titanium nitride coating across the surface of a metallic sample. Kim[87] (1992) reported the variation of calcium concentration with depth for a sample of steel.

1.5.2 Liquid phase

Only a few applications of laser-induced plasma emission spectrometry have been made with liquid samples. Cremers et al[97] (1984) fired the laser through a window in the side of a teflon cell to generate a submerged spark in the liquid. The laser was focused by a pair of 5 cm focal length lenses and the light produced was transferred through a second window to a monochromator with photomultiplier tube detection. Limits of detection were of the order 1 mg l^{-1} in water with RSD values of 4-8% for various elements (Li, Na, K, Rb, Cs. Be, Mg, Ca, B and Al). In the case of lithium, calibration was linear over four orders of magnitude. The effect of sample flow was found to have no effect upon analytical performance. Species were also detected in organic solvents (methanol, ethanol, acetone).

Two studies have examined the determination of uranium in nitric acid solution for use in the nuclear reprocessing industry. Cremers et al[88] (1987) compared the focus of the laser at the surface and into the bulk of the liquid. The surface measurement was found to be more sensitive because it produced a higher plasma temperature, necessary for uranium excitation (U II 409.0 nm). The detection limit was 0.1 g l^{-1}. Mauchien et al[89] (1993) used a nitrogen laser (337 nm) to measure uranium in nitric acid solution in an on-line application of laser-induced spectrofluorometry. The more sensitive technique used by Mauchien et al enabled lower detection limits to be achieved, between 5 μg l^{-1} and 1 mg l^{-1}.

The analysis of dry aerosols produced by a nebuliser and desolvator was studied by Radziemski et al[98] (1988) for the determination of cadmium, lead

and zinc. The aerosol was presented to the focal point of the laser and detection limits estimated to be of the 0.2 $\mu g\ g^{-1}$. Crouch et al[99] (1988) used an isolated droplet generator as a sample introduction system. The generator produced droplets at a rate of 1,000 to 50,000 s^{-1} with volumes in the nl range. A flow injection manifold (sample volume 70 ml to 1.5 ml) was used to introduce sample solution and laser light from a Nd:YAG laser (1064 nm) was focused into the stream of droplets. Calibration curves linear over three orders of magnitude were obtained with detection limits in the low mg/l (Na, Li, In, Al, Ga, Mg, K and Sr). Winefordner et al[100] (1992) used a concentric glass nebuliser to produce an aerosol that was ablated by an Ar-F excimer laser (193 nm). They obtained detection limits similar to those obtained by Crouch and co-workers.

In a geochemical application of laser-induced plasma emission spectrometry , Mermet et al[101] (1991) investigated the analysis of calcium, magnesium, sodium and potassium in individual fluid inclusions. The analysis of the fluid inside an inclusion can provide information about the history of the parent rock, such as the minerals that the rock was formed from originally. Good analytical data were obtained for synthetic fluid inclusions suggesting that the method should be further explored.

1.5.3 Gas phase

Radziemski and Loree[102] (1981) studied the real-time analysis of gas samples. With the addition of time-resolved detection[103] (1981), the authors reported significant improvements in analytical performance. The limit of detection was improved from 690 to 15 ppm (m/m) and from 120 to 60 ppm (m/m) for phosphorus and chlorine respectively. Radziemski et al[104,105] (1983, 1983) detected beryllium in air, and chlorine and fluorine in air[106] (1983). Detection limits were 0.5 ng g^{-1} (m/m), 8 and 38 ppm (m/m), respectively. Eden et al[107]

(1991) measured the trace concentrations of polyatomic species (B_2H_6, PH_3 and AsH_3) in helium with detection limits of about 1 ppm.

Radziemski et al[92,93] (1989, 1991) monitored in-situ the composition of coal particles in a flowing gas stream. The semi-quantitative analysis enabled four coals to be analysed for silicon, aluminium, iron, titanium, calcium and magnesium. Radziemski et al[108] (1985) measured the variation of temperature and electron density with time for a plasma induced in air with a CO_2 laser. The results implied that there was thermodynamic equilibrium between the oxygen species monitored. Singh et al[94] (1993) successfully used a Nd:YAG laser at 532 nm to measure relative concentrations of calcium, aluminium, barium, manganese, magnesium, iron strontium and titanium in the combustion environment of a coal-fired power station.

1.5.4 Studies to improve analytical performance

Several researchers have made studies into the parameters affecting performance, such as laser energy, distance of sample from laser focal point, presentation of sample (same spot or fresh area for ablation), number of cumulative laser shots, type of gas atmosphere and pressure at point of ablation, sample matrix, etc. Additionally, work has been directed into techniques which might improve aspects of performance, such as precision, a major limitation in semi- and full quantitative laser ablation. Much of this centres on using some form of internal standard to reduce errors and increase repeatability, e.g., ratio the line intensities of analyte and matrix elements, measure the crater volume produced by each ablation and normalise this with the emission data to standards, measure and use the primary plasma intensity as with the crater volume method. Studies have generally used time-resolved measurement to improve analytical performance. Other investigations include

spatial resolution where only a specific part of the plasma is spectrally analysed, the remainder being masked.

Buffer gas type and pressure

Buffer gas type and pressure have been investigated by several groups: Niemax et al,[109,110] Iida et al,[111,42] Kuzuya et al,[112] Piepmeier et al,[113] Marich et al,[37] Sneddon et al.[32,34] Gases studied include air, argon, neon and helium at different pressures for a range of sample types. General conclusions were that reduced pressures of argon gave improved analytical performance, and helium may be better than air at atmospheric pressure. The studies are reviewed below.

Niemax[109] (1989) measured silicon, chromium and iron emission as a function of argon gas pressure and time delay (time between start of laser pulse and start of measurement). A 30-fold increase in line intensity for silicon (288.2 nm) was obtained when the pressure was reduced from 1000 mbar to 140 mbar. When the gas pressure was reduced further, the signal intensity decreased. The main reason for this maximum appeared to be that this pressure is an optimum in the atomisation process, despite the fact that the size and temperature of the plasma change with argon pressure. The argon pressure determined the mean free path of the particles, which penetrate the hot argon plasma, and thus the atomisation, excitation and ionisation processes. The background intensity was also measured and was found to have a similar temporal behaviour but decreased faster, thus the S/B ratio increased with time. The maximum S/B ratios at pressures of 5, 140 mbar were at time delay 4-6, 8-12 μs respectively. In another study, Niemax et al[110] (1992) found that argon was the best buffer gas at reduced pressure (300 mbar), and suggested that for atmospheric pressure, neon should be used.

Piepmeier and Olsten[113] (1971) observed that the emission spectra, crater size, and amount of material vaporised were affected by the gas pressure. At 760 Torr, the crater diameter and amount of material vaporised remained fairly constant when the laser energy was increased, but with reduced pressure, (1 Torr), both parameters increased with laser energy. The results appeared to be caused by absorption of a large fraction of the laser energy by the atmospheric plasma at higher pressure, reducing the amount of laser energy available at the sample surface to ablate material. In an earlier study, Piepmeier[115] (1969) made time and spatially resolved measurements of aluminium in air. These suggested the rapid formation of an atmospheric plasma initially containing little sample material. The resulting intense background spectra lasted only a few tenths of a μs and could be time-resolved from the analyte emission lines that last for many μs. It was also noted that a large fraction of the laser energy was absorbed by the plume, and that the hot plume continued to cause sample vaporisation after the laser pulse had finished.

Iida[111] (1989) studied the emission characteristics of the laser induced plasma in argon at reduced pressures using time- and spatially- resolved emission profiles. In comparison to atmospheric pressure ablation, the emission period was lengthened to over 100 μs and the plasma extended to a few tens of millimetres above the sample surface at reduced pressure. The emission intensities of atomic lines were observed to increase several fold in argon relative to air at the same pressure. It was suggested that the chemical inertness and thermal characteristics of the argon plasma, and the decrease in absorption of the laser pulse by the plasma plume, accounted for these results. In another paper, Iida[42] (1991), made simultaneous, spatial mapping measurements of the laser induced plasma with a novel optical imaging spectrometer. This instrument focused the spectrally-resolved image of the

plasma onto a charge coupled device detector to produce an emission intensity contour map. Measurements were made for the ablation of aluminium metal, (Al (I) 396 nm, background 400 nm), in different gases (air, Ar and He) at a range of pressures (10, 100, 760 Torr). Contour maps were prepared of the aluminium 396 nm signal with the background subtracted, and of the background. It was observed that the most intense aluminium emission in argon and air was at the reduced pressure of 100 Torr. At this pressure the background emission was very small relative to that detected at 760 Torr. The helium atmosphere produced strong aluminium emission with little background at 760 Torr, and both signals decreased with a reduction of pressure. The explanation proposed was that the plasmas developed in argon or air were more absorptive of the laser light than those in He. This is because argon, nitrogen and oxygen are more easily ionised than helium and this produces more electrons at the beginning of plasma formation. This results in more energy absorption from the laser through electron-dependent processes such as electron-neutral and electron-ion inverse Bremsstrahlung. In addition the pressure of the ambient gas relates directly to the plasma density, so that an increase in pressure results in an increase in absorption coefficient. This absorption of laser energy by the plasma induces higher plasma temperatures and greater background continuum emission, and a corresponding decrease in laser energy reaching the sample and so less material is vaporised. Iida concluded that argon at reduced pressure would be the most suitable for emission analysis, and for atmospheric measurements, helium gas could be used, but air at atmospheric pressure was not a good atmosphere.

The effect of argon buffer gas pressure on the copper and aluminium alloys was studied by Kuzuya and Mikami[112] (1992). It was found that self-absorption was reduced with a reduced-pressure argon atmosphere, but increased emission intensity was obtained with higher pressures due to the confining

effects of the plasma. Overall, it was concluded that a reduced argon pressure would be most useful.

Kuzuya et al[116] (1993) found that the emission characteristics of the laser-induced plasma were strongly influenced by the ablation atmosphere and laser energy. Increases in laser energy and gas pressure resulted in high emission intensities for the ablation of a nickel alloy. At atmospheric pressures, however, higher laser energy did not produce higher intensities, and the highest intensities were achieved at reduced pressure of argon with high laser energy. Sneddon et al[32,34] (1992) ablated copper using an ArF laser (193 nm) and concluded that improved signal/background ratio was obtained at reduced pressures with argon, and at atmospheric pressure with helium.

Effect of laser wavelength

Niemax et al[25] (1992) studied the effects of laser wavelength upon ablation. Two wavelengths from a Nd:YAG laser, 266 nm (fourth harmonic) and 1064 nm (fundamental wavelength) were compared, and it was observed that, although the UV radiation ablated more sample mass with the same pulse power, element emission intensities were much lower because the plasma was more constricted. It was concluded that laser ablation with UV laser radiation required an additional atomisation step such as ICP-AES. Lorenzen et al[52] (1992) used a wavelength of 248 nm (excimer KrF) in preference to 1064 nm (Nd:YAG) for the analysis of rubber materials because it did not produce thermal side-effects on the sample surface. Mermet et al[117] (1993) obtained results for UV ablation (nitrogen 337 nm) in air at atmospheric pressure which were only slightly degraded compared to reduced pressure ablation. They suggested that these conditions were suitable for analytical applications. Mermet et al[118] (1994) compared infrared (Nd:YAG, 1064 nm) and ultraviolet (excimer XeCl 308 nm, ArF 193 nm) laser ablation with copper metal, and found that UV ablation

removes more material per laser shot and produced a simple, more reproducible plasma than IR ablation. They concluded that UV ablation was to be preferred with coupled techniques (LA-ICP-MS) as analytical performance (reproducibility, matrix effects, sensitivity) was significantly improved over IR ablation.

Use of internal standard

Niemax[109] (1989) obtained precision of typically 6 % RSD when calibration curves were obtained for silicon and chromium using five or ten measurements of thirty laser shots each, but was improved to 2.4% when an appropriate iron line was used as internal standard. Detection limits were 30 μg/g and 200 μg/g for chromium and silicon respectively. It was noted that there was negligible loss in precision when 10 laser shots were used instead of 30. The standard deviation was partly caused by micro-inhomogeneities in the sample. In a further study of internal standardisation, Niemax et al[114] (1989) observed that the zinc and copper emissions showed different temporal behaviour, the zinc line reached a maximum intensity at 2 μs, copper at 5 μs. Fractional evaporation from the ablated droplets occurred because zinc and copper have very different vapour pressures. Niemax concluded that if the same criteria were adopted as for iron/chromium above, i.e. similar wavelength and excitation energy, taking the ratio of zinc to copper would not improve analytical performance. Niemax et al[99] (1989) calculated the temperature of the plasma as a function of time for a series of binary iron-chromium alloys by measuring simultaneously the relative line intensities of four iron lines (299.04, 300.96, 301.15, 302.65 nm). It was observed that the temperature decreased very rapidly initially (3-6 μs), but was much slower at later times (9-12 μs). It was assumed that at early times, the sample plume was not completely mixed with the argon plasma and as mixing took place the temperature decreased. At later times the mixing was almost complete and so the temperature decreased

slowly. The temperature obtained for the different samples varied considerably, the temperature decreased with increasing chromium content. It was shown by measuring crater volume that, as the chromium content increased more material was ablated, and a lower plasma temperature was recorded. It was concluded that this strong matrix dependence implies that calibration should be made with standards of composition as close as possible to the samples, and, reference lines for ratioing should have a similar temperature behaviour to the analytical line, (i.e. comparable excitation energies).

Effect of magnetic field

The effect of a pulsed magnetic field on the laser-induced plasma was studied by Goldberg and Mason[119,120] (1991) with aluminium metal samples. Two to five-fold enhancements of the emission intensity were obtained with the magnetically compressed plasma, but it was not considered a significant analytical advantage with the low magnetic coupling achieved in the studies.

Other studies

Kuzuka[121] (1987) developed a calculation procedure to correct for self-absorption of spectral lines. It was found that calibration curves for copper in aluminium alloy became unity after correction for self-absorption. Yeung et al[122] (1988) monitored the acoustic signal associated with plume generation as an internal standard. It was shown that the acoustic signal could be used to normalise fluctuations in emission intensity over three orders of magnitude, and it was thought that the technique could be used where experiment conditions vary significantly such as depth profiling. Radziemski et al[123] (1989) modelled the emission spectra formed on a carbon surface to obtain the behaviour of the intensity profiles of the carbon atom (247.8 nm) and carbon ion (251.1 nm) lines and the carbon atom Stark shifts. Kagawa et al[124] (1993) used a tube (dimensions 7 x 7 x 20 mm) in front of the sample to confine the laser-induced

plasma. The CO_2 laser was fired down the tube at the sample and the confinement caused element intensities to increase. The authors concluded that sensitivity may be improved for certain elements and this may be useful for elements such as the halogens.

1.6 Conclusions

From the discussion of laser-material interactions, it can be seen that several complex processes are involved in laser-induced plasmas. This complexity is a major cause of the relatively poor analytical performance (precision and sensitivity) of the spectrometric technique compared to more conventional approaches such as inductively coupled plasma spectrometry. Additional sources of error centre on the relatively small amounts of material sampled by the laser leading to problems if samples are not sufficiently homogenous. Other laser ablation techniques, such as laser ablation inductively coupled plasma emission and mass spectrometry's, also suffer from poor precision for these reasons. The laser-induced plasma emission technique retains many advantages, such as rapid, in situ and simultaneous multi-element capabilities, such that many groups continue to research the method and develop new applications.

Improved performance, i.e. sensitivity and precision, can be achieved for different applications by optimising operating parameters, such as laser energy, sample position relative to the laser focus, and by using methods such as time-resolved measurement, etc. Some studies have utilised different buffer gases of various pressures at the ablation site to improve performance. Many studies have used correction methods, such as internal standardisation, to improve precision, but these need to be applied with care. For example, different rates of volatilisation were reported for copper and zinc from a copper/zinc alloy by Baldwin et al[56] and Niemax et al,[109] resulting in worse performance if one

element was used as internal standard for the other. Although improved performance can be achieved with the use of buffer gases such as argon at partial pressures, industrial applications such as process monitoring have utilised atmospheric pressures because high sensitivity is not necessarily required and it may not be feasible to achieve partial pressures.

Instrumentation for laser-induced plasma emission spectrometry generally consists of a Q-switched Nd:YAG laser and an optical multi-channel analyser fitted with an intensified photodiode array detector. The Q-switched Nd:YAG laser is rugged, relatively compact and low cost compared to other lasers. The fundamental wavelength of 1064 nm from the Nd:YAG is normally used because this wavelength is readily absorbed by almost all materials to produce laser ablation and a laser-induced plasma for analytical measurement. More recently, the use of ultraviolet laser wavelengths has been examined. A fibre optic is generally used to collect and transfer radiation from the laser-induced plasma to the spectrometer because it facilitates easy alignment and capture of radiation and allows remote location of the spectrometer if required. For detection, an optical multi-channel analyser fitted with an intensified photodiode array detector is generally used because it enables simultaneous, multi-element analysis with time-resolved measurement.

Industrial applications such as process monitoring have been developed that have exploited the advantages of laser-induced emission spectrometry. For example, the rapid, remote sensing capabilities have enabled the in situ monitoring of steel and rubber production. The speed of analysis has been utilised in recent environmental analysis applications, such as the detection of heavy metals in soils, to provide a rapid, survey analysis capability. Laser-induced plasma emission spectrometry has been widely applied to the analysis of metals, but few applications to the analysis of polymeric, ceramic, or organic

materials, liquids, or coatings on substrates have been reported. There has also been little development of methods to rapidly process laser-induced emission data towards real-time data analysis. Artificial intelligence techniques have not been applied to the pattern recognition of laser-induced emission spectra. There is considerable potential for research in these areas for the development of new applications, which will further the understanding of the laser-induced emission technique.

1.7 Aims and objectives of this work

The aim of this research is to further the understanding of laser-induced plasma emission spectrometry through the study of new applications. The objectives are to configure an integrated laser-induced plasma emission spectrometer system using the most appropriate instrumentation. This includes a Q-switched Nd:YAG laser with an infrared laser wavelength that is readily absorbed by most materials, fibre optic for collection and transmission of the emitted radiation, and an optical multichannel analyser with an intensified photodiode array detector to provide a time-resolved, simultaneous multi-element analysis capability. The performance of the optical multichannel analyser will be first evaluated with a stable emission source (an inductively coupled plasma emission source), and then with the laser-induced plasma emission source. Studies will investigate basic aspects of laser-induced plasma emission spectrometry to provide information about laser-induced plasma characteristics. Novel applications will be devised to provide insight into the processes of laser-induced emission spectrometry. The areas to be studied are the rapid survey analysis of polymeric materials, and the depth profile measurement of coatings on substrates. The influence of key operating parameters upon emission characteristics and performance will be examined for both types of materials. The polymer studies will exploit the capabilities of the technique towards bulk

analysis of non-conducting materials, and may enable samples to be rapidly identified by their elemental composition. The depth profile investigations will utilise the in situ, micro-analysis capabilities of the technique, and may provide a new method for the rapid measurement of coating thickness. In addition, a new, rapid data processing technique will be devised to exploit the real-time analysis capabilities of laser-induced plasma emission spectrometry. In this study, the rapid pattern recognition capabilities of artificial neural networks, a form of artificial intelligence, will be applied to laser-induced emission spectra.

1.8 References

1. Montaser A. and Golightly D. W., in *Inductively Coupled Plasmas in Analytical Spectrometry,* Montaser A. and Golightly D.W., Editors, VCH Publishers, New York, 1987, pp 1-15.
2. Slickers K., *The Automatic Atomic Emission Spectroscopy*, Brühl Universitätsdruckerei, Giessen, Germany, Second Edition, 1993.
3. Harrison T. S., *Handbook of Analytical Control of Iron and Steel Production*, Ellis Horwood Ltd., Chichester, U.K., 1979.
4. Bengston A. and Danielsson L., Thin Solid Films, 1985, **124**, 231-236. Depth Profiling Of Thin Films Using A Grimm-type Glow Discharge Lamp
5. Brech F. and Cross L., Applied Spectroscopy, 1962, **16**, 59. Optical micro emission stimulated by a ruby laser.
6. Maiman T. H., Physics Review Letters, 1960, **4**, 564.
7. Moenke-Blankenburg L., *Laser Micro Analysis*, Wiley, New York, 1989.
8. Cremers D. A. and Radziemski L. J., "Laser Plasmas for Chemical Analysis", in *Applications of Laser Spectroscopy*, Marcel Dekker, New York, 1986, pp 351-415
9. Tyson J. and Darke S. A., Journal of Analytical Atomic Spectrometry, 1993, **8**, 145-209. Interaction of laser radiation with solid materials and its significance to analytical spectrometry.
10. Routh M., and Tikkanen M. W., in *Inductively Coupled Plasmas in Analytical Spectrometry,* Montaser A. and Golightly D.W., Editors, VCH Publishers, New York, 1987, pp 468-475.
11. Schrenk W. G., *Analytical Atomic Spectroscopy*, Plenum Press, London, 1975.
12. Skoog D. A. and Leary J. L., *Principles of Instrumental Analysis*, Harcourt Brace College Publishers, London, Fourth Edition, 1992.

13. Harrison G. R., *Wavelength Tables with Intensites in Arc, Spark or Discharge Tube*, M.I.T. Press, Cambridge, Mass., USA, 1969

14. Winge R. K., Fassel V. A., Peterson V. J. and Floyd M. A., *Inductively Coupled Plasma-Atomic Emission Spectroscopy, An Atlas Of Spectral Information*, Elsevier, New York, USA, Volume 20.

15. Ready J. F., *Effects of High Power Laser Radiation*, Academic Press, New York, 1971.

16. Kim Y. W., "Fundamentals of Analysis of Solids by Laser-Produced Plasmas", in: *Laser-Induced Plasmas and Applications*, Cremers D. A., Radziemski L. J., Editors, Marcel Dekker, New York, 1989, pp 327-346.

17. Piepmeier E. H., "Laser Ablation for Atomic Spectroscopy", in *Analytical Applications of Lasers*, Piepmeir E.H., Editor, Wiley, New York, 1986, pp 627-669.

18. Hein S., Piepmeier E. H., Trends in Analytical Chemistry, 1988, **7** (4), 137-142. Laser Ablation And The Laser Microprobe.

19. Sneddon J., Hwang Z. W., Teng Y. Y. and Li K. P., Analytical Letters, 1992, **25** (11), 2143-56. Studies of space and time resolved emission measurements of an ArF excimer laser ablated plasma.

20. Scott R. H. and Strashheim A., Spectrochimica Acta, 1970, **25B**, 311-332. Laser Induced Plasmas For Analytical Spectroscopy.

21. Piepmeier E. H. and Osten D. E, Applied Spectroscopy, 1971, **25**, 642-652. Atmospheric Influences On Q-Switched Laser Sampling And Resulting Plumes.

22. Van Deijck W., Balke J. and Maessen M. J., Spectrochimica Acta, 1979, **34B**, 359-369. An Assessment Of The Laser Microprobe Analyzer As A Tool For Quantitative Analysis In Atomic Emission Spectrometry.

23. Jarrell Ash Laser Microprobe, Jarrell Ash literature, Thermo Jarrell Ash Corporation, USA, 1975.

24. Cremers D. A. and Archuleta F. L., Proceedings of the 5th Process Tech. Conf. on Sensors Steel Industry, Detroit, Michigan, April 14-17, 1985, pp157-162. Rapid Analysis Of Steels Using Laser-Based Techniques.
25. Niemax K., Sdorra W. and Brust J., Mikrochim Acta, 1992, **108**, (1-2), 1-10. Basic Investigation For Laser Micro Analysis IV: The Dependence Of Laser Wavelength In Laser Ablation.
26. Kagawa K. and Yokoi S., Spectrochimica Acta, 1982, **B37**, 789-795. Applcation Of The N_2 Laser To Laser Microprobe Spectrochemical Analysis.
27. Kagawa K., Matsuda Y., Yokoi S. and Nakajima S., Journal of Analytical Atomic Spectromertry, 1988, **2**, 415-419. Nitrogen Laser Ablation Analysis Using The Primary Plasma As A Standard For The Quantification Of Vapourised Atoms.
28. Chau F. T., Lau K. S., Wong K. H., Mak C. H. and Wong W. K., Laboratory Microcomputer, 1990, **9**, (3), 88-93. A Software Package For Spectrum Processing Of A Laser-Induced Spectrometer.
29. Hoffman A., Super Conductor Science & Technology, 1990, **3**, (8), 395-403. A Comparative Study Of The ArF Laser-Ablation-Induced Plasma Plume Of Y YO Cu YCuO & YBaCuO By Fluoresence Spectroscopy.
30. Lorenzen C. J., Carlhoff C., Hahn U. and Jogwich M., Journal of Analytical Atomic Spectrometry, 1992, **7**, 1029-1035. Applications Of Laser-Induced Emission Spectral Analysis For Industrial Process And Quality Control.
31. Petit A., ICP Infromation Newsletter, **17**, January 1992, 114. (1992 Winter Conference on Plasma Spectrochemistry) Optical Emission Spectroscopy On Laser Produced Plasma For Analytical Determination In Solid Sample.
32. Sneddon J., Lee Y. I., Kim G. H. and Teng Y. Y., Applied Spectroscopy, 1992, **46**, 11, 1597-1604. Interation Of An Excimer Laser Beam With Metals 3: Effect Of A Controlled Atmosphere In Laser-Ablated Plasma Emission.

33. Sneddon J. and Lee Y. L., Spectroscopy Letters, 1992, **25**, (6), 881-891. Quantitative Elemental Analysis Of Solid Samples By ArF-Excimer Laser - Ablated Atomic Emission-Specrometry.

34. Sneddon J., Hwang Z. W., Teng Y. Y. and Li K. P., Analytical Letters, 1992, **25** (11), 2143-56. Studies Of Space And Time Resolved Emission Measurements Of An ArF Excimer Laser Ablated Plasma.

35. Weimer W. A. and Geyer J. J., Applied Spectroscopy, 1990, **44** (10), 1659-1664. Parametric Effects On Plasma Emission Produced During Excimer Laser Ablation Of $YBa_2Cu_3O_{7-X}$.

36. Beatrice E. S and Glick D., Applied Spectroscopy, 1969, **23**, 260-263. A Direct-Reading Polychromator For Emission Spectroscopy.

37. Marich K. W., Treytl W. J., Hawley W. J., Peppers N. A., Myers R. E. and Glick D., Journal of Physics, 1974, **E7**, 830-834. Improved Q-Switched Ruby Laser Microprobe For Emission Spectroscopic Element Anaysis.

38. Moenke-Blankenburg L., Progress Analytical Spectroscopy, 1986, **9**, 335-427. Laser Micro Analysis.

39. Talmi Y. and Sieper H. P., Analytical Chimica Acta, 1981, **127**, 71-85. Laser-Microprobe Elemental Determinations With An Optical Multichannel Detection System.

40. Radziemski L. J. and Loree T. R., Journal of Plasma Chemistry and Plasma Processing, 1981, **1**, 271-279. Laser Induced Breakdown Spectroscopy: Time-Integrated Applications.

41. Denton M. B., Sweedler J. V. and Jalkian R. D., Applied Spectroscopy, 1989, **43** (6), 953-962. A Linear Charge-Coupled Device Detector System For Spectroscopy.

42. Iida Y., Analytical Science, 1991, **7** (1), 61-64. Laser Induced Plasmas With An Optical Imaging Spectrometer.

43. Peipmeier E. H. and Malmstadt H. V., Analytical Chemistry, 1969, **41**, (6), 700-707. Q-Switch Laser Energy Absorption In The Plume Of An Aluminium Alloy.
44. Marich K. W., Treytl W. J., Glick D. and Orenberg J. B., Applied Spectroscopy, 1971, **25**, 376-379. Photoelectric Time Differentiation In Laser Microprobe Optical Emission Spectroscopy.
45. Allemand C. D., Spectrochimica Acta, 1972, **B27**, 185-204. Spectroscopy Of Single Spike Laser Generated Plasmas.
46. Schroeder W. W., Spectrochimica Acta, 1971, **B26**, 33. A New Electronic Time Resolution System For Direct Reading Spectrometers And Some Applications In The Diagnosis Of Spark And Laser Radiations.
47. EG&G Literature OMA 4, EG&G Instruments, Sorbus House, Wokingham, RG11 2GY, UK, 1993.
48. Campos J., Aguilera J. A. and Aragon C., Applied Spectroscopy, 1992, **46** (9), 1382-1387. Determination Of Carbon Content In Steel Using Laser-Induced Breakdown Spectroscopy.
49. Cremers D. A., Applied Spectroscopy, 1987, **41** (4), 572-579. Analysis Of Metals At A Distance Using Laser-Induced Breakdown Spectroscopy.
50. Grant K. J., Paul G. L. and O'Neill J. A., Applied Specroscopy, 1991, **45** (4), 701-705. Quantitative Elemental Analysis Of Iron Ore By Laser Induced Breakdown Spectroscopy.
51. Kuzuya M. and Mikami O., Journal of Analytical Atomic Spectrometry, 1992, **7** (3) 493-497. Effect Of Argon Pressure On Spectral Emission Of A Plasma Produced By A Laser Microprobe.
52. Lorenzen C. J., Carlhoff C., Hahn U. and Jogwich M., Journal of Analytical Atomic Spectrometry 1992, **7**, 1029-1035. Applications Of Laser-Induced Emission Spectral Analysis For Industrial Process And Quality Control.
53. Runge E. F., Minck R. W. and Bryan F. R., Spectrochimica Acta, 1964, **20**, 733. Spectrochemical Anaylsis Using A Pulsed Laser Source.

54. Runge E. F., Bonfiglio S. and Bryan F. R., Spectrochimica Acta, 1966, **22**, 1678-1680. Spectrochemical Anaylsis Of Molten Metal Using A Pulsed Laser Source.

55. Felske A., Hagenah W. D. and Laqua K., Spectrochimica Acta, 1972, **B27**, 1-21.

56. Baldwin J. M., Applied Spectroscopy, 1970, **24**, 429-435. Q-Switched Laser Sampling Of Copper-Zinc Alloys.

57. Ishizuka T., Analytical Chemistry, 1973, **45**, 538-541. Laser Emission Spectrography Of Rare Earth Elements.

58. Furuta K., Yago H., Ishikawa K. and Komura H., Physical Status Solidi B, 1993, **179** (1), 223-32. Time-Resolved Emission Spectra From Laser-Induced Plasma In Sodium Chloride

59. Marich K. W., Treytl W. J., Carr P. W. and Glick D., Analytical Chemisty, 1970, **42**, 1775. Effect Of Matrix Material On Laser-Induced Element Spectral Emission.

60. Marich K. W., Treytl W. J., Glick D. and Orenberg J. B., Applied Spectroscopy, 1971, 25, 376-379. Photoelectric Time Differentiation In Laser Microprobe Optical Emission Spectroscopy.

61. Treytl W. J., Marich K. W, Orenberg J. B., Carr P. W. and Glick D., Analytical Chemistry, 1971, **43** (11), 1452-1456. Effect Of Atmosphere On Spectral Emission From Plasmas Generated By The Laser Microprobe.

62. Treytl W. J., Marich K. W. and Glick D., Analytical Chemistry, 1972, **44** (11), 1903-1904. Detection Limits In Analysis Of Metals In Biological Materials By Laser Microprobe Optical Emission Spectrometry.

63. Marich K. W., Treytl W. J. and Glick D., Analytical Chemistry, 1975, **47** (8), 1275-1279. Spatial Differentiation Of Optical Emission In Q-Switched Laser-Induced Plasmas And Effects On Spectral Line Analytical Sensitivety

64. Cremers D. A., SPIE 1986, **644**, Remote Sensing 7-12. An Evaluation Of Factors Affecting The Analysis Of Metals Using Laser-Induced Breakdown Spectroscopy.

65. Cremers D. A. and Archuleta F. L., Proceedings of the 5th Process Techniques Conference on Sensors in Steel Industry, Detroit, Michigan, April 14-17, 1985, p157-162. Rapid Analysis Of Steels Using Laser-Based Techniques.

66. Cremers D. A., Applied Spectroscopy, 1987, **41** (4), 572-579. Analysis Of Metals At A Distance Using Laser-Induced Breakdown Spectroscopy.

67. Radziemski L. J., Millard J. A., and Dalling R. H., SPIE 1986, **644**, Remote Sensing, 13-15. Time Resolved Laser-Induced Breakdown Spectrometry For Rapid Alloy Analysis.

68. Radziemski L. J., Millard J. A. and Dalling R. H., Applied Spectroscopy, 1986, **40** (4), 491-494. Time-Resolved Laser-Induced Breakdown Spectrometry For The Rapid Determination Of Beryllium In Beryllium - Copper Alloys.

69. Yoo K. M., Applied Physics Letters, 1989, **54**, (3), 1278-1279. Time Resolved Emission Spectroscopy Of The High TC Superconductor $YBa_2Cu_3O_{7-x}$ Under Laser Ablation.

70. Geyer J. W., Applied Physics Letters, 1989, **54** (5), 469-471. Spectral Characteristics of Plasma Emission During ArF Excimer Laser Ablation of $YBa_2Cu_3O_7$.

71. Deshmukh S., Applied Physics Letters, 1988, **53** (26), 2698-2700. Emission Spectra From ArF Laser Ablation of High Temperature Superconductor $Bi_2CaSr_2Cu2O_9$.

72. Chita G., Conference proceedings, 1991, 29. Quantum Electronics and Plasma Engineering, 471-475. Spectroscopy Of Laser Produced Plasma During Aluminium Welding With CO_2 Laser.

73. Pramanick S. and Narayan J., Materials Research Society Symposium Proceedings, 1992, **250**, 125-9. In-Situ Optical Emission Of Titanium Nitride (TiN) And Titanium Silicide ($TiSi_2$) Plasma During Thin Film Growth By Pulsed Laser Evaporation.
74. Grant K. J., Paul G. L. and O'Neill J. A, Applied Specroscopy, 1991, **45** (4), 701-705. Quantitative Elemental Analysis Of Iron Ore By Laser Induced Breakdown Spectroscopy.
75. Sneddon J. , Hwang Z. W. and Li K. P., Applied Specroscopy, 1991, **45** (3), 435-441. Interation Of A Laser Beam With Metals Part L Quantitative Studies Of Plasma Emission.
76. Sneddon J., Lee Y. I. and Sawan S. P., Applied Specroscopy, 1992, **46** (3), 436-441. Interation Of A Laser Beam With Metals Part II: Space Resolved Studies Of A Laser-Ablated Plasma Emission.
77. Niemax K., Zhao XZ., Shen LJ., Applied Physics B-Photophysics And Laser Chemistry, 1992, **55** (4), 327-330. Spatial Distributions Of Electron Density In Microplasmas Produced By Laser Ablation Of Solids.
78. Esmiller B., Baudinaud V. and Autric M., SPIE, 1992, Gas Flow and Chemical Lasers, 692-695. Characterisation By Space-Time Resolved Emission Spectroscopy Of Laser Produced Plasma On Solid Materials.
79. Majidi V. and Ning X. U., Applied Spectroscopy, 1993, **47** (8), 1134-1139. Wavelength And Time-Resolved Investigation Of Laser-Induced Plasmas As A Continuum Source.
80. Cremers D. A. and Radziemski L. J., Applied Spectroscopy, 1985, **39** (1), 57-63. Direct Detection Of Beryllium On Filters Using The Laser Spark
81. Hardjoutomo W., Munechika H., Kurniawan H., Hattori I., Kobayashi T. and Kagawa K., Optics And Laser Technolology, 1992, **24** (5), 273-277. A Compact TEA Carbon Dioxide Laser For Field Based Spectrochemical Analysis Of Geochemical Samples.

82. O'Shea D. C., Callen W. R. and Rhodes W. T., *Introduction To Lasers And Their Applications*, Addison Publishing Company, London, 1977.

83. Wisbrun R., Schechter I., Niessner R. and Schroder H., Proceedings SPIE Int. Soc. Opt. Eng., 1992, **1716**, 2-15. Laser-Induced Breakdown Spectroscopy For Detection Of Heavy Metals In Environmental Samples

84. Wisbrun R., Schroder H. and Niessner R., Analytical Methods and Instrumentation, 1993, **1** (1), 17-22. Laser-Induced Breakdown Spectrometry For Environmental Analysis Of Trace Amounts Of Heavy Metals In Soils.

85. Cremers D. A., Ferris M. J. and Kane K. Y., Portable Laser Spark Surface Mass Analyser, Los Alamos Information Sheet (LALP 92-63), Los Alamos National Laboratory, Los Alamos, USA, 1992.

86. Jowitt R., British Steel/BISPA Chemist Conference, June 26th, 1985, 19-29. Direct Analysis Of Liquid Steel By Laser.

87. Kim Y. W., Advanced Sensing, Modelling and Control of Material Processing, 1992, 45-47. Compositional Control Via Laser Sensing Of Plasma Generated From Steel Melts.

88. Cremers D. A. and Wachter J. R., Applied Spectroscopy, 1987, **41** (6), 1042-1048. Determination Of Uranium In Solution Using Laser-Induced Breakdown Spectroscopy.

89. Mauchien P., Deniau H. and Moulin C, Radiochimica Acta, 1993, **61**, 23-28. Time-Resolved Laser-Induced Spectroflurometry Of UO_2^{2+} In Nitric Acid Solutions. Preliminary Results For On-Line U Monitoring Applications

90. Adrain R. S., Airey D. R. and Ormerod E. J., IEE Conference Publication (1978 International Conference on Gas Discharges, 5th), 70-73. Spectro-Chemical Analysis Of Steels With Laser Initiated Plasmas.

91. Personnal Communication, Shuttleworth S., Manchester University, Manchester, UK.

92. Radziemski L. J., Appled Spectroscopy, 1989, **43**, (6) 967-976. Real Time Laser Spark Spectroscopy Of Particulates In Combustion Environments.

93. Radziemski L. J., Energy and Fuels, 1991, **5** (2), 304-312. Laser Spark Emission Spectroscopy For In-Situ Monitoring Of Coal.

94. Singh J. P., Zhang H., Fang-Yu Y. and Cook R. L., Proceedings of Intersociety Energy Conversion Engineering Conference, 1993, **1**, 1995-1100. Laser-Induced Breakdown Spectra In A Coal-Fired MHD Facility.

95. Krupp Literature, RELMA: On-Line Quality Control In The Rubber Mixing Room Using Laser Analysis, Technishe Mitteilungen Krupp, 2, 1992.

96. Cremers D. A. and Radziemski L. J., *in Laser-Induced Plasmas and Applications*, Editors Cremers D. A. and Radziemski L. J., Marcel Dekker, New York, USA, 1989, p314.

97. Cremers D. A., Radziemski L. J. and Loree T. R., Applied Spectroscopy, 1984, **38** (5), 721-729. Spectrochemical Analysis Of Liquids Using The Laser Spark.

98. Radziemski L. J., Essien M. and Sneddon J., Journal of Analytical Atomic Spectrometry, 1988, **3**, (7), 985-988. Detection Of Cadmium, Lead And Zinc In Aerosols By Laser-Induced Breakdown Spectrometry.

99. Archontaki H. A. and Crouch S. R., Applied Spectroscopy, 1988, **42**, (5), 741-746. Evaluation Of An Isolated Droplet Sample Introduction System For Laser-Induced Breakdown Spectroscopy.

100. Winefordner J. D., Ng K. C., Ayala N. L. and Simeonsson J. B., Analytica Chimica Acta, 1992, **269**, 123-128. Laser-Induced Plasma Atomic Emission Spectrometry In Liquid Aerosols.

101. Mermet J. M. and Boiron M. C., Geochemica et Cosmochimica Acta, 1991, **55**, (3), 917-923. Analysis Of Mono-Atomic Ions In Individual Fluid Inclusions By Laser-Produced Plasma Emission Spectometry.

102. Radziemski L. J. and Loree T. R., Journal of Plasma Chemistry and Plasma Processing, 1981, 1, 271. Laser Induced Breakdown Spectroscopy: Time-Integrated Applications.

103. Radziemski L. J. and Loree T. R., Journal of Plasma Chemistry and Plasma Processing, 1981, **1**, 281-293. Laser Induced Breakdown Spectroscopy: Time Resolved Spectrochemical Applications.

104. Cremers D. A., Radziemski L. J. and Loree T. R., Spectrochimica Acta, 1983, **38B** (1-2), 349-355. Detection Of Beryllium By Laser-Induced Breakdown Spectroscopy.

105. Cremers D. A and Radziemski L. J., Analytical Chemistry, 1983, **55** (8), 1246-1252. Time-Resolved Laser-Induced Breakdown Spectrometry Of Aerosols.

106. Cremers D. A. and Radziemski L. J., Analytical Chemistry, 1983, **55** (8), 1252-1256. Detection Of Chlorine And Fluorine In Air By Laser-Induced Breakdown Spectrometry.

107. Cheng E. A., Fraser R. D. and Eden J. G., Applied Spectroscopy, 1991, **45** (6), 949-952. Detection Of Trace Concentrations Of Column III And V Hydrides By Laser-Induced Breakdown Spectroscopy.

108. Radziemski L. J., Cremers D. A. and Neimczk T. M., Spectrochimica Acta, 1985, **40B**, 3, 517-525. Measurement Of The Properties Of A CO2 Laser Induced Air-Plasma By Double Floating Probe And Spectroscopic Techniques.

109. Niemax K. , Leis F., Sdorra W. and Ko J. B., Mikrochimica Acta, 1989, **2** (4-6), 185-199. Basic Investigation For Laser Micro Analysis: 1. Optical Emission Spectrometry Of Laser-Produced Sample Plumes.

110. Niemax K., Sdorra W., Quentmeir A., Mikrochimica Acta, 1989, **2**, (4-6), 201-218. Basic Investigation For Laser Micro Analysis Part 2: Laser-Induced Fluorescence In Laser-Produced Sample Plumes.

111. Iida Y., Applied Spectroscopy, 1989, **43** (2), 229-234. Atomic-Emission Characteristics Of Laser-Induced Plasmas In An Argon Atmosphere At Reduced Pressure.

112. Kuzuya M. and Mikami O., Journal of Analytical Atomic Spectrometry, 1992, **7** (3), 493-497. Effect Of Argon Pressure On Spectral Emission Of A Plasma Produced By A Laser Microprobe.

113. Piepmeier E. H. and Osten D. E., Applied Spectroscopy, 1971, **25**, 642. Atmospheric Influences On Q-Switched Laser Sampling And Resulting Plumes.

114. Niemax K., Ko J.B. and Sdorra W., Fresnius' Z. Analytical Chemistry, 1989, **335** (7), 648-651. On The Internal Standardisation In Optical Emission Spectrometry Produced By Laser Ablation Of Solid Samples.

115. Peipmeier E. H. and Malmstadt H. V., Analytical Chemistry, 1969, **41** (6), 700-707. Q-Switch Laser Energy Absorption In The Plume Of An Aluminium Alloy.

116. Kuzuya M., Matsumoto H., Mikami O. and Takechi H., Applied Spectrosopy, 1993, **47** (10), 1659-1664. Effect Of Laser Energy And Atmosphere On The Emission Characteristics Of Laser-Induced Plasmas.

117. Autin M., Briand A., Mauchien P. and Mermet J. M., Spectrochimica Acta, 1993, **48B** (6/7), 851-862. Charcaterization Of A Laser-Produced Plasma From A Copper Target In Air At Atmospheric Pressure.

118. Geersten C., Briand A., Chartier F., Lacour J. L., Mauchien P., Sjostrom S. and Mermet J. M., Journal Of Analytical Atomic Spectroscopy, 1994, **9**, 17-22. Comparison Between Infrared And Ultraviolet Laser Ablation At Atmoshperic Pressure - Implications For Solid Sampling Inductively Coupled Plasma Spectrometry.

119. Goldberg J. M. and Mason K. J., Applied Spectroscopy, 1991, **45** (3), 370-379. Charcaterisation Of A Laser Plasma In A Pulsed Magnetic-Field 1. Spatially-Resolved Emission Studies.

120. Goldberg J. M. Mason K. J., Applied Spectroscopy, 1991, **45** (9), 1444-1455. Charcaterisation Of A Laser Plasma In A Pulsed Magnetic-Field 2. Time Resolved Emission And Absorption Studies.

121. Kuzuya M., Mikami T. and Mikami O., Bunko-Kenkyu, 1987, **36** (5), 333-340. Studies On The Analysis Precision Of Laser Micro-Probe Analyser: II. Improvement Of Analysis Precision By Correcting Self-Absorption.

122. Yeung E. and Chen G., Analytical Chemistry, 1988, **60** (20), 2258-2263. Acoustic Signal As An Internal Standard For Quantitation In Laser Generated Plumes.

123. Radziemski L. J., Journal of Applied Physics, 1989, **65** (8), 2946-2950. Modelling Of Time Dependant Laser Induced Plasma On Carbon Surface.

124. Kagawa K., Ueda T. H., Sasaki M. and Mizukami K., Applied Spectroscopy, 1993, **47** (10), 1562-1566. TEA CO2 Laser-Induced Plasma With A Plane Shock Wave Structure.

2.1 Introduction

This chapter describes the instrumentation and methods used to study laser-induced plasma emission spectrometry (LIPS). An integrated LIPS system was configured in which an optical multi-channel analyser (OMA) was used to monitor light emitted from the laser-induced plasma produced by a Q-switched Nd:YAG laser. The method of integrating the operation of the laser and OMA is described together with details of the system components. In addition, inductively coupled plasma (ICP) instrumentation is described.

2.2 Laser-induced plasma emission spectrometry

Laser

A Spectra Physics Quanta Ray DCR II Nd:YAG laser was used in these studies. It is a pulsed, solid state laser with an output of 1064 nm, a repetition rate of 10 Hz (10 pulses s^{-1}), and can be Q-switched. Key components include a neodymium doped yttrium aluminium garnet (Nd:YAG) excitation medium, a xenon flash lamp, a Q-switch and a resonant cavity, (Figure 1).[1,2,3]

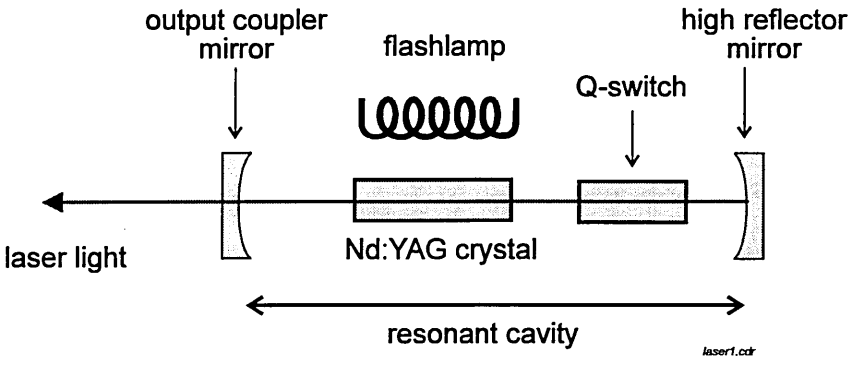

Figure 1 Schematic diagram of the Nd:YAG laser

The principle of laser action (light amplification by stimulated emission of radiation) is depicted in Figure 2 and is as follows.

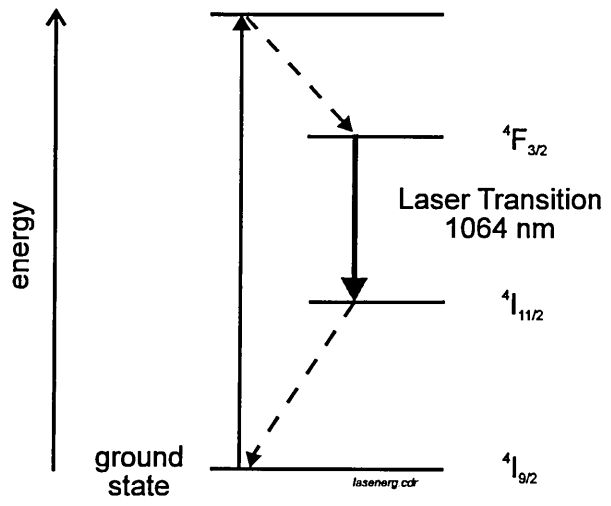

Figure 2 Diagram of the 4-level energy transition scheme for the Nd:YAG laser

The active medium (Nd^{3+} ions in a host aluminium garnet crystal) is optically pumped by the pulsed flash lamp causing electrons to gain energy and move to high energy levels. The excited electrons quickly decay to the upper lasing transition level ($F_{3/2}$), which is metastable, where they can remain for a relatively long period of time (~230 μs). The most probable transition is to the $I_{11/2}$ state, from where electrons quickly decay to the ground state. Thus, a population inversion is easily built up at the $F_{3/2}$ level. This energy is released through stimulated emission to produce laser light at 1064 nm. In stimulated emission, a photon of specific wavelength, i.e. 1064 nm, impinges on an excited electron (at $F_{3/2}$) resulting in 2 photons of the same energy travelling in the same direction and in phase. The first photons are produced by random, spontaneous emission. The mirrors at either end of the optical cavity only reflect light that is travelling along the axis of the cavity, perpendicular to the mirrors, and stimulated emission in other directions passes out of the cavity. Light passes back and forth within this resonant cavity causing further

stimulated emission. It is released by the output coupler as a pulse of laser light lasting ~200 μs, the duration of the flash lamp illumination. The output coupler in this diffraction coupled resonator (DCR) laser is a small, high reflector mounted on a clear substrate on the optical axis of the resonant cavity. Light escapes from the resonator by diffraction around this dot.

Laser energy can be released in two modes, long pulse (normal) and Q-switched. In the long pulse mode, the energy is released as above, to produce a train of laser pulses lasting about 200 μs. In the Q-switched mode, the Q-switch acts as a high speed shutter. It is closed initially to prevent lasing action causing the build up of a large population inversion at the upper lasing transition level ($F_{3/2}$). When the maximum population inversion is achieved, (~220 μs after the start of the flash lamp), the Q-switch is opened and the energy is released as a single giant pulse. The pulse width is less than 10 ns, and the peak optical power is of the order of megawatts. This Q-switched mode is used in LIPS as the high peak power, when focused to a small spot size, will produce a high power density sufficient to induce a plasma at the surface of a sample.

Q-switching means changing the Q (quality factor) of the cavity resonator. When the Q factor is high, the cavity stores the energy well (Q-switch closed, large population inversion builds up), and when the Q factor is low, the cavity emits laser light rapidly (Q-switch open). The Q-switch in this laser is an electro-optic device consisting of a Pockels cell, quarter-wave plate and a polariser, (Figure 3). When a high voltage is applied to the Pockels cell crystal, the polarisation characteristics of the cell are changed which determines whether light is returned to the cavity and the cavity can resonate or not. When the Q-switch is closed, no voltage is applied and so the Pockels cell does not affect the polarisation of light passing through it. Light entering the Q-switch is

vertically polarised by the polariser and then circular polarised by the quarter-plate polariser. When the light returns from the reflector, it is converted to horizontal polarised light by the quarter-plate polariser. This light is reflected out of the cavity by the polariser as it will only transmit vertically polarised light and so lasing does not occur. When the Q-switch is opened, a fast high-voltage pulse is applied to the Pockels cell which cancels the polarisation of the quarter-plate and so the vertically polarised light is transmitted by the polariser and lasing will occur. In the long pulse mode, the Q-switch is open throughout the flash lamp illumination and so laser light is released as a train of pulses lasting the duration of the flash lamp.

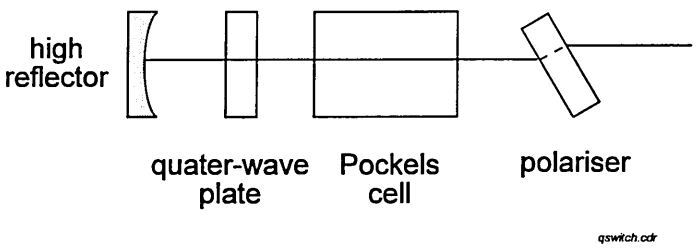

Figure 3 Diagram of the laser Q-switch

Laser radiation has several unique properties. It is monochromatic, unidirectional, intense, and coherent (same phase and polarisation). A laser beam has low divergence so that the beam diameter, 6.4 mm here, is maintained over relatively large distances. These properties enable laser light to be focused to a small spot size with very high irradiance, typically 10^{11} W cm^2 in Q-switched mode, such that a plasma will be induced at the laser focal point. Emission from the laser-induced plasma is monitored in this study with an optical multichannel analyser, described in the next section.

Irradiance is defined as power per unit area, and is calculated from the laser energy per pulse and the area of the laser spot.[4,5] Below are the calculations to obtain values for irradiance produced by two laser energies (laser flash lamp energies 70 and 40 J) with the focus lens that is used in these studies (focal length 500 mm).

a. calculation of laser power

(1) power = energy / unit time (watt = joule second^{-1})

Laser power is ideally measured directly from the laser with a power meter, but it is calculated here from the laser manufacturer's specification because no power meter was available.

- from laser manufacturer's specification:

70 J laser flash lamp energy = 275 mJ laser energy

laser pulse width = 8-9 ns, assume = 10 ns

therefore, laser power = 275 mJ per 10 ns

as power (watt) = J s^{-1}, laser power per s = 27.5 x 10^6 W

b. calculation of the area of the laser spot from the focal spot diameter

for a Gaussian beam, the focal spot diameter (d) is given by:

(2) $$d\ (\mu m) = \frac{4}{\pi} \lambda \frac{F}{D}$$

where: λ = wavelength of laser radiation

F = focal length of focus lens

D = diameter of laser beam

for these studies: λ = 1.064 μm

F = 500 mm

D = 6.4 mm

$\therefore$ focal spot diameter (d) = 105.8 μm

= 1.058×10^{-2} cm

(3) area of laser focal spot (cm^{-2}) = $\frac{\pi \ d^2}{4}$

$\therefore$ area of laser focal spot = 0.8791×10^{-4} cm^{-2}

c. Calculation of irradiance

(4) irradiance = power / unit area (watt cm^{-2})

irradiance for laser flash lamp energy 70 J = power / unit area (watt cm^{-2})

$$= \frac{27.5 \times 10^{6}}{0.8791 \times 10^{-4}}$$

irradiance for laser flash lamp energy 70 J = 3.1×10^{11} W cm^{-2}

irradiance for laser flash lamp energy 40 J = 7.8×10^{10} W cm^{-2}

calculation of irradiance for laser flash lamp energy of 40 J:

the estimated laser energy for this laser flash lamp energy is 70 mJ, from:

- assuming laser flash lamp energy is proportional to laser energy
- lasing threshold is at laser flash lamp energy 30 J = 0 laser energy

and laser flash lamp energy 70 J = 275 mJ laser energy

$\therefore$ laser flash lamp energy 40 J = 7.0 mJ laser energy

laser power = 6.87×10^{6} watt

From (2), it can be seen that the laser spot size is governed by the focal length of the focus lens, the diameter of the laser beam, and the wavelength of the laser. From (4), irradiance is increased by reducing the size of the laser spot. To decrease the size of the laser spot size and thereby increase the irradiance, the laser wavelength or the focal length of the focus lens can be decreased. Calculated values are shown in Table 1 of the laser spot diameter produced by a shorter laser wavelength (266 nm), and a shorter focal length focus lens (100 mm), than the laser wavelength and focus lens used in these studies (1064 nm, 500 mm, respectively).

Laser Wavelength (nm)	Focal Length of Focus Lens (mm)	Calculated Laser Spot Diameter (μm)
1064*	500*	105.8
1064	100	21.16
266	100	5.29

* laser wavelength and focus lens used in these studies

Table 1 Calculated laser spot diameters for different laser wavelengths and focus lenses

The depth of focus (DOF) for a Gaussian beam is given by:

(5) $$\text{DOF} = \left(\frac{8\lambda}{\pi}\right)\left(\frac{F}{D}\right)^2$$

where F = focal length of focus lens (500 mm)

D = diameter of laser beam (6.4 mm)

$\therefore$ DOF for 500 mm focal length lens = 16.5 mm

This indicates that when a focus lens of focal length 500 mm is used, the sample should be placed more than 16.5 mm from the laser focal point for the sample to be ablated with defocused laser radiation.

Optical multichannel analyser

An optical multichannel analyser (OMA) is a versatile spectrometer system that can be configured to measure light for a wide variety of experiments. The OMA used here (EG&G OMA III) was purpose-configured to measure ultra violet (UV) to visible radiation on the sub-μs time scale, suitable for use in laser-induced plasma emission spectrometry (LIPS). It is depicted in Figure 4 and consists of an intensified photodiode array detector mounted onto the exit port of a compact spectrometer, and several electronic units to control the operation of the spectrometer, detector and data acquisition. The components are summarised in Table 2 and are described below.[6]

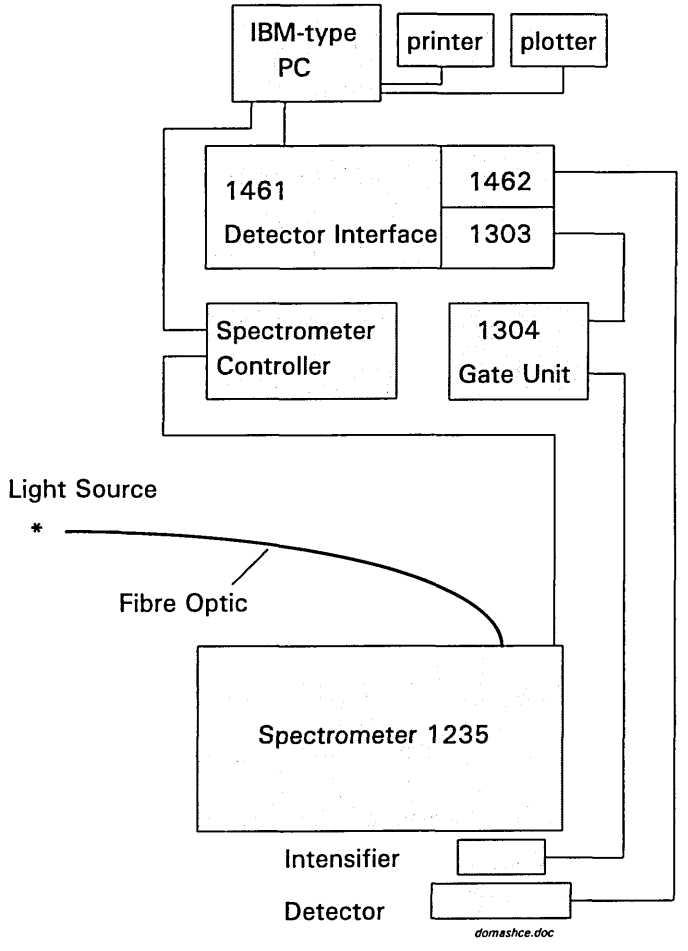

Figure 4 Schematic diagram of the optical multichannel analyser (OMA) system

EG&G Model Number	Description
1455B-700HQ	Detector: gateable, intensified, silicon photodiode array, photosensitive material (multi-alkali on quartz) with blue enhanced response, 1024 pixels, >700 active pixels, pixel dimensions 25 μm x 2.5 mm (width x height)
1235	Spectrometer: Czerny-Tuner mount, focal length 0.275 m, aperture ratio f/3.8, entrance slit 25 μm x 18 mm, 3 grating turret fitted with two gratings
1235 / 86	Grating 1: ruled grating 1200 groove/mm, blaze 250 nm, spectral window ~50 nm, dispersion 0.07 nm/pixel
1235 / 72	Grating 2: holographic grating 2400 groove/mm, blaze 250-500 nm, spectral window ~25 nm, dispersion 0.03 nm/pixel, effective resolution 0.20 nm
1461	Detector interface unit: electronics and microprocessor to control detector; contains electronic cards 1462, 1303
1462	Detector interface card (in 1461)
1303	Gate pulse interface card (in 1461)
1304	Gate pulse amplifier: controls gate width, gate delay
M1235 /52	Fibre optic cable: length 2 m, bundle of 19 x 200 μm UV grade fused silica, acceptance angle 25° SMA input (diameter 1.2 mm)
Viglen Vig SX-20	IBM-compatible personal computer running OMA2000 software
OMA2000	Software package to control detector interface (1461)

Table 2 Components of the optical multi-channel analyser, EG&G OMA III

Spectrometer

Radiation is collected and transmitted from the light source by the fibre optic cable to the spectrometer. The light is dispersed spectrally by the grating and detected by the intensified photodiode array. The spectrometer has a crossed path Czerny Turner optical layout, Figure 5. It is equipped with a choice of two gratings of different dispersions mounted on a turret. The chosen grating is

positioned by a microprocessor-controlled stepper motor with worm-gear drive. This rotates the turret until the desired wavelength region covers the detector. Selection of grating and spectral region are made through the spectrometer control unit or the OMA2000 software.

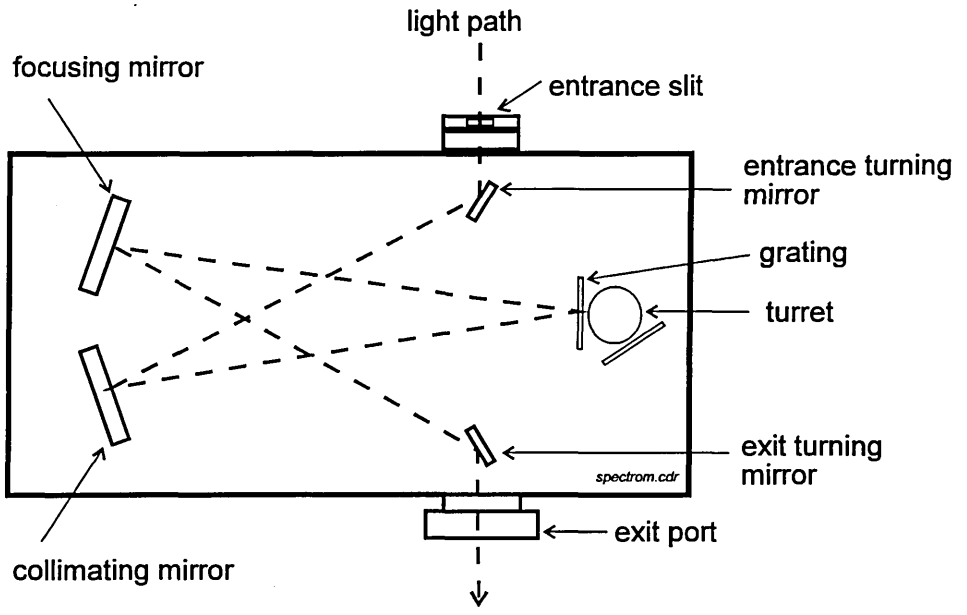

Figure 5 Diagram of the spectrometer of the optical multichannel analyser

Intensified photodiode array detector

This comprises a microchannel plate (MCP) image intensifier coupled via fibre optics to a linear, silicon photodiode array, Figure 6. The photodiode array (EG&G Reticon) consists of 1024 photodiodes mounted on a single integrated circuit. This also contains electronic circuits to read each photodiode. Each photodiode, or detector element (pixel) is a photo-sensitive area of dimensions 25 μm length by 2.5 mm width. Thus the array is 25.6 mm long by 2.5 mm wide. It is mounted on a Peltier-effect cooler to reduce the array temperature to a fixed level of 5 °C in order to reduce the 'dark current', signal resulting from heat rather than light. The intensified detector is purged with dry nitrogen at 5 cubic feet per hour to prevent condensation and damage.

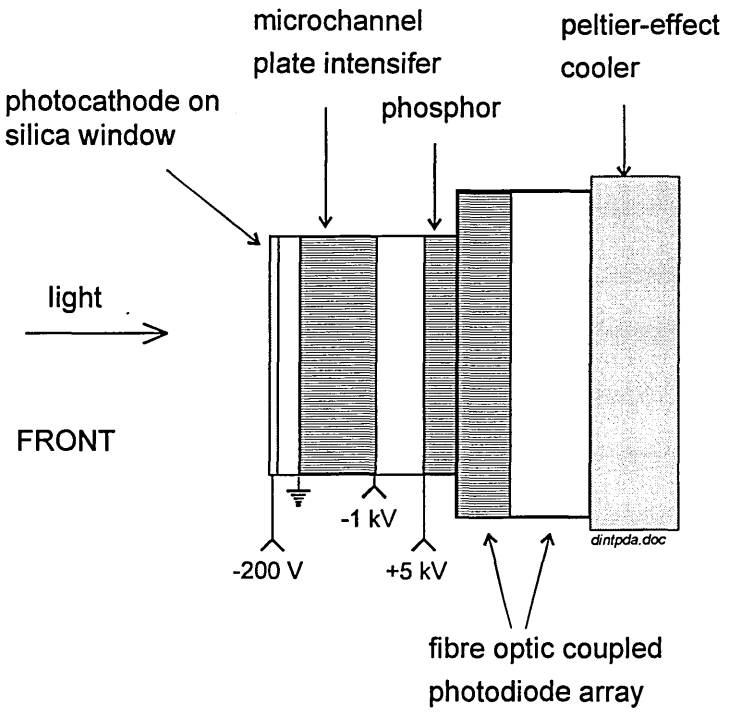

Figure 6 Schematic diagram of the intensified photodiode array detector

At the front of the intensifier is a photocathode (Pk) that emits electrons when struck by photons. These electrons are accelerated by a Pk to MCP voltage and most enter the MCP after crossing the small distance between the Pk and MCP. The MCP consists of a bundle of fine glass tubes which have partially conducting walls. The electrons are accelerated by the potential difference of ~700 V between the ends of the microchannels which causes them to collide with the microchannel walls. The microchannels act as electron multipliers and each collision causes more electrons to be liberated. The electrons leaving the MCP are accelerated towards a phosphor screen by a 5 kV potential difference between the MCP and the phosphor. This causes photons to be emitted from the phosphor which are transferred by fibre optics to the photodiode array for detection.

The intensifier can be rapidly switched on and off, i.e. gated, because the close proximity of the photocathode and the entrance of the MCP requires only a small change in voltage to prevent electrons entering the MCP. It amplifies the signal reaching the detector with a gain of up to 25000. This enables the detector to be used with very short integration times, down to 100 ns with this system. The intensifier is 18 mm in diameter enabling more than 700 pixels to be active, (~730).

The photodiodes are reverse-biased so that they are, in effect, charged capacitors. When light strikes a photodiode, electrons are freed that discharge the capacitance. The charge is dissipated at a rate proportional to the intensity of the light flux. This process takes place until the pixel is read by the measuring circuits which connect each photodiode in turn to the detector's amplifier. This signal is measured for each pixel and these data comprise a spectrum. As each pixel is read in turn and the time per pixel is 28 μs, the cycle time for each scan of the array is 30 ms which includes overhead time for any processor decisions or triggers to be made. Thus the integration time is 30 ms. As described above, the intensifier can be rapidly switched on and off to enable gating of the light signal. This enables the detector to be used in two ways. (1) In the free running mode, the intensifier is always on and the array is read every 30 ms with a fixed integration time of 30 ms. This is suitable for the OMA to be used with a light source such as an ICP or a discharge lamp. (2) In the gated mode the intensifier acts as a high speed shutter, being turned on and off very rapidly, to enable measurement at a precise time for a variable integration period. Here the timing sequence is: intensifier off and array is read to clear each pixel; after required delay, intensifier switched on for pre-set time to integrate light signal; at the end of the integration time, the intensifier is switched off; the array is read and the process can then be repeated. The time delay and the integration time can be varied separately, from a minimum of

100 ns to several seconds. This gating and the increase in gain provided by the intensifier are exploited in LIPS to undertake time-resolved measurements.

A disadvantage of a photodiode array fitted with an image intensifier is that the spectral resolution of the spectrometer is degraded by the intensifier. This is because the fibres of the fibre optic, which couple the output of the intensifier to the photodiode array, are a different size to the individual photodiode pixels. The widths are 10 and 25 μm, respectively. Each fibre does not exactly illuminate a single pixel, which means that a dispersed spectral line is spread to a larger area of the array than if an intensifier was not fitted. The effective resolutions at full width half maximum (FWHM) are 2 and 3 pixels for non-intensified and intensified detectors, respectively, as quoted by the manufacturer when a 25 μm wide line is focused onto the detector.[6]

Detector interface

The detector interface (EG&G 1461) contains electronics, a microprocessor and electronic cards (EG&G 1462 and 1303) to control detector operation and data acquisition. The 1462 detector interface card controls the scanning of the array detector and the acquisition of data. The 1303 with the 1304 gate pulse amplifier control the operation of the intensifier. Operation of the 1461 unit is directed by the OMA2000 program running on an IBM-type personal computer (PC). Data acquisition is described in the next section.

Laser - optical multi-channel analyser system

Overview

A schematic diagram of the integrated laser and OMA system is shown in Figure 7, and details are given in Table 3. Laser light is delivered to the sample by a mirror. A lens is used to focus the light from a beam diameter of 6.4 mm down to about 100 μm on the sample surface positioned at the laser focal point.

A laser-induced plasma is formed at the surface of the sample and radiation is captured and transmitted to the OMA by the fibre optic cable for time resolved detection. Sample can be manipulated in three dimensions relative to the laser spot using the XYZ stage. The fibre optic is positioned independently using a second XYZ stage, 12 mm from the laser point and 1 mm above the sample surface, as shown in Figure 7. Below are descriptions of the laser table / sample ablation cabinet and the synchronisation of the operation of the laser and OMA.

Reflecting mirror	45° high purity silica, 25.4 mm diameter (Newport 10 QM 20 HM-15)
Focus lens	500 mm focal length bi-convex, high purity fused silica 25.4 mm diameter (Newport SBX 040 AR.18)
Ablation gas	air at atmospheric pressure
Fibre optic observation position	
From laser point	12 mm
Above sample surface	1 mm

Table 3 Details of optics and parameters used for laser- induced plasma emission spectrometry

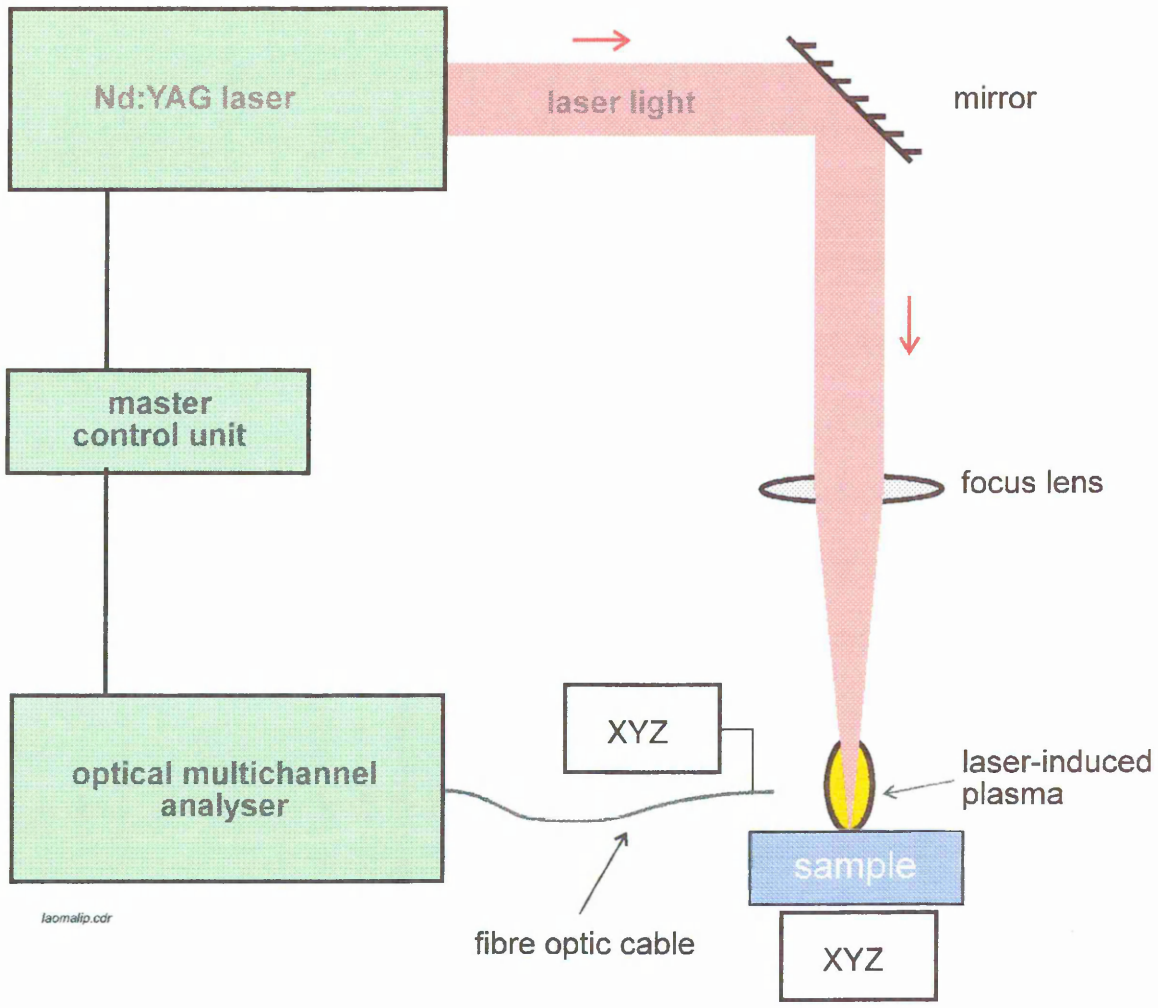

Figure 7 Schematic of the laser - optical multi-channel analyser system used for laser- induced plasma emission spectrometry

Laser table and sample ablation cabinet

A steel table of welded construction was specially modified to house the laser and sample ablation chamber, (Figure 8). The large sample chamber was 0.54 x 0.82 x 1.0 m (width x depth x height). It was purpose-designed and built to be light-tight and accommodate a variety of laser optics and sample sizes. A steel box with an internal baffle was provided on the side of the cabinet to facilitate easy input of the fibre optic cable, gas pipes and wires for electric illumination. The inside of the steel cabinet was painted matte black to minimise any reflections of laser light and was illuminated by an electric lamp. Extraction was provided so that any fumes produced from sample ablation were removed to outside of the building. The large, hinged door enabled easy access to the inside of the cabinet and all four sides of the door wrapped around the cabinet opening to provide a light-tight seal. The laser table had legs with adjustable feet so that the table could be levelled. The laser head was bolted onto a high steel shelf so that laser light entered near the top of the chamber enabling a long focal length lens to be used. The power supply was located on the floor underneath the laser table. Laser light entered the chamber through a steel tunnel. With the chamber door closed, the design and construction of the chamber prevented the escape of laser radiation permitting Class 1 laser operation. Laser safety is described in section 2.4.

A versatile mounting system for the optical components was built inside the sample chamber. This consisted of a vertical, stainless steel mounting bar (0.96 m high x 38 mm diameter) bolted to the base of the chamber. The laser optics, mirror and focus lens, and a mounting for the fibre optic cable were

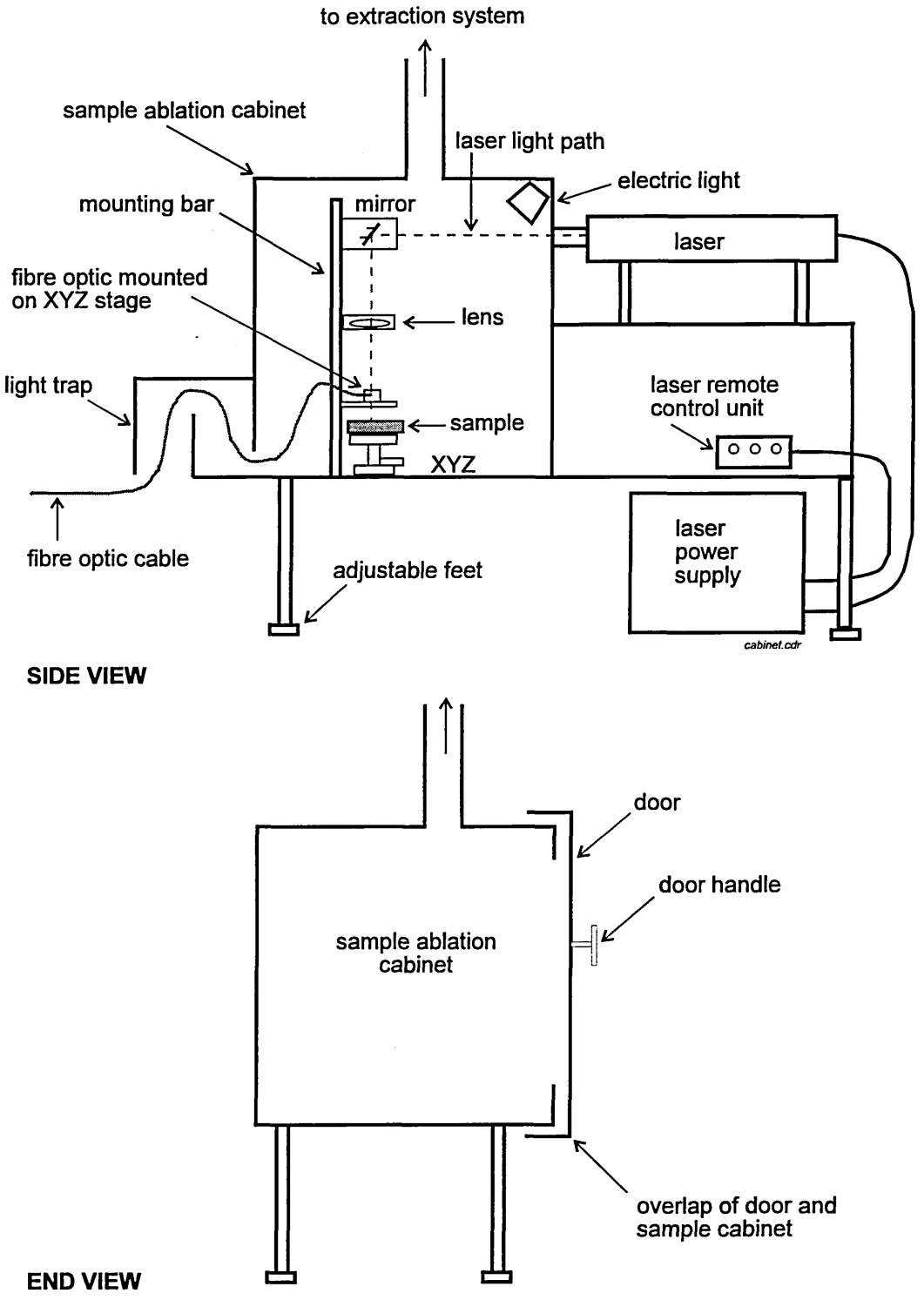

Figure 8 Diagram of the laser table and sample ablation cabinet. The end view shows the overlap of door and cabinet to provide a light seal

independently attached to this. Each item could be moved up or down, or rotated about the bar and clamped in any desired position. The laser mirror and focus lens were mounted separately on modified steering units (LBS-1, Photon Control, Cambridge) attached to clamps. The fibre optic mounting consisted of a holder for the fibre end attached via a bracket to a micro-adjustable XYZ stage which had 10 mm travel in each direction. This was attached to the mounting bar via a plate and clamp. The threaded end cap (SMA fitting) of the fibre screwed onto the hollow holder which was clamped against the XYZ bracket by the nut to provide a secure mounting for the fibre optic, (Figure 9). A quartz window, attached with blutak onto a plastic sleeve, protected the end of the fibre from any ablation product. All engineering work was undertaken by the Engineering Workshops, School of Engineering, Sheffield Hallam University.

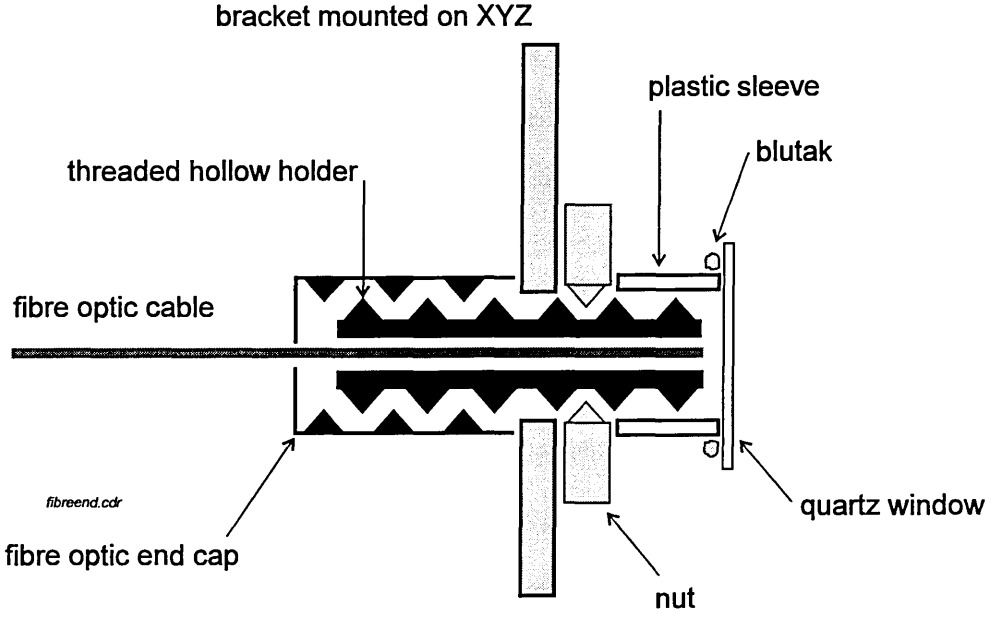

Figure 9 Schematic diagram of the fibre optic holder arrangement

Synchronisation of the laser and OMA operation

The operation of both laser and OMA systems was studied so that the firing of the laser would be synchronised with the scanning of the photodiode array. It is necessary to co-ordinate several events in order to have a working system. The photodiode array needs to be scanned at the same frequency as, and in phase with, the flashing of the laser flash lamp. The two frequencies are normally 33 and 10 Hz, respectively. In addition, the laser Q-switch needs to be opened a set time after the start of the laser flash lamp illumination in order to fire the laser, and has to be synchronised with the gating of the detector.

Following experiments and discussions with the respective manufacturers of the laser and OMA, a master control unit was designed and was specially built by EG&G, (EG&G 1310). This consists of a master pulse generator with electronic trigger outputs to the photodiode array and laser flash lamp, and a variable control for operation of the laser Q-switch. The master pulse generator replaced the timing units of the laser and OMA, and the OMA detector interface (1461) was modified to enable timing to be controlled by this external source.

The OMA and Nd:YAG laser were configured with the master control unit to produce an integrated laser-induced plasma emission spectrometry system. Operation of the laser and the OMA is synchronised electronically at 10 Hz using the master control unit. This frequency of operation was selected because it is an optimum repetition rate for operation of the Spectra Physics laser. The unit controls the timings of the laser flash lamp and Q-switched laser firing, and the detector gating and scanning of the detector array. The number of detector scans / laser shots is controlled by the OMA-2000 program.

The timing sequence for a typical experiment is depicted in Figure 10 and is as follows. At the start of the experiment, a trigger pulse from the master control unit causes the photodiode array to be scanned in order to clear each pixel. A trigger from the OMA to the master control unit tells it to fire the laser, i.e. open the Q-switch, during the next flash of the flash lamp. A trigger pulse to the laser, 50 ms later, starts the flash lamp illumination. After the Q-switch delay, a trigger pulse to the laser opens the Q-switch to cause the laser to fire. At the same time, a trigger pulse to the OMA starts the delay / integration sequence. The delay and integration times are pre-set in the OMA-2000 program. The next pulse, 50 ms later, causes the photodiode array to be scanned, i.e. read. This 50 ms cycle time enabled the photodiode array to be read between separate firings of the laser and allowed each individual laser-induced plasma to be monitored. The sequence of laser firing / detector integration / detector read is 100 ms and is repeated at 10 Hz. The number of repeats is set within the OMA-2000 program.

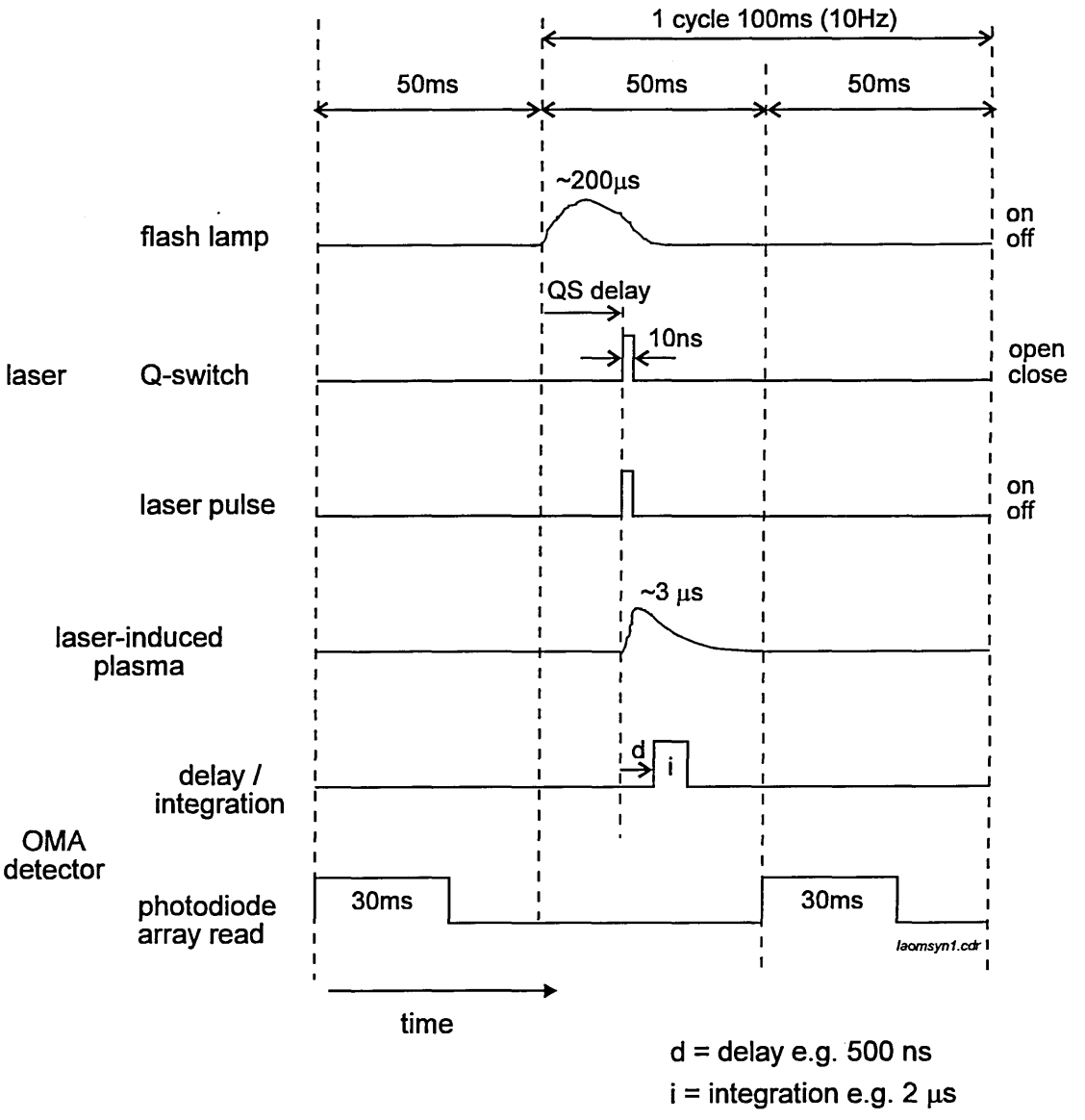

Figure 10 Schematic of the laser - optical multichannel analyser timing sequence

Data acquisition

Data acquisition was controlled by proprietary software (EG&G OMA2000) running on an IBM-compatible personal computer. The detector interface (EG&G 1461) allows versatile data acquisition and storage through the use of memories. An individual scan of the array, i.e. a spectrum, can be stored separately in a memory, or multiple spectra can be accumulated into several memories. For example, 1 spectrum in 20 memories gives a total of 20 spectra; 5 spectra in each of 40 memories provides 200 spectra in total. These values can be tailored to a specific experiment. A maximum of 250 memories can be used. Other parameters such as sending and receiving trigger pulses, subtraction of blank spectra, are set by writing a simple OMA Data Acquisition Design (DAD) routine.

In addition, there are different modes of data acquisition. In the Live mode, spectra are displayed after every scan of the array with no automatic saving of data. In the Accumulation mode, a pre-set number of scans are made which are stored in the 1461 unit until the end of the experiment when data are transmitted to the PC.

The OMA was used with the time-gating capability in two ways to address the problem of complex, time-dependent emission from the laser-induced plasma. (1) The OMA was used in an incremental program mode which allowed the spectra to be time-resolved to produce an emission-wavelength-time profile of emission from the plasma. Study of the transient signal responses within these profiles enabled suitable values for delay and integration times to be chosen. (2) A fixed time mode (FT) was used with these timing values such that the start of the integration time was delayed by a set time, the delay time, to enable rejection of the initial intense background signal, and the integration period captured the analyte emission signal response.

In the OMA incremental mode, each scan of the array was stored in a separate memory, and the integration window (100 ns) was stepped sequentially through the lifetime of the plasma by the increment time (100 ns). Each scan was taken from a separate laser-induced plasma. This yielded an emission-wavelength-time profile for ablation of a sample.

For the OMA fixed time programs (FT), fixed delay and integration times were set, e.g. delay time 500 ns, integration time 1 μs. Scans were either stored in individual memories or accumulated into a single memory. Both of the OMA programs were used with a blank spectrum subtraction method. The laser flash lamp and the OMA detector were both operated at 10 Hz. The laser was fired during alternate flashes of the flash lamp only, i.e. 5 Hz, and the OMA recorded a blank spectrum during the flash lamp cycles when the laser did not fire. Each blank spectrum was automatically subtracted from the previous emission spectrum to yield a net signal from the plasma. In this way, the run time for 5 laser shots was 1 s.

After a LIPS experiment, spectra could be viewed on screen using the OMA2000 software, printed either as overlays or in a variable 3D view, and stored on disk for later use. The data produced by both OMA programs was manipulated as needed using separate computer routines. Individual pixels from the 3D plots were selected and plotted against memory number (time), to give an emission - memory number (time) response. These were then extracted into a spreadsheet program (Microsoft Excel) to facilitate graph plotting and statistical calculations to be made, such as signal/noise signal/background ratios, precision, etc.

Procedure

Samples were generally analysed as received with no sample preparation. The sample was mounted on the XYZ manipulator and a fresh area of material positioned at the laser spot. The manipulator was moved in height (Z) until the sample was at the laser focal point, 500 mm from the focusing lens. The sample chamber door was closed. The spectrometer was set-up with the chosen grating, i.e. grating 2, to monitor the required spectral region, e.g. 307-332 nm. The number of detector scans / laser shots and OMA memories was selected, e.g. 2 scans / laser shots in each of 10 OMA memories resulting in 20 scans / laser shots in total. A blank subtraction program was used so that the experiment run time for 20 laser shots was 4 s with the laser firing at 5 Hz. The laser flash lamp energy was set on the laser remote control unit to a suitable value, e.g. 40 J, and the acquisition was started. The laser fired under control of the OMA software and the master control unit, and the resulting spectra were stored on the computer for later manipulation and printing as required.

2.3 Inductively coupled plasma emission spectrometry

Introduction

Inductively coupled plasma - atomic emission spectrometry (ICP-AES) is a versatile chemical analysis technique, able to determine elements over a wide range of concentrations, from trace through minor to major levels, and is well established in laboratories world-wide.[7] An ICP instrument consists of a sample introduction system, an inductively coupled plasma emission source and a spectrometer to analyse the light emitted by the plasma. Sample is introduced as a liquid and a nebulizer is used to produce an aerosol that is swept into the plasma by a flow of argon carrier gas. The ICP source (Figure 11) comprises a torch of concentric quartz tubes and a water-cooled copper induction coil which surrounds the top of the torch.

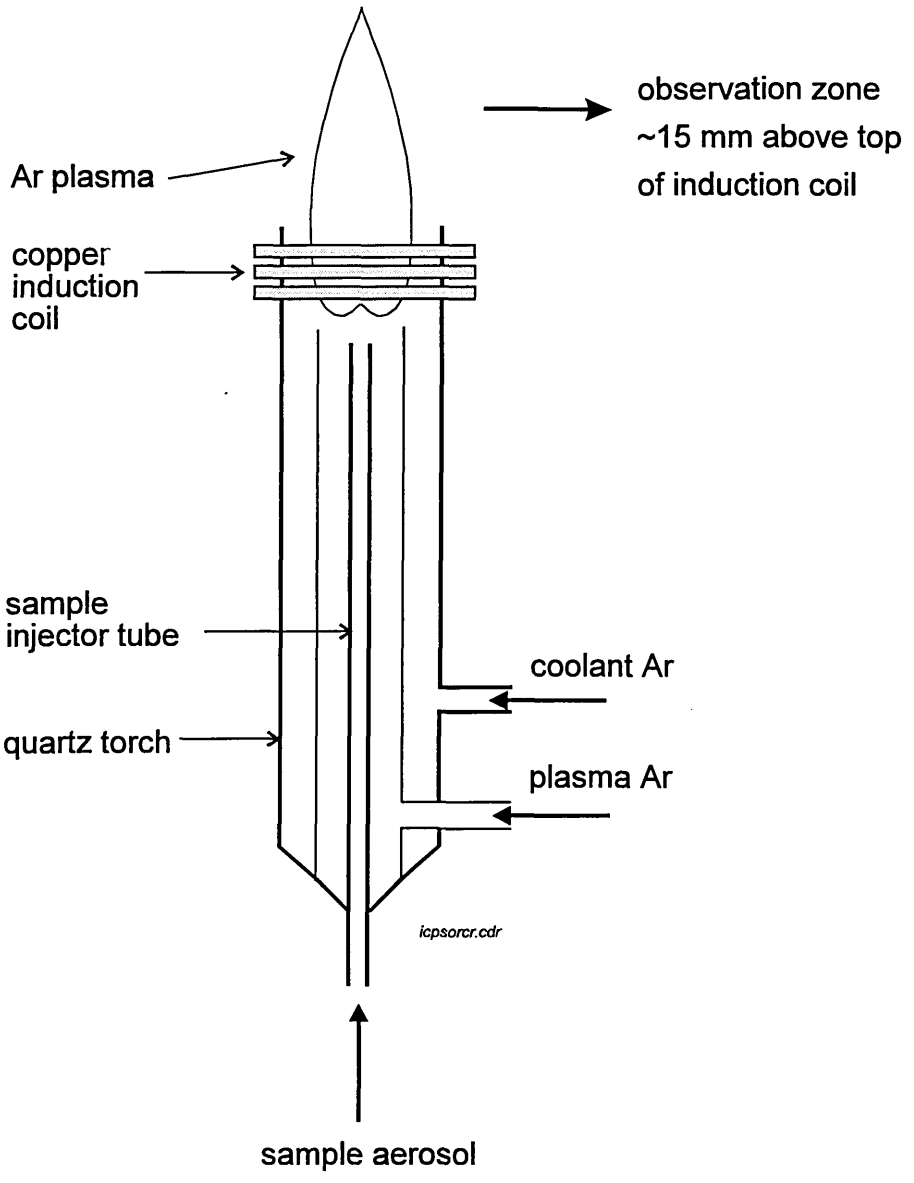

Figure 11 Diagram of the ICP source

The high temperature argon plasma (6 - 10,000 K) is sustained by inductively-coupled radio-frequency energy from the induction coil. The coolant and plasma argon gas flows are introduced tangentially and the plasma is initiated by a tesla coil which provides a seed of electrons. Sample aerosol is introduced through the sample injection tube and the analyte is confined to a central axial channel within the ICP discharge. Drying, atomisation and/or ionisation, and excitation of the analyte takes place. Light is emitted that is characteristic in wavelength of the analyte elements. In a conventional ICP spectrometer, the

emitted light is dispersed by a diffraction grating and wavelengths of interest are detected by photo multiplier tubes (PMT). The technique benefits from several advantages, such as, simultaneous multi-element analysis capability, wide dynamic range, and relative freedom from inter-element interference effects.

In this study, light from the ICP is collected and transmitted by fibre optic to an optical multichannel analyser (OMA) that utilises an intensified photodiode array for detection. This enables simultaneous spectral monitoring over a window approximately 25 nm wide, and offers the possibility of simultaneous multi-element analysis. Different wavelength regions can be selected by scanning the grating of the spectrograph to the region of interest. A feature of the OMA is the ability to store a spectrum electronically in memory. This can be used to simultaneously remove the background signal of a previously recorded blank, from the spectrum of a sample as it is measured.

Instrumentation

Details of the instruments and operating parameters used are given in Table 4. The sample introduction system for normal ICP - AES is depicted Figure 12a in which sample is continuously pumped to the nebulizer to achieve a steady state emission signal. The sample introduction manifold for flow injection (Figure 12b) incorporates an injection valve to inject sample into the carrier stream, distilled water. This transports the sample to the ICP where transient signal responses are obtained.

ICP Instrument	Thermo Jarrell Ash ICAP 9000
Forward Power	1.1 kW
Gas Flows Plasma	0 litre minute
Coolant	15 litre minute
Nebulizer	0.4 litre minute
Carrier / Sample Flow Rate	2 ml $minute^{-1}$
Observation Position	15 mm above load coil
	15 mm from load coil
Detection System	EG&G OMA III
Spectrometer	
grating (holographic)	2400 g/mm, blaze 250-550 nm
dispersion	0.027 nm/pixel
view band	25 nm
Detector	
Intensifier (0-1000 units)	500
Mode	Free-running
Exposure Time	30 ms

Table 4 Details of instrumentation for ICP-AES studies

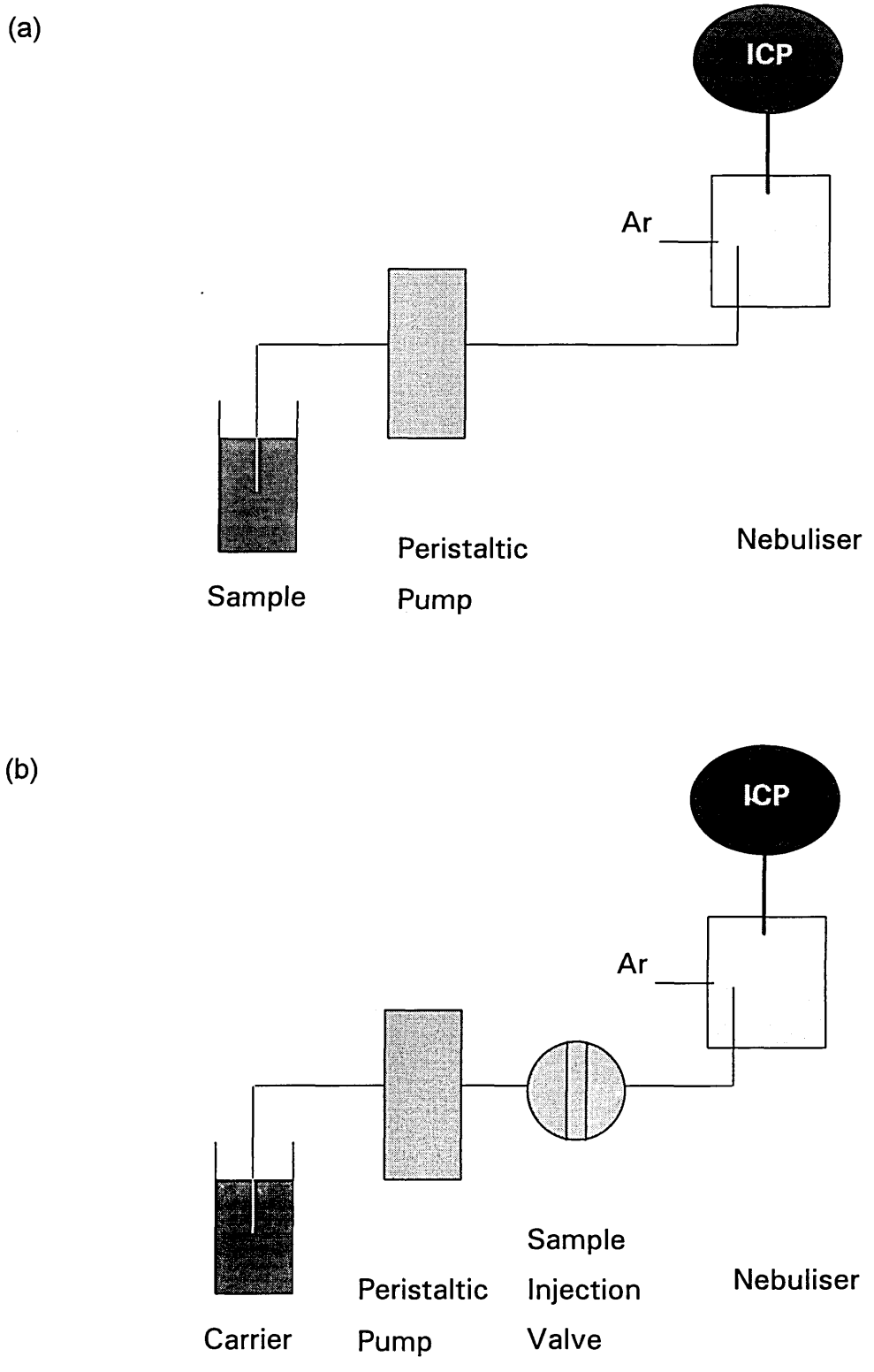

Figure 12 Schematic diagram of sample introduction system into ICP-AES with, (a) conventional, direct nebulization, (b) flow injection

Procedure

Normal - direct nebulisation

The fibre optic was positioned as described in Table 4 and the plasma lit and allowed to stabilise for 30 minutes. The centre wavelength of the OMA was set. Sample solution was introduced into the ICP and measurements made after the solution had been in the plasma for 30 seconds. The recorded spectra were stored on the computer and printed. Emission-time plots were obtained for chosen pixels (wavelengths), and these data points were transferred to another program for numerical calculations such as signal/background and precision.

Flow injection

The instrumentation and procedure is the same as above but a flow injection valve was used to introduce sample into the ICP (Figure 12). Sample was loaded into the loop (250 μl) of the valve, and injected into the ICP by bringing the loop on-line. OMA measurement was started when the sample reached the nebuliser.

Reagents

Solutions were prepared fresh from commercial stock solutions (BDH Spectrosol Solutions, Merck Ltd., Lutterworth, Leicestershire, UK).

2.4 Additional instrumentation

To examine the craters produced in samples by laser ablation, two techniques were used, scanning electron microscopy (SEM) and Talysurf surface analysis. The SEM used was a Phillips XL40. The sample was irradiated by a beam of electrons in a vacuum, and the collected backscattered electrons, or secondary electrons, were used to produce a magnified image of the sample surface. Photographs were recorded of the sample surface at different magnifications.

The Talysurf instrument was a Rank Taylor Hobson Form Talysurf 120L. A diamond-tipped stylus traversed the sample surface and the vertical movements of the stylus were magnified by a laser interferometric transducer mechanism to reveal surface texture information. The radius of the stylus tip was 2 μm and the vertical resolution was 0.020 μm. A typical profile was recorded using 164 scans in a 1.63 mm square to produce a magnified, three dimensional view of surface features. The data were stored and manipulated on an IBM-compatible personal computer using proprietary software. The software enabled the three dimensional profile to be viewed from different angles and individual scans, such as the profile through the centre of a laser crater, to be viewed separately. The profiles were recorded photographically direct from the computer screen.

2.5 Laser Safety

Warning

A Class IV high power laser has been used in this work. This classification means that the output power is above 500 mW and it is a **safety and fire hazard**. It is a pulsed Nd:YAG laser with an output wavelength of 1064 nm and this infrared wavelength is **invisible to the human eye** and is therefore **extremely hazardous**. Infrared radiation passes easily through the cornea of the eye which focuses the laser light on the retina, where it can cause instantaneous permanent damage. Diffuse and specular reflections can cause severe eye and skin damage. The laser light must not be viewed directly and precautions should be taken to prevent accidental exposure to both direct and reflected beams. In addition, the laser head and power supply both contain lethal high voltage components which are accessed if the respective covers are removed.

Precautions

The laser is used in a laser-designated area where only authorised personnel are allowed and a strict code of practice is followed. Access to the laser room and laser is by key which are only issued to authorised laser users. A warning sign is illuminated outside the room during laser operation. The room is blacked out to prevent the escape of laser light, and bright illumination is provided to reduce the pupil size of the eye. For all experimental work, the laser is used with the sample chamber door closed and laser light is confined to the steel sample cabinet. For alignment work, the laser is used in the long pulse mode only, with the laser energy as low as possible, i.e. at the laser threshold. Eye protection must be worn (laser goggles for 1064 nm radiation) and watches, jewellery, etc. that may reflect the laser light must be removed. Laser light is located with an infrared laser card. For further information about laser safety precautions and the hazards of laser radiation, a manual such as that of Sliney and Wolbarsht [8] should be consulted.

2.6 References

1. Quanta-Ray DCR-II Instruction Manual, Spectra Physics, Hemel Hempstead, Hertfordshire, UK, 1987.
2. Andrews D. L., *Lasers in Chemistry*, Second Edition, Springer-Verlag, London, 1990.
3. O'Shea D. C., Callen W. R. and Rhodes W. T., *Introduction to Lasers and Their Applications*, Addison-Wesley Publishing Company, London, 1977.
4. Hecht E., *Optics*, Addison-Wesley Publishing Company, Wokingham, Berkshire, UK, Second Edition, 1987.
5. Optics Tutorial, Newport Catalogue, Newport Ltd., Harpenden, Hertfordshire, UK., 1990.
6. EG&G OMA III Instruction Manuals, EG&G Instruments, Wokingham, Berkshire, UK, 1990.
7. Montaser A., Golightly D. W., *Inductively Coupled Plasmas in Analytical Atomic Spectrometry*, VCH Publishers, New York, USA, 1987.
8. Sliney D. and Wolbarsht M., *Safety with Lasers and Other Optical Sources, A Comprehensive Handbook*, Plenum Press, London, 1985.

Chapter 3

Studies Of Laser-Induced Plasma Emission Spectrometry With An Optical Multichannel Analyser

3.1 Introduction

The aim of this work was to evaluate the performance of the optical multichannel analyser and to investigate laser-induced plasma emission spectrometry. The operation of the optical multichannel analyser (OMA) was first tested and evaluated with an inductively coupled plasma (ICP) emission source because the laser-induced plasma is transient and emission spectra are complex. An ICP emission source was chosen because it is a well characterised, stable emission source and is relatively easy to monitor. In addition, emission spectra for different elements can be easily obtained over a range of element concentrations. The basic analytical performance of the optical multichannel analyser (OMA) was examined, and parameters studied include spectral resolution, wavelength accuracy (ability to position the grating to a set wavelength), and analytical performance (effect of integration time, precision, sensitivity, limit of detection and dynamic range). In addition, special advantages of the OMA spectrometer were demonstrated compared to a conventional atomic emission spectrometer as used in ICP instrumentation, such as concurrent background subtraction, and simultaneous spectrum measurement during a transient event.

Following the ICP work, the optical multichannel analyser (OMA) was used with a Q-switched Nd:YAG laser in laser-induced plasma emission spectrometry. Here, the optical multichannel analyser was used to monitor the laser-induced plasma produced by focused radiation from a Nd:YAG laser. The purpose was to evaluate the performance of the integrated laser and OMA instrument system and to study laser-induced plasma emission spectrometry in order to obtain basic analytical performance data. The influence of operating parameters such as laser energy upon laser-induced plasma emission characteristics was examined for the ablation of copper metal. The lifetime of the plasma was

established for different laser energies. Performance data were obtained for the determination of copper in aluminium alloys.

3.2 Experimental

For the inductively coupled plasma (ICP) emission studies, the optical multichannel analyser (OMA) was used with the ICP emission source of a Thermo Jarrell Ash instrument, as described in Chapter 2 (section 2.3). The photodiode detector of the OMA was operated in the free-running mode with an integration time of 30 ms. A variable number of photodiode array scans were accumulated into an OMA memory, the number depending on the experiment. Solutions were prepared fresh from commercial stock solutions (BDH Spectrosol Solutions, Merck Ltd., Lutterworth, UK).

For laser-induced plasma emission spectrometry studies, the OMA was used in an integrated laser-induced plasma emission spectrometer system. The system consisted of a Q-switched Nd:YAG laser, an OMA and a master control unit, and is described with details of operation in Chapter 2 (section 2.2). The blank-spectrum subtraction method was utilised with the laser fired at 5 Hz. Different modes of OMA operation were used. The incremental mode was used with various time settings to study the transient signal responses from the laser-induced plasma. Time settings were: delay time of 0 ns, integration time of 100 ns (or 1 μs), and increment time of 100 ns (or 1 μs). Fixed time (FT) programs were also used, FTa, FTb, and FTc, with delay times of 700 ns and integration times of 1 μs. Method FTa consisted of firing 30 laser shots at the same spot, each shot being stored individually, i.e. 1 laser shot in each of 30 OMA memories (30 laser shots total). Method FTb accumulated 10 laser shots into each of 30 memories, all at the same sample site (300 shots total), and method FTc repeated FTb seven times at fresh site each time (2100 shots total). The run times for FTa, FTb and FTc were 6, 60 and 420 s, respectively,

with a further 25 s required for sample manipulation for method FTc. Laser energy (laser flash lamp energy, LFLE) was varied for some experiments.

The materials examined were copper metal (BDH Analar, Merck Ltd., Lutterworth, UK), pure aluminium metal (BAS BCS198e, Bureau of Analysed Standards, Newham Hall, Newby, Cleveland, UK), and a range of aluminium alloy standards (BAS SS502, SS503, SS506, Bureau of Analysed Standards) containing various amounts of copper (0.001 to 0.40 % m/m Cu).

3.3 Results and Discussion

3.3.1 Inductively coupled plasma emission spectrometry

Emission spectra for the 307 - 332 nm spectral region recorded with the OMA are shown in Figure 1 for distilled water and a copper solution (10 mg l^{-1}). This region was monitored because it encompasses two strong emission lines for copper (324.754 and 327.396 nm). An increase in intensity can be seen for the background spectrum due to the continuum emission from the ICP source. The two regions of low intensity at either side of the spectra correspond to the pixel regions which are not intensified. Of the 1024 pixels of the photodiode array, the central 720 pixels are intensified. The effective resolution of the OMA spectrometer was calculated to be 0.20 nm at full width half height from the spectrum for copper solution depicted in Figure 1.

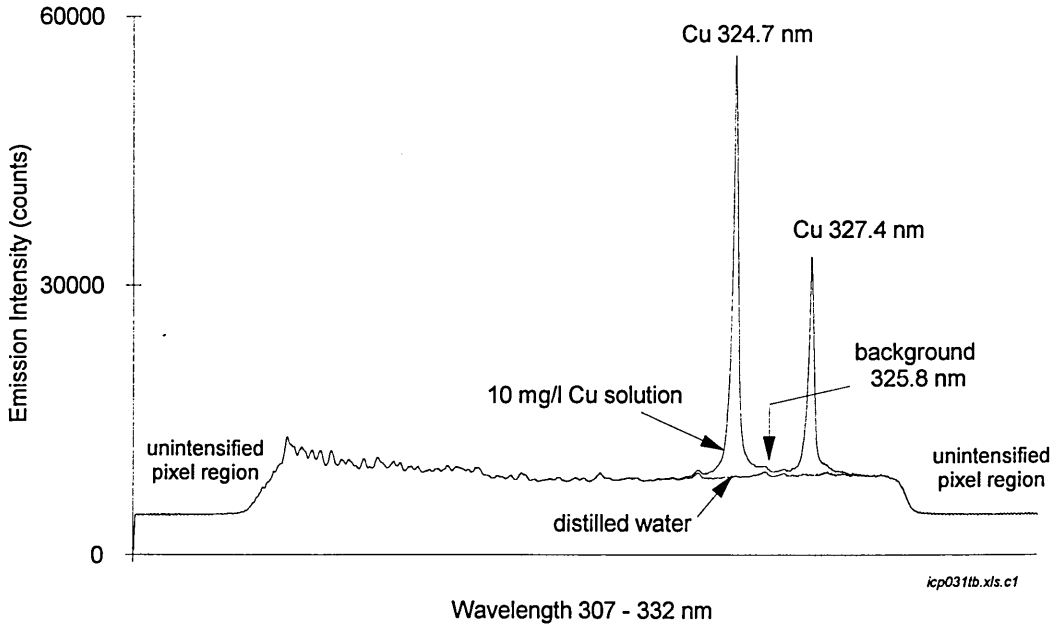

Figure 1 Overlay of spectra for copper solution (10 mg l^{-1}) and distilled water from ICP emission spectrometry recorded with the OMA. The integration time for each spectrum was 6 s (20 scans of the photodiode array into each OMA memory).

The effect of integration time upon performance was examined. Spectra were recorded for distilled water and a solution of copper (10 mg l^{-1}) using a range of integration times from 0.3 to 30 s. To change the integration time, the number of scans of the photodiode array accumulated into an OMA memory was varied. Ten OMA memories were used for each experiment. The emission intensity for copper 324.7 nm was measured for each memory and the data are shown, together with the integration times, in Table 1. Precision (% relative standard deviation, % RSD) did not vary significantly with integration time for either the distilled water or the copper solution. The signal/noise ratio increased with integration time as would be expected. The signal/background ratio, approximately 6.3, was very similar for each integration time. The values for precision are similar to those of the Jarrell Ash ICP spectrometer and those

reported in the literature for the ICP technique.[1] Data indicate, therefore, that the OMA spectrometer is capable of achieving good levels of precision.

Total integration time (s)		0.3	3	6	15	30
No. of photodiode array scans per OMA memory		1	10	20	50	100
Integration time of each OMA memory (s)		0.03	0.3	0.6	1.5	3.0
Mean signal (counts)	distilled water	459.6	4601	9200	23010	45701
	10 mg l^{-1} Cu	2895	29064	57724	143500	288100
% RSD	distilled water	0.68	0.37	0.18	0.17	0.28
	10 mg l^{-1} Cu	0.40	0.54	0.54	0.37	0.50
S/N ratio	10 mg l^{-1} Cu	4244	78551	318919	829480	1018021

S = Cu 324.7 nm N = % RSD of Cu 324.7 nm measured with distilled water

Table 1 Effect of integration time upon analytical performance for the OMA monitoring an ICP emission source

The wavelength accuracy was tested by measuring the emission intensity of copper 324.7 nm after the grating had been driven from centre wavelength 700 nm to 320 nm. This was repeated ten times. Each measurement had an integration time of 6 s (20 photodiode array scans into 1 OMA memory). The spectra were examined and the copper 324.7 nm emission line was found to be at the same pixel number on the photodiode array each time (pixel 684). The precision was slightly worse, 0.9 % RSD, compared to the same measurements when the grating was fixed at centre wavelength 320 nm, 0.5 % RSD. The data indicate that the grating drive mechanism is reproducible in operation to within

1 pixel (± 0.024 nm), which is the manufacturer's spectrometer specification. It is recommended, however, that the pixel positions of analyte emission lines should be confirmed for each spectrum following movement of the grating.

Analytical performance data are shown in Table 2 for copper, cadmium and lead. Copper signals were recorded with the 307 - 332 nm spectral region as above, and the spectral region 216 - 242 was used to monitor cadmium and lead signal responses.

element	Cu I	Cd I	Pb II
emission wavelength (nm)	324.754	228.802	220.353
limit of detection (mg l^{-1}) (3σ, distilled water)	0.017	0.011	0.135
signal / background (10 mg l^{-1})	6.45	2.67	1.06
% RSD	0.57	0.43	0.51

I neutral atom emission line II singly ionised atom emission line

n = 10 for statistical calculations

Table 2 Analytical data for the OMA monitoring the ICP emission source. The integration time was 6 s (20 scans of the photodiode array into each OMA memory).

The emission lines for copper and cadmium are relatively sensitive compared to lead, and therefore have lower limits of detection than lead. The % RSDs are similar to those obtained by the spectrometer of the Jarrell Ash ICP instrument (0.6 % RSD for similar integration times), but limits of detection and signal /background ratios are poorer; the limit of detection for copper was 0.005 mg l^{-1} and the signal/background ratio was 51 (10 mg l^{-1}). The performance of the OMA might be improved by varying the fibre optic observation position.

Results obtained here are similar to those reported by Furuta at al [2] (1980) who utilised a silicon intensified target image detector.

The dynamic range of the OMA photodiode array detector was studied by aspirating solutions that had a wide range of concentrations (Cu, Cd and Pb, 0.1 to 100 mg l^{-1}). A typical calibration graph of emission intensity versus concentration of cadmium is shown in Figure 2. Linear plots were obtained over 3 to 4 orders of magnitude, indicating that the photodiode array detector has the potential to exploit the wide dynamic range of the ICP source. Dynamic range is limited compared to that of a photomultiplier tube because of the image intensifier fitted to this photodiode array. This could be shown with further study using solutions that cover a wider range of concentration than used here.

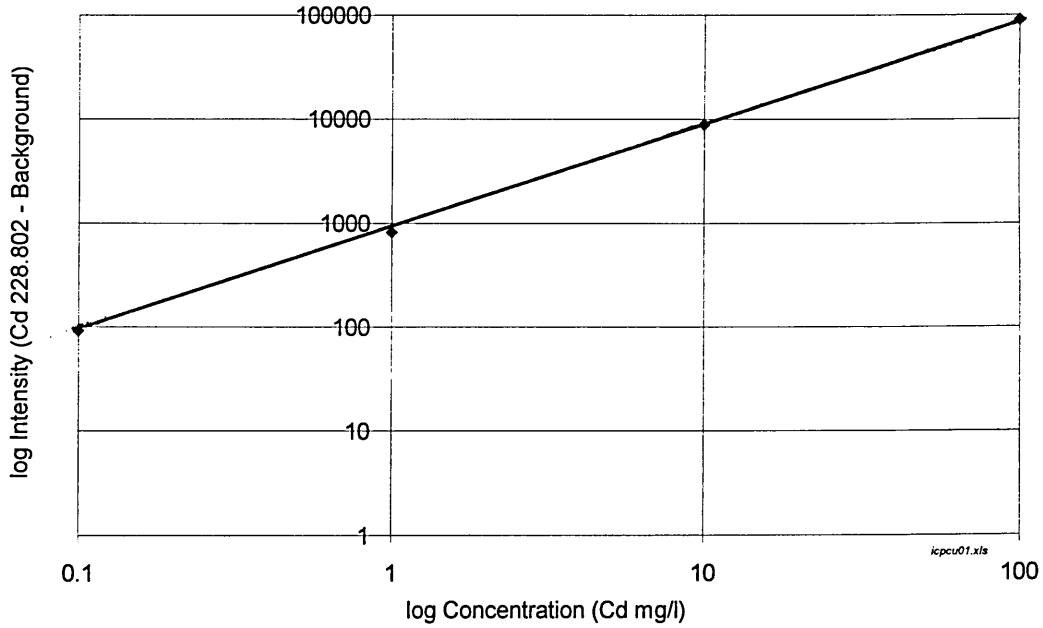

Figure 2 Plot of log emission intensity versus log concentration of cadmium for the OMA monitoring the ICP emission source. The integration time was 6 s (20 scans of the photodiode array into each OMA memory).

The background subtraction capability of the OMA photodiode array detector is depicted in Figure 3 with spectra for copper solution (10 mg l^{-1}) with, and without, the background signal. For the subtracted spectrum, a spectrum of distilled water was recorded first and this was simultaneously subtracted from the copper solution spectrum when it was recorded. The spectrum resulting from the background subtraction technique is clearly much simpler. With further work, this subtraction technique could be used to simplify complex spectra from sample solutions containing a strong matrix, such as digested steels, serum samples, etc. A spectrum for a matrix blank solution would be recorded first, and this used to correct the spectrum for the sample solution.

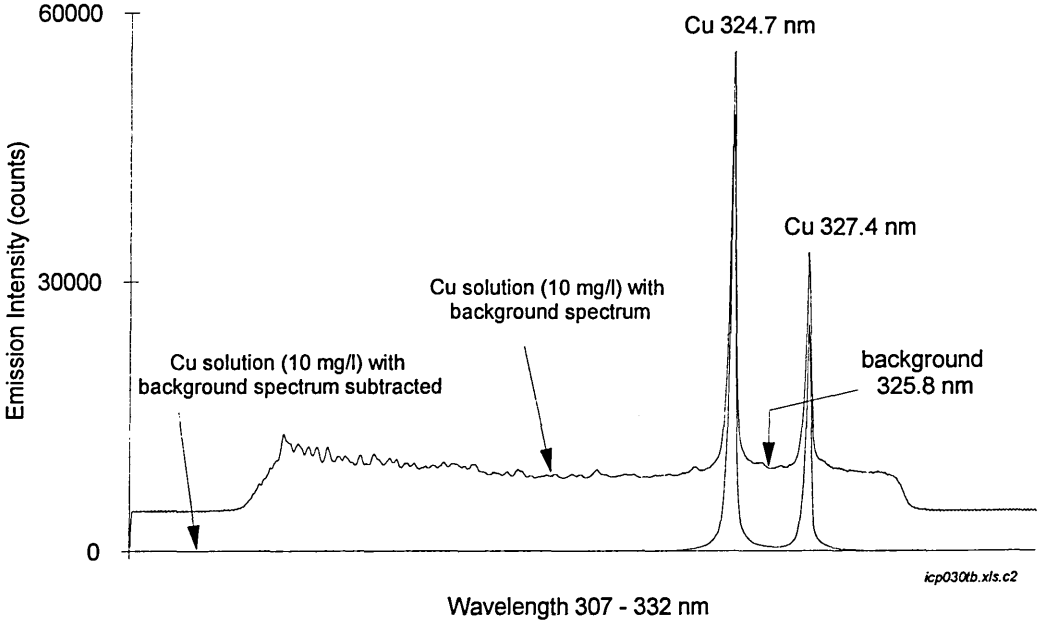

Figure 3 Overlay of spectra for copper solution (10 mg l^{-1}) with background spectrum (upper spectrum) and with the background spectrum subtracted (lower spectrum). The spectra were recorded with the OMA monitoring the ICP emission source, and the integration time for each spectrum was 6 s (20 scans of the photodiode array into each OMA memory).

The OMA was used to monitor transient signals of the ICP source resulting from the introduction of sample solutions by a flow injection technique. Instead of continuous nebulization of sample solution to achieve a steady state, as used above, small, discrete sample volumes are introduced into the ICP source using an injection valve. An emission-wavelength-time response for the introduction of a copper solution (10 mg l^{-1}) is depicted in Figure 4a. The sample volume was 250 μl and the flow rate was 1 ml $minute^{-1}$. Transient emission responses for copper are observed. The spectral background is monitored simultaneously, together with other emission lines within this spectral region 307 - 332 nm. Spectra for a repeat injection with background subtraction are shown in Figure 4b. Here, spectra were first recorded for a blank injection of distilled water, and these were subtracted from the spectra for the subsequent injection of copper solution. The responses in Figure 4b are clearer and simpler than those of Figure 4a without background subtraction. The technique could be advantageous in more complex flow injection applications, such as samples with organic matrices, e.g. oils, blood serums and organic solvents that cause signal depression in the ICP source, because any background shifts can be simultaneously monitored with the analyte signals and such shifts can be easily corrected.

The technique of using an OMA spectrometer with photodiode array detection to monitor transient signals from an ICP source is advantageous over a conventional ICP spectrometer because the conventional spectrometer uses photomultiplier tube detectors for single element wavelength detection. Simultaneous background measurement is not normally possible. This photodiode array detection technique could also be very useful to record signals when other sample introduction devices are used, such as laser ablation, electro-thermal atomisation, hydride generation.

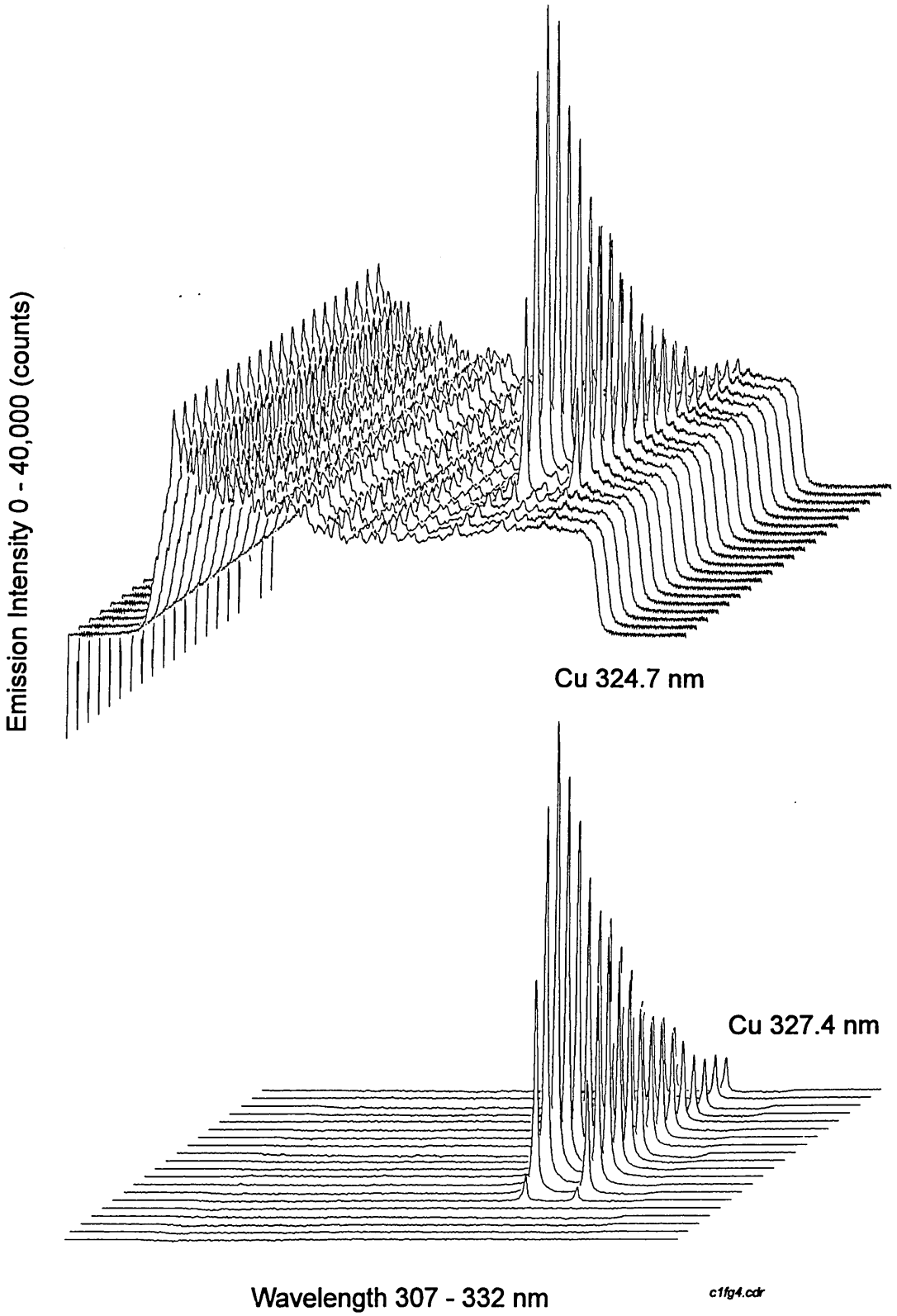

Figure 4 Emission-wavelength-time responses for the introduction of copper solution (10 mg l^{-1}) into the ICP source with flow injection: (a) with the background signal present, (b) with the background signal subtracted.

3.3.2 Laser-induced plasma emission spectrometry

Studies of the laser-induced plasma

Previous work established the performance of the optical multichannel analyser with a well characterised and stable emission source, an inductively coupled plasma emission source (section 3.3.1). Here, the optical multichannel analyser is used to monitor a transient laser-induced plasma produced by the focused radiation from a Q-switched Nd:YAG laser. A sample of copper metal was ablated at the laser focal point with laser flash lamp energy (LFLE) 40 J, (irradiance ~8 x 10^{10} W cm^{-2}). The OMA incremental mode was used to enable spectra to be time-resolved so that the transient signals from the plasma could be studied. There were 30 OMA memories with 1 laser shot in each memory. The increment time after each memory was 100 ns and so the total time was 2.9 μs. Copper metal was examined because copper has a relatively simple emission spectrum and is available in relatively high purity at low cost.

An emission-wavelength-time response for the ablation of copper metal is depicted in Figure 5, spectral overlays are shown in Figure 6, and an emission-time response for selected wavelengths is depicted in Figure 7. The figures show that initially the emission spectrum is dominated by a very intense background continuum from the plasma, and only a broad continuum is visible near the two copper emission lines (Cu 324.754 and 327.396 nm). This indicates that the plasma temperature is very high, of the order 1.5 to 3.0 x 10^4 K.[3,4] At time 300 ns, broad copper emission lines are evident superimposed on the intense background continuum. These lines are shifted to the red by about 0.07 nm (Figure 6b). The background has reduced considerably by time 400 ns because plasma temperature has decreased, caused by sample material entering the plasma.

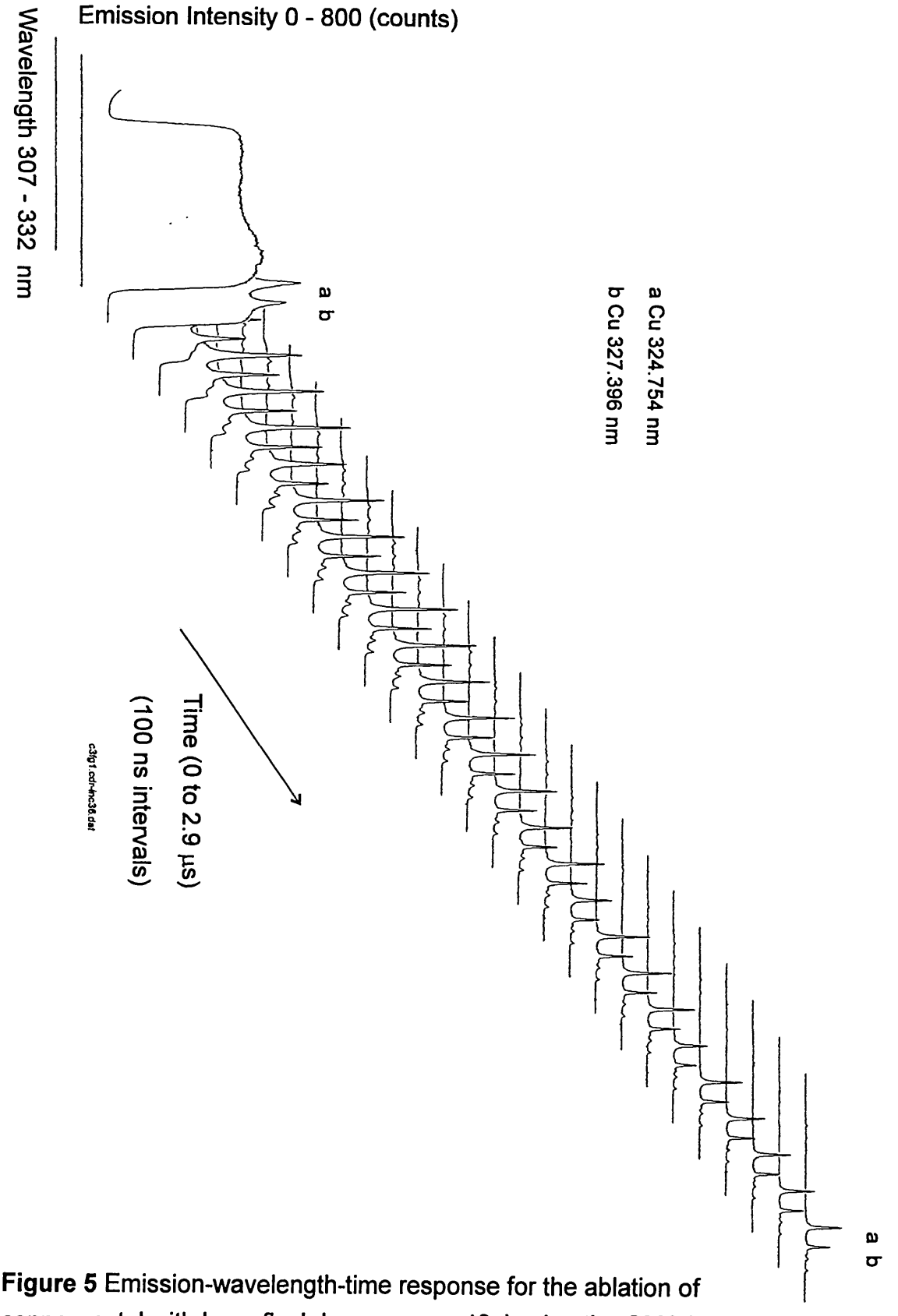

Figure 5 Emission-wavelength-time response for the ablation of copper metal with laser flash lamp energy 40 J using the OMA incremental program (increment time 100 ns, integration time 100 ns) .

(a)

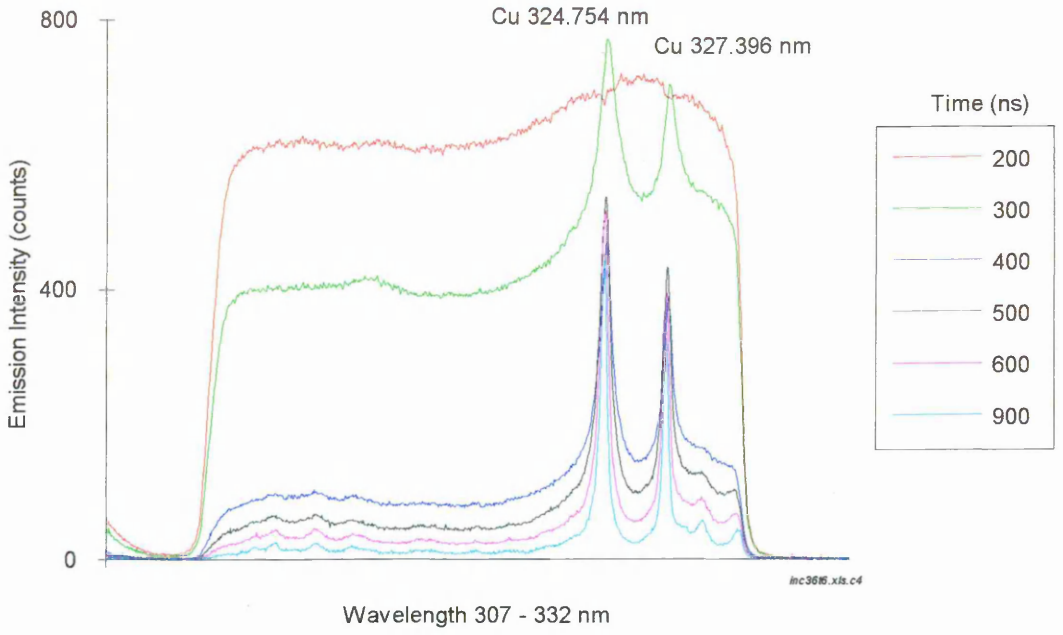

(b)

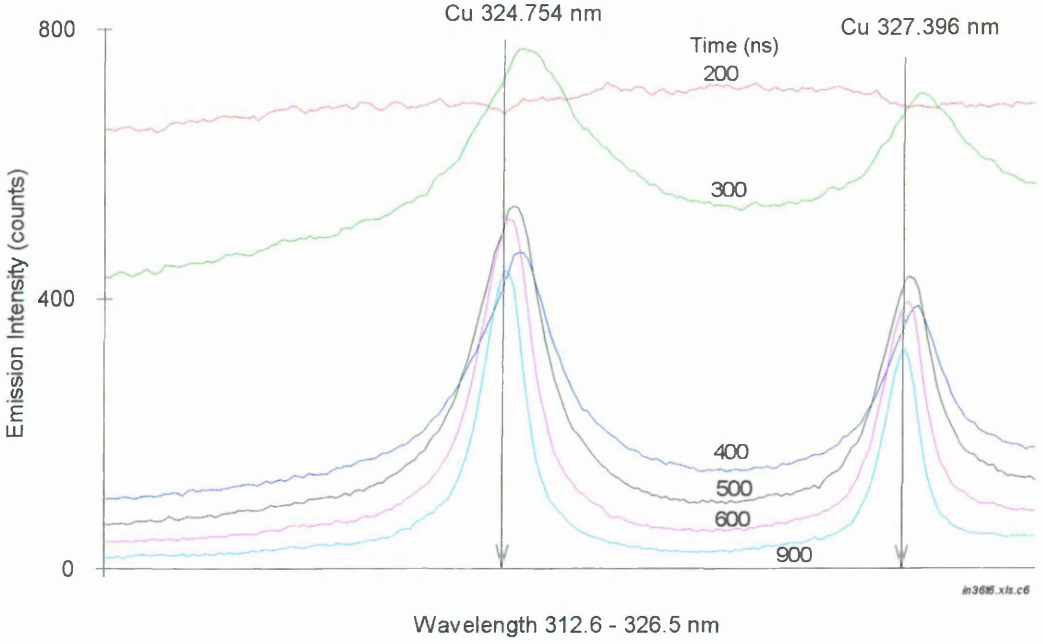

Figure 6 Emission spectra for the ablation of copper metal with laser flash lamp energy 40 J using the OMA incremental method (integration time 100 ns, increment time 100 ns). The spectra are for the times shown and the wavelength regions are: (a) 307 - 332 nm, (b) 312.6 - 326.5 nm, a magnified portion of (a).

After time 400 ns, the background intensity continues to decrease and line widths become narrower as the plasma temperature decreases. The amount of emission line shift to the red also reduces with time as the plasma temperature decreases. By time 900 ns, the lines have ceased to be red shifted, the background response is minimal and element emission responses are dominant.

The emission-time response (Figure 7) shows the rapid decrease in background intensity after time 300 ns. Element emission signals are clearly seen after time 400 ns. They continue to be observed as they decrease slowly until the plasma has extinguished at about 35 μs. The plasma lifetime (examined below) is relatively long-lived compared to the laser pulse width (10 ns).

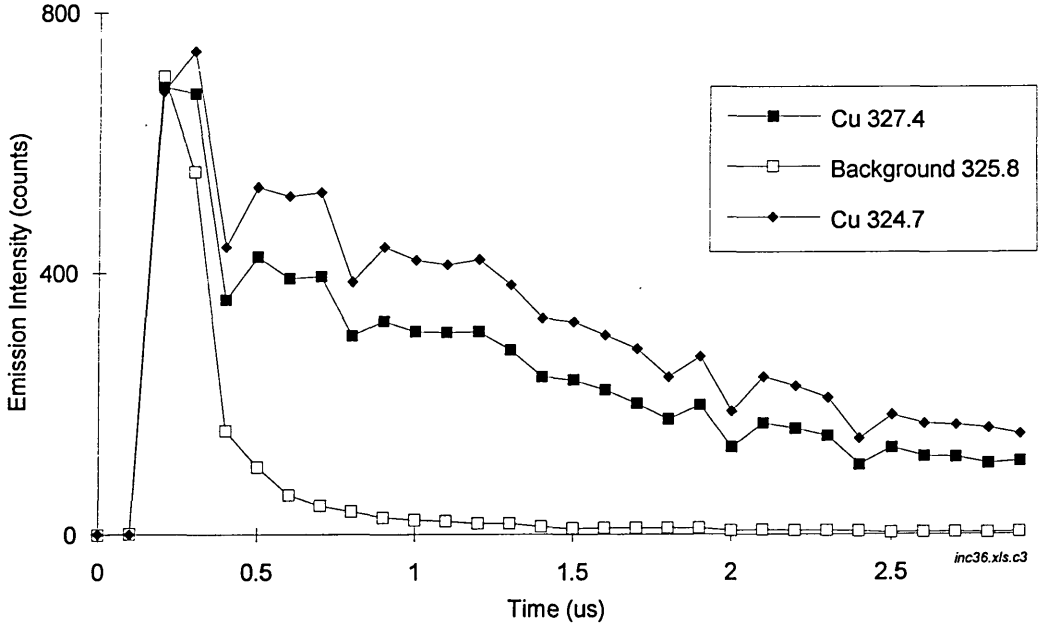

Figure 7 Emission-time response for the ablation of copper metal with laser flash lamp energy 40 J using the OMA incremental method (integration time 100 ns, increment time 100 ns, total 2.9 μs).

Useful analytical data can be obtained by resolving the analyte emission signals in time from the initial, intense background continuum. This can be achieved using an OMA fixed time program with suitable time settings. A delay time of 700 ns would minimise background contributions as the background has reduced considerably by then, and an integration time of about 1 μs is appropriate to measure analyte emission responses.

The peak broadening and line shifts at early times are due to pressure broadening effects, and suggest very high plasma temperatures, pressures and electron densities. Scott and Strasheim[5] have previously reported red line shifts (~0.16 nm) and line broadening for the ablation of aluminium which they attributed to pressure effects. Niemax and Sdorra,[3] and Kim[6] have also reported line broadening due to pressure broadening effects (Stark broadening). Pressure broadening (Stark broadening) is due to perturbation of the emitting species by charged particles in the laser-induced plasma.[7]

The experiment was repeated with the maximum laser energy available (LFLE 70 J, irradiance ~3.1 x 10^{11} W cm^{-2}). An emission-wavelength-time response is shown in Figure 8, spectra overlays in Figure 9, and an emission-time response in Figure 10. Compared to ablation with LFLE 40 J (Figures 5 and 6), emission signals are greater (~7000 vs. ~800) and line shifts are larger (~0.12 vs. 0.07 nm) suggesting that the laser-induced plasma is more intense and has a higher initial temperature, (1.5 to 3.0 x 10^4 K). The plasma also has a longer lifetime compared to LFLE 40 J ablation, (~80 μs vs. ~35 μs). The temperature of the plasma for the ablation of different materials with different laser energies could be estimated from spectrometric measurement at selected times of the plasma lifetime. Niemax[3] measured the relative intensities of four copper lines to obtain temperature measurements for the ablation of copper, but this would require a more detailed study of other spectral regions than is reported here.

It can be seen from the comparison of ablation with LFLE 40 and 70 J that the copper signals are more intense for the higher laser energy. However, signal /background ratios (Cu 324.7/background 325.8 nm) were higher for LFLE 40 J than for 70 J as the background intensities were greater for the higher laser energy. For example, signal/background ratios for LFLE 40 and 70 J were 19.1 and 8.3 at time 1 μs, and 31.3 and 18.8 at time 2 μs, respectively, suggesting that high laser energy may not be required to obtain the most sensitive analyte emission responses.

The different time behaviours of the copper and background signals for ablation with LFLE 40 and 70 J suggest that a longer detector delay time may be required for LFLE 70 J in order to minimise the effect of the background signal and optimise analytical performance, e.g. 1.5 μs instead of 700 ns.

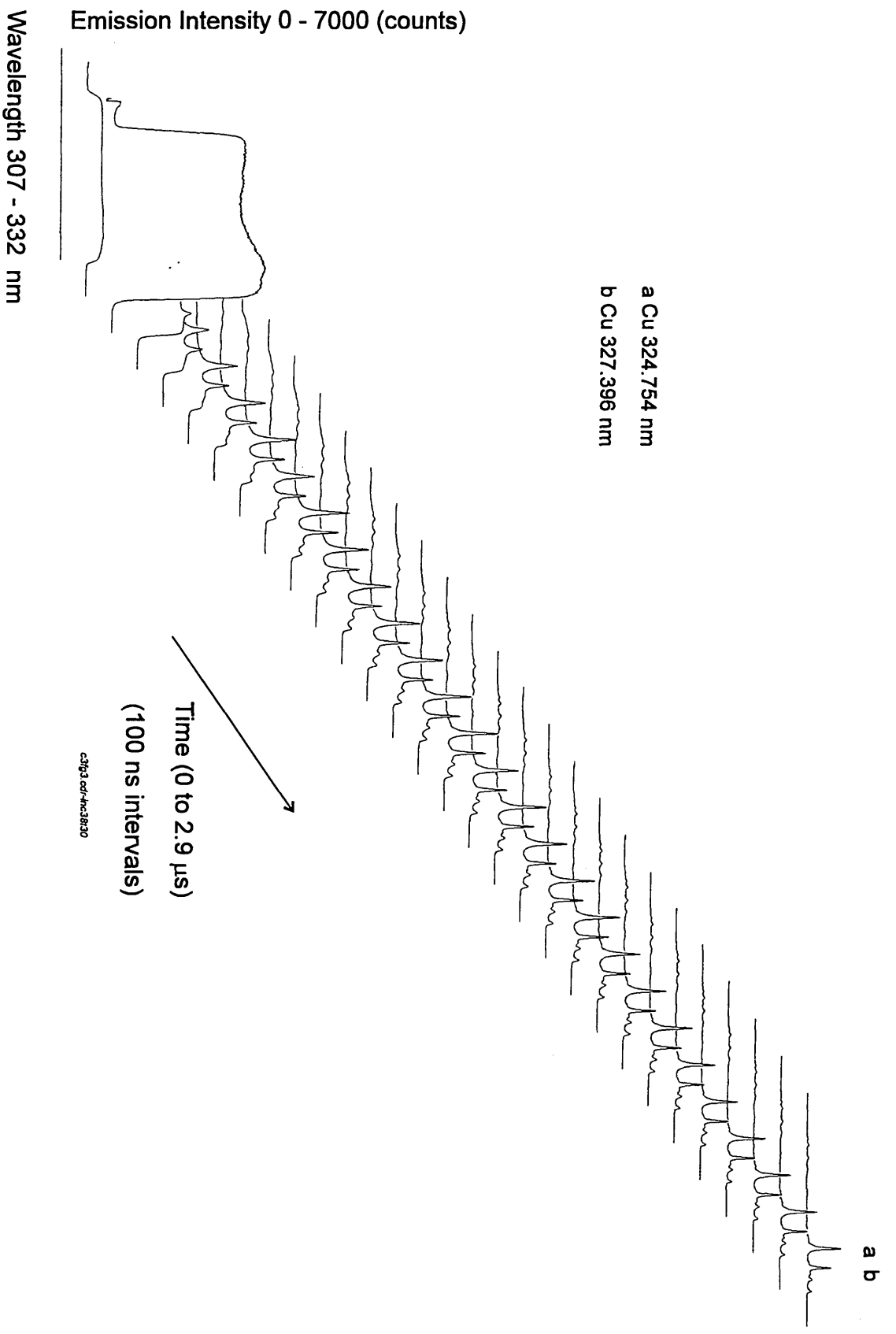

Figure 8 Emission-wavelength-time response for the ablation of copper metal with laser flash lamp energy 70 J using the OMA incremental program (increment time 100 ns, integration time 100 ns).

(a)

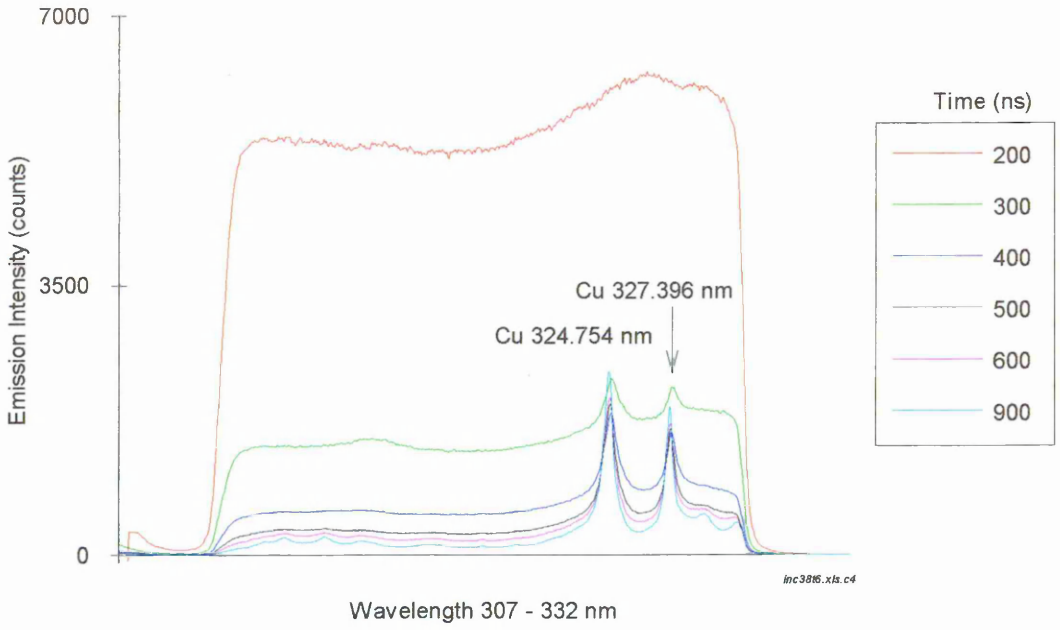

(b)

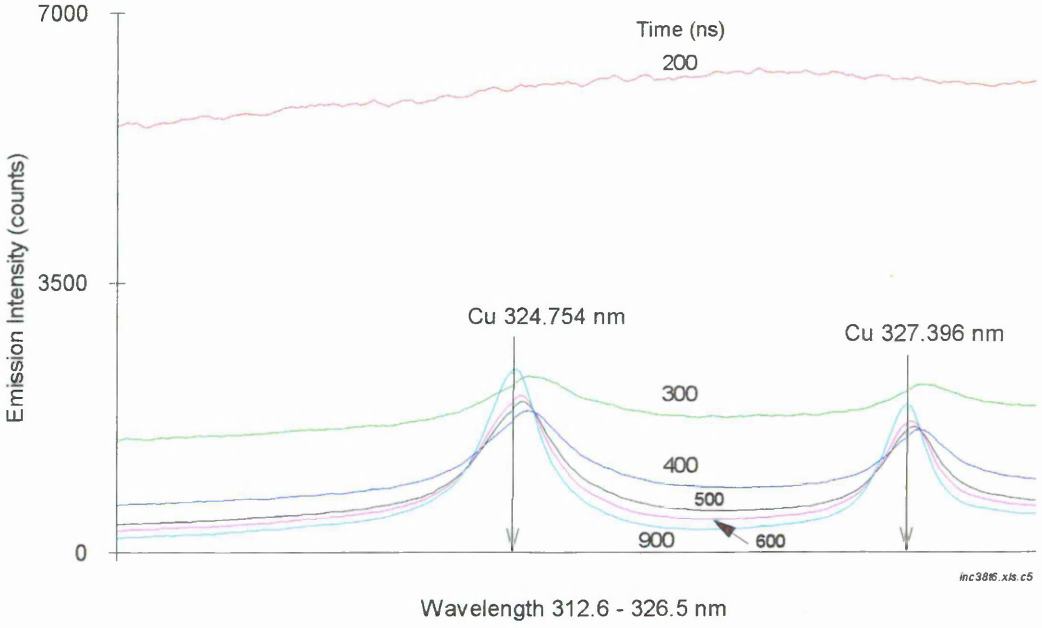

Figure 9 Emission spectra for the ablation of copper metal with laser flash lamp energy 70 J using the OMA incremental method (integration time 100 ns, increment time 100 ns). The spectra are for the times shown and the wavelength regions are: (a) 307 - 332 nm, (b) 312.6 - 326.5 nm, a magnified portion of (a).

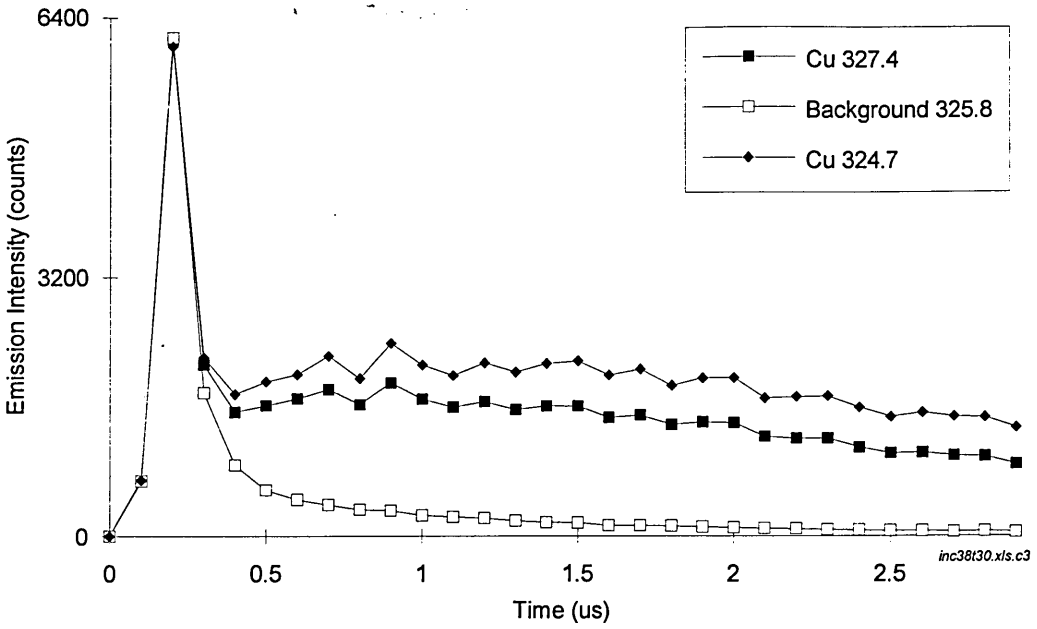

Figure 10 Emission-time response for the ablation of copper metal with laser flash lamp energy 70 J using the OMA incremental method (integration time 100 ns, increment time 100 ns, total 2.9 μs).

The plasma lifetime for ablation with different laser energies (LFLE 40 and 70 J) was estimated using an OMA incremental program. The time settings used were increment time of 1 μs and integration time of 1 μs with 100 memories to enable a total measurement time of 99 μs. Emission-wavelength-time responses are depicted in Figures 11 and 12 for ablation with LFLE 40 and 70 J, respectively.

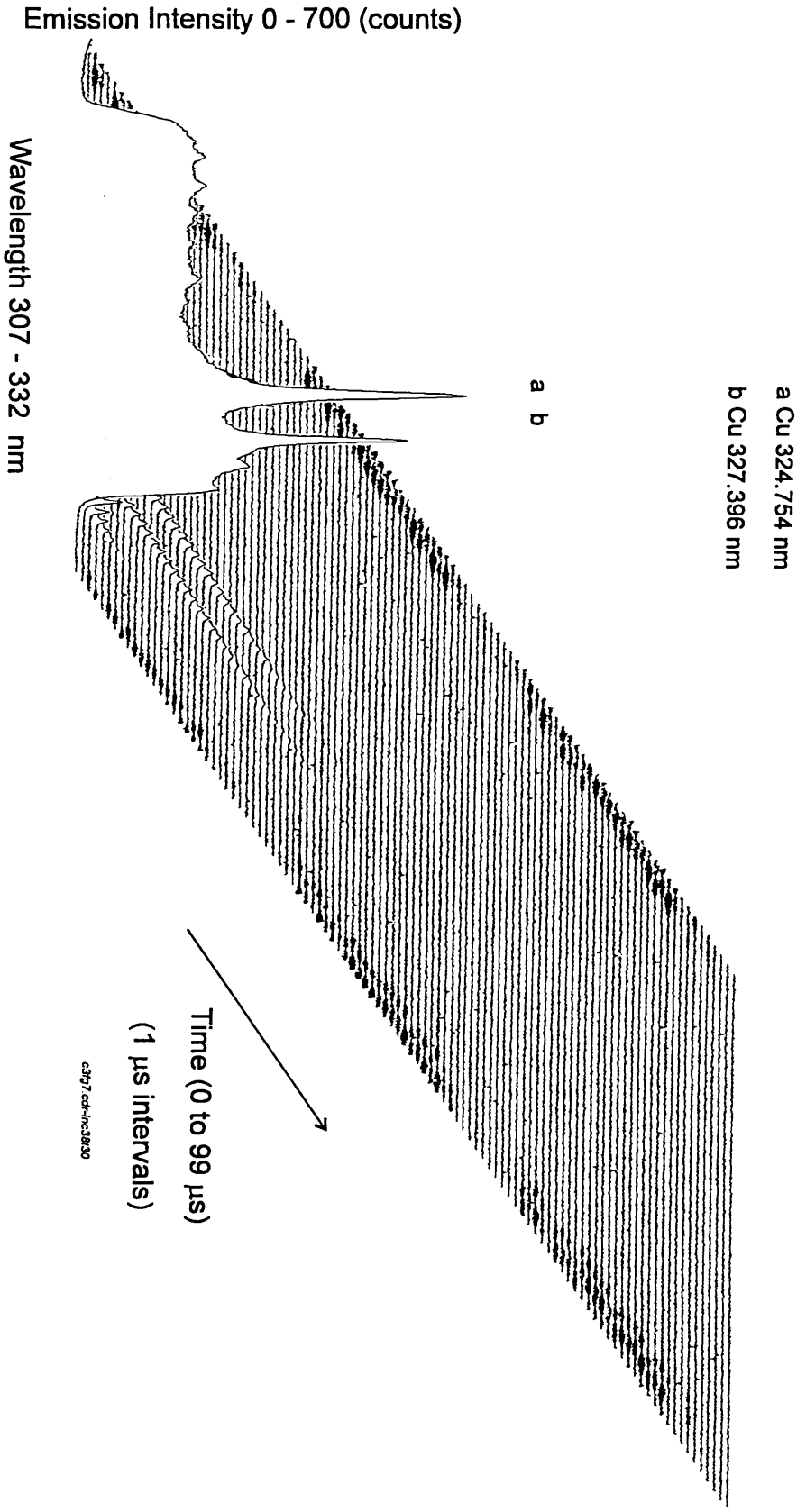

Figure 11 Emission-wavelength-time response for the ablation of copper metal with laser flash lamp energy 40J using the incremental program (increment time 1 μs, integration time 1 μs) to estimate the lifetime of the plasma.

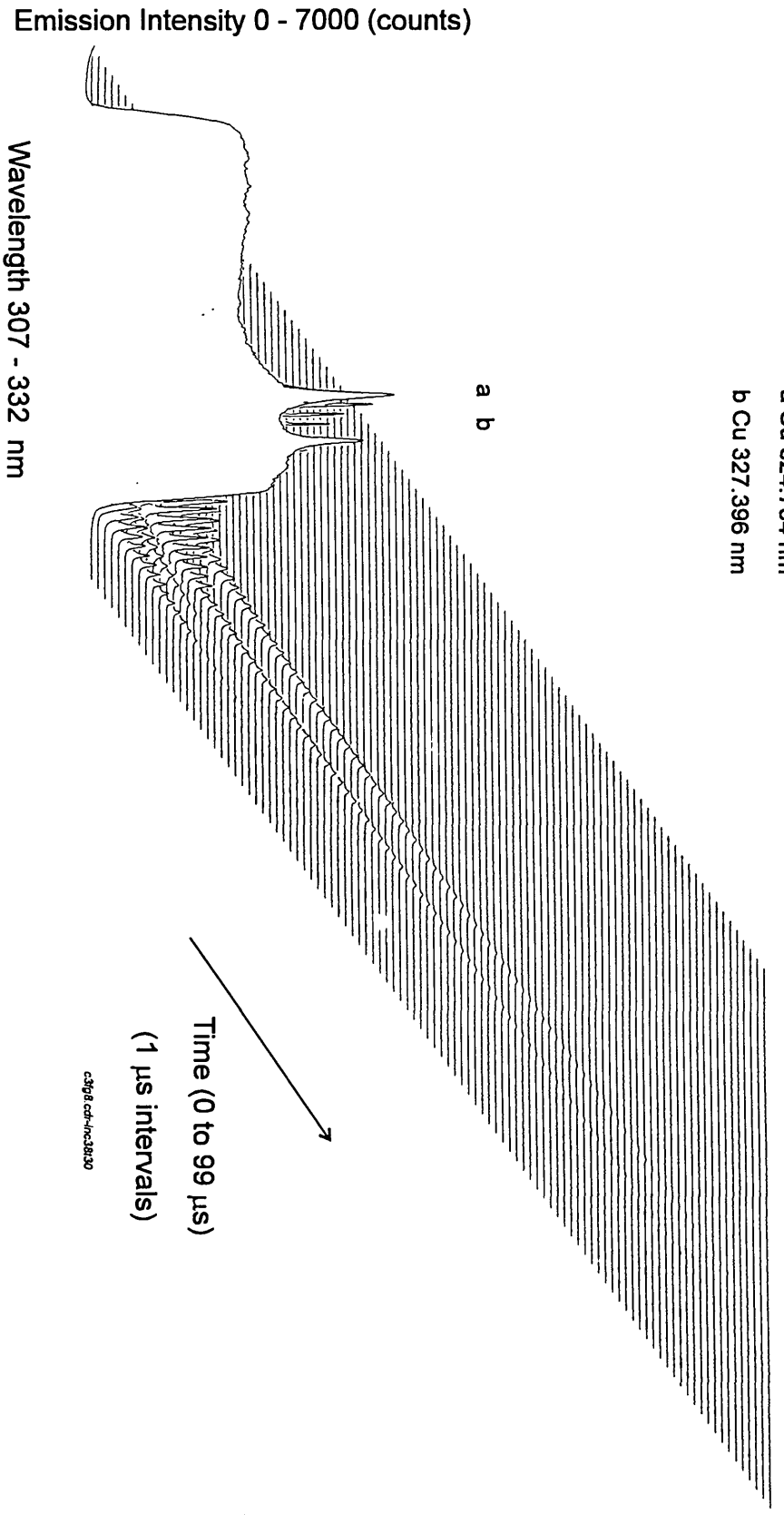

Figure 12 Emission-wavelength-time response for the ablation of copper metal with LFLE 70J using the incremental program (increment time 1 μs, integration time 1 μs) to estimate the lifetime of the plasma.

These show that element emission responses for both copper lines became indistinguishable from the background at about 37 and 80 μs for LFLE 40 and 70 J, respectively, indicating that the plasma had extinguished by these times. Emission intensities for both copper lines were less than 5 counts. Examination of the spectra for both ablations at time 99 μs confirms that there are no element emission responses (Figure 13).

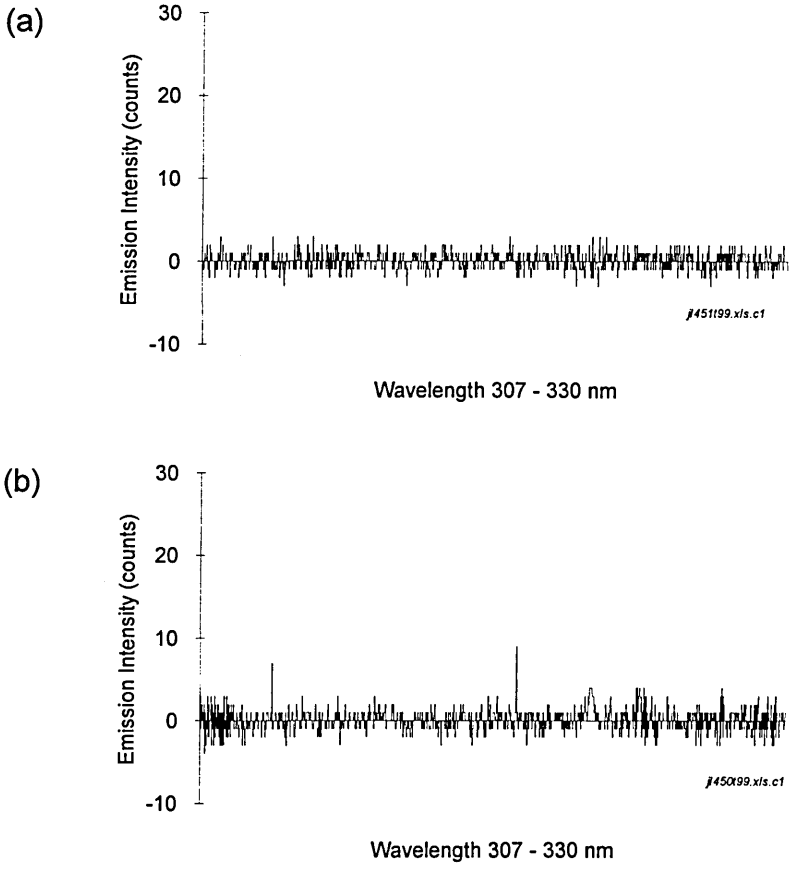

Figure 13 Spectra at time 99 μs for the ablation of copper metal recorded with the OMA incremental program (increment time 1 μs, integration time 1 μs) using laser flash lamp energy: (a) 40 J, (b) 70 J.

The lifetime of the plasma produced by ablation with LFLE 55 J was ~44 μs, a value between those for LFLE 40 and 70 J, i.e. increased laser energy lengthens the plasma lifetime. Kim[5] reported plasma lifetimes ranging from 300 ns to 40 μs depending on operating parameters such as laser energy and ablation gas and pressure. Sneddon et al[8] reported plasma lifetimes of 100 μs for the ablation of copper, zinc, iron and nickel targets with an excimer laser (ArF 193 nm). The published values are comparable to those obtained here. It is noted that with the laser firing at 5 Hz, as in these experiments, the time interval between laser shots is 200 ms. The plasma is therefore extinguished for approximately 199.9 ms prior to the next laser shot, (plasma lifetime ~0.1 ms).

Analytical performance

The effect of operating parameters upon analytical performance was examined for the ablation of copper metal. An OMA fixed time program (FTa), consisting of 30 memories with 1 laser shot in each memory, was used (delay time 700 ns, integration time 1 μs) with LFLE 40 J. The observation position for the end of the fibre optic was varied and it was found that increased signal/background (S/B) and signal/noise (S/N) ratios were obtained with the fibre positioned 1-2 mm above the sample surface and in direct line with the laser spot. The sample was placed at different positions relative to the laser focal point and increased S/B and S/N were obtained with the sample positioned at the laser focal point. The effect of repetitive laser firing at a sample site upon performance was considered using three fixed time programs, FTa (1 laser shot in each of 30 memories, 30 shots total), FTb (10 laser shots in each of 30 memories, 300 total), and FTc (method FTb was repeated 7 times at a fresh site each time to give 2100 shots in total). Data for each method are given in Table 3.

These data indicate that precision (relative standard deviation, RSD) and S/N ratio improve with the number of laser shots used for measurement. The S/B ratio was reduced, however, with a larger number of laser shots. Emission-time profiles showed that this was because the background signal increased with time, i.e. with the number of laser shots. This effect might be minimised by increasing the delay time. The results suggest that precision is improved by accumulating a large number of laser shots, e.g. from 17.1 (30 shots) to 3.8 (2100 shots), (% RSD, Cu 324.7 nm). Precision was further improved to 0.6 (% RSD) when a ratio of the two copper lines was taken, suggesting that the use of an appropriate internal standard is beneficial. The precision data are comparable to those reported by other workers, for example, Cremers and Romero[9] obtained % RSD values between 0.4 and 14 for various elements in steel using iron signals from the steel matrix as internal standard. Niemax et al[10] achieved precision of 6 % RSD for silicon and chromium in steel, which was improved to 2.4 when an iron signal was used as internal standard.

Method	n	mem	shots /mem	total shots	% RSD Cu 324.7	% RSD Cu 327.4	% RSD Cu 324.7 /Cu 327.4	S/B	S/N
FTa	30	30	1	30	17.1	18.6	1.7	17.7	183
FTb	30	30	10	300	10.2	12.2	2.7	11.7	2424
FTc	7	210	10	2100	3.8	3.5	0.6	11.9	18613

shots = number of laser shots
mem = number of OMA memories used
B = Background (325.8 nm)
n = number for statistical calculation
S = Signal (Cu 324.7 nm)
N = RSD of Background response

Table 3 Data for copper metal from laser-induced plasma emission spectrometry. Different OMA fixed time programs were used.

In order to quantify the effect that time resolved measurement has upon performance, copper metal was ablated with an OMA fixed time program using different delay times. With time resolution, the delay time was 700 ns, and with no time resolution, the time delay was 0 ns. An OMA program (FTa) was used to record 30 laser shots, each into a separate memory. The integration time was 1 μs for both, and the laser flash lamp energy was 40 J. A typical spectrum from each experiment is shown in Figure 14. The spectrum recorded with time resolution (delay time of 700 ns) has minimal spectral background and sharp, intense emission peaks for the two copper lines. Conversely, the spectrum recorded with no time resolution (delay time 0 ns) has an intense spectral background and broader copper emission lines. Although the copper lines are as intense as those recorded with time resolution, the signal/background ratio was considerably worse because of the intense background signal. The

signal/background ratios (Cu 324.7 / background 325.8) were 15.4 and 2.5 for time resolved measurement and no time resolution, respectively. This clearly shows the increase in sensitivity that is achieved by the use of time resolved detection in laser-induced plasma emission spectrometry.

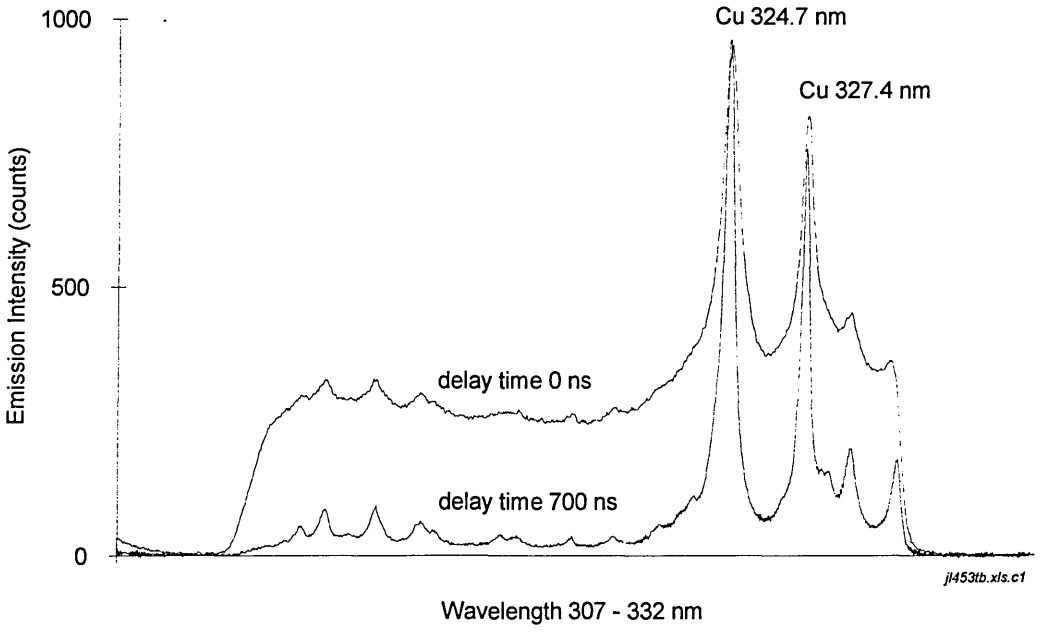

Figure 14 Spectra for the ablation of copper metal with laser flash lamp energy 40 J and an OMA fixed time program (FTa), 1 laser shot into each memory. The upper spectrum was recorded with no time resolution (delay time 0 ns), and the lower spectrum recorded with time resolution (time delay 700 ns). The integration time for both spectra was 1 μs.

These copper spectra can be compared to that obtained for copper solution from the inductively coupled plasma (ICP) emission source (Figure 1). The emission lines of the ICP source spectrum are considerably narrower and the baseline is simpler compared to the laser-induced plasma spectra. The differences are due to the higher temperatures and more complex interaction processes of the laser-induced plasma. In addition, the laser-induced plasma is in air and these gases may contribute to the spectra, whereas the ICP emission

source is an argon plasma, which has a relatively simple emission spectrum, and the emitting species are effectively shielded from air.

To study the quantitative analysis capability of the technique, a range of aluminium alloy standards was examined for copper content, (Table 4). The samples were ablated with LFLE 70 J and data acquired with a fixed time OMA program, FTb (10 laser shots in each of 30 memories at same site, 300 shots total). The spectral region 307 - 332 nm was monitored. A spectrum for the ablation of BAS SS 502 is shown in Figure 15 in which emission lines for aluminium and copper are clearly seen.

Standard	Cu Concentration (% m/m)
pure Al BCS198e	0.00
BAS SS 506	0.03
BAS SS 503	0.11
BAS SS 502	0.40

Table 4 Copper content of aluminium metal and a range of aluminium alloys

The two aluminium emission lines are not fully resolved and there is a small background shift seen across the spectrum, (Figure 15). The use of a longer time delay might reduce the background intensity and enable the aluminium lines to be resolved.

Calibrations for copper 324.7 nm and copper 324.7 ratioed to aluminium 309.2 nm were both linear, although the ratioed values provided a better fit when the value for the blank was omitted, (Figure 16). The line equations and correlation coefficients were: $y = 12049x + 5353$, 0.9632 (Cu 324.7), and $y = 122x + 53.3$, 0.9989 (Cu 324.7 / Al 309.2), respectively.

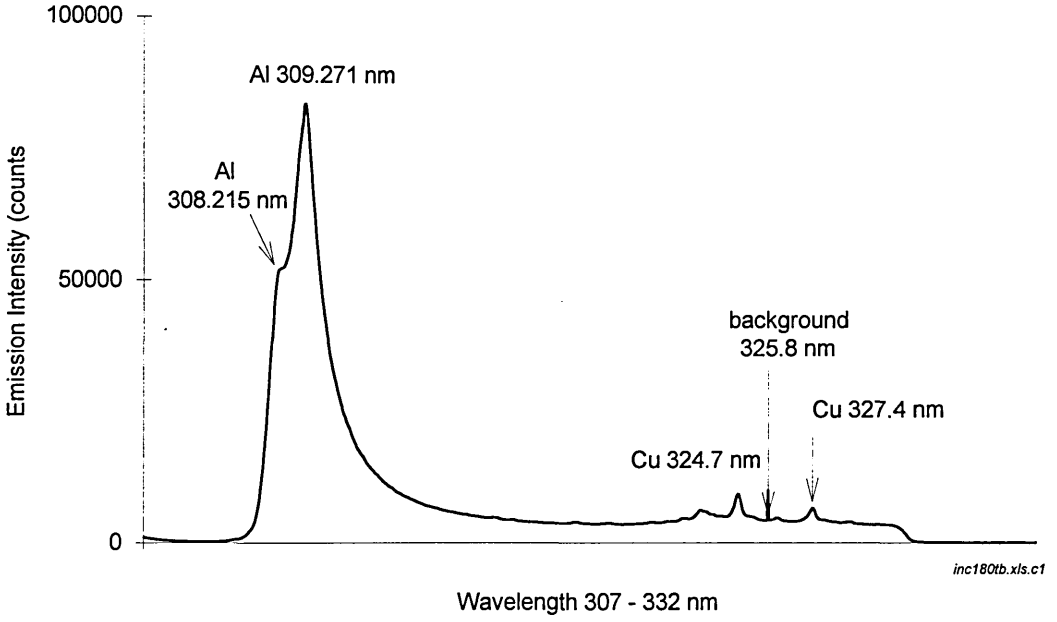

Figure 15 Emission spectrum for aluminium alloy containing copper 0.40 % m/m (BAS SS 502). Sample was ablated with laser flash lamp energy 70 J and data were acquired with fixed time OMA program FTb, (delay time 700 ns, integration time 1 μs).

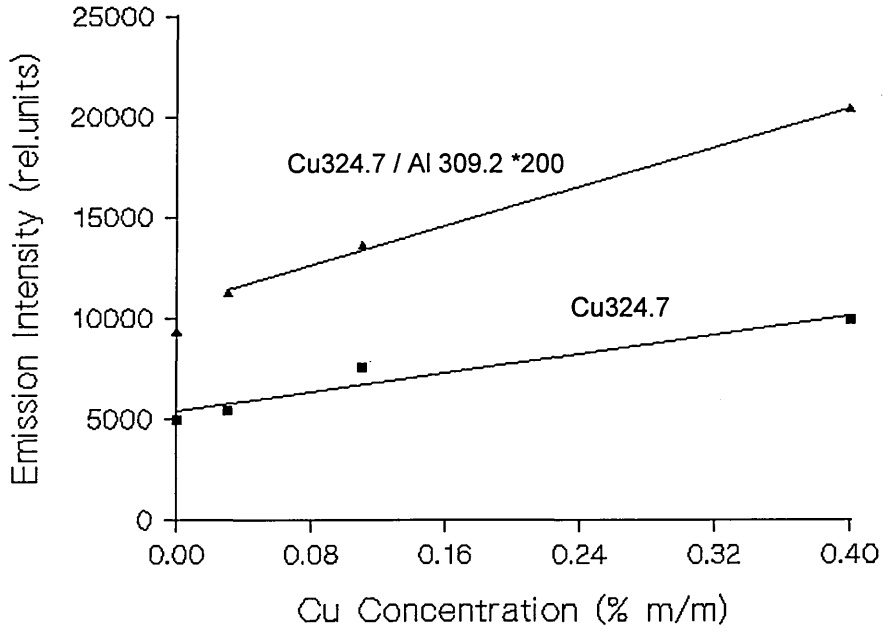

Figure 16 Calibration plot for copper in aluminium alloy. Samples were ablated with LFLE 70 J and data were acquired with OMA fixed time program FTb. The samples are listed in Table 4. The values for the copper/aluminium plot were multiplied by 200 in order to obtain both graphs on the same scale.

The limit of detection for copper was estimated to be 0.010 % m/m based on 3σ (measurement of pure aluminium standard). The calibration shows that emission signals are representative of the samples ablated and that quantification is possible when suitable standard reference materials are available. Precision of 5.3 % RSD was obtained for copper 324.7 nm (n=30), and this was improved to 3.0 % when the copper was ratioed to the aluminium 309.2 nm emission signal. The values are better than those obtained by Scott and Strasheim (1970),[5] who obtained values of between 5-8 % RSD for copper in aluminium alloy, and comparable to those reported by Niemax et al (1989)[10] for the determination of chromium and silicon in steel. Niemax[10] achieved better limits of detection than here, 0.003 % m/m (3σ), by using an argon buffer gas at reduced pressure. The performance achieved here, however, is appropriate for process monitoring and industrial applications such as the rapid sorting of alloy types.

3.4 Conclusions and Recommendations for Further Work

An optical multichannel analyser with a photodiode array detector has been successfully used to monitor an ICP emission source. Analytical performance was comparable to a conventional ICP spectrometer although sensitivity was lower. Sensitivity could probably be improved by optimising the fibre optic observation position relative to the ICP discharge. Spectral resolution was about an order of magnitude lower than that of a conventional ICP spectrometer because of the compact size of the OMA spectrometer and the intensifier. The wavelength accuracy of the optical multichannel analyser spectrometer was found to be reproducible in positioning the grating to a selected wavelength region.

The integrated laser and OMA system was found to operate satisfactorily, and it was possible for the spectrometer to discreetly monitor the laser-induced plasma from each laser shot. The versatility of the OMA data acquisition modes indicates that the system is appropriate to investigate new applications. Study of the laser ablation of copper metal showed that sensitivity was considerably improved when time resolved measurement of the laser-induced plasma was used. For the ablation of copper metal, the signal/background ratio (Cu 324.7 /background 325.8) was 6.2 times larger for measurement with time resolution than measurement without. Increasing the laser energy was found to increase the intensity of the initial background continuum and increase the lifetime of the laser-induced plasma. Analytical performance was established for the ablation of copper metal and copper in aluminium alloy. It was found that a larger number of laser shots (2100 vs. 30) improved precision (17.1 vs. 3.8 % relative standard deviation, RSD). Performance was comparable to other published studies.[5,9,10] The limit of detection for copper in aluminium alloy was 0.010 % m/m. The use of an internal standard for the determination of copper in aluminium alloy also improved the performance (5.3 vs. 3.0 % RSD), and provided a calibration graph of improved linearity.

Comparing the performance of the OMA with the ICP emission source and the laser-induced plasma source, precision and sensitivity (signal/background ratio) were better with the ICP source, as expected. Values for precision were 0.5 % RSD for the ICP source (10 mg l^{-1} Cu solution, Cu 324.7 nm) and 3.5 % RSD for the laser-induced plasma (pure copper metal, Cu 324.7 nm). The signal/background ratio was 6.3 for the OMA monitoring the ICP source (10 mg l^{-1} Cu 324.7 nm / distilled water 324.7 nm), compared to 11.9 for the OMA with the laser-induced plasma source (pure copper metal, Cu 324.7 nm / background 325.8 nm). The signal for the ICP was only for a dilute solution whereas the signal for the laser-induced plasma source was for pure metal.

These results show that the OMA can achieve good levels of precision with a relatively precise emission source, and that the relatively poor precision obtained with the laser-induced plasma emission source can probably be attributed to complex laser ablation processes.

3.5 References

1. Thompson M., in *Inductively Coupled Plasmas in Analytical Spectrometry,* Montasser A. and Golightly D. W., Editors, VCH Publishers, New York, 1987, pp 163-199.
2. Furuta N., McLeod C. W., Haraguchi H. and Fuwa K., Applied Spectroscopy, 1980, **34** (2), 211-216. Evaluation Of A Silicon-Intensified Target Image Detector For Inductively Coupled Plasma Emission Spectrometer.
3. Niemax K. and Sdorra W., Mikrochimica Acta, 1992, **107**, 319-327. Basic Investigations for Laser Microanalysis III: Application Of Different Buffer Gases For Laser-Produced Plumes.
4. Moenke-Blankenburg L., *Laser Micro Analysis*, Wiley, New York, 1989.
5. Scott R. H. and Strasheim A., Spectrochimica Acta, 1970, **25B**, 311-332. Laser Induced Plasmas For Analytical Spectroscopy.
6. Kim Y. W., in *Laser-Induced Plasmas and Applications*, Cremers D. A. and Radziemski L. J., Editors, Marcel Dekker, New York, 1989, p327-346.
7. Miller M., in *Inductively Coupled Plasmas in Analytical Spectrometry,* Montasser A. and Golightly D. W., Editors, VCH Publishers, New York, 1987, pp 17-65.
8. Sneddon J., Hwang Z. W., Teng Y. Y. and Li K. P., Analytical Letters, 1992, **25** (11), 2143-56. Studies Of Space And Time Resolved Emission Measurements Of An ArF Excimer Laser Ablated Plasma.
9. Cremers D. A., SPIE 1986, **644**, Remote Sensing, 7-12. An Evaluation Of Factors Affecting The Analysis Of Metals Using Laser-Induced Breakdown Spectroscopy.
10. Niemax K., Leis F., Sdorra W. and Ko J. B., Mikrochimica Acta, 1989, **2**, 185-199. Basic Investigation For Laser Micro Analysis: 1. Optical Emission Spectrometry of Laser-Produced Sample Plumes

Chapter 4

Survey Analysis of Polymeric Materials

4.1 Introduction

Polymeric materials generally contain a wide variety of additives which are used to give specific properties to the material.[1] These include, pigments for colour (e.g. white TiO_2), fillers (e.g. $CaCO_3$), stabilisers (e.g. Zn, Pb, Ba), flame-retarding agents (e.g. Sb, P), smoke suppressants (e.g. Zn), etc. These inorganic components vary in concentration from trace (μg/g) to minor (%) levels. Samples can be in different forms such as granular, extruded shape, or sheet of different thicknesses (mm to several cm).

Analytical techniques currently in use for such analyses include solution-based atomic spectrometric methods[2,3] which require time-consuming dissolution of sample and X-ray fluorescence spectrometry. For example, Belarra et al[2] digested samples of poly (vinyl chloride) (PVC) by heating sample material (0.1 g) first in concentrated sulphuric acid, and then in hydrogen peroxide solution. Concentrated ammonia solution and EDTA solution were added to the cooled solution to dissolve the precipitate. Calcium, aluminium and antimony were determined by atomic absorption spectrometry. Precision varied from to 6.9 to 1.1 % RSD and recoveries were within the range 93 to 103 % m/m. Sample preparation took about 1 hour. DiPasquale et al[3] determined sulphur in polymeric materials by inductively coupled plasma emission spectrometry following sample dissolution, and obtained RSD values of less than 2 %.

Energy dispersive X-ray fluorescence spectrometry was used by Warren et al[4] to measure calcium, silicon and strontium in nylon samples, and calcium, titanium lead, barium and cadmium in PVC materials. Analysis time was much faster than the techniques above that required sample dissolution, 100 s vs. about 1 hour. Limits of detection were of the order 1 % m/m, and precision

varied from 0.5 to 10 % RSD depending on element and sample type. Samples were placed in a 30 mm diameter cup for analysis, either as nylon granules, or by cutting PVC sheet to size. Sample homogeneity was found to influence analytical performance because X-ray fluorescence signals originated from different depths of the sample depending on the element measured. For example, the critical depth (depth beyond which no significant radiation emerges) for silicon was 0.05 mm compared to 17.1 mm for strontium. The authors concluded that performance was suitable for off-line monitoring of the composition of polymeric materials in the plastics industry.

An alternative technique is direct spectrochemical analysis by laser ablation, either by direct spectral measurement of the laser-induced plasma (laser-induced plasma emission spectrometry), or by coupling to an another analytical technique. For example, laser ablation with inductively coupled plasma (ICP) - atomic emission spectrometry has been used for the survey analysis of liquid paints and polymeric materials in sheet form.[5] In situ micro-sampling and rapid elemental monitoring capabilities were demonstrated for a range of elements including aluminium, chromium, lead and titanium. Measurement times were typically 30 s. Laser ablation with ICP - mass spectrometry was applied to the determination of trace elements (Al, Si, P, Co, Zn, Sb) in plastic materials by Marshall et al.[6] Higher sensitivity than X-ray fluorescence spectrometry was demonstrated with limits of detection at the $\mu g\ g^{-1}$ level, but precision was significantly worse, ~10 % RSD. Quantitative analysis was limited in most of the above studies because of the absence of suitable standards and certified reference materials.

This study has examined the application of laser-induced plasma emission spectrometry to the rapid survey analysis of poly (vinyl chloride) (PVC) samples. Potential advantages of the technique include in situ measurement of

analyte and rapid measurement times. The small area sampled by the laser may enable samples to be tested for homogeneity of inorganic additives, and bulk analysis may be possible by ablating several sites of the sample material. The twelve elements selected to be monitored, (Al, Ba, Ca, Cu, Fe, Mg, Pb, P, Sb, Sn, Ti, Zn) are used in various chemical forms in polymeric materials. The effects of key operating parameters, (laser energy and sample position relative to the laser focal point) upon analytical performance (signal/background ratio) are characterised for antimony and calcium, and performance data for the determination of antimony, zinc and calcium in PVC samples are obtained. Part of this study has been published.[7]

4.2 Experimental

The laser-induced plasma emission spectrometry system was used as described in Chapter 2, with the blank-spectrum subtraction method and the laser fired at 5 Hz. The incremental mode of optical multichannel analyser (OMA) operation was used with time settings of zero delay time, increment time of 100 ns and an integration time of 100 ns. Two fixed time (FT) programs were also used, FT1 and FT2, with a 500 ns delay time, and a 1 μs integration time. Method FT1 consisted of firing 30 laser shots at the same spot, the emission spectrum from each shot being stored individually, i.e. 1 laser shot in each of 30 OMA memories (30 shots total). Method FT2 accumulated 5 laser shots into one memory at one sample site, and repeated this 7 times in total, with a fresh site each time, i.e. 5 laser shots in each of 7 memories (35 laser shots total). The run times for FT1 and FT2 were 6 s and 7 s respectively, with a further 25 s required for sample manipulation for FT2. Laser energy (laser flash lamp energy, LFLE) and sample position relative to the laser focal point (F-) were varied for some experiments

Three spectral windows, 237 - 262, 267 - 292 and 307 - 332 nm of centre wavelengths 250, 280 and 320 nm, respectively, were used to detect the elements selected (Al, Ba, Ca, Cu, Fe, Mg, Pb, P, Sb, Sn, Ti, Zn). The emission lines monitored are given in Table 1. In addition, two barium lines were utilised (230.423 nm and 233.527 nm) at centre wavelength 230 nm. Emission lines were identified for each spectral region from the ablation of pure materials (Table 2). Wavelength values for element emission lines were taken from standard tables.[8]

Materials

Samples of PVC were prepared by FMC Process Additives (UK) Ltd. The samples were supplied in sheet form and were identified as A to K. The elemental compositions as supplied by the manufacturer are listed in Table 3. Sample X was industrial grade PVC (Darvic), obtained locally. All samples were analysed as received with no sample preparation.

Wavelength Range (nm)					
237 - 262 nm		267 - 292 nm		307 - 332 nm	
240.549	Cu	279.553	Mg II	308.215	Al I
241.949	Sn	280.199	Pb I	308.802	Ti II
247.857	C I	280.270	Mg II	309.271	Al I
250.200	Zn II	283.306	Pb I	315.887	Ca II
250.911	C II	283.999	Sn I	317.502	Sn I
251.203	C II	285.213	Mg I	317.933	Ca II
251.743	Ti II	286.333	Sn I	322.579	Fe II
252.560	Ti II	286.426	Pb	322.775	Fe II
252.852	Sb I	287.792	Sb I	323.252	Sb I
253.401	P I			323.452	Ti II
253.565	P I			323.612	Ti II
254.480	Cu II			323.904	Ti II
255.328	P I			324.199	Ti II
255.493	P I			324.754	Cu I
255.796	Zn II			326.233	Sn I
256.253	Fe II			326.751	Sb I
259.806	Sb I			327.396	Cu I
259.881	Cu II			328.233	Zn I
261.418	Pb			328.321	Sn II
				330.259	Zn I

Table 1 List of element emission lines for each spectral region monitored in this study

Material	Details
Al	aluminium metal, BCS198e, Bureau of Analysed Standards, Newham Hall, Newby, Cleveland, UK
Ba	barium chloride powder, pressed in die into pellet, Proanalysis, May and Baker, Rhône-Poulenc, Manchester, UK
C	Spectroscopic grade solid carbon, Spectrochem, Spectro Supplies Ltd, Hornsea, UK
Ca	calcium carbonate powder, pressed in die into pellet, BDH Analar, Merck Ltd, Lutterworth, Leicestershire, UK
Cu	copper metal foil, BDH Analar
Fe	iron metal rod, Specpure, Johnson Matthey, Royston, Hertfordshire, UK
Mg	magnesium metal turnings, pressed in die into pellet, BDH Analar
Pb	lead metal sheet, BDH Analar
P	sodium phosphate powder, pressed in die into pellet, Proanalysis, May and Baker, Rhône-Poulenc
Sb	antimony metal rod, Specpure, Johnson Matthey
Sn	tin metal rod, Specpure, Johnson Matthey
Ti	titanium metal, IMI Titanium Ltd, Witton, Birmingham, UK
Zn	zinc metal, BCS194d, Bureau of Analysed Standards

Table 2 List of materials used to identify element emission wavelengths

Sample Reference	Element Composition (% m/m)											
	Al	Ba	Ca	Cu	Fe	Mg	P	Pb	Sb	Sn	Ti	Zn
A	-	-	-	-	-	-	2.6	-	4.9	0.05	-	-
B	-	0.1	6.8	-	-	-	-	-	2.8	-	-	0.1
C	z	-		-	-	z	-	3	-	-	-	-
D	-	-	0.7	-	-	-	-	3	-	-	-	-
E	3.0	-	-	-	-	-	2.6	-	-	1.0	-	-
F	0.1	0.1	0.1	-	-	0.1	2.8	0.1	0.1	0.1	0.1	0.2
G	1.0	1.0	1.0	-	-	1.0	2.8	1.0	1.0	1.0	1.0	2.0
H	10	-	-	-	-	-	-	1.0		-	-	10.0
I	-	-	-	-	-	-	-	1.0	10	-	-	10.0
J	-	10.0	-	-	-	-	-	1.0	-	10.0	-	-
K	-	10.0	-	-	-	10.0	-	1.0	-	-	10.0	-

z: may be present at trace level

frncsamp.xls

Table 3 Elemental composition of PVC samples A to K. The composition values were supplied by the manufacturer.

4.3 Results and Discussion

4.3.1 Preliminary studies

An emission-wavelength-time response, recorded with the optical multichannel analyser incremental program, is depicted in Figure 1 for the ablation of sample A (4.9 % m/m Sb, 2.6 % m/m P). The sample was ablated with laser flash lamp energy (LFLE) 40 J with the sample positioned at the laser focal point (F0), (irradiance ~ 8 x 10^{10} W cm^{-2}). The wavelength region monitored was 237 - 262 nm. The response shows the intense background continuum at early times, and the emergence of atom/ion emission at later times. Carbon ion emissions (C ion 250.9, 251.2 nm) were evident initially, and carbon atom (C atom 247.9 nm) later. The intense background signal and carbon ion emissions reflect the high temperatures of the plasma at early times, but as the plasma expanded and cooled, the background signal decayed rapidly and atomic emission lines for antimony and phosphorus became prominent. An emission-time response for selected wavelengths (Figure 2a) shows that carbon, antimony and phosphorus responses were indistinguishable from the background until 400 ns. After this, emission signals for carbon, antimony and phosphorus remained above background until about 1.5 μs. These observations enabled suitable detector settings to be obtained for time-resolved measurement of analyte signal with the OMA fixed time mode. As the background signal had reduced significantly by 500 ns, selection of a time delay of 500 ns minimised background contributions. An integration time of 1 μs was appropriate for monitoring analyte emission.

An emission-time response for this experiment repeated with maximum laser energy (LFLE 70 J, irradiance ~ 3 x 10^{11} W cm^{-2}) is depicted in Figure 2b. Element emission responses for carbon, antimony and phosphorus remained above the baseline until about 3 μs, indicating that the micro-plasma was longer lived than that produced by ablation with LFLE 40 J.

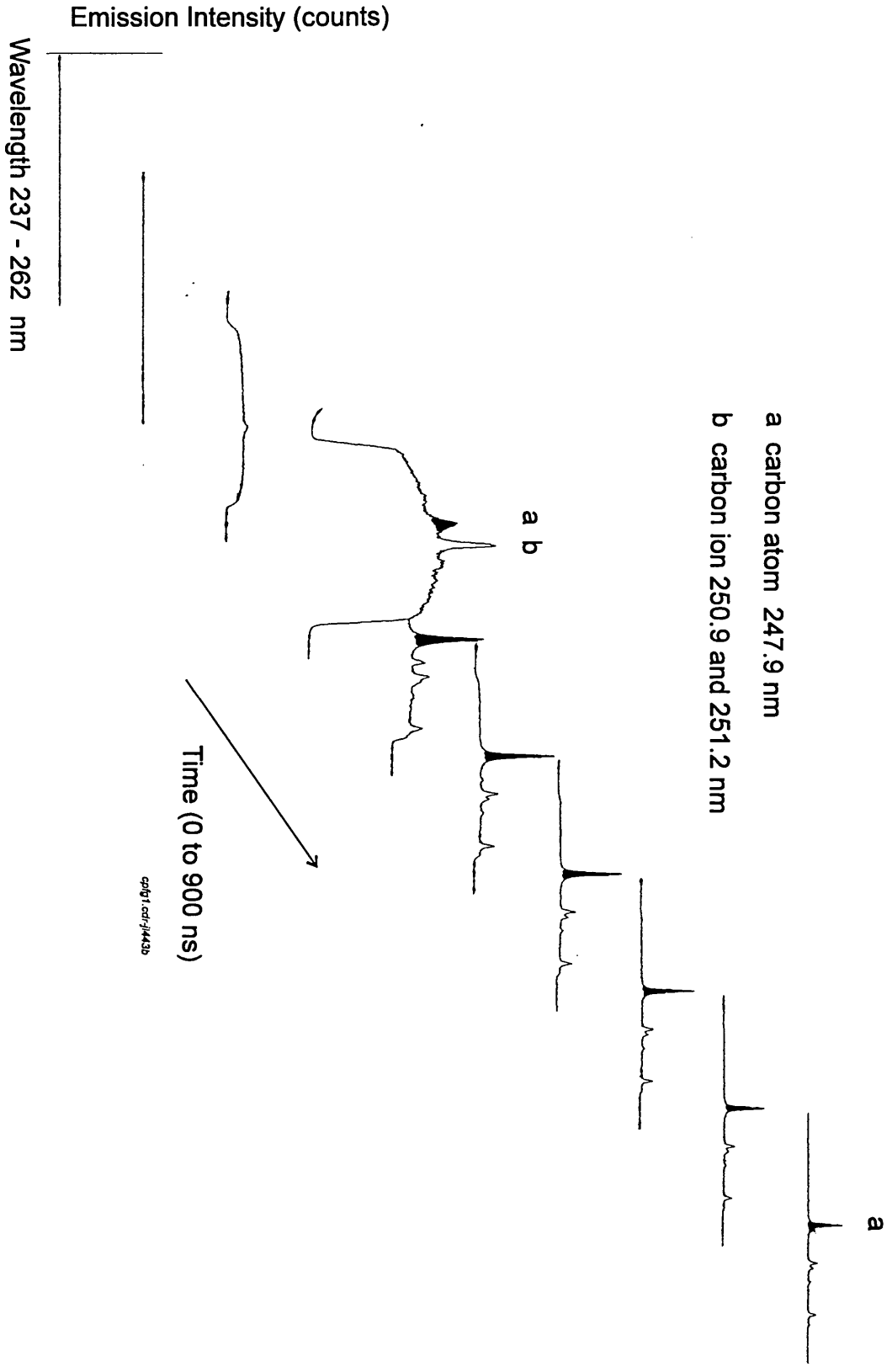

Figure 1 Emission-wavelength-time response for ablation of sample A using the incremental program, (increment time 100 ns, integration time 100 ns), with LFLE 40 J at sample position F0.

(a)

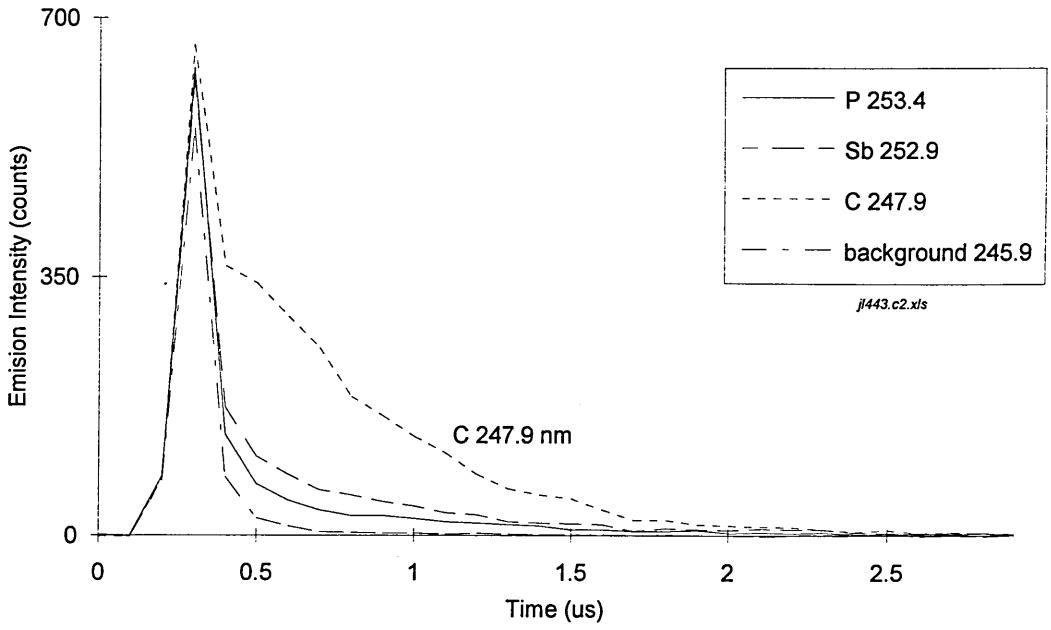

(b)

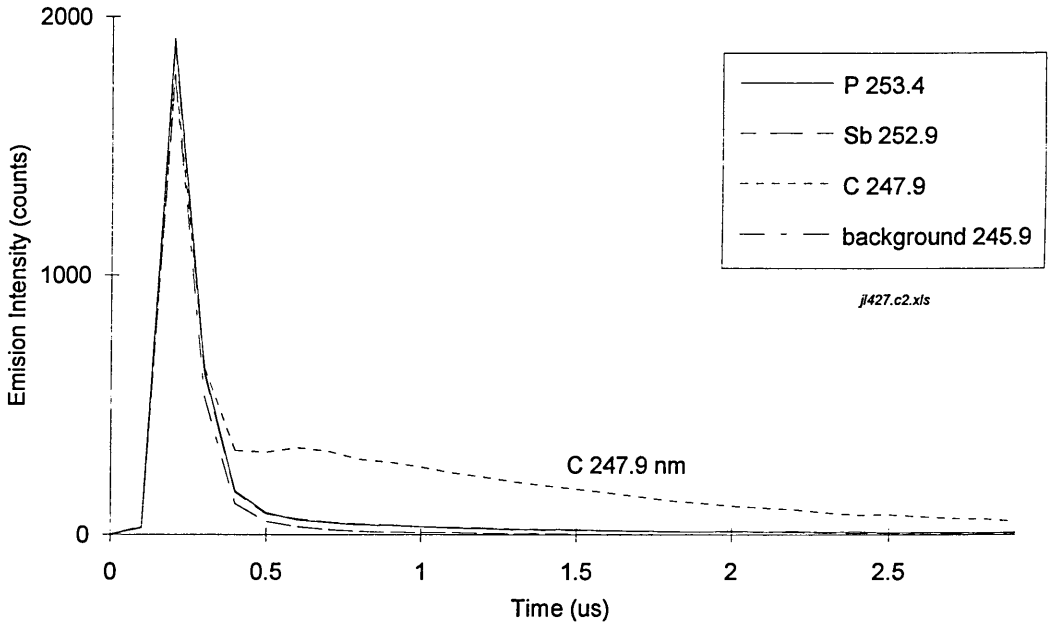

Figure 2 Emission-time profile for ablation of sample A using the incremental program, (increment time 100 ns, integration time 100 ns) at sample position F0 with laser flash lamp energy: (a) 40 J, and (b) 70 J.

Results obtained with the 307 - 332 nm spectral region for the ablation of sample B with LFLE 40 and 70 J suggested that the timing values selected above were appropriate.

There are differences between the laser ablation of polymer and metal, in particular, in the rate of material removal and the emission characteristics of the laser-induced plasma. Laser ablation of PVC samples results in a crater approximately 1 mm in diameter and 50 μm deep (10 laser shots at the same site with LFLE 40 J). A Talysurf surface analysis of a crater is shown in Figure 3. The base of the crater is relatively flat and the crater walls steep. A darkened region, about 2 mm in width, is observed around each crater. The rate of material removal is estimated to be 5 μg/laser shot, which is significantly higher than that obtained for the ablation of metal under very similar conditions, (0.45 μg/laser shot, Zn/Ni coating on steel, Chapter 5).
(The calculation for the rate of material removal is given in Appendix 1.)

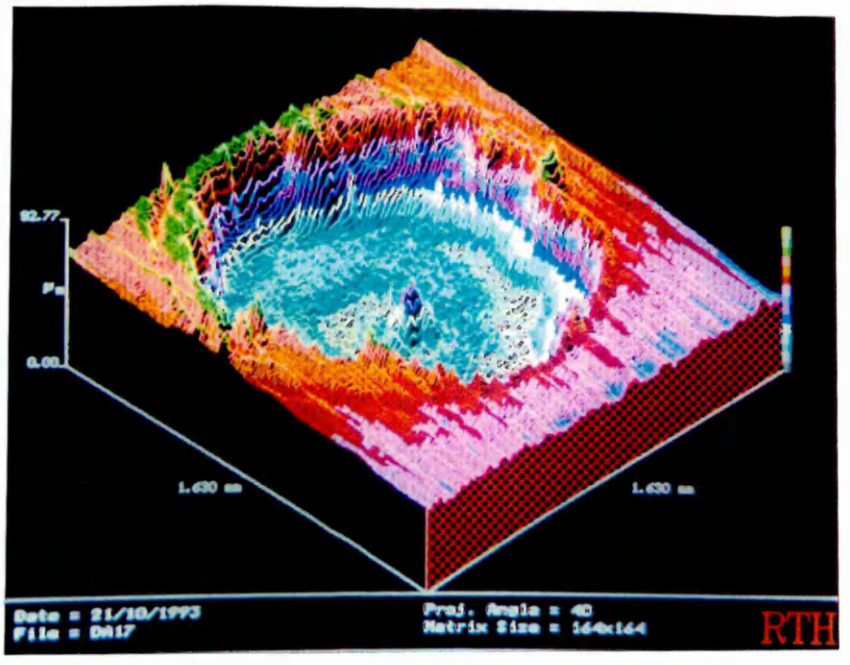

Figure 3 Three dimensional Talysurf surface analysis of crater in PVC (sample X). The x and y-axis correspond to distance across the sample surface, both 1.63 mm total. The z-axis is the vertical height, with total height 92.8 μm. The crater was produced by 10 laser shots with LFLE 40 J.

Comparing the emission-time responses for the ablation of PVC (Figure 2a) and pure copper metal (Chapter 3, Figures 7 and 11) shows that the plasma lifetime for ablation of copper metal (~35 μs) is much longer than for the polymer (~2.5 μs). Ablation conditions and measurement times were similar for both experiments. Initial intensities for the matrix elements, carbon from the polymer and copper from the metal, are similar (~ 800 counts).

The differences between ablation of polymer and metal are probably because of the difference in material properties. For ablation of metal, the free electrons of the conducting material are able to couple with the energy of the laser pulse through inverse-Bremsstrahlung processes, to produce a plasma of higher energy, electron density and temperature. This relatively energetic plasma will therefore have a longer lifetime. The plasma may shield the metal from part of the laser pulse, thereby reducing direct laser-material interaction, and reducing the amount of material removed per laser shot.

For ablation of polymer, the insulating nature of the material means that there is less coupling with the laser pulse, and therefore a less energetic plasma is induced which has a shorter lifetime. The rate of material removal is higher for the polymer because of the lower temperature needed to volatilise and decompose polymeric material compared to metal. The plasma is cooled as the relatively large amount of ablated polymer material enters the plasma, further reducing the plasma lifetime. The result is that the rate of material removal is higher and the plasma lifetime is shorter for the ablation of polymeric material compared to the ablation of metal.

4.3.2 Characterisation of operating conditions

The objective was to study the effects of operating conditions (laser energy and sample position relative to the laser focal point) upon analytical performance, and thereby obtain the conditions required for maximum sensitivity of key elements (Sb and Ca). Sample B (6.8 % m/m Ca, 2.8% m/m Sb) was ablated using fixed time method FT1 (30 laser shots at same site, delay time 500 ns, integration time 1 μs) with different laser energies (LFLE 40, 55 and 70 J) and at different sample positions (F-20, F-5, F0, F+5 and F-20). A fresh sample site was used for each experiment. The signal/background ratio was calculated for antimony 323.3 and calcium 317.9 nm for each experiment, where the background wavelength was 312.9 nm. The signal/background values are plotted in Figure 4. Maximum values of the ratio for calcium and antimony were obtained at F0 with LFLE 40 J. Although the analyte emission intensities were more intense with the higher laser energies, the background intensites were also more intense, resulting in maximum signal/background values at low laser energy, LFLE 40J. These conditions were adopted for subsequent studies.

Sample positions of F-5 and F-20 also produced similar results for antimony with this laser energy. Initial studies, as reported,[7] suggested that sample position F-0.5 gave improved performance, but the more detailed study here found no significant differences between F-0.5 and F0. The timing values (delay and integration) used for this experiment were selected for LFLE 40 J ablation. Sensitivity increased a little when the integration time for LFLE 70 J was increased from 1 to 2 μs to take advantage of the longer plasma lifetime (Figure 2b). However, the increase was small and LFLE 40 J at sample position F0 still produced maximum sensitivity.

(a)

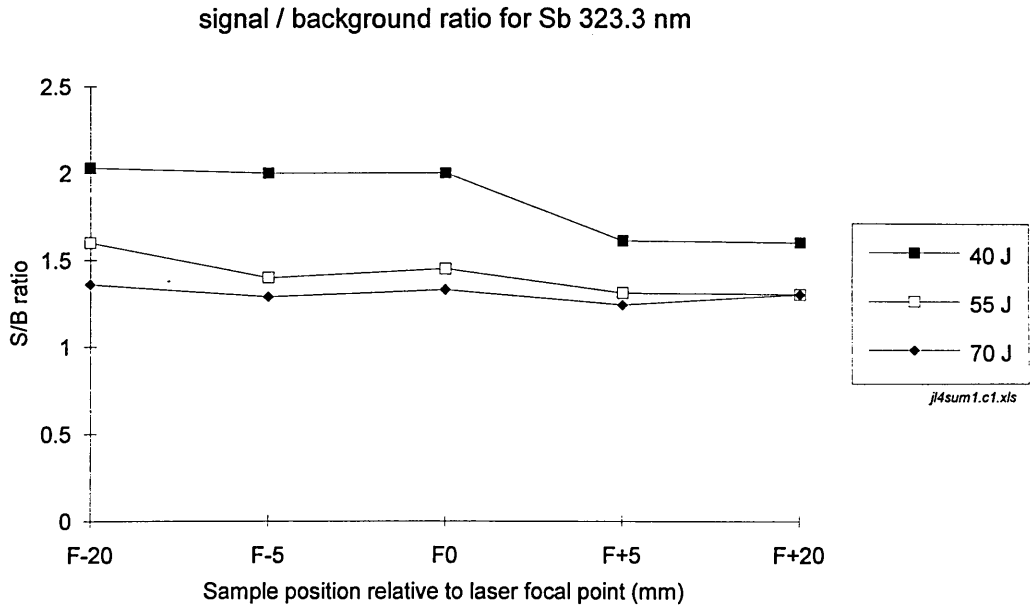

(b)

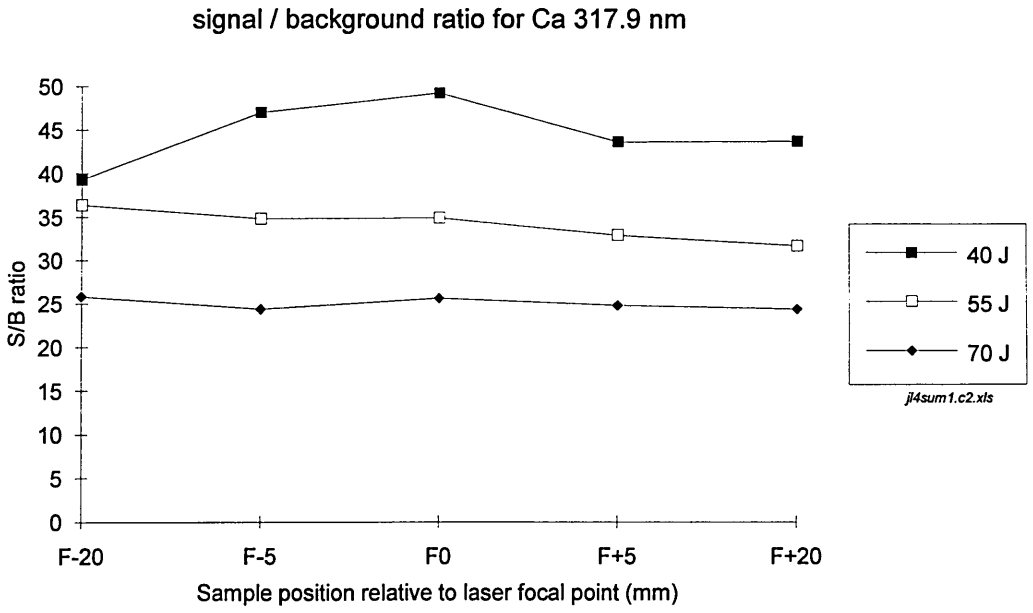

Figure 4 Plot of signal/background ratios obtained for ablation of sample B with different laser energies and sample positions relative to laser focal point; (a) Sb 323.3, and (b) Ca 317.9 nm. The background wavelength was 312.9 nm.

In the case of transparent polymeric samples, no emission signals were obtained when material was ablated at F0 with LFLE 40 J. Faint tunnelling through the material and ablation of the metal support underneath the sample were observed, suggesting that a plasma was not induced on the surface of the polymer, and the laser light was transmitted through the plastic to the metal. The tunnelling was due to the self-focusing of the laser beam within the material, which trapped the light and prevented it from spreading, to produce a waveguide.[9] This was not evident in the opaque samples because the laser light was absorbed leading to ablation and production of the laser-induced plasma. When the transparent sample was moved away from the laser focus position, e.g. F+5, emission signals and laser damage on the sample surface were obtained. The plasma was induced in the air above the sample surface, and the plasma was responsible for volatilising sample material and creating the crater. As the PVC samples in this study were opaque, the conditions identified above (LFLE 40 J and F0) were adopted.

A further consideration was the effect of repetitive laser firing upon performance, i.e. the number of laser shots at a given site. Emission-time responses for the ablation of sample A with fixed time methods FT1 (30 shots at same site) and FT2 (5 shots at each of 7 sites) are depicted in Figure 5. With method FT1, the antimony responses were not similar throughout the experiment, although the carbon, phosphorus and background responses were reasonably constant. The intensity of both antimony signals increased initially, then decreased until about memory number 8, after which a relatively constant signal was observed. In contrast, all emission responses were fairly constant with method FT2. Preliminary calibrations indicated that the emission response for antimony was not linear with concentration with method FT1 although the response for calcium was linear. Method FT2, however, produced linear responses for calcium and antimony. A probable explanation is that the

antimony in the vicinity of the laser spot was selectively volatilised during the first few laser shots, possibly through formation of volatile antimony chloride, leading to a depletion of antimony for the remaining shots. The effect was not due to higher concentration levels of antimony at the surface as similar emission responses were obtained from the ablation of material beneath the sample surface. The effect was also observed for the antimony emission lines in the 307 - 332 nm wavelength region. Reasonably constant signals for carbon, phosphorus and calcium were obtained by FT1, suggesting that these elements were not selectively volatilised and it was still possible to make representative measurements after firing 30 laser shots at the same site.

Method FT2 was selected for subsequent use because the effects of antimony volatilisation were minimised, and FT2 provided improved analytical performance compared to method FT1. Data are shown in Table 4. Precision (% relative standard deviation, % RSD) improved from 13.6, 16.0 and 11.0 (FT1) to 6.9, 7.1 and 7.3 (FT2) for carbon, antimony and phosphorus, respectively, and the signal/noise ratios for antimony and phosphorus increased from 20.6 and 16.2 to 746 and 250, respectively.

	Method FT1	Method FT2
Number of shots per site	30	5
% RSD C 247.8 nm	13.6	6.9
% RSD Sb 252.9 nm	16.0	7.1
% RSD P 253.4 nm	11.0	7.3
S/N (Sb 4.9 % m/m)	20.6	746
S/N (P 2.6 % m/m)	16.2	250
n for statistical calculation	30	7

Table 4 Comparison of data from fixed time methods FT1 and FT2 for the ablation of sample A

(a)

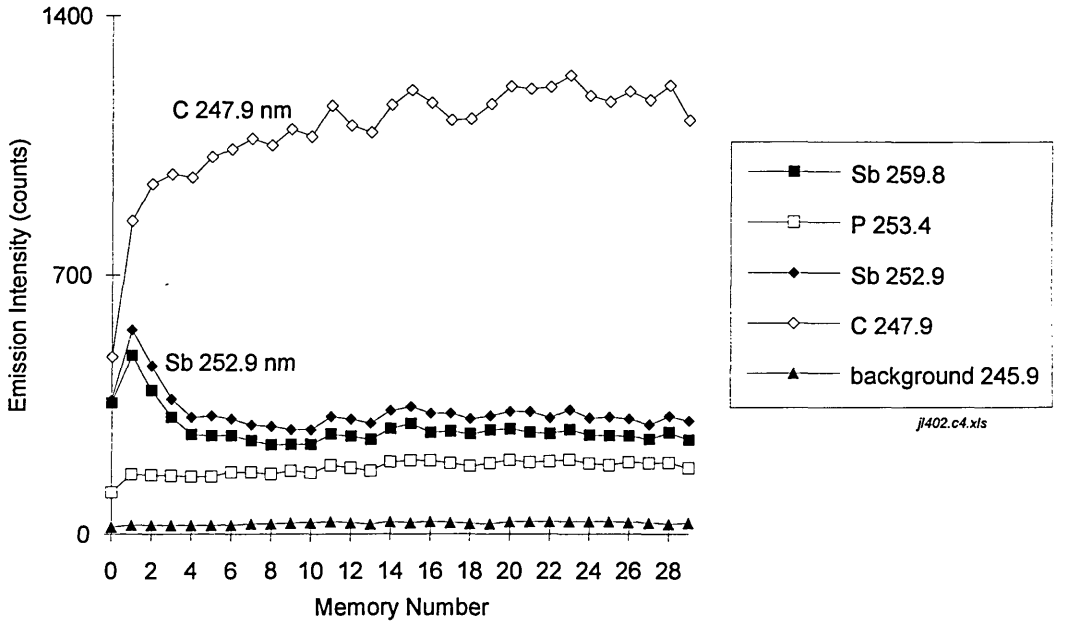

(b)

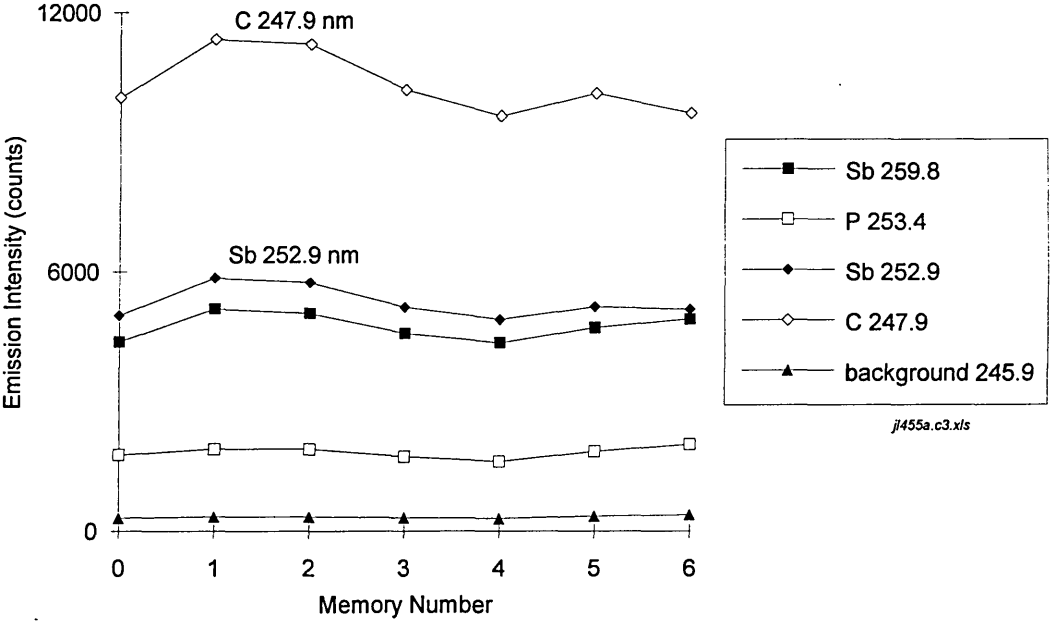

Figure 5 Emission-time profile for ablation of sample A with fixed time programs: (a) FT1, 30 shots at same sample site; (b) FT2, 5 shots in each memory, 7 memories, fresh site each memory.

4.3.3 Analytical performance

Full quantitative measurement of inorganic additives in polymeric materials is considered to be difficult because of the absence of suitable certified reference materials necessary to prepare calibration graphs. Quantitative measurements in this work were based on using characterised samples as calibration standards. The operating conditions used were as identified above, LFLE 40 J, sample position F0 and method FT2 (5 laser shots at each of 7 fresh sample sites). An emission-wavelength-memory number response (Figure 6) for ablation of sample A clearly indicates good repeatability for successive laser firings. The emission-time response for this experiment is shown in Figure 5b. Results suggest that the sample is relatively homogenous, and indicate that the technique can be used for bulk analysis to check for sample heterogeneity.

Performance data are given in Table 5. Typical values for precision (% relative standard deviation, % RSD) were 7.3, 5.6 and 3.2 for antimony 252.9, calcium 317.9 and zinc 330.3 nm, respectively. Precision improved from 7.3 to 1.8 for antimony 252.9 when the carbon signal (C atom 247.86 nm) from the polymer matrix was used as an internal standard. This internal standard can only be used for element emission signals that are within a spectral region that contains a carbon emission signal, e.g. 237 - 262 nm.

Element		Wavelength (nm)	Limit of Detection (% m/m)	% RSD
Ca		317.9	0.04	5.6
Zn		330.3	0.07	3.2
Sb		252.9	0.09	7.3
Sb / C *	Sb	252.9	--	1.8
	C	247.9		

Table 5 Analytical performance data for Sb, Ca and Zn in PVC samples. Operating conditions were LFLE 40 J, sample position F0 with 5 laser shots in each of 7 memories, fresh sample site each memory (method FT2).

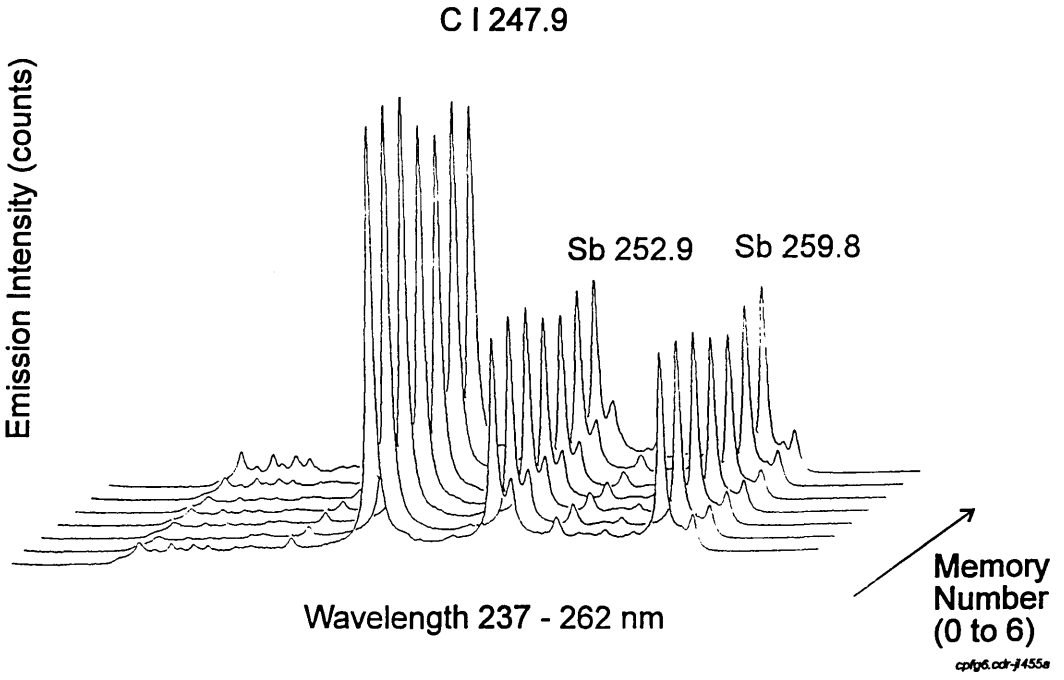

Figure 6 Emission-wavelength-memory number response for the ablation of sample A at sample position F0 with LFLE 40 J and 5 laser shots in each of 7 memories, fresh sample site each memory (method FT2).

Linear calibration graphs, shown in Figures 7 and 8, were generated for calcium 317.9, zinc 330.3 and antimony 252.9 nm for up to 10 % m/m of each element. The line for calcium was a straight line, ($y = 320.2x + 29.7$, correlation coefficient 0.9985) and the lines for antimony and zinc were curves. The line for antimony was improved (Figure 8b), i.e. was less curved, when the ratio of antimony to carbon 247.9 nm was plotted, indicating that the use of an internal standard can provide better performance. The curvature of the antimony and zinc lines suggests that there was some enhancing effect for the responses of zinc and antimony at higher concentrations. The ablation efficiency was possibly higher when these elements were present in the polymer at greater concentrations, leading to increased mass removal per laser shot and enhanced analyte emission responses. This effect was partly corrected for for antimony by using the carbon signal from the polymer matrix as internal standard.

Limits of detection based on 3σ (measurement of blank PVC sample) were estimated at 0.09, 0.04 and 0.07 % m/m for antimony 252.9, calcium 317.9 and zinc 330.3 nm, respectively. The limits of detection are similar to values obtained for elements in steel (Ni, Cr, Si and Mn) by Cremers et al [9] using LIPS.

Ca

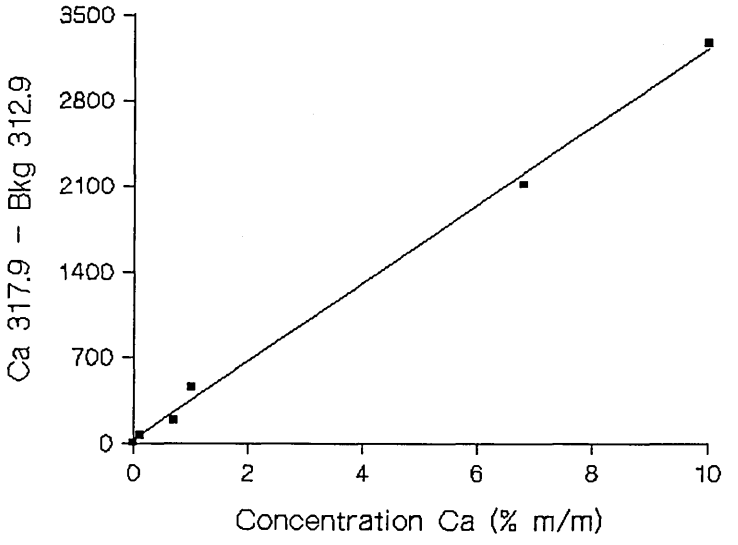

zinc

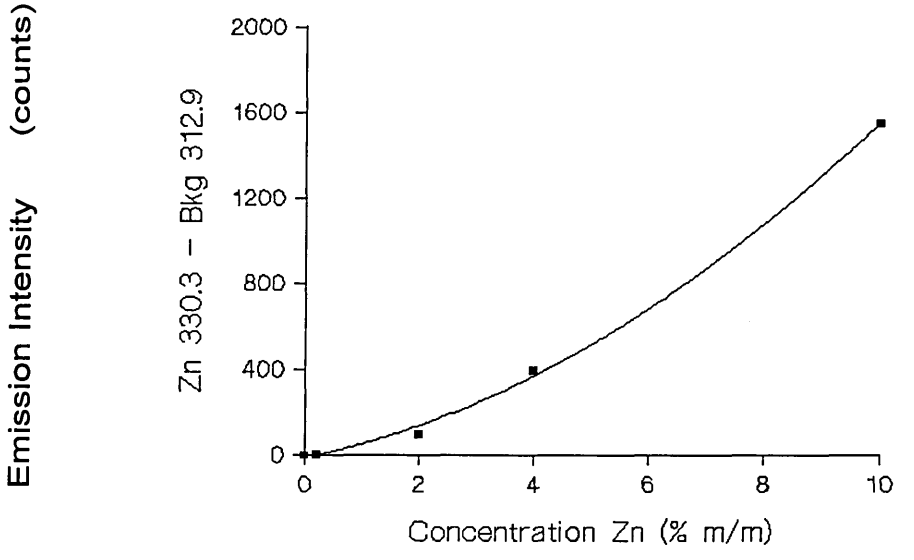

Figure 7 Calibration graphs for Ca and Zn in PVC samples using laser-induced plasma emission spectrometry.

(a)

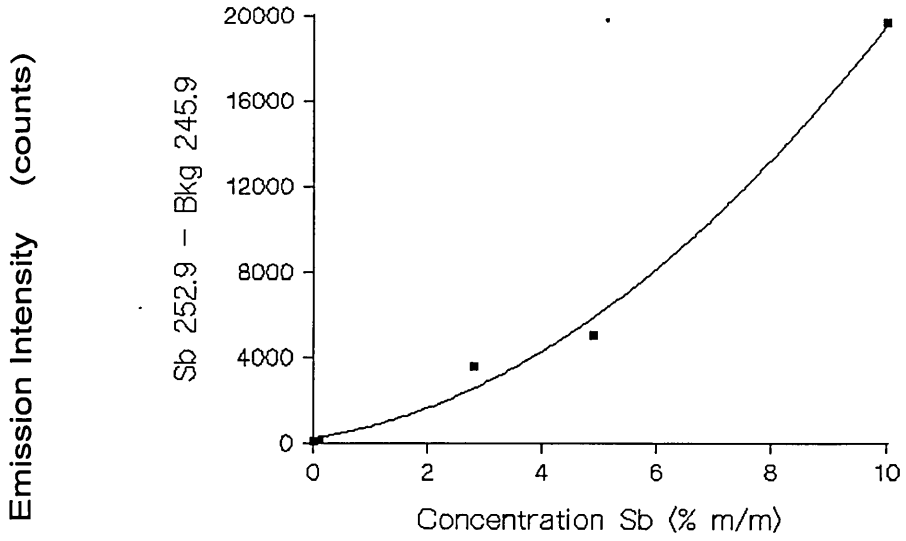

(b)

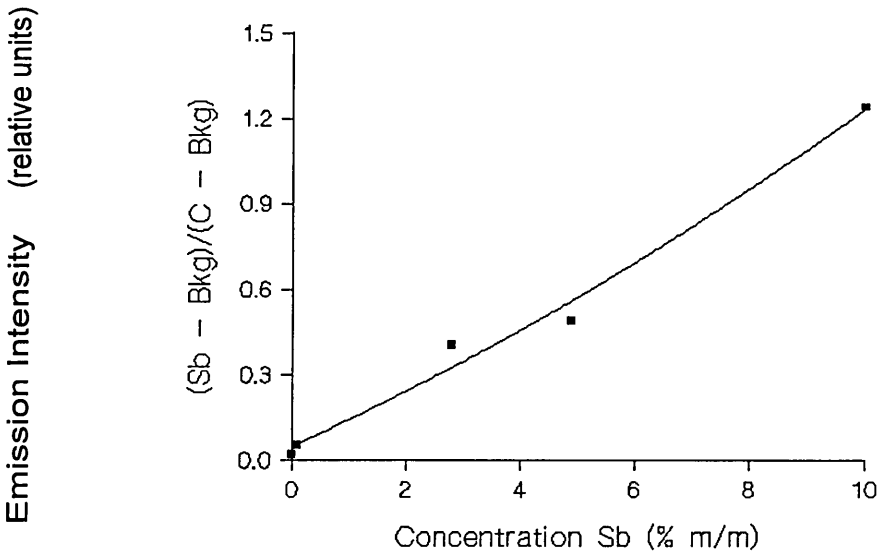

Figure 8 Calibration graphs for Sb in PVC samples using laser-induced plasma emission spectrometry; (a) Sb 252.9 - background 245.9 nm, (b) using a carbon signal from the polymer matrix as internal standard,
(Sb 252.9 - background 245.9) / (C 247.9 - background 245.9)

4.3.4 Survey analysis

To demonstrate the rapid analysis capability of laser-induced plasma emission spectrometry, the range of PVC samples listed in Table 3 was examined. The composition values quoted were supplied by the manufacturer. Spectra from four samples (A, B, D and E) are shown in Figure 9 for three spectral regions. Samples A and B are clearly seen to contain antimony, as the emission lines for antimony are identified within all three spectral windows for both samples. The greater emission intensity for A compared to B indicates the higher concentration present in A (Sb: A, 4.9 % m/m; B, 2.8 % m/m). Tin and phosphorus are present in sample A (P 2.6 % m/m, Sn 0.05 % m/m). Calcium emission lines are evident in samples B and D, the greater emission intensity of B indicating the higher concentration present (Ca: B, 6.8 % m/m; D, 0.4 % m/m). Emission lines of magnesium lines were observed for all four samples. Barium was detected in sample B (Ba: 0.1 % m/m), the barium emission lines (230.423 nm and 233.527 nm) are not shown in Figure 8. Lead (3.0 % m/m) is present in sample D, and aluminium, phosphorus, tin and zinc are evident in E. Iron and copper were not detected in the samples tested here.

The technique can rapidly differentiate between samples by the inorganic content without the need for time-consuming sample dissolution with associated possible loss of volatile elements. Each spectrum was acquired in 1 s and so it took about 3 s to examine each sample (excluding sample manipulation time). In comparison, similar testing by energy dispersive X-ray fluorescence took 100 s, and required a minimum sample size of 30 mm diameter and ~17 mm thickness. Testing by laser-induced plasma emission spectrometry was possible on small samples only ~5 mm in diameter and 2 mm thick. The small sample site enables sample material to examined for localised homogeneity. The results indicate that laser-induced plasma emission spectrometry can be used for rapid survey analysis of polymeric materials.

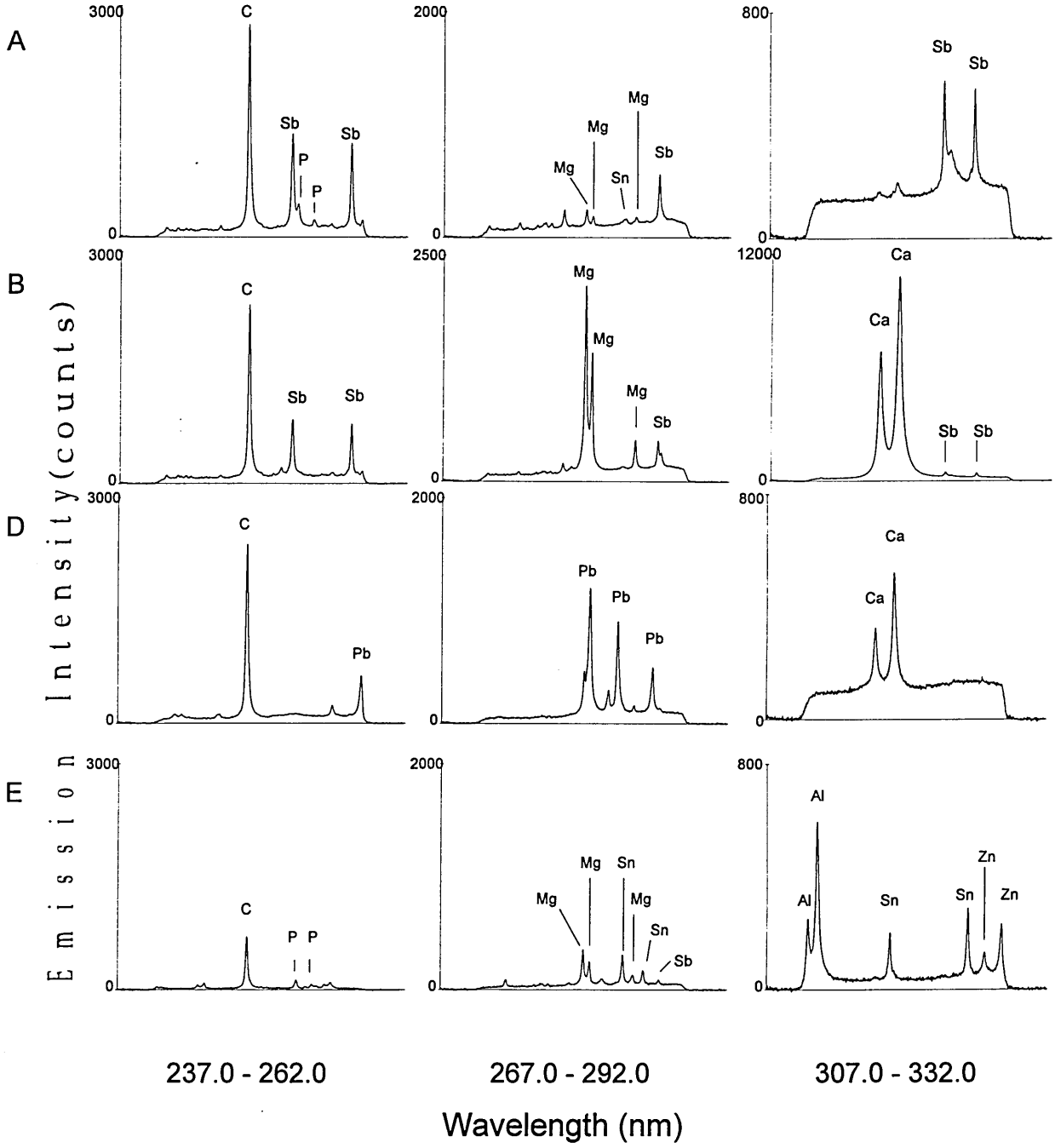

Figure 9 Laser-induced plasma emission spectra from samples A, B, D and E. Spectra were recorded with fixed time method FT2 and emission wavelengths are given in Table 1.

4.4 Conclusions and Recommendations for Further Work

The laser ablation of polymeric materials was found to be different from that of metals. The lifetime of the plasma was shorter and rate of material removal was higher for the ablation of polymer, and were attributed to differences in the properties in the two types of material. Samples of poly (vinyl chloride) were successfully monitored for a range of twelve elements (Al, Ba, Ca, Cu, Fe, Mg, Pb, P, Sb, Sn, Ti and Zn). The study examined the effects of operating conditions (laser energy and sample position relative to the focal point) upon analytical performance (signal/background ratio), and obtained improved performance at relatively low laser energy (laser flash lamp energy 40 J) with the sample positioned at the laser focal point. Selective volatilisation of antimony was found to interfere with the determination of this element when a relatively large number of laser shots (30) was directed at the same sample site. The effect was minimised by using a smaller number of laser shots (5) at 7 fresh sample sites. This method also provided improved analytical performance in terms of precision and sensitivity.

Full quantitative measurement was limited by the availability of characterised samples. Limits of detection and precision were obtained for key elements (Ca 0.04, Zn 0.07, Sb 0.09 % m/m) and linear calibration graphs were achieved for these elements to 10 % m/m. Precision (% relative standard deviation) improved from 7.3 to 1.8 for antimony when the carbon signal from the polymer matrix was used as an internal standard. The speed of analysis, compactness of instrumentation and simplicity of operation suggest that the technique has the potential for compositional monitoring of polymeric materials in industrial processes, such as manufacture and recycling. Compared to energy dispersive X-ray fluorescence, the technique is considerably faster (1 vs. 100 s), requires a smaller sample size, and is more sensitive (limit of detection 0.09 vs. estimated 1 % m/m).

Calibration and performance data for all twelve elements could be obtained with further work if suitable characterised standards could be obtained. The range of elements could be extended to include other elements of interest to the polymer industry, bromine, chlorine, silicon, cadmium, sulphur and bismuth. The use of carbon as an internal standard could be applied to other elements if other carbon lines could be used, or if a larger wavelength region could be monitored around a suitable carbon emission line. Further work could utilise a lower resolution spectrometer grating to achieve this, and examine, for each element, the effects of using an internal standard upon performance. Possible spectral interferences would need to be considered if a lower resolution spectrometer was to be used. Further studies could investigate the effects of other operating parameters, such as type and pressure of buffer gas. Improved performance might be realised with a reduced pressure of argon buffer gas, as reported by Niemax et al[10] for the determination of silicon and chromium in steel.

4.5 References

1. Gächter R. and Müller H., *Plastic Additives Handbook*, Hanser, New York, USA., 1983.
2. Belarra M. A., Gallarta F., Anzano J. M. and Castillo J. R., Journal of Analytical Atomic Spectrometry, 1986, 1, 141-144. Determination Of Metals In Poly (vinyl chloride) By Atomic Absorption Spectrometry
   Part 1. Determination Of Calcium, Aluminium and Antimony In Samples Of Poly (vinyl chloride) With A High Content Of Alkaline Earths.
3. DiPasquale G. and Casetta B., Atomic Spectroscopy, 1984, **5**, 209.
   ICP Determination Of Sulphur In Polymeric Materials.
4. Warren P. L., Farges O., Horton M. and Humber J., Journal of Analytical Atomic Spectrometry, 1987, **2,** 245-248. Role Of Energy Dispersive X-ray Fluorescence Spectrometry In Process Analysis Of Plastic Materials.

5. Booth P. K. and McLeod C. W., Mikrochimica Acta, 1989, **3**, 283-289. Rapid Survey Analysis of Polymeric Materials by Laser Ablation-Inductively Coupled Plasma Spectrometry. An Analytical Note.
6. Marshall J., Franks J., Abell I. and Tye C. J., Journal of Analytical Atomic Spectrometry, 1991, **6** (2), 145-150. Determination of Trace Elements in Solid Plastic Materials by Laser Ablation-Inductively Coupled Plasma Mass Spectrometry.
7. Anderson D. R., McLeod C. W. and Smith A. T., Journal of Analytical Atomic Spectrometry, 1994, **9** (2), 67-72. Rapid Survey Analysis of Polymeric Materials Using Laser Induced Plasma Emission Spectrometry.
8. Harrison G. R., *Wavelength Tables with Intensities in Arc, Spark or Discharge Tube*, M.I.T. Press, Cambridge, Mass., USA, 1969.
9. Ready J. F., *Effects of High Power Laser Radiation*, Academic Press, New York, 1971.
10. Niemax K., Leis F., Sdorra W. and Ko J. B., Mikrochimica Acta, 1989, **2**, 4-6, 185-199. Basic Investigation for Laser Micro Analysis: 1. Optical Emission Spectrometry of Laser-Produced Sample Plumes.

5.1 Introduction

In the previous chapters, studies have investigated laser-induced plasma emission spectrometry for the bulk chemical analysis of metal alloys and polymeric materials. The technique also has a micro-analysis capability which was used to test the homogeneity of inorganic additives in samples of polymeric materials. This chapter applies the micro-analysis capabilty to the depth profile measurement of coatings deposited on steel substrates. Coatings are widely used in industry to give enhanced properties to materials. For example, metallic coatings such as zinc, nickel and chromium are applied to steel to provide resistance to corrosion for products ranging from car bodies to oil rig structures.[1] Improved resistance to wear in abrasive environments, such as drill bits and scissors, can be achieved with the use of hard coatings such as titanium nitride, and zirconium nitride.[2] In the jewellery and electronics industries, gold coatings are used for cosmetic or electrical purposes.

The quality of these coatings can be investigated by a number of techniques depending on the information required. Techniques such as Auger and X-ray photoelectron spectroscopy have been utilised to study surface chemistry on the atomic scale, and can be used to probe into the coating by removing material through ion bombardment to yield depth profile data.[3] Thicker coatings can be measured mechanically with ball cratering methods, and analytically using X-ray spectrometry and Rutherford backscattering techniques. Glow discharge optical emission spectrometry (GD-OES)[4] and glow discharge mass spectrometry (GD-MS)[5,6] have been used to measure coatings over the thickness range 0.01 μm to over 50 μm. The quantitative aspects of GD-OES have been reported by Bengtson[7] and both techniques are now widely accepted. Measurement times are about 15 minutes with depth resolution typically around 100 nm and crater diameter of ~10 mm. An improved measurement technique would be more rapid (seconds vs. minutes) and

examine smaller areas to provide higher spatial resolution. The base of the crater produced by the depth profile should be as flat as possible so that good depth resolution is achieved.

This study considers the feasibility of utilising laser-induced plasma emission spectrometry (LIPS) for the depth profiling of coatings. Possible advantages when compared to glow discharge techniques include small crater size, ~1 mm diameter, and rapid analysis time, ~40 s. The application of LIPS to depth profiling has been limited and is discussed in Chapter 1. In this study, a pulsed Nd:YAG laser is fired repetitively at the same site to erode the coating and then ablate the substrate. The laser-induced plasma from each laser shot is discreetly monitored by a gated photodiode array spectrometer system to yield an emission-wavelength-time signature, i.e. depth profile.

The aim of the investigation is to evaluate the capability of laser-induced plasma emission spectrometry to depth profile metallic coatings over a range of coating thickness, i.e. to measure the coating thickness, and to provide information about the distribution with depth of the components of the coating. The influence of key operating conditions on signatures is characterised for zinc/nickel coatings in order to obtain suitable operating conditions. Depth profile performance is established for zinc/nickel and tin coatings over a coating thickness range of 0.38 to 7.2 μm. The technique is also applied to a titanium nitride coating and the detection of an ultra-thin chromium coating (20 nm). Detailed depth profile studies with laser-induced plasma emission spectrometry are reported here for the first time and part of this work has been submitted for publication.[8]

5.2 Experimental

The laser-induced plasma emission spectrometry system was used as described in Chapter 2 with the blank-spectrum subtraction method and the laser fired at 5 Hz. A fixed time OMA program was utilised with time settings of time delay 1.5 μs and integration time 1 μs. Two main operating parameters were varied to obtain optimum conditions for depth profile measurement: the laser energy, by changing the laser flash lamp energy (LFLE); and the sample position relative to the laser focal point, which affected the amount of laser defocusing and consequently the laser irradiance. This was achieved by positioning the sample at different distances from the laser focal point, expressed as F±x, where x was the distance in mm from the laser focal point, and the - or + sign indicated either towards, or away from, the laser source.

Materials

A series of samples with different coatings over a range of coating thickness was examined in the study, (Table 1). Samples of low alloy steel with different coatings were prepared at British Steel Technical, Swinden Laboratories, Rotherham, UK. The zinc/nickel coating contained 13% m/m nickel and was deposited by a hot-dip process. The thickness of each tin coating, electrolytically deposited, was calculated from the coating weight (Appendix 1). A low alloy steel reference standard was used as an uncoated blank (BAS SS401, Bureau of Analysed Standards, Newby Hall, UK). A sample of stainless steel (AISI-340) with a coating of titanium nitride deposited by physical vapour deposition (PVD) was prepared by G. Williams (Materials Research Institute, Sheffield Hallam University). Sample Zn-A was hot-dipped galvanised steel (coating: Zn metal with minor levels of Al and Pb), supplied by A. Bengtson (Swedish Institute for Metals Research, Stockholm, Sweden). Samples were rinsed in acetone and air dried prior to use.

Sample Reference	Coating	Coating Thickness (μm)	Coating Weight (gm^{-2})
P1	Zn/Ni	2.7	-
P2	Zn/Ni	2.7	-
P4	Zn/Ni	2.7	-
P5	Zn/Ni	5.0	-
P6	Zn/Ni	7.2	-
Sn1/1	Sn	1.48	10.8
Sn3/1	Sn	0.82	6.0
Sn1/2	Sn	0.58	4.2
Sn4/1	Sn	0.49	3.6
Sn4/2	Sn	0.47	3.4
Sn3/2	Sn	0.44	3.2
Sn5/1	Sn	0.38	2.8
Cr-1	Cr	0.020	-
TiN-1	TiN	2.0	-
Zn-A	Zn	8.0	-

Note: the coating thickness of the tin samples was calculated from the coating weight (the calculation is given in Appendix 1)

Table 1 Details of the coated samples used in the depth profile studies.

5.3 Results and Discussion

5.3.1 Preliminary studies

The feasibility of depth profile measurement using laser-induced plasma emission spectrometry was examined in preliminary studies with zinc/nickel coatings. Three spectral regions were identified that encompassed strong emission lines for zinc and nickel and iron: 237 - 262, 287 - 312, and 307 - 332 nm. Initial studies with sample P2 (zinc/nickel coating thickness 2.7 μm) showed that an experiment consisting of 200 laser shots with maximum laser energy (laser flash lamp energy, LFLE 70 J) was sufficient to ablate through the coating and obtain strong element emission responses from the iron of the steel base. This was achieved by accumulating 5 laser shots/scans of the detector array into 1 memory of the optical multichannel analyser (OMA); 40 memories were used to record 200 laser shots. With the laser firing at 5 Hz, the experiment run time was 40 s. The sample was ablated at the laser focal point (sample position F0) with laser flash lamp energy (LFLE) 70 J.

Spectra for the ablation of sample P2 at the three spectral regions are depicted in Figures 1a, 1b, and 1c. Each figure depicts a spectrum from memory 0 (laser shots 1-5) and from memory 39 (laser shots 196-200). Useful information about the coating and ablation process can be gained from examination of these spectra. For each spectral region, zinc and nickel lines were evident for the first spectrum (laser shots 1 - 5) and there were no responses for iron. The absence of iron indicated that the surface of the coating did not contain iron, either as a contaminant of the zinc/nickel alloy, or from diffusion of iron from the substrate, and that the laser had not penetrated through the coating into the steel substrate in the first 5 laser shots.

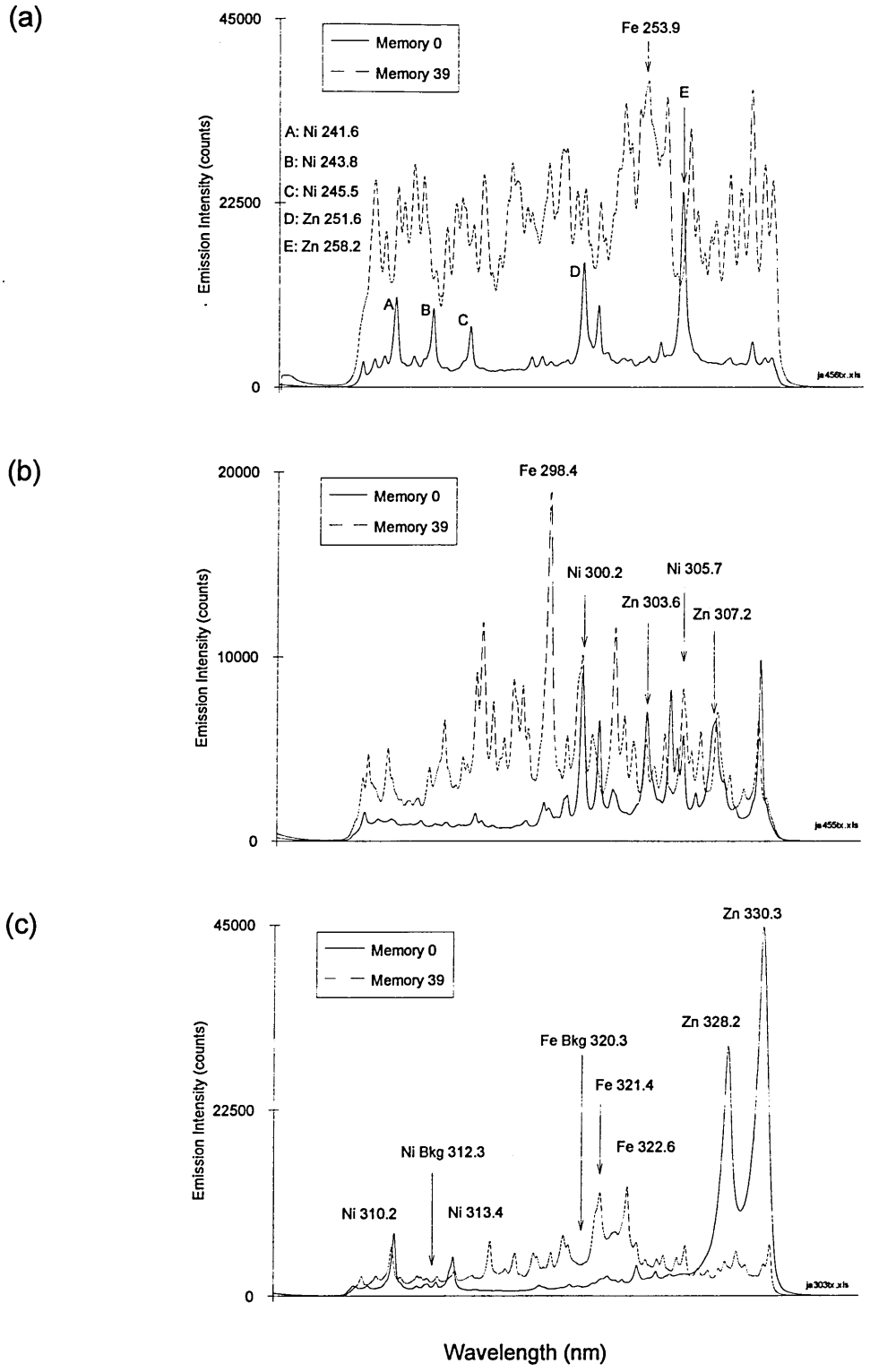

Figure 1 Overlay of spectra for the ablation of Zn/Ni coating on steel (sample P2, coating thickness 2.7 μm) with LFLE 70 J at sample position F0. Emission wavelengths (nm). Memory 0: laser shots 1-5. Memory 39: laser shots 196-200. Spectral regions are: (a) 237-262, (b) 287-312, (c) 307-332 nm.

The last spectrum (laser shots 196-200) for each spectral region contained strong emission lines for iron, which showed that ablation of the substrate had been achieved. This spectrum for the spectral region 307 - 332 nm contained minimal responses for zinc and nickel, which indicated that the coating had been removed. This was not particularly clear for the last spectrum within spectral regions 237 - 262 and 287 - 312 nm (Figures 1, 2) because of spectral interference problems discussed below.

The spectral region 237 - 262 nm (Figure 1a) showed an intense increase in background signal between ablation of the zinc/nickel coating (memory 0) and the steel substrate (memory 39). This was because of the large number of iron emission lines present in this region, which caused an increase in the spectral baseline. This region was not selected as the zinc and nickel emission lines were effectively swamped by the iron signals when ablation of the substrate commenced. The spectral region 287 - 312 nm (Figure 1b) was not selected because the zinc emission lines suffered from spectral interference from iron emission lines.

The spectral region 307- 332 nm (Figure 1c) was therefore selected for use in the study of all the zinc/nickel and zinc coated samples because emission lines for nickel, zinc and iron were relatively free from interference either from the background or from other emission lines. Aluminium was also monitored in this wavelength region for sample Zn-A. Emission wavelengths with the corresponding detector pixel position are listed in Table 2. The last spectrum within this region had a higher background level because the spectrum was predominantly iron from the ablation of the steel compared to memory 0 which was mainly zinc that has a lower background spectrum. To observe the behaviour of the background during the profile measurement, two wavelengths

(312.3 and 320.3 nm) close to nickel and iron lines were selected and monitored, (Table 2, Figure 3).

An emission-wavelength-time response for the ablation of sample P2 is depicted in Figure 2. Nickel and zinc emissions were observed during the removal of the coating until memory 9, after which these emission intensities decreased and signal responses for iron commenced. An emission-time response (depth profile) was constructed by plotting specific emission and background wavelengths against memory number (time), (Figure 3a). The zinc emission signals were very intense and the zinc values were therefore divided by 10 in order to obtain a response with all the signal responses on the same scale. The responses depicted in Figures 2 and 3a show that the zinc emission signal was reasonably constant until memory 9, (50 laser shots), after which it decreased sharply. The emission intensity for nickel increased during the removal of the coating which suggested that the nickel content of the coating was not uniform with depth. The iron signal increased after about memory 6 and became reasonably constant after about memory 15. This suggested that about 30 laser shots were required to ablate through the coating. The region in which the iron increased and the zinc and nickel decreased (memory 9 to 18) corresponds to an interface region between the coating and the substrate. The background intensity also increased within the interface region and is discussed in the next section.

Wavelength (nm)	Element	Pixel Number	
309.271	Al I	185	m
310.155, 310.188	Ni I, I	212	
312.3	Ni Background	280	m
313.411	Ni I	315	m
320.342	Fe Background	539	m
321.321* 321.404 *	Fe II, I	572	
322.638* 322.672 *	Fe II, I	619	m
328.233	Zn I	794	
330.259	Zn I	856	m

* unresolved emission lines m = monitored for emission-time response

Table 2 List of main element emission lines used in the study of Zn/Ni and Zn coatings. The spectral region was 307-332 nm, (centre wavelength 320 nm).

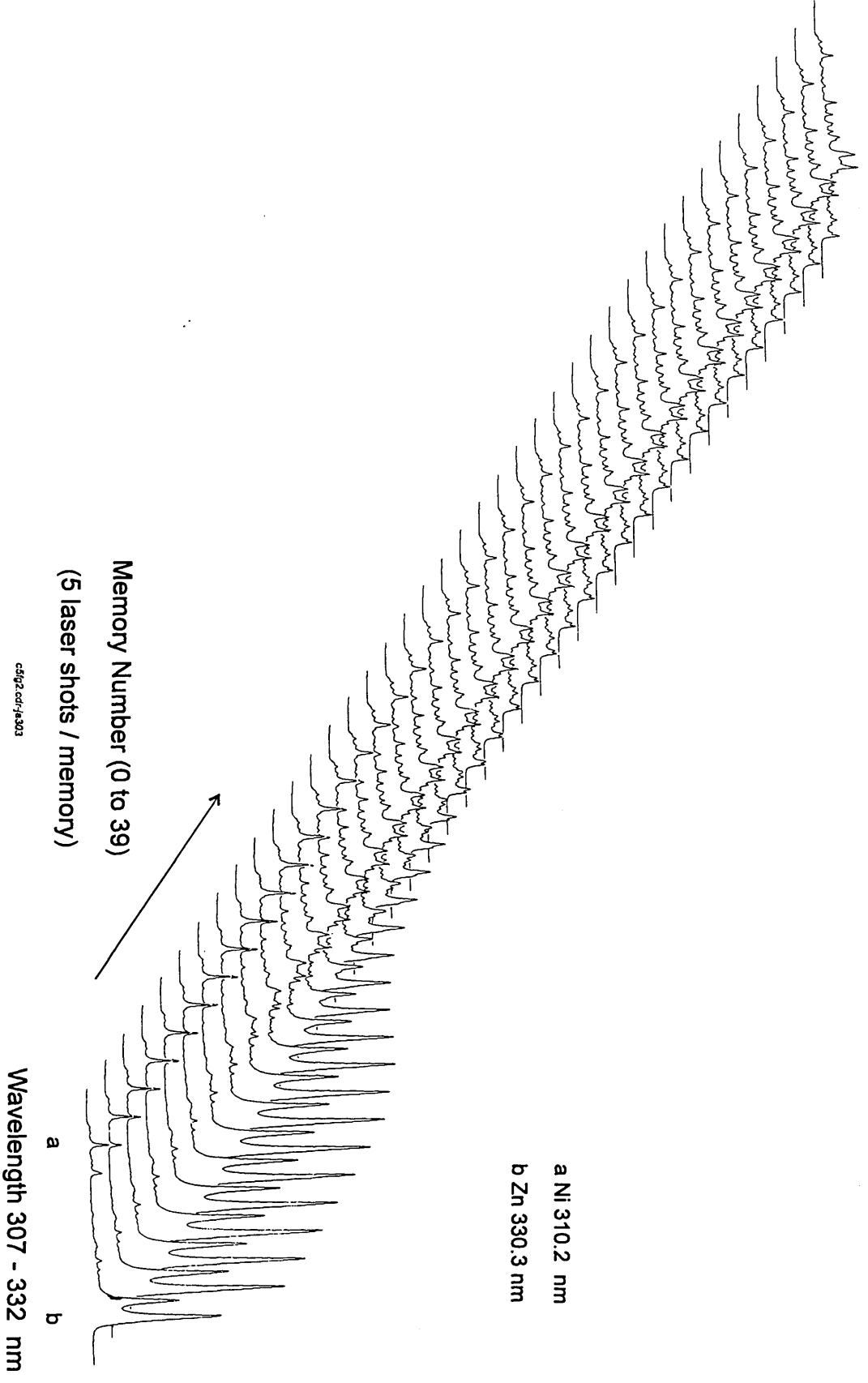

Figure 2 Emission-wavelength-time response for the ablation of Zn/Ni coating on steel (sample P2, coating thickness 2.7μm) with LFLE 70J at sample position F0. Experiment run time 40 s.

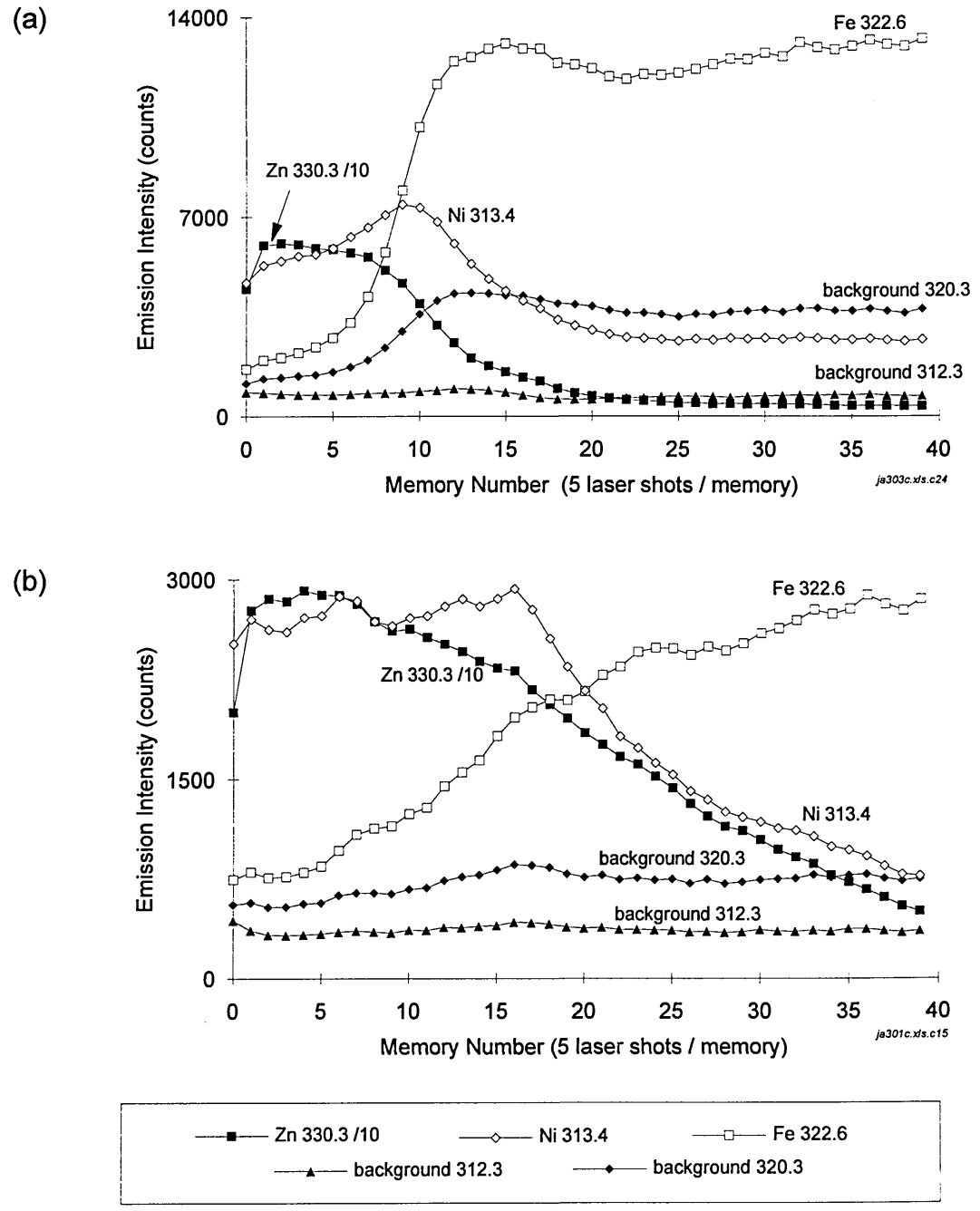

Figure 3 Emission-time response for the ablation of Zn/Ni coating on steel (sample P2, coating thickness 2.7 μm) at sample position F0 with LFLE: (a) 70 J; (b) 40 J.

5.3.2 Basic characterisation studies

In order to provide insight into ablation processes and to obtain optimum operating conditions for depth profile measurement, key operating parameters (laser energy and sample position relative to laser focal point) were varied systematically. The effect of laser energy upon depth profile characteristics is seen for zinc/nickel coatings in the comparison of Figures 3a and 3b. These depict emission-time responses for the ablation of sample P2 with LFLE 70 and 40 J, respectively, at the laser focal point (F0). Signal characteristics varied with laser energy: the emission intensities of the iron, nickel and zinc increased with laser energy, from ~2500 to ~6000 counts for zinc and nickel (40 to 70 J), and ~2000 to ~9000 counts for iron; the gradient of the profile lines during the transition period also increased with energy. These features may be explained by examination of the craters which resulted from these ablations, and by consideration of the effect of laser energy upon laser - material interaction processes.

Talysurf surface analyses of these craters, each produced by 200 laser shots, are depicted in Figures 4 and 5. Figure 4 shows a three dimensional view and Figure 5 shows a profile through the centre of each crater. Electron micrographs from examination of each crater with scanning electron microscopy (SEM) are shown in Figures 6. The crater produced by ablation with LFLE 40 J contained a central 'volcano' feature which consisted of walls ~10 μm higher than the unablated surface with a hole inside that was deeper than the base of the crater. The hole and crater were ~100 μm and ~1.3 mm in diameter, respectively, and the crater was ~4.0 μm deep. By contrast, the crater produced by ablation with LFLE 70 J appeared to be larger in diameter (~1.4 mm) and deeper (~7.4 μm) . The crater bottom was considerably flatter with no central volcano 'feature'. Both craters were surrounded by walls higher than the surface of the sample.

It is proposed that the differences between the craters, and therefore the emission-time signatures, were caused by different sampling processes. For ablation with LFLE of 40 J (irradiance ~ 8 x 10^{10} W cm^{-2}, Appendix 1), two processes occurred: plasma-sampling, where the plasma induced by each laser pulse vaporised solid material from the surface leading to the production of the crater; and laser-sampling, where direct laser-material interaction produced the hole feature within the crater. The hole diameter was approximately the same as the calculated laser spot diameter, ~100 μm, which suggested that the hole was formed by laser-material interaction. The crater, ~1.3 mm in diameter, probably approximated to the size sampled by the laser-induced plasma. The laser-induced plasma was optically thin and allowed significant laser radiation to reach the sample surface. Direct heating by the laser took place at the sample surface[9] which caused rapid heating and phase changes that produced ejection of material leading to the formation of the deep hole. Electron micrographs of this crater (Figure 6a, b) appear to show the presence of a large number of bubbles at the surface in the vicinity of this hole, suggesting that gas was evolved from a molten state and that sub-surface heating had taken place. Some of the ablated material was removed into the plasma where excitation and atomic / ionic emission took place, the remainder was deposited at the top of the hole to produce the 'volcano' walls. As the hole was deeper than the crater, sampling in effect took place at 2 different depths at the same time. The hole penetrated the substrate before complete removal of the coating was achieved within the crater, which caused iron signals to be observed from the steel during the removal of the coating and a very indistinct interface region to be obtained, (Figure 3b).

(a)

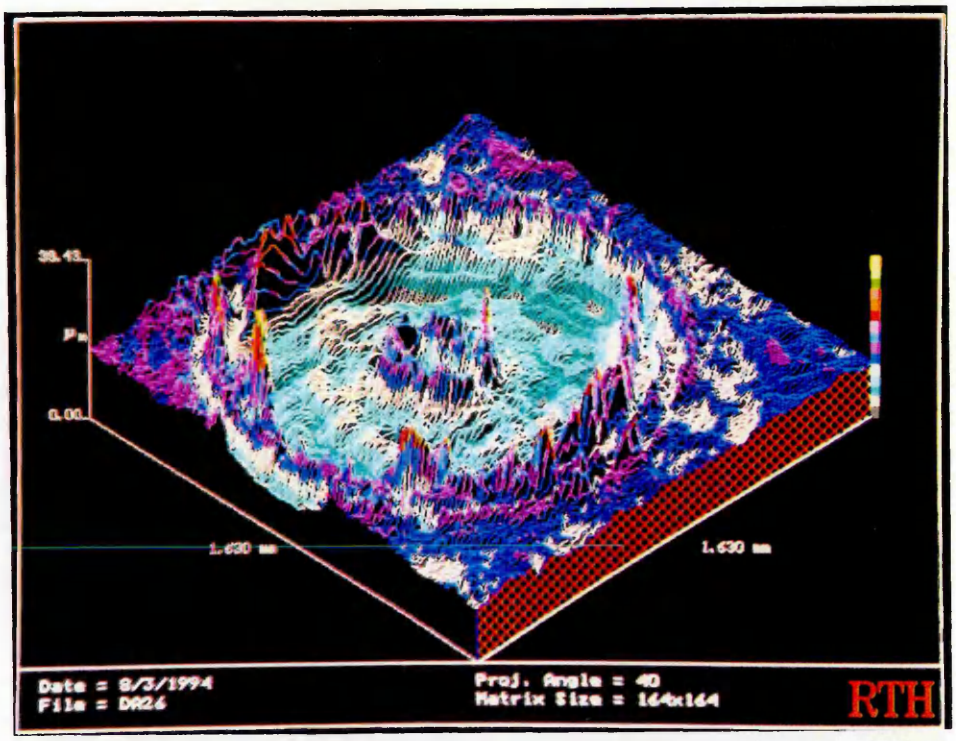

(b)

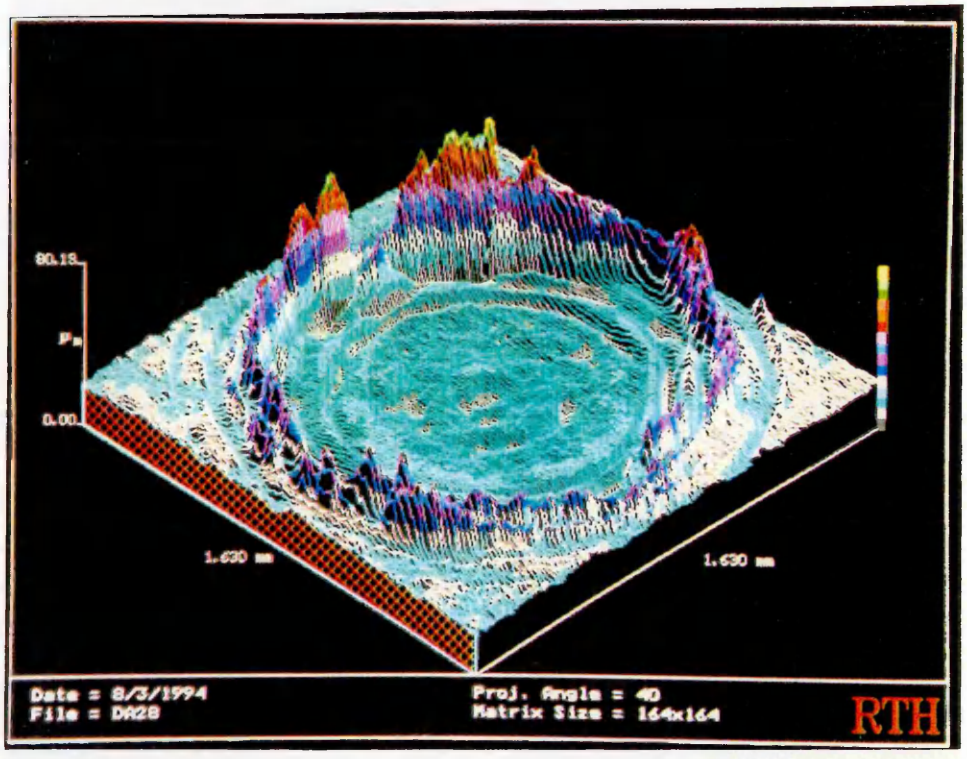

Figure 4 Three dimensional Talysurf analysis of craters in Zn/Ni coating on steel. The x and y-axes correspond to distance across the sample surface, both 1.63 mm total. The z-axis is the vertical height, with total heights: (a) 38.4 µm (b) 80.2 µm. The craters were produced by 200 laser shots with LFLE: (a) 40 J, (b) 70 J.

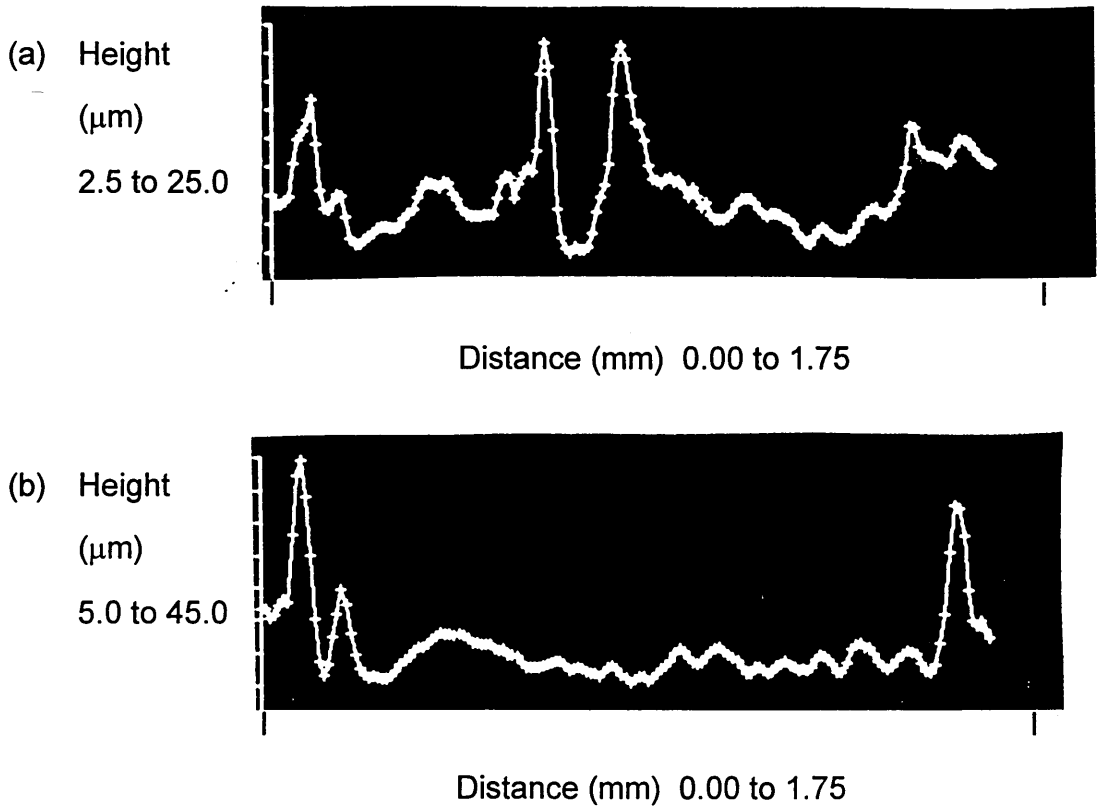

Figure 5 Single Talysurf profiles through centre of craters in Zn/Ni coating on steel. The y-axis corresponds to vertical height and the x-axis is the horizontal distance across the sample surface. The craters were produced by 200 laser shots with LFLE: (a) 40 J, (b) 70 J.

In the case of ablation with LFLE of 70 J (irradiance ~ 3 x 10^{11} W cm^{-2}), it is proposed that there was little or no direct laser interaction, and that the main process of material removal was by volatilisation by the laser-induced plasma. An electron micro-graph (Figure 6c) shows a generally flat, featureless crater. Here, a plasma of greater density, intensity and temperature was induced by each laser pulse which absorbed the incoming laser pulse preventing significant laser light from reaching the sample surface. The plasma shielded the sample from the laser pulse. The high temperature plasma vaporised material from the sample surface to produce a relatively flat-based crater.

(a)

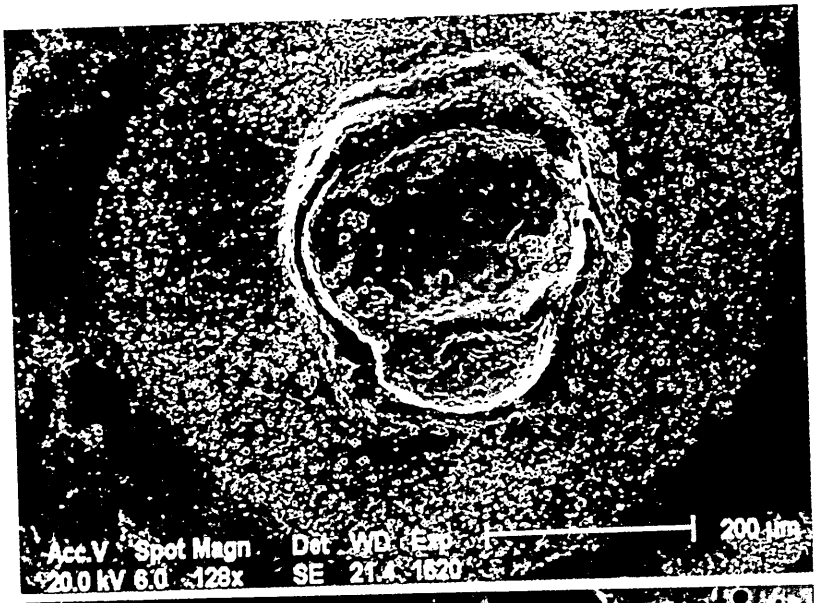

(b)

(c)

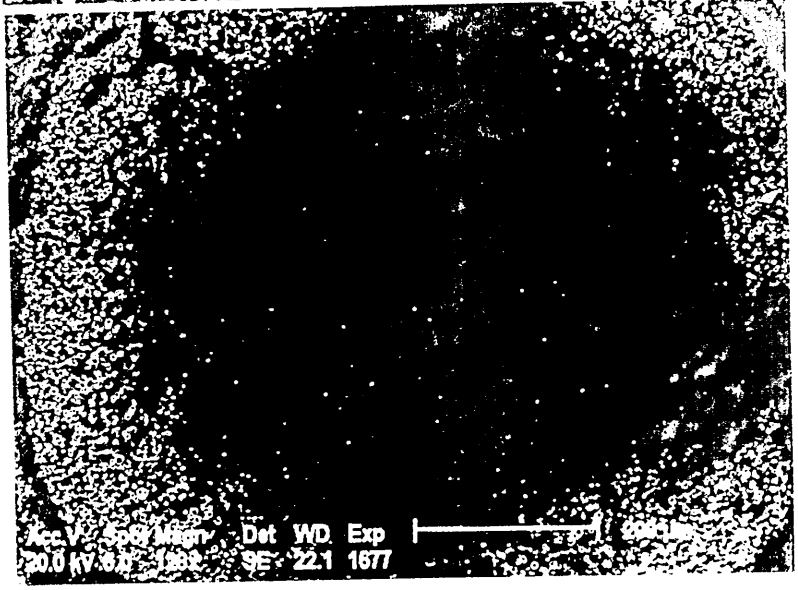

Figure 6 Scanning electron micro-graphs of craters in Zn/Ni coating on steel produced by 200 laser shots: (a) & (b) LFLE 40 J, (a) central volcano feature within crater, x128 magnification; (b) hole within volcano, x514; (c) crater produced by LFLE 70 J, x128.

As material removal took place at only one level for each laser shot compared to two levels for the 40 J ablation above, removal of the coating was completed before ablation of the interface and substrate started. Thus a depth profile was obtained (Figure 3a) that showed a sharp interface region and relatively level plots corresponding to coating and substrate removal.

The diameter of the crater was probably governed by the size of the laser-induced plasma. A larger plasma was produced by the higher energy ablation (LFLE 70J) compared to that of LFLE 40 J ablation, which sampled a larger area of material and resulted in a crater of larger diameter. The emission intensities for LFLE 70 J ablation were more intense than for the LFLE 40 J ablation through a combination of reasons (Figure 3). The higher energy of the laser pulse (LFLE 70J) induced a hotter, larger, more intense plasma that produced more intense atomic and ionic emissions; the plasma sampled a larger area of material resulting in more material bieing removed per shot (larger crater); and the higher temperature enabled more material to be removed per laser shot (deeper crater). The rate of material removal was 0.18 and 0.45 μg/laser shot for ablation with LFLE 40 and 70 J, respectively, estimated from the size of the craters measured by the Talysurf analysis, (calculation given in Appendix 1).

The background intensity varied during the depth profile, particularly in the vicinity of the iron emissions, (321.4 and 322.6 nm), depicted in Figure 3. The background response 320.3 nm was relatively constant during the ablation of the coating, increased in the interface region, and then remained reasonably constant for the ablation of the steel substrate. The other background response, 312.3 nm also varied in this manner but to a lesser extent. To correct the nickel and iron emissions for these changes, the respective background value was subtracted from the nickel and iron values for each memory number,

i.e. iron 322.6 - background 320.3 nm (Fe-Bkg); nickel 310.2 - background 312.3 nm (Ni-Bkg). These background-corrected responses were used in subsequent studies.

The effects of sample position and laser energy were next examined. Several complex interdependent processes were affected by changing these operating conditions. The characteristics of the laser-induced plasma changed with laser energy, i.e. increased LFLE increased the energy density, size, temperature, and intensity of the plasma, and by positioning the sample away from the laser focal point, the laser spot was defocused which increased the laser spot size and decreased the energy density. Emission-time responses for the ablation of sample P2 with LFLE 40, 55, 70 J at different sample positions are shown in Figure 7 (F-20, F0, F+20), Figure 8 (F+10, F+20, F+30) and Figure 9 (F-50, F+50). From Figure 7, two general observations can be made for sample positions F-20, F0 and F+20: (1) the gradient of the profile lines in the interface region generally increased with laser energy, indicating that laser energy had a greater effect than sample position upon material removal and the corresponding emission-time signature, and (2) emission intensities for each sample position increased with laser energy. The energy of the plasma increased with laser energy which increased the rate of material removal and the element emission intensities. In the case of ablation with LFLE 55 and 70 J, line gradients also increased as the sample was positioned further from the laser, i.e. F-20 through F0 to F+20. The signatures for LFLE 40 J were less affected by the change in sample position. This suggested that sample position had more influence on the main material removal process for ablation with LFLE 55 and 70 J (plasma-material interaction) than for ablation with LFLE 40 J (laser-material interaction).

Depth resolution (Δd) [6, 10] was calculated as the difference in depths at 84% and 16% of the maximum zinc signal (Figure 10a). The time-axis was converted to depth by equating the known coating thickness to D½, where D½ was the distance along the x-axis from the origin to half of the maximum zinc signal (Figure 10b). For ablation with LFLE 70 J at different sample positions, Δd was 1.5 μm (F-20), 1.8 μm (F0), 1.6 μm (F+10), 1.1 μm (F+20) 1.9 μm (F+30), and 1.5 μm (F+20) for LFLE 55 J. These data and comparison of the emission-time signatures for these sample positions (Figures 7 and 8) suggested that the plasma sampling process was modified such that sharper gradients and improved Δd were achieved at sample position F0 with LFLE 70 J. This consisted of the longest 'level' signals for zinc and iron as the coating was being removed, and the steepest gradients in the interface region. This sample position with LFLE 70 J was probably an 'optimum' distance from the laser focal point such that plasma characteristics were 'optimised' for controlled vaporisation across the sampling site. At F+10 with LFLE 70 J, the energy density was higher and the plasma positioned closer to the surface such that sampling was more aggressive and less even, indicated by faster penetration into the coating (Fe increase after 25 laser shots) and shallower gradients. At F+30 with LFLE 70 J, the plasma was probably induced further from the surface with a lower energy density leading to less even-sampling. Talysurf analysis of the crater produced by 200 laser shots at F+20 showed that the crater base was flatter than that produced by ablation at F0 with LFLE 70 J. The rate of material removal was estimated at 0.38 μg/laser shot compared to 0.45 μg/laser shot for LFLE 70 J at F0. (The calculation used to obtain the rate of material removal is given in Appendix 1).

Ablation at sample positions of F-50 and F+50 showed that large defocusing either towards or away from the laser degraded depth profile performance significantly, (Figure 9). In the case of ablation with LFLE 40 J, line gradients

increased with distance from the laser focal point, i.e. F+10 to F+30, (Figure 8). As the sample was positioned further from the focal point, a more intense plasma was induced near the focal point which absorbed more of the laser radiation and decreased the amount of laser sampling.

For all the emission-time responses (Figures 7-9), the zinc and nickel lines decreased at the same rate, indicating that zinc and nickel were removed at a similar rate and selective volatilisation of zinc had not occurred. If boiling of the sample at the laser spot had been a major process of material removal, it might have been expected that zinc would be removed preferentially as it has a much lower boiling point compared to nickel, (Zn 907 vs. Ni 2732 °C).

In summary, experiments have demonstrated that profile performance and depth resolution were influenced by key operating parameters. Optimal depth profile data were obtained using the operating parameters of sample positioned 20 mm from the laser focal point (away from the laser source, F+20), with maximum available laser energy (laser flash lamp energy 70 J).

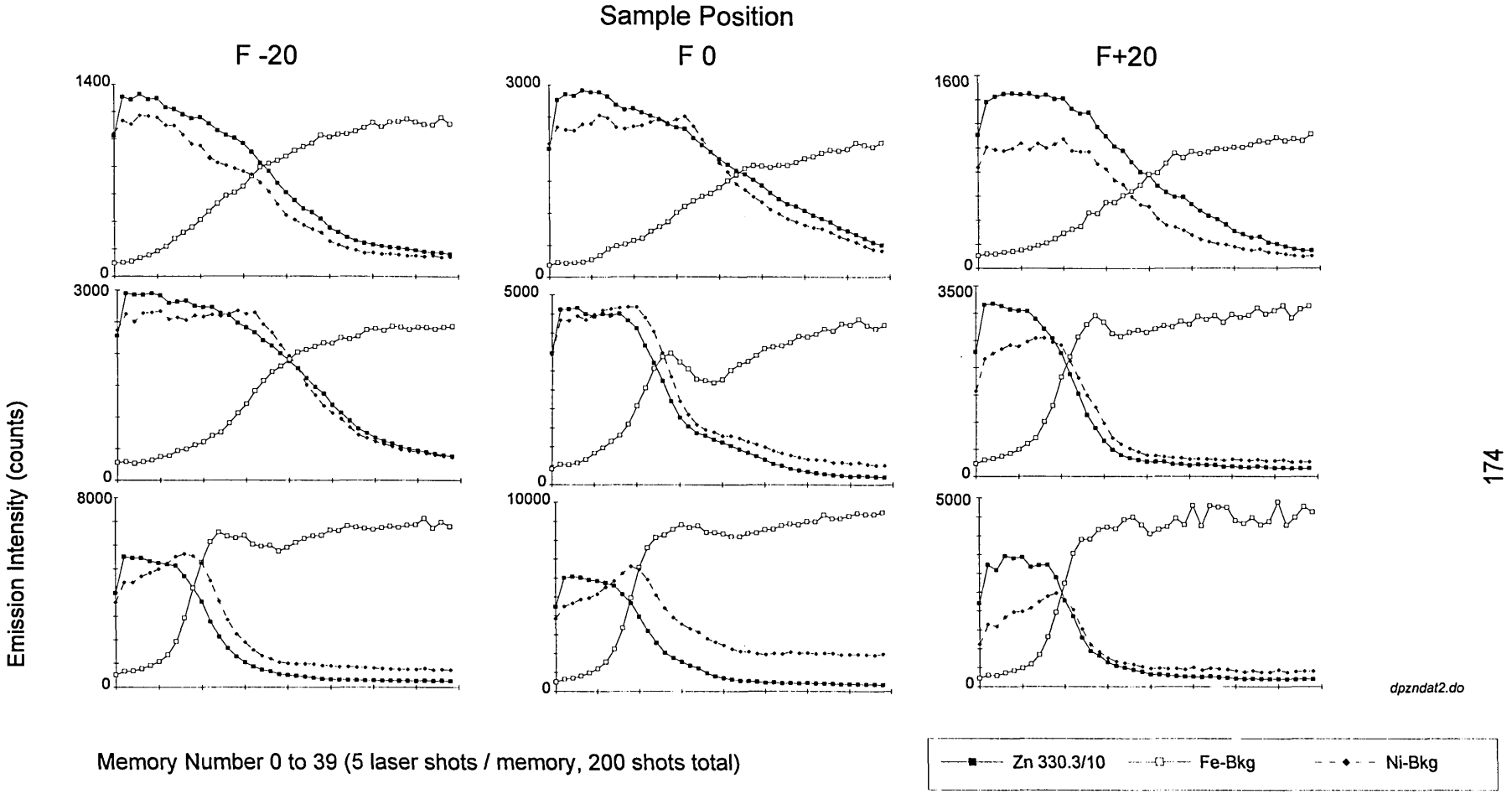

Figure 7 Emission-time responses for the ablation of Zn/Ni coating on steel (sample P2, 2.7 μm) at sample positions F-20, F0 and F+20 with LFLE 40, 55 and 70J.

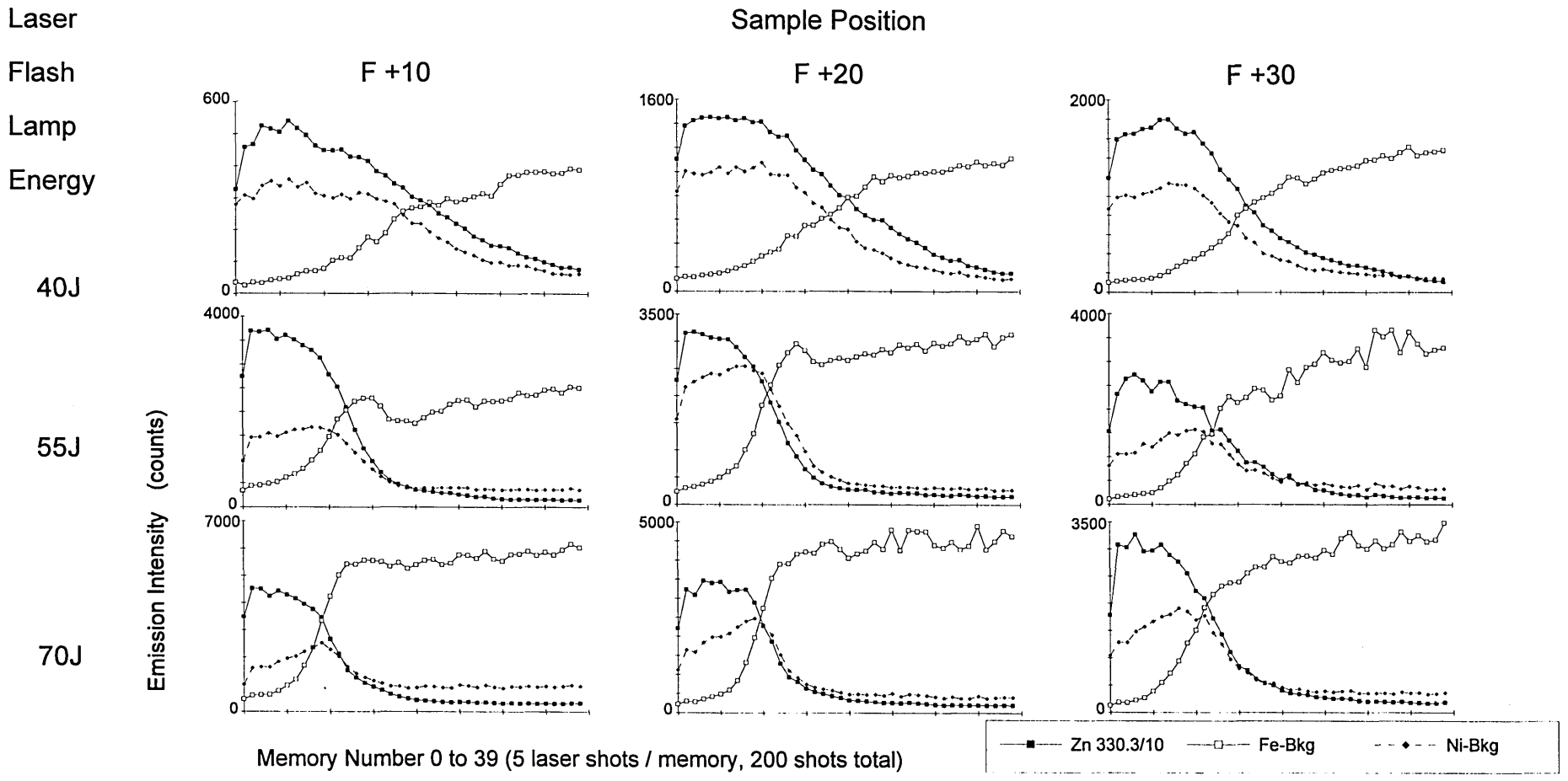

Figure 8 Emission-time response for the ablation of Zn/Ni coating on steel (sample P2, 2.7 μm) at sample positions F+10, F+20 and F+30 with LFLE 70J.

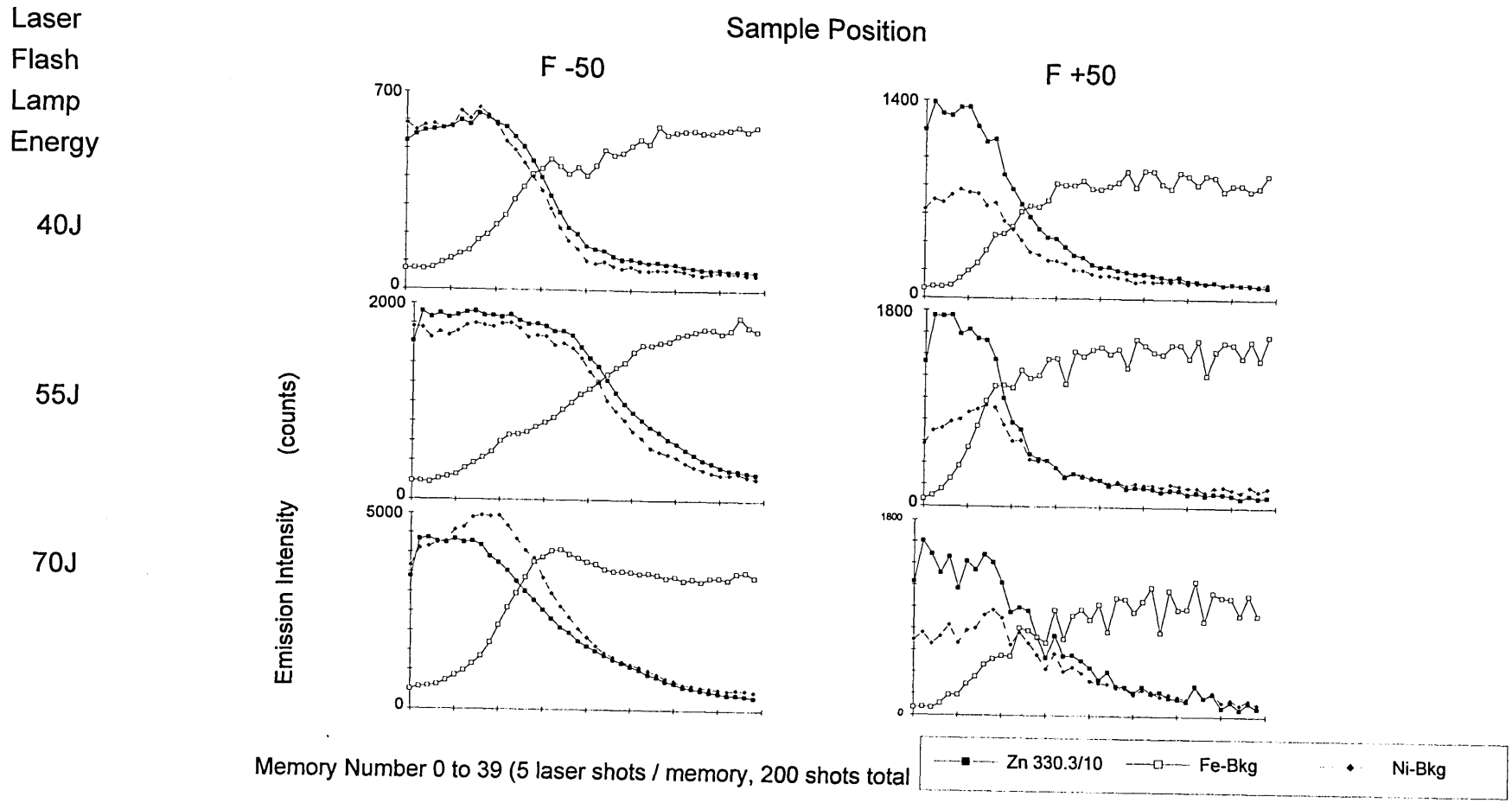

Figure 9 Emission-time responses for the ablation of Zn/Ni coating on steel (sample P2, 2.7 μm) at sample positions F-50, F+50 with LFLE 40, 55 and 70J.

(a) Depth Resolution (Δd)

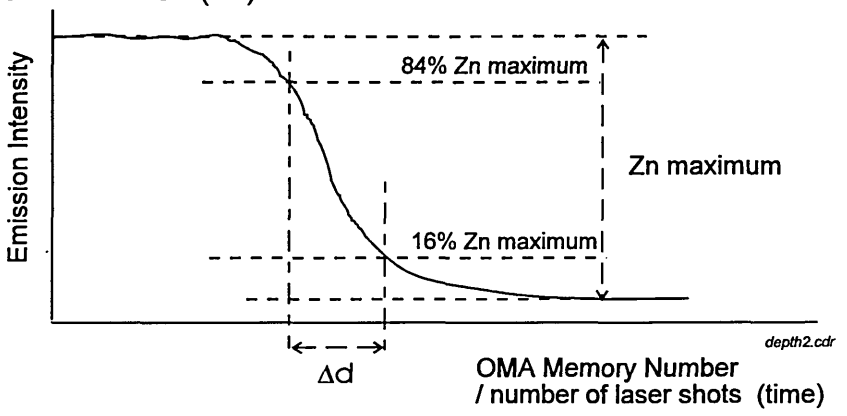

(b) D½

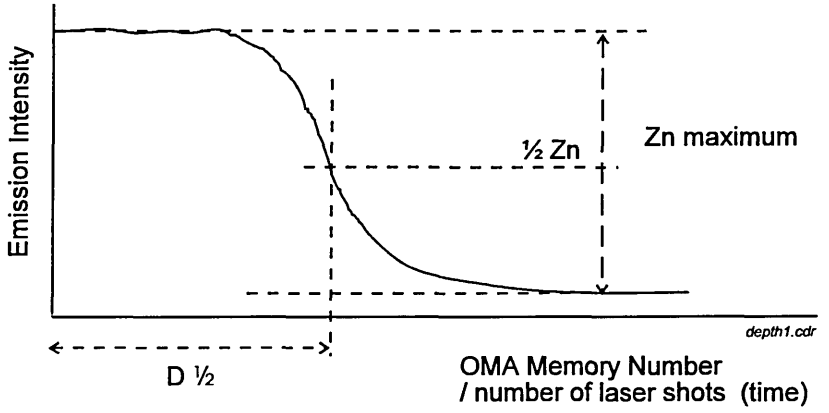

(c) Dx

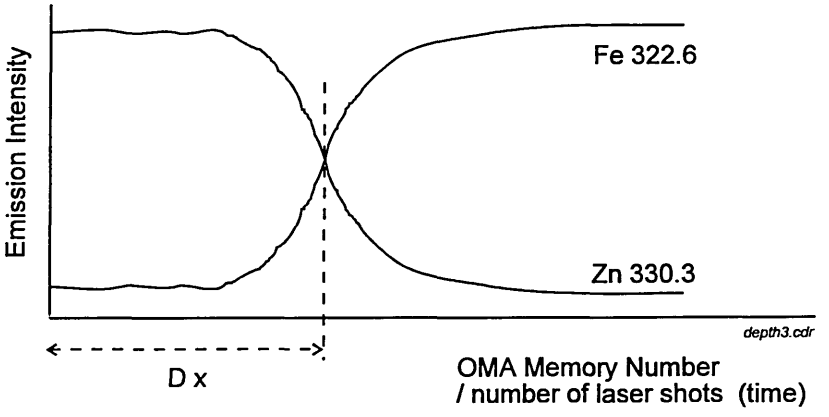

Figure 10 Emission-time responses of Zn 330.3 nm for the depth profile measurement of zinc/nickel coating on steel showing the calculation of: (a) depth resolution (Δd), (b) D½, and (c) Dx.

5.3.3 Depth profile performance and applications

This section examines depth profile performance and the application to a range of different coatings on steel, zinc/nickel, zinc, tin, titanium nitride and an ultra-thin chromium coating.

Zinc/nickel coatings

To demonstrate depth profile performance, laser-induced plasma emission spectrometry measurements were performed on zinc/nickel-coated steels with a range of coating thickness. Samples P4, P5 and P6 with coating thickness 2.7, 5.0, and 7.2 μm, respectively, were each ablated in triplicate. Operating parameters were as above except the total number of laser shots utilised was 250 instead of 200 (5 laser shots in each of 50 OMA memories) in order to remove the thicker coatings. Typical emission-time responses are depicted in Figure 11 for each sample. These showed that the number of laser shots needed to remove the coating increased with coating thickness; the number of laser shots needed before the zinc signal decreased were 35, 60, and 90 for 2.7, 5.0, and 7.2 μm, respectively. The zinc and iron signals remained relatively constant during the removal of the coating for each sample, and the nickel response appeared to increase a little.

A correlation between output parameters for laser-induced plasma emission spectrometry and coating thickness has not been previously reported. Possible output parameters include D½ (distance along the x-axis from the origin to half of the maximum zinc signal), Dx (the distance along the x-axis from the origin to where the Zn and Fe lines cross), and zinc-area or nickel-area (the area under a coating element profile line, Zn or Ni). The calculation of D½ and Dx is depicted in Figure 10 b and 10c, respectively.

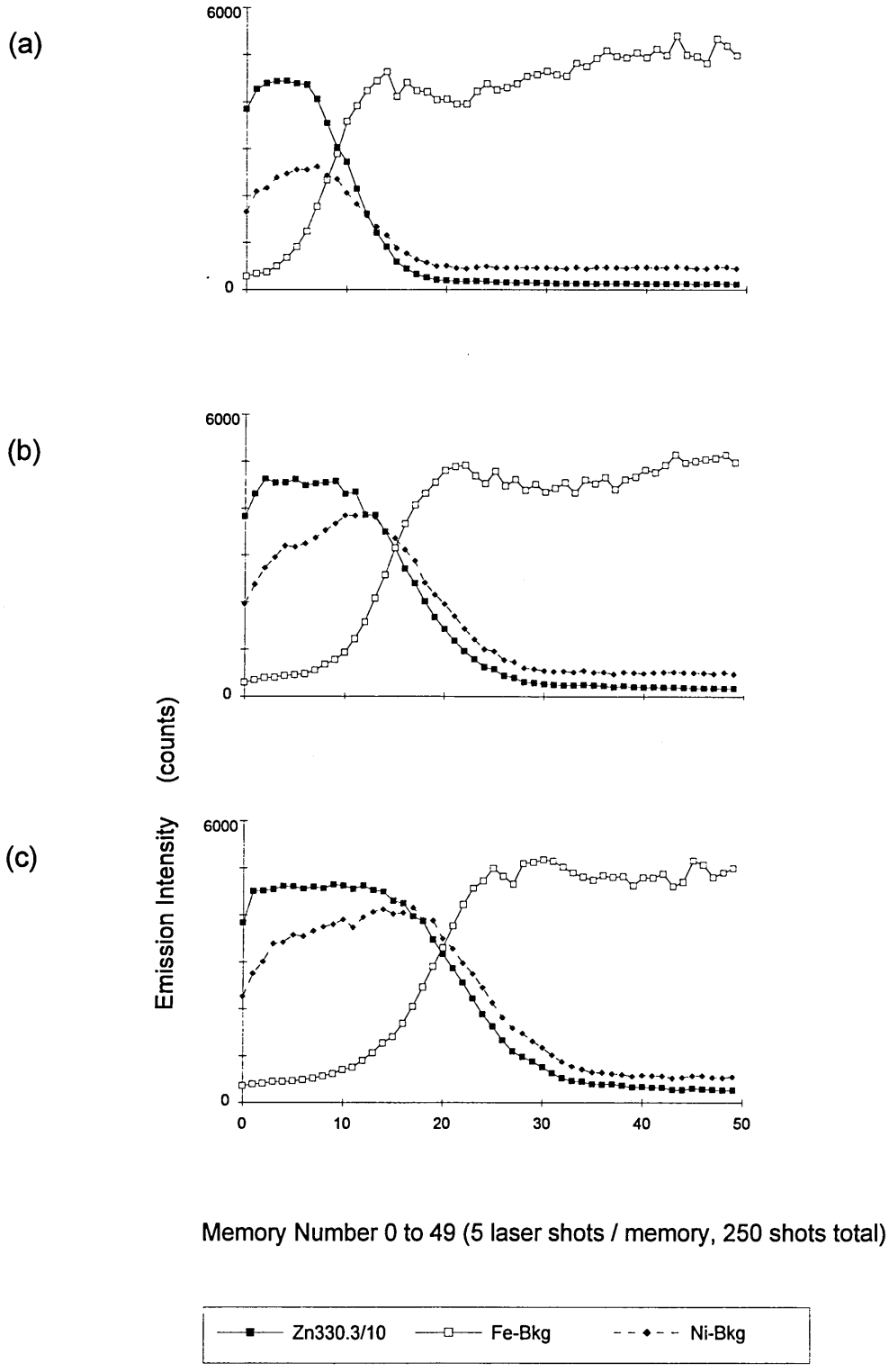

Figure 11 Emission-time responses for the ablation of samples P4, P5 and P6 at sample position F+20 with laser flash lamp energy 70 J. Experiment run time 50 s. Coating thicknesses were: (a) P4 2.7 μm; (b) P5 5.0 μm; (c) P6 7.2 μm.

Linear plots of D½, Dx and zinc-area against coating thickness were obtained, but the nickel-area plot was curved. The curvature was probably caused by spectral interference from iron on the nickel emission line, which had less effect as the coating thickness increased. The line equations and correlation coefficients were, respectively: (D½) y = 8.66x + 13.28, 0.99986; (Dx) y = 8.22x + 9.64c, 0.99942; (zinc-area) y = 128854x + 203881, 0.99999. These results suggest that the LIPS output parameters D½, Dx and Zn-area are proportional to coating thickness. This indicates that the rate of penetration into the coating is constant with depth, i.e. the rate of material removal is constant with depth, suggesting that each laser shot removes the same amount of material. The linear relationship between these output parameters to coating thickness indicates that laser-induced plasma emission spectrometry can provide a measurement of coating thickness.

The repeatability of the coating measurement was calculated by ablating sample P6 (7.2 μm) at eight different locations. Good precision (RSD) for the zinc-area and nickel-area measurements were obtained, 4.0 and 3.7 % respectively, suggesting that there was uniform coating thickness across the area of material tested. This indicates that the technique can rapidly undertake a coating thickness survey of coated samples.

To investigate the capability of the laser-induced plasma emission spectrometry technique to provide spatial-depth information, two samples of zinc/nickel coated steels (samples P1 and P2, both 2.7 μm thick) and a sample with a zinc coating (Zn-A) were examined. Both zinc/nickel-coated samples were ablated eight times and typical emission-time responses are depicted in Figure 12.

(a)

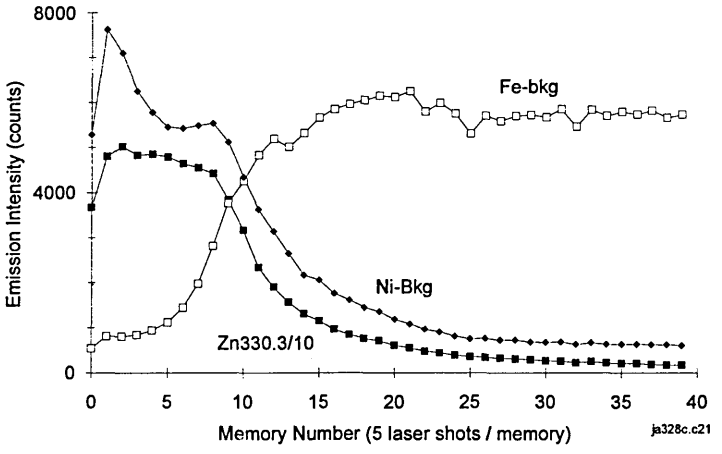

(b)

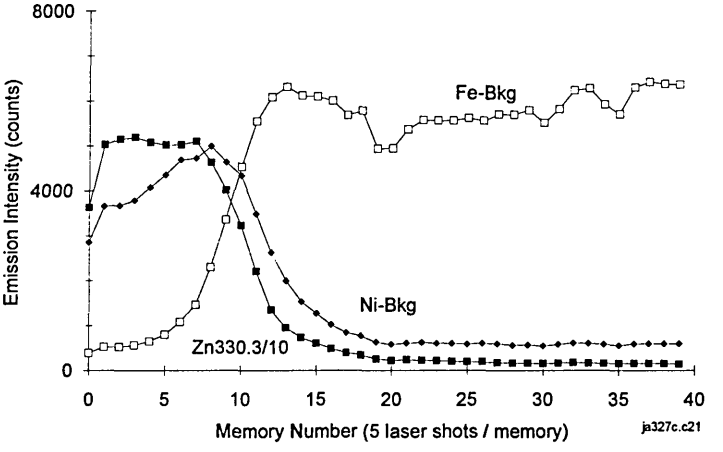

Figure 12 Emission-time responses for the ablation at sample position F+20 with LFLE 70 J of two samples of Zn/Ni coating on steel (2.7 μm):
(a) P1, (b) P2.

The technique revealed differences within these coatings, although the samples were suposedly very similar.[11] In the case of P1, a larger number of laser shots were required for the zinc and iron signals to reach minimum and maximum levels, respectively, from the interface region to removal of the substrate. This may indicate that the interface region for sample P1 was larger, suggesting that the surface finish of the steel substrate was rougher which allowed the coating deeper into the surface of the steel. There was a significant difference in the

profiles for nickel during the removal of the coating. For sample P1, the nickel signal initially increased to ~7500 counts, then decreased to ~5500 and became level until memory number 8 before decreasing in the interface region. For sample P2, the nickel signal increased steadily through the coating from ~3000 to ~5000 counts. These observations suggest that for sample P1, the concentration of nickel was decreasing through the coating, i.e. nickel was richer near the surface, and for sample P2 the nickel concentration increased slightly through the coating. These results suggest that depth profile measurement using LIPS may be appropriate in the quality control of zinc/nickel coatings on steel.

An emission-time response for the ablation of zinc on steel (sample Zn-A, 8 μm) at sample position F+20 with 400 laser shots of LFLE 70 J is shown in Figure 16a. This depicts emission responses for zinc, aluminium and iron; the emission wavelengths are listed in Table 2. The coating did not contain nickel so the response for nickel is not shown. The emission-time response showed an increase in the response for aluminium within the coating, with a maximum at memory number 5 corresponding to 60 laser shots. This indicated that a region of the coating, not at the surface, contained a significant amount of aluminium. This was confirmed by analysis of the sample using glow discharge optical emission spectrometry (GD-OES), undertaken by the sample supplier. Figure 16b depicts the GD-OES emission-time profile with total time 800 s. The aluminium layer appeared to be present at the interface region between the zinc coating and steel substrate. Although the LIPS profile was not optimal, the aluminium layer was clearly shown and the profile was much quicker to measure by LIPS than by GD-OES, 80 vs. 800 s.

(a)

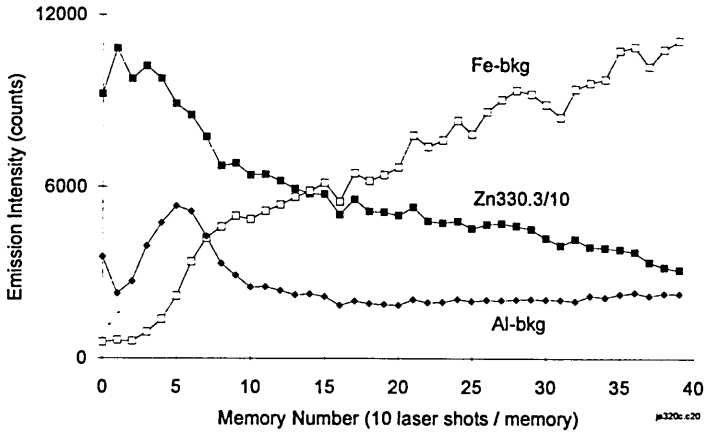

(b)

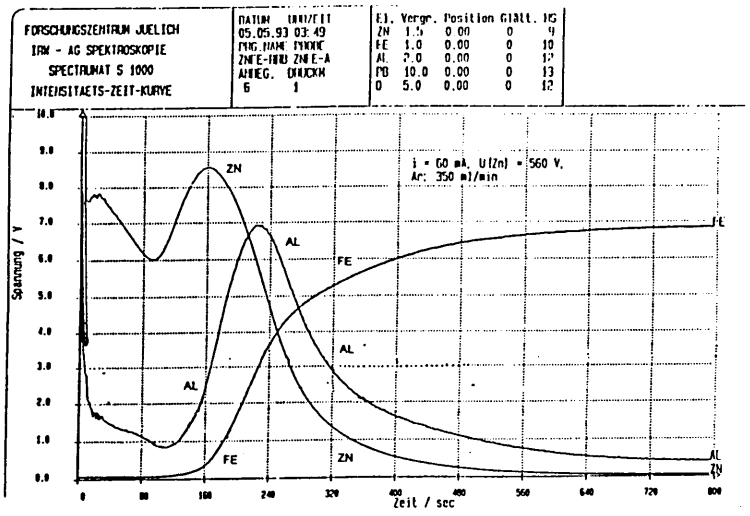

Figure 13 Emission-time response for the depth profile of sample Zn-A (8 μm Zn on steel): (a) using LIPS at sample position F+20 with laser flash lamp energy 70 J, 400 laser shots total, experiment run time 80 s; (b) using glow discharge - optical emission spectrometry, experiment run time 800 s

The emission-time characteristics from the ablation of this coating were different from the zinc/nickel coatings discussed above. The zinc and iron signatures did not exhibit a relatively constant signal response or sharp line gradients corresponding to coating removal and interface region, respectively. Also, considerably more laser shots were required to remove the zinc coating

compared to a sample of zinc/nickel coating, ~150 vs. ~400, respectively, although the zinc coating was only ~10% thicker than sample P6 above (7.2 vs. 8.0 μm). These results suggested that the process of ablation for a zinc coating was different from a zinc/nickel coating. The rate of material removal for the zinc coating was estimated to be 0.19 μg/laser shot, lower than for zinc/nickel (0.45 μg/laser shot), both ablated under similar operating conditions. It is proposed that this was caused by a matrix effect. During the laser pulse and at the start of the plasma lifetime, a larger amount of zinc was vaporised than for the zinc/nickel coating, because of the lower vaporisation temperature of zinc compared to the zinc/nickel alloy. This extra material quickly cooled the plasma as it entered, resulting in less material being removed during the remainder of the plasma lifetime. Further studies including measurement of plasma temperatures are required to investigate this effect and obtain operating parameters suitable for optimised profile measurement of zinc coatings.

Tin coatings

Two spectra for the ablation of sample Sn1/1 are depicted in Figure 14. The coating thickness of the sample was 1.48 μm, calculated from the tin coating weight 10.8 gm^{-2}, (the calculation is given in Appendix 1). The sample was ablated using 1 laser shot / OMA memory and 60 shots total with the preferred operating conditions described above. The spectral region utilised was 287-312 nm and the main emission wavelengths are listed in Table 3.

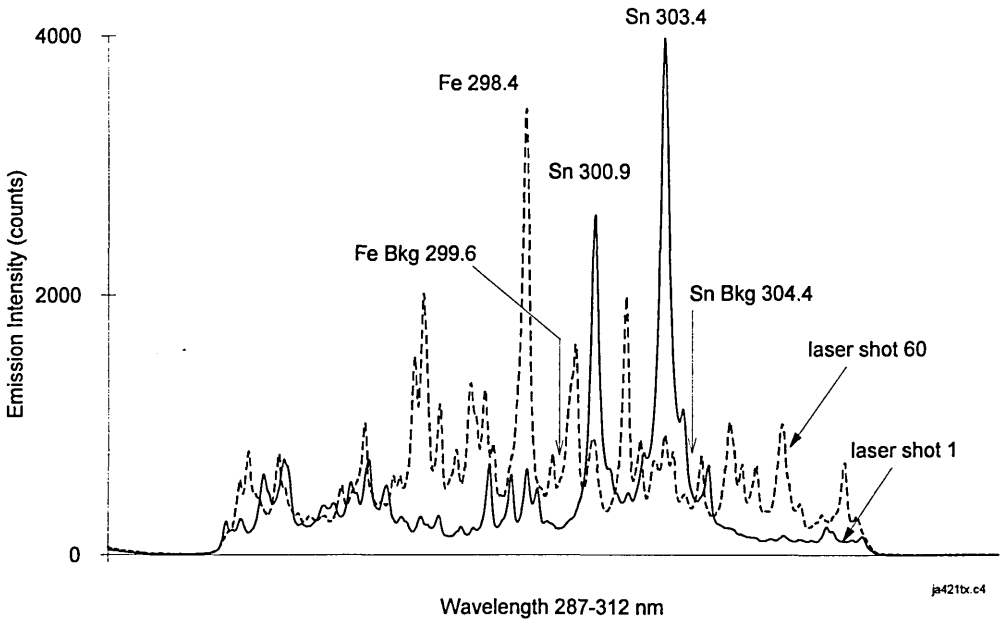

Figure 14 Spectra for the ablation of Sn coating on steel (sample Sn1/1, coating weight 10.8 gm^{-2}) with LFLE 70 J at sample position F+20. Emission wavelengths (nm).

Wavelength (nm)	Element	Pixel Number	
298.357	Fe I	480	m
299.621	Fe Background	520	m
300.914	Sn I	560	
303.412	Sn I	640	m
304.391	Sn Background	671	m

m = monitored for emission-time response

Table 3 List of main element emission lines used in the study of tin coatings, (spectral region 287 - 312 nm, centre wavelength 300 nm)

The spectrum for laser shot 1 showed intense tin emissions from the coating and small responses for iron, suggesting that the coating may contain iron or that the steel substrate was penetrated with the first laser shot. Intense iron signals from the ablation of the steel were observed for laser shot 60 together

with a small response for tin suggesting that removal of the tin was not complete with 60 laser shots. It was found that 100 laser shots were sufficient to remove the tin (50 OMA memories, 2 laser shots/OMA memory). A shift in the spectral background, between the first and last shot, was caused by the change in matrix from tin to iron as ablation of the steel substrate took place. The background spectrum from iron was more intense than from tin, and so the intensity of the background increased. Values for the intensity of the background at 299.6 and 304.4 nm close to iron 298.4 and tin 303.4 nm lines, respectively, were subtracted from the element emissions to correct for this shift.

The samples with a tin coating (Table 1) and an uncoated steel blank (BAS SS401) were analysed in duplicate to study the relationship of coating weight with signal output. The repeatability of the technique was studied by ablating samples Sn1/1 and Sn3/2 (10.8 and 1.44 gm^{-2}) eight times. Emission-time responses (tin, Fe and tin/Fe ratio) for the ablation of samples Sn1/1, 3/1 and 5/1 are shown in Figure 15. Both the number of laser shots needed to remove the tin coating and the initial tin emission intensity increased with coating weight. The number of laser shots required to reach a relatively constant iron signal also increased, and the iron intensity corresponding to ablation of the substrate was ~5000 counts in each case. A sharp transition in the tin and iron signals was not observed, unlike the zinc and iron signals of the zinc on steel, because there is no sharp interface between the tin and steel substrate. In the manufacturing process,[11] a tin-iron alloy approximately 0.1 μm deep was produced at the tin-steel interface by heating of the material above the melting point of tin (230°C). During the ablation process, signal responses from the tin coating were observed followed by tin and iron from the interfacial tin-iron, and finally iron from the steel substrate. Coating weights have been quoted for tin coatings in the study as this better describes the total quantity of tin in the tin

and tin/iron layers. The rate of material removal was estimated from Talysurf analysis to be 0.32 μg/laser shot.

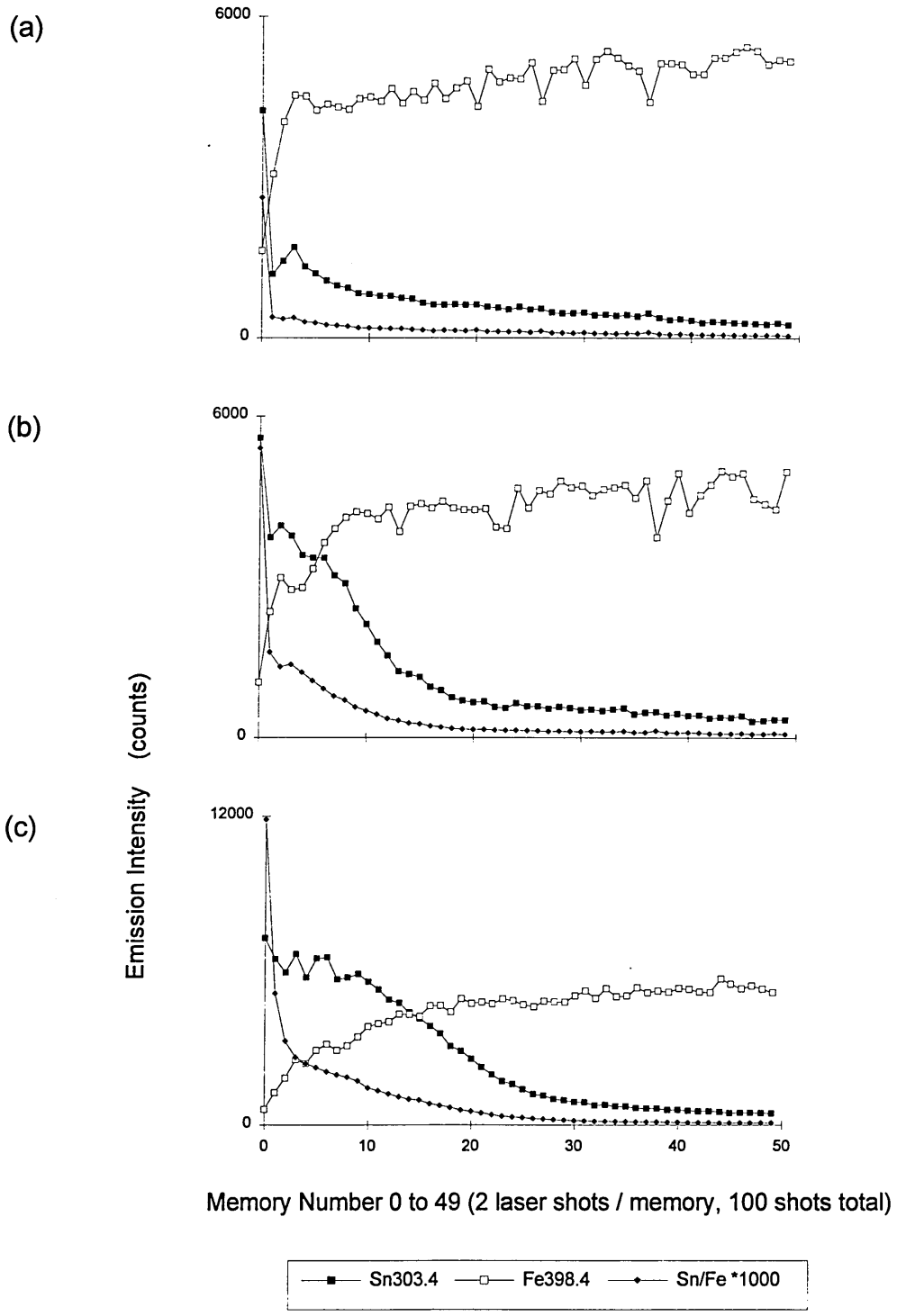

Figure 15 Emission-time response for the ablation of Sn on steel. The experiment run time was 20 s using 100 laser shots. The Sn/Fe was x1000 to obtain the responses on the same scale. Samples were of different coating weight (a) Sn5/1, 2.8 gm^{-2}, (b) Sn3/1, 6.0 gm^{-2}, (c) Sn1/1, 10.8 gm^{-2}.

The area under the tin profile line (tin-area), which combined the tin intensity measurement with the number of shots needed to remove the coating, was calculated as a measure of the tin coating weight. A linear calibration graph was obtained for the plot of tin-area against coating weight (Figure 16). This indicated that the output parameter, tin-area, was proportional to the amount of tin deposited onto steel, and that LIPS could be used to measure coating weights of tin on steel. Precision (% RSD) for the repeat measurements of samples Sn1/1 and Sn3/2 was calculated for tin-area to be 3.5 and 6.6 %, respectively. The result for sample Sn1/1 indicated that coating depth measurements using LIPS can be achieved with good precision, and that the tin coating was uniformly distributed across the steel. The poorer precision obtained for Sn3/2 may be caused by the lower coating thickness, or it may indicate that the tin was less-evenly distributed across the sample surface. By comparison, Ka'ntor et al[12] obtained an RSD value of 9.4 % for the replicate measurements of gold coatings using a single shot laser ablation - flame atomic absorption spectrometry technique.

In summary, the linearity of the calibrations and precision achieved with the tin-area and zinc-area values suggest that these are suitable methods to measure tin coating weight / zinc/nickel coating thickness in depth profile measurements by LIPS. This performance coupled with the respective analysis times of 20 and 50 s indicates that laser-induced plasma emission spectrometry can provide rapid depth profile data for tin and zinc/nickel coatings over the thickness range 0.3 to 7.2 μm.

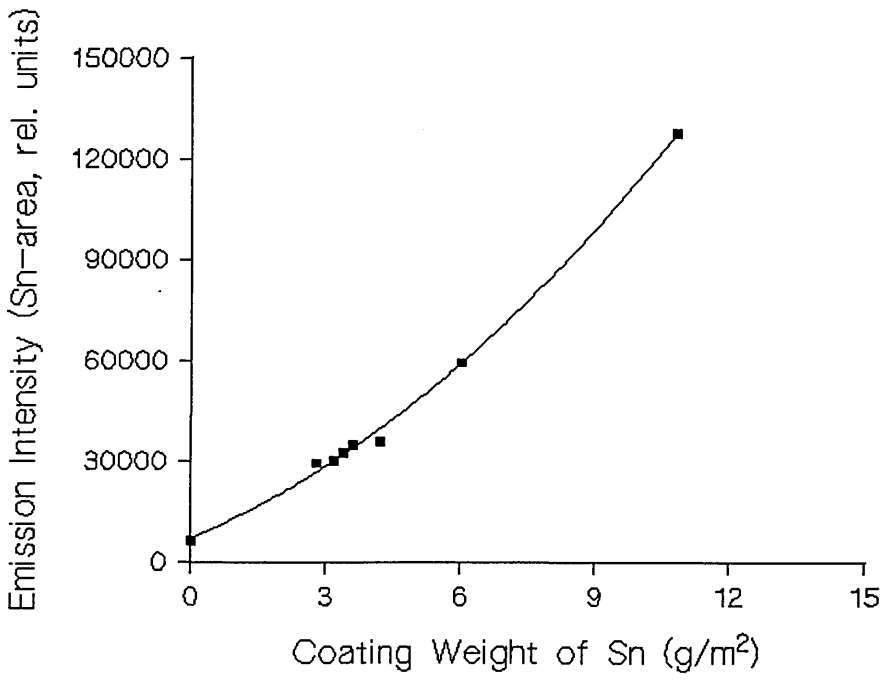

Figure 16 Plot of area under Sn profile line (Sn-area) against Sn coating weight for the ablation of different samples of Sn coating on steel.

Titanium nitride coating

The ablation of a titanium nitride coating (coating thickness 2 μm) is shown in Figure 17, which depicts spectra for laser shot number 1 and 100. The spectral region 287-312 nm was selected because it contained titanium and iron emission lines that were relatively free from spectral interference. The first laser shot (1) showed intense emission responses for titanium from the coating and no responses for iron and chromium from the stainless steel substrate. This suggested that the coating did not contain iron or chromium and the first laser shot did not penetrate the coating. The last laser shot (100) showed strong emission responses for iron and chromium form the substrate and minimal responses for titanium, indicating that ablation of the substrate had taken place and removal of the coating was virtually complete. An emission-time response

is shown in Figure 18 using the emission wavelengths listed in Table 4. To correct for the observed shifts in background, the emission intensity values for chromium, iron and titanium were corrected by subtraction of the intensity value from the corresponding background wavelength, e.g. chromium 288.9 - Background 289.3 nm (Cr-Bkg).

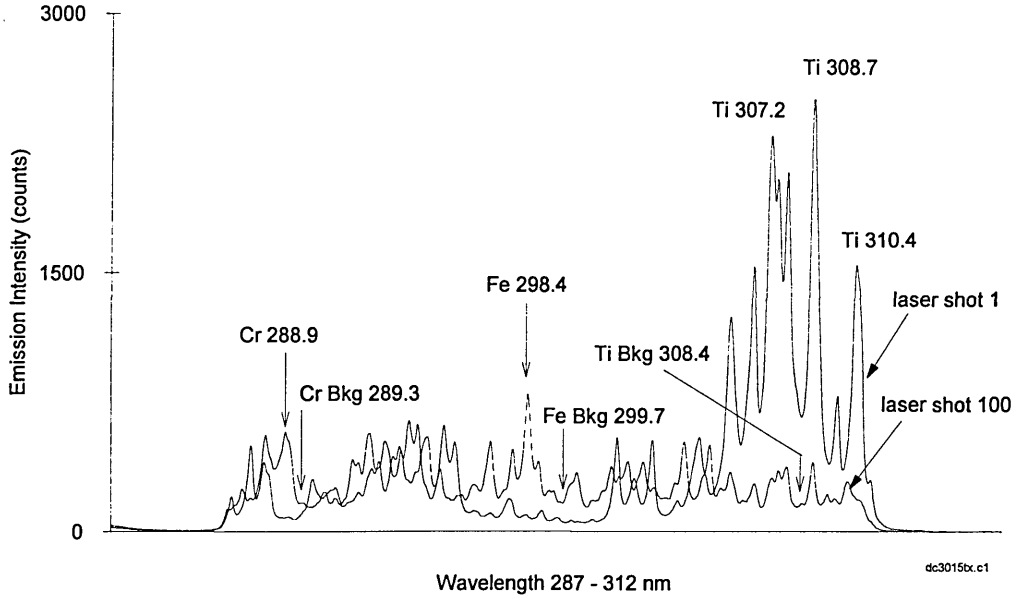

Figure 17 Overlay of spectra for the ablation of titanium nitride coating on steel (sample TiN-1, coating thickness 2μm) at sample position F0 with LFLE 40 J. Spectral region 267-312 nm, emission wavelengths (nm).

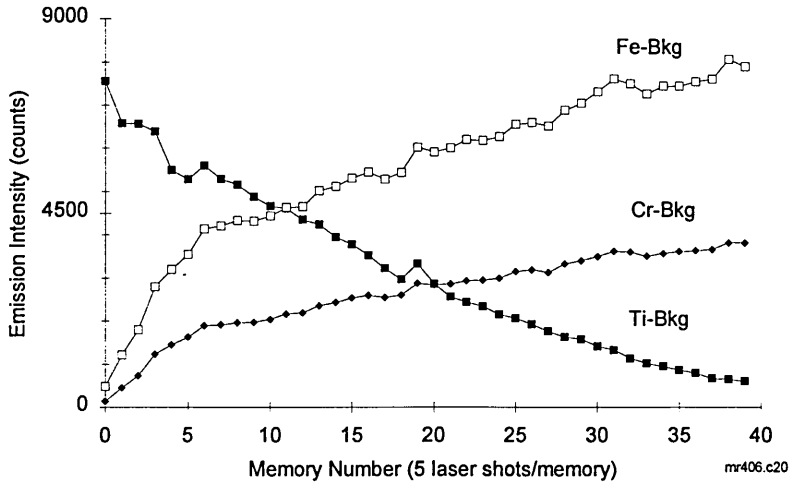

Figure 18 Emission-time response for the ablation of titanium nitride on steel (sample TiN-1, coating thickness 2 μm) at sample position F+20 and LFLE 70 J.

Wavelength (nm)	Element	Pixel Number	
288.929	Cr II	202	m
289.302	Cr Background	212	m
298.357	Fe I	479	m
299.747	Fe Background	520	m
307.211* 307.297 *	Ti II, II	762	m
308.373	Ti Background	795	m
308.718	Ti II	809	

* unresolved emission lines m = monitored for emission-time response

Table 4 List of main element emission lines used in the study of titanium nitride coatings. Spectral region 287-312 nm, centre wavelength 300 nm.

The emission-time signatures were different from those of the zinc/nickel coating discussed above. There were no sharp line gradients for titanium, chromium or iron corresponding to an interface region. The titanium signal showed a gradual decrease through the profile while the chromium and iron signals increased quite steeply until about memory number 5, then increased gradually for the remainder of the profile. The rate of material removal was estimated to be 0.17 μg/laser shot from Talysurf analysis of the resultant crater. The differences in the emission-time signatures were probably caused by matrix effects, as with the zinc coating above, which may influence the ablation process in a number of ways and require further study. Different physical properties of the coating elements may have affected plasma characteristics which in turn influenced the relative rate of material removal and depth profile performance. The high affinity of titanium for oxygen may have caused the formation of titanium dioxide during the ablation process which interfered with the material removal process. Ablation in an oxygen-free buffer gas is likely to reduce this possible interference. Further investigation of the effects of operating conditions with this coating may enable improved emission-time signatures and depth profile calibrations to be achieved.

Ultra-thin chromium coating

The above studies have shown that useful depth profile data can be obtained for coatings with thickness ranging from 0.4 to 8 μm. This section examines the feasibility of utilising LIPS to obtain information about an ultra-thin coating of chromium on steel. Spectra for the ablation of chromium on steel (coating thickness 20 nm) using operating conditions of LFLE 40 J and sample position F0 are depicted in Figure 19. The spectral region utilised was 267-292 nm because iron and chromium emission signals could be monitored with minimal spectral interference. The experiment run time was 2 s with 10 laser shots.

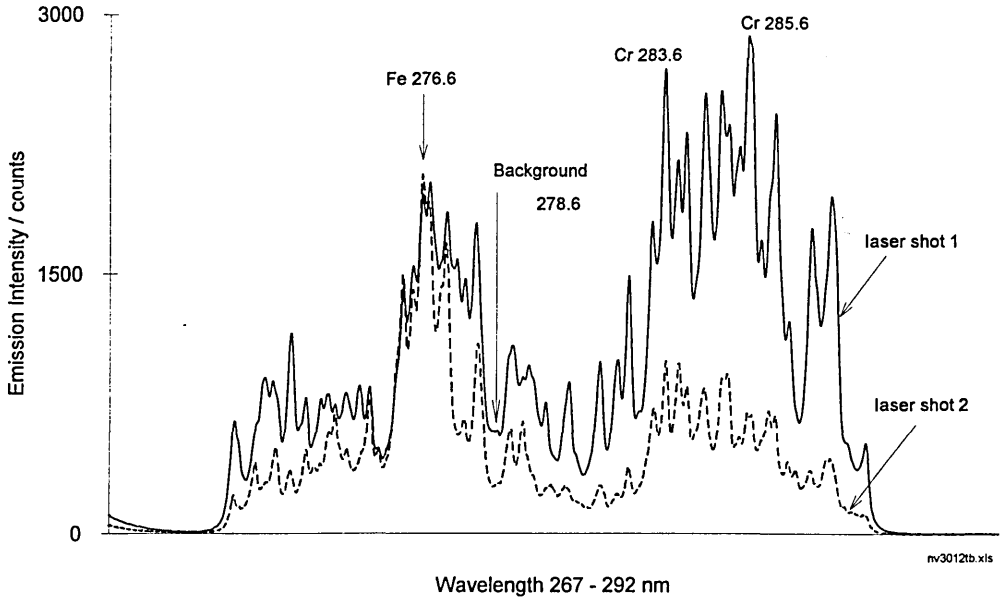

Figure 19 Spectra for the ablation of Cr on steel (coating thickness 20 nm) with LFLE 70 J at sample position F+20.

The spectrum for laser shot 1 showed intense emissions for chromium and strong responses for iron, while the spectrum for laser shot 2 showed similar responses for iron but only small signals for chromium. This indicated that the chromium coating was detected with the first laser shot. In Figure 20, an emission-time response of iron 276.6, chromium 283.6, Background 278.6 nm and the chromium/iron ratio shows the chromium signal to decrease sharply from laser shot 1 to 2 and then increase a little. The chromium/iron ratio was initially very large when the chromium was removed, but was constant after memory number 1 as the substrate was ablated. The iron response increased after memory number 1 for the remainder of the profile; also there was a small increase in the background intensity during the profile. These observations suggested that the first laser shot removed the chromium coating and a substantial amount of steel substrate. Laser shot 2 and the following laser shots ablated substrate only. The amount of chromium detected with the first laser shot was estimated to be 0.22 μg, (calculation in Appendix 1).

These results indicate that LIPS can be applied to the rapid detection of ultra-thin coatings, but more work is required to develop a measurement capability. Further study may enable the amount of substrate removed by the first laser shots to be significantly reduced in order that coating only is ablated with the first laser shot. Towards this aim, it may be advantageous to use the laser solely as a sampling tool so that laser operating parameters are optimised for minimal mass removal and are not compromised by the requirements of *in situ* emission spectrometry. This could be achieved by removing ablated material to a separate analytical measurement system such as an inductively coupled plasma mass spectrometer. However, measurement times would be greatly increased to allow for discreet transport and detection of material ablated by each laser shot.

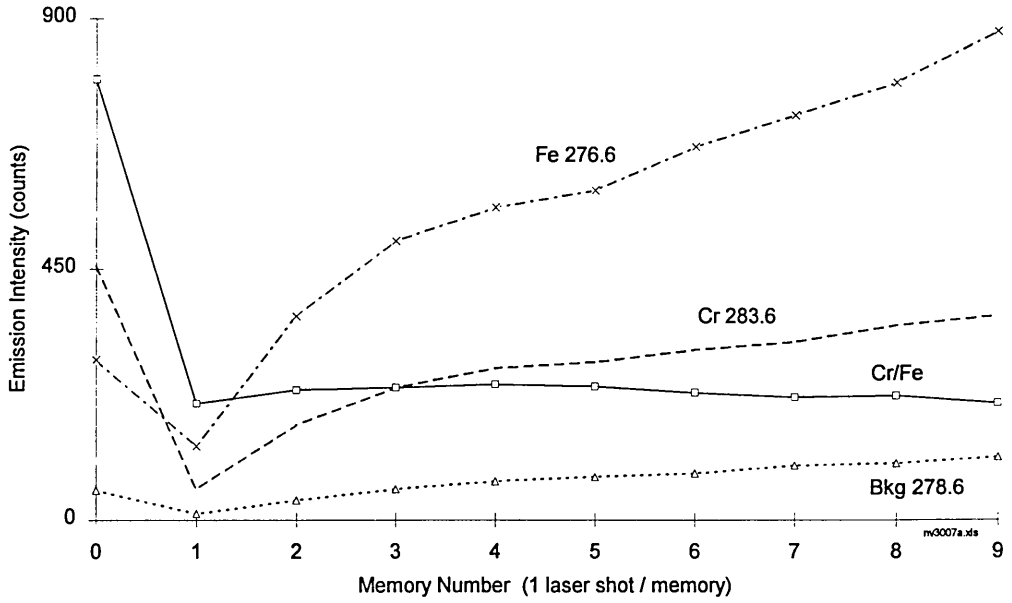

Figure 20 Emission-time response for the ablation of Cr on steel (coating thickness 20 nm) with LFLE 40 J at sample position F0.

5.4 Conclusions and Recommendations for Further Work

This study has shown that rapid depth profiling of coatings can be achieved with laser-induced plasma emission spectrometry. Emission-time signatures for the ablation of zinc/nickel coatings on steel were greatly influenced by operating parameters such as laser energy and sample position relative to the laser focal point. Improved performance was realised with high laser energy (laser flash lamp energy 70J) and the sample positioned 20 mm from the focus position, away from the laser source. The use of these operating conditions enabled linear calibration against coating thickness for zinc/nickel and tin coatings to be achieved with good precision (3.5 % RSD). Advantages include rapid measurement time (50 s for zinc/nickel, 7.2 μm) and small area of damage (~1 mm diameter) compared to glow discharge techniques (15 minutes, 10 mm diamter crater). A simple measurement strategy was utilised which involved ablation in air at atmospheric pressure. A limitation of the technique is absolute depth resolution (Δd) compared to glow discharge methods, 1.1 vs. 0.1 μm, although differences in depth of 0.02 μm for tin coatings were distinguished by the technique. This performance combined with an in situ measurement capability indicates that the technique may be valuable in industrial situations where rapid coating measurements are required.

Different emission-time signatures and rates of material removal were obtained for the ablation of different coatings, which indicated that the composition of the coating influenced plasma characteristics through complex matrix effects. This suggested that the processes involved in depth profiling with LIPS were complex and that different operating conditions may be required for each coating type. Studies with additional techniques e.g. high speed photography, imaging spectroscopy [13,14] would provide more information regarding plasma characteristics which may further understanding of the material removal processes and matrix effects.

Further work could apply the technique to the study of coatings of greater thickness such as 50 or 100 μm. Measurement times could be reduced by removing the coating at a higher rate, either by ablation at a higher repetition rate, or by using a shorter focal length focus lens that would produce a smaller laser spot with associated higher irradiance. In both cases, more energy per unit area and time would be delivered to the sample surface causing additional heating in the vicinity of the laser spot. Further work would address the effects of these changes and study other parameters which may influence profile performance. For example, sample cooling, e.g. cryogenic, could be required to dissipate the additional heat input, and the use of a buffer gas such as argon, helium, might improve analytical performance. For example, in an argon atmosphere, a denser plasma would be induced that may reduce laser-material interaction and promote more even sampling.

5.5 References

1. Silman H. and Isserlis G., *Protective and Decorative Coatings for Metals*, Averill AF, Finishing Publications Ltd., Teddington, UK, 1978.
2. Grissler W. and Jehn H. A., Editors, *Advanced Techniques for Surface Engineering*, Kluwer Academic Publishers, London, UK, 1992.
3. Briggs D. and Seah M. P., Editors, *Practical Surface Analysis by Auger and X-ray Photoelectron Spectroscopy*, Wiley, New York, 1985.
4. Bengtson A. and Danielson L., Thin Solid Films, 1985, **124**, 231-236. Depth Profiling of Thin Films Using A Grimm-type Glow Discharge Lamp.
5. Hall D. J. and Sanderson N. E., Surface and Interface Analysis, 1988, **11**, 40-44. Quantitative Depth Profiling By Glow Discharge Mass Spectrometry.
6. Raith A., Hutton R. C. and Huneke J. C., Journal of Analytical Atomic Spectrometry, 1993, **8** (6), 867. Optimisation Of Quantitative Depth Profiling With Glow Discharge Mass Spectrometry. Part 1: Optimisation Studies On Crater Shapes And Time - Depth Conversion.
7. Bengtson A., Spectrochimica Acta, 1985, **40B** (4), 631-639. A Contribution To The Solution Of The Problem Of Quantification In Surface Analysis Work Using Glow Discharge Atomic Emission Spectrometry.
8. Anderson D. R., McLeod C. W., English T., and Smith A. T., submitted to Applied Spectroscopy, 7, 1994. Depth Profile Studies Using Laser-Induced Plasma Emission Spectrometry.
9. Piepmeier E. H., in *Analytical Applications of Lasers*, editor Piepmeier E. H., Wiley New York, 1986, pp 635-639.
10. Oechsner H., Editor, *Thin Film and Depth Profile Analysis*, Springer-Verlag, Berlin, 1984.

11. Personal Communication, English T., British Steel Technical, Swinden Laboratories, Rotherham, UK.
12. Ka'ntor T., Bezur L., Pungor E., Fodor P., Nagy-Balogh J. and Heincz G., Spectrochimica Acta, 1979, **34B**, 341-357. Determination Of The Thickness Of Silver, Gold, And Nickel Layers By A Laser Microprobe And Flame Atomic Absorption Techniques.
13. Iida Y., Morikawa H., Tsuge A,. Uwamino Y. and Ishizuka T., Analytical Science, 1991, **7** (1), 61-64. Laser Induced Plasmas With An Optical Imaging Spectrometer.
14. Geersten C., Briand A., Chartier F., Lacour J. L., Mauchien P., Sjostrom S. and Mermet J. M., Journal of Analytical Atomic Spectroscopy, 1994, **9**, 17-22. Comparison Between Infrared And Ultraviolet Laser Ablation At Atmospheric Pressure - Implications for Solid Sampling ICP Spectrometry.

Chapter 6

The Discrimination Of Laser-Induced Plasma Emission Spectra Using Artificial Neural Networks

6.1 Introduction

Laser-induced plasma emission spectrometry has been used in several demanding applications such as the monitoring of steel and rubber productions, etc. because of its unique advantages, non-invasive, in situ, rapid elemental analysis. One disadvantage of the technique, however, is complex emission spectra. Emission spectra are complex because of the high temperatures of the laser-induced plasma. Intensified photodiode arrays allow time-resolved measurement, which enables analyte emission signals to be separated in time from the initial, intense background continuum. This reduces the problem somewhat, but plasma temperatures are still relatively high, resulting in complex emission spectra for many elements. In addition, many elements produce spectra with complicated baselines that contain background shifts. These spectral problems cause spectral interferences in the identification and measurement of emission lines.

The photodiode array generally requires wavelength calibration for each spectral region monitored. This can be achieved by locating known emission lines on the array from a discharge lamp or from the ablation of pure metals. The identification of unknown spectra requires each emission line to identified as a wavelength value (nm) and this value compared to wavelength tables.[1] This is achieved manually, which is usually very time consuming, or alternatively, a specially-written computer software routine is employed. For example, Chau et al [2] recently reported such a package that combined wavelength calibration with a database for identification of elements for unknown spectra. Langsam et al [3] developed a computer program which matches spectra against standard wavelengths from tables.

In this study, a novel alternative approach is devised which is based on the application of artificial neural networks (ANNs) to laser-induced plasma emission spectra. Artificial neural networks are a form of artificial intelligence (AI). An important feature of ANNs is the ability to learn by example. Conventional computer programs use techniques such as logic-tree routines to process data. In the case of identifying an element from emission lines within a spectrum, this requires the prior knowledge of the position and identification of emission wavelengths for the elements of interest. In this study, each spectrum is presented to the ANN and the network selects appropriate features and learns to recognise these patterns. The network can then identify one of these spectra when a spectrum is presented again.

An ANN is a greatly simplified computer model of the human brain and can be trained to recognise different signals or patterns.[4] When the ANN has been successfully trained, it can very rapidly identify unknown signals corresponding to the trained patterns. Artificial neural networks are particularly effective when signals are noisy and conventional statistical methods such as discriminant analysis are not suitable. They have been used in several pattern recognition applications which produce complex signals, such as spectrum analysis of electro-encapholograph data (EEG)[5] in order to identify patients with brain disorders. Other applications include radar signal processing,[6] optical character recognition,[7] and speech recognition and synthesis.[7] In the field of chemical engineering, ANNs have been applied to problems such as predicting flow rates in stirred tank reactors.[8] In analytical chemistry, ANNs have been used to successfully differentiate spectra for different polymeric materials produced by laser ablation ion mobility spectrometry (LA-IMS).[9] Artificial neural networks were applied to the calibration of iron/nickel/chromium samples in X-ray fluorescence spectrometry[10] and to the processing of signals from ion-selective electrodes.[11] Meyer et al[12] applied ANNs to the interpretation of infrared

spectra from a low resolution spectrometer. The trained ANNs were able to recognise the functional groups of 50 compounds with a success rate of 76.2 %. A tutorial review has been presented by Bos et al.[13] Hieftje and Glick[14] applied ANNs to glow discharge optical emission spectrometry in order to classify a range of metal alloys. Emission wavelengths were selected manually for 7 elements representative of the different alloy types, and the intensity values of these wavelengths were presented to the ANN.

The aim of this study is to assess the application of ANNs to the identification of emission spectra (patterns) from LIPS in order to differentiate materials. Emission spectra for 7 elements (Cu, Sn, Ti, Zn, Sb, Al and Ca) covering a 25 nm wavelength region have been directly applied to ANNs following a computerised feature extraction procedure. These elements were selected so that the ANNs would examine a range of spectral characteristics. For example, within the spectral region 307 - 332 nm, the spectrum for copper is relatively simple with just 2 emission lines, the spectrum for antimony contains 9 emission lines, and the spectrum for titanium is very complex with more than 20 lines and several background shifts. This ANN approach has several potential advantages: element emission wavelengths are not identified or assigned, wavelength calibration of the array is not required, and spectral interferences may not be problem. Although only 7 elements were included in the study, the technique may be applicable to any number of elements. The feature extraction procedure and ANNs are described, and results for the training and test modes of operation are presented. Aspects of this work are being prepared for publication.

6.2 Artificial neural networks

6.2.1 Historical

The biological origins of neural networks stem from research and theories of processes of the brain in the 1890s by James, and in the 1940s by McCulloch and Pitts.[4] Rosenblatt in 1958 modelled a neural network structure, called a perceptron, on a computer using these biological ideas, and hence the term, artificial neural network. In 1960, Widrow and Hoff simulated ANNs on a computer and developed a hardware device, an adaline (adaptive linear), that consisted of a single neuron with several inputs. However, in 1969, research in this field effectively stopped with the publication of a book by Minsky and Papert entitled Perceptrons.[15] They showed that ANNs available then had very limited capabilities. The ANNs were simple structures of only two layers, input and output, and the neurons had only on or off values. It was not until 1986 that major interest was revived with the publication of Parallel Distributed Processing, edited by McClelland and Rumelhart.[16] They presented multi-level perceptrons (input, hidden, output layers) and the derivation of the error back-propagation learning rule for this structure. These were combined with other works, the sigmoid transfer function (Grossberg, 1973), and continuously-valued neurons (Hopfield, 1984), to provide powerful ANNs that have the capability to solve complex problems. Since then, these ANNs have been used in many diverse applications.

6.2.2 Theory

The type of ANN used in this work is a multi-layer perceptron and consists of three layers of neurons: input, one or more hidden layers and an output layer. A simple network is shown in Figure 1. A neuron (neurode, node or unit) is a simulated device that receives and sends signals. Each neuron is connected to every neuron of the adjacent layer(s). Each connection has an associated connecting weight that controls the amount of influence that the input has upon

a neuron. Data flows from the input through the hidden layer to the output, i.e. a feedforward network.

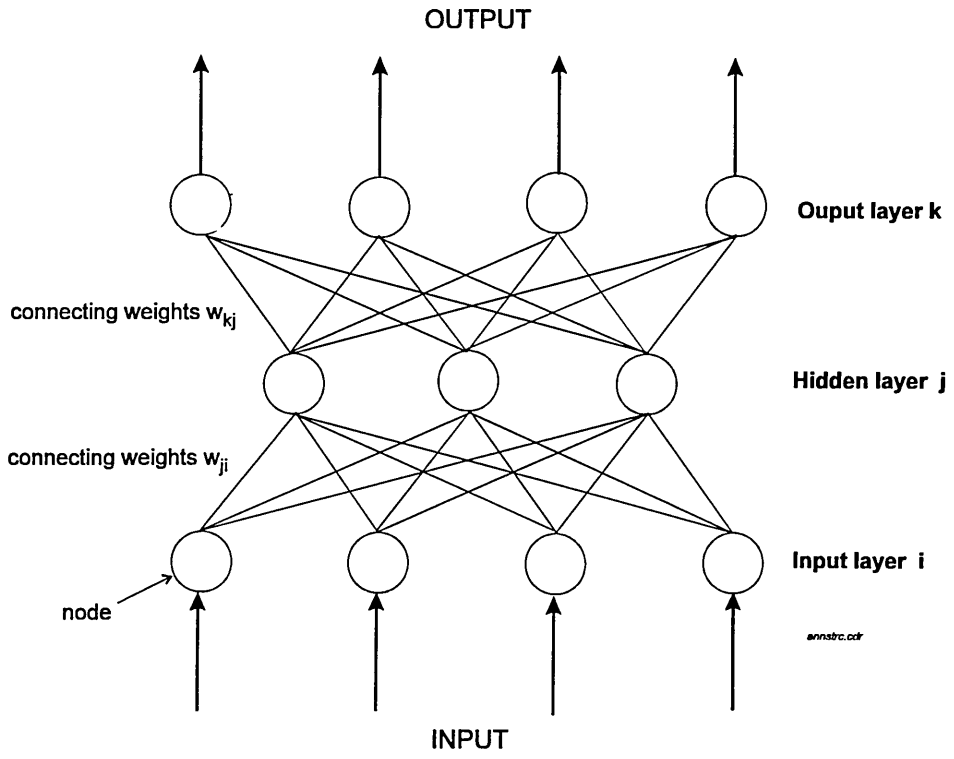

Figure 1 Structure of a back-propagation ANN

When a hidden layer neuron receives signals from the input neurons, it sums the signals, transforms the sum, and sends the result to the neurons in the next layer. The output layer repeats this process and displays the result of the test, i.e. output values that correspond to the input pattern.

The ANNs are used in two modes, training and test (use). Supervised, back-propagation networks are used here, which means that the training phase is supervised, i.e. the network is presented with the patterns and the desired output values. The input patterns and the resulting output values are compared with the desired output values. The connecting weights are adapted via an error back-propagation method to cause the output values to be changed so that

they become closer in value to the desired outputs. This learning process is repeated until the ANN can correctly discriminate between the categories. In the test mode, unknown patterns are presented for the ANN to recognise. This process is very rapid due to the parallel structure of the network. The unknown patterns must be of the same types as the training classes.

In the training and test modes, feedforward calculations are used by the hidden and output neurons to process the input data and produce the output response of the network, (Figure 2). The first calculation (combining function) combines the inputs by multiplying each input by its associated weight. The net input is the sum of these results.

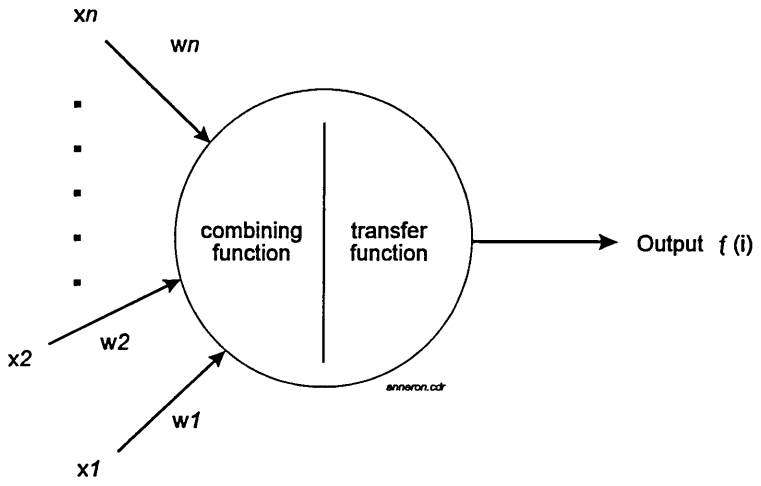

Figure 2 Diagram of a neuron in a neural network

The second calculation (transfer function) transforms this net input (i) with a non-linear sigmoid function, shown in Figure 3.

$$\text{output} = f(i) = \frac{1}{1+\exp[-(i+\theta_j)/\theta_o]}$$

where θ_j is the threshold value (or bias) which shifts the transfer function along the horizontal axis, and θ_o is a constant which determines the slope of the sigmoid.

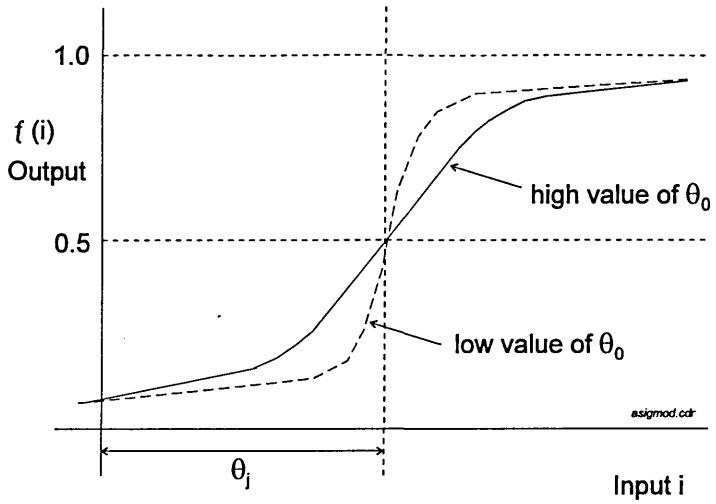

Figure 3 Sigmoid transfer function

During the training mode, these calculations are combined with additional calculations that represent the learning of the network. The output values obtained are compared to the desired values and the difference is defined by an error function, E. The aim of the learning process is to reduce the error E as quickly as possible. This is achieved using the error back-propagation rule (generalised delta rule) that propagates the error back through the network in order to adjust the connecting weights. This is described in detail elsewhere.[7,16,17] The change in weight value (Δw_{ji}) is calculated as:

$$\Delta w_{ji} = \beta E f(i) + \alpha \Delta w_{ji} \text{ (previous)}$$

where α is the momentum factor and is used to overcome a problem called 'local energy minima' and β is the learning rate which affects the speed of learning. Both have values of between 0 and 1. This learning process is repeated many times until training is complete, i.e. the network can successfully identify the input patterns.

6.3 Feature extraction

Feature extraction is a procedure used to identify the most discriminating variables of a pattern and thereby reduce the number of input data points. Ideally, all of the data from a spectrum would be presented to the ANN, i.e. the values from all 1024 pixels of the photodiode array. However, this would require an unacceptably large computer memory and a very long processing time. A more appropriate method is to extract features from the spectrum that will adequately describe the spectrum.

There are several possible methods to achieve the feature extraction. In the study of the discrimination of polymeric materials by laser ablation-ion mobility spectrometry,[7] a moving average window was used that averaged the values of each group of three pixels. This procedure performed well because the ion mobility spectrometry signatures were relatively simple broad peaks. In this study, a new feature extraction procedure, peak intensity-wavelength identification (PIWI), was devised because the spectra are more complex and contain more information than the ion mobility spectrometry signatures. The peak intensity-wavelength identification procedure is depicted in Figure 4.

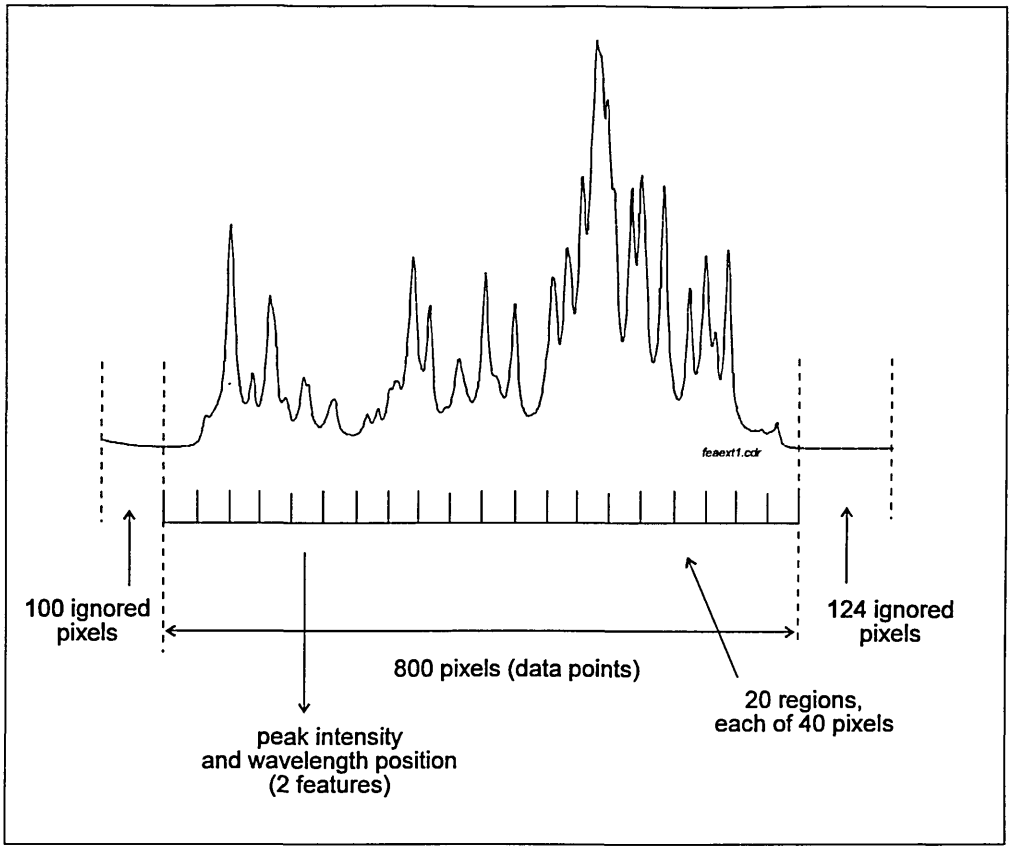

Figure 4 Schematic of the feature extraction procedure, peak intensity - wavelength identification (PIWI)

Each spectrum consisted of 1024 pixels (data points), of which the central ~730 were intensified. The procedure ignores the first 100 and last 124 because these pixels are not intensified and their values are always 0. A region of 800 pixels remained which approximated to the intensified pixels. This even number of pixels was divided into smaller regions, i.e. 20 regions each of 40 pixels. For each region the intensity value of the highest point and the corresponding pixel position (wavelength) were identified, i.e. 2 features per region. The procedure resulted in 40 features and these were presented to the ANN.

Two advantages of the PIWI procedure are that main features of each spectrum are extracted, i.e. the pixel position (wavelength) and intensity of major peaks, and it is relatively easy to change the size of the regions so that

feature resolution could be increased for later studies, if necessary, e.g. 40 to 20 pixels.

6.3 Experimental

The laser and spectrometer system used are described in Chapter 2. The background subtraction routine was utilised with the laser firing at 5 Hz and with laser flash lamp energy 40 J. A fixed time OMA program was used with time settings of time delay of 700 ns and integration time of 1 μs. The spectral region 307-332 nm was monitored by the photodiode array using grating 2 (2400 grooves/mm). The seven materials listed in Table 1 were each ablated with 20 laser shots at the same site, (experiment run time 4 s). A pellet was made of the calcium carbonate powder by pressing in a die to a pressure of 10 tons per square inch.

Material	Details
Cu	copper metal foil, BDH Analar, Merck Ltd., Lutterworth, Leicestershire, UK
Sn	tin metal rod, Specpure, Johnson Matthey, Royston, Hertfordshire, UK
Ti	titanium metal, IMI Titanium Ltd, Witton, Birmingham UK
Zn	zinc metal, BCS194d, Bureau of Analysed Standards, Newham Hall, Newby, Cleveland, UK
Sb	antimony metal rod, Specpure, Johnson Matthey
Al	aluminium metal, BCS198e, Bureau of Analysed Standards
Ca	calcium carbonate powder, BDH Analar

Table 1 Details of the materials used in the study

6.3.1 Data manipulation

The ablation of the samples resulted in a data file for each sample which contained 20 spectra. Each data file was divided in 2 files to provide training and test data, i.e. a training file and a test file, each containing 10 spectra. These files were converted into ASCII format and were subjected to the feature extraction routine (PIWI) using a purpose-written program.[18] The maximum intensity of each spectrum was normalised to 1.0 relative to the most intense spectrum of the entire group.

The data files from this step were taken into a spreadsheet program (Microsoft Excel) and each material was assigned a binary code that could be used by the ANN (Table 2). All the training files were merged in a spreadsheet to produce a single training file, and all the test files were merged to give a single test file. The layout of each file is shown in Table 3. The order of the training file was more mixed so that possible bias in the training of the network was minimised.

	Material	Code
1	Cu	0 0 0 0
2	Sn	0 0 0 1
3	Ti	0 0 1 0
4	Zn	0 0 1 1
5	Sb	0 1 0 0
6	Al	0 1 0 1
7	Ca	0 1 1 0

Table 2 Output codes for each material

TRAINING				TEST			
material	1	spectrum	1	material	1	spectrum	1
	2		1		1		2
	3		1		1		3
	4		1		1		4
	5		1		1		5
	6		1		1		6
	7		1		1		7
material	1	spectrum	2		1		8
	2		2		1		9
	3		2		1		10
	4		2	material	2	spectrum	1
	5		2		2		2
	6		2		2		3
	7		2		2		4
material	1	spectrum	3		2		5
	2		3		2		6
	3		3		2		7
	4		3		2		8
	5		3		2		9
	6		3		2		10
	7		3	material	3	spectrum	1
etc.		etc.		etc.		etc.	

Table 3 Layout of training and test data files

6.3.2 Artificial neural networks

The program used was a commercially available package (NeuralWare Pittsburg, USA) and was run on an IBM-compatible personal computer (Viglen 486 DX2 66 MHz, Alperton, Middlesex). The program allowed different network structures to be constructed, containing up to a maximum of 100 neurons. The ANNs used always had 40 input and 4 output neurons. This enabled differentiation of up to 16 materials (classes). The values of the output neurons were always between 0 and 1.

The error back-propagation method of learning was used and values of α,β,θ_o were 0.6, 0.9 and 1, respectively. The patterns in the training file were used to train the ANN. The training was stopped after 100,000 iterations, and the ANN was then used in the test mode and tested with the training and test files.

6.4 Results and Discussion

A typical spectrum for the ablation of each material is depicted in Figure 4 and principal emission lines are listed in Table 4. The spectrum for titanium is very complex with many emission lines and several shifts in background. The other spectra are less complex but antimony and tin also contain several emission lines. Emission lines for titanium, copper, antimony, tin and zinc are similar in wavelength and there are several spectral overlaps. The 7 spectra are overlaid in Figure 5 which illustrates the potential complexity of the problem and closeness of many emission lines. The large variation in emission intensities between laser shots, shown for calcium in Figures 7 and 8, might also present problems in the discrimination process. The precision was estimated to be ~18 % relative standard deviation (% RSD) for both Ca emission lines. The ablation of other materials resulted in precision of typically ~9 % RSD (copper). The pixel positions for the emission lines did not vary and were the same for each laser shot.

Element	Wavelength (nm)
Al I	308.215
Al I	309.271
Ca II	315.887
Ca II	317.933
Cu I	324.754
Cu I	327.396
Sb I	323.252
Sb I	326.751
Sn I	317.502
Sn I	326.233
Sn II	328.321
Ti II II *	323.612, 323.904 *
Zn I	328.233
Zn I	330.259

* unresolved emission lines

Table 4 Principal emission wavelengths of the elements studied

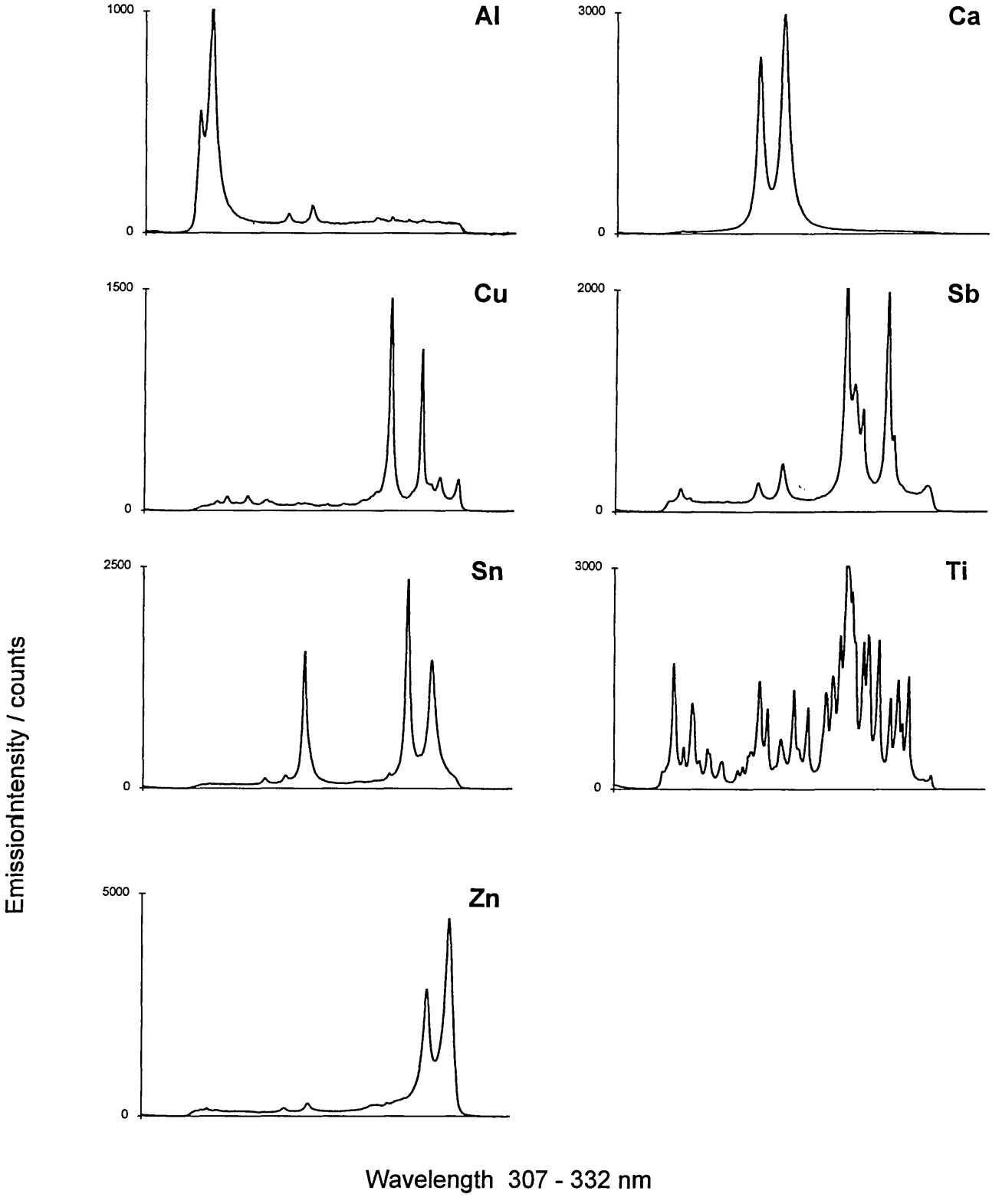

Figure 5 Emission spectra for the ablation of the seven materials.

(Principal emission lines are listed in Table 4)

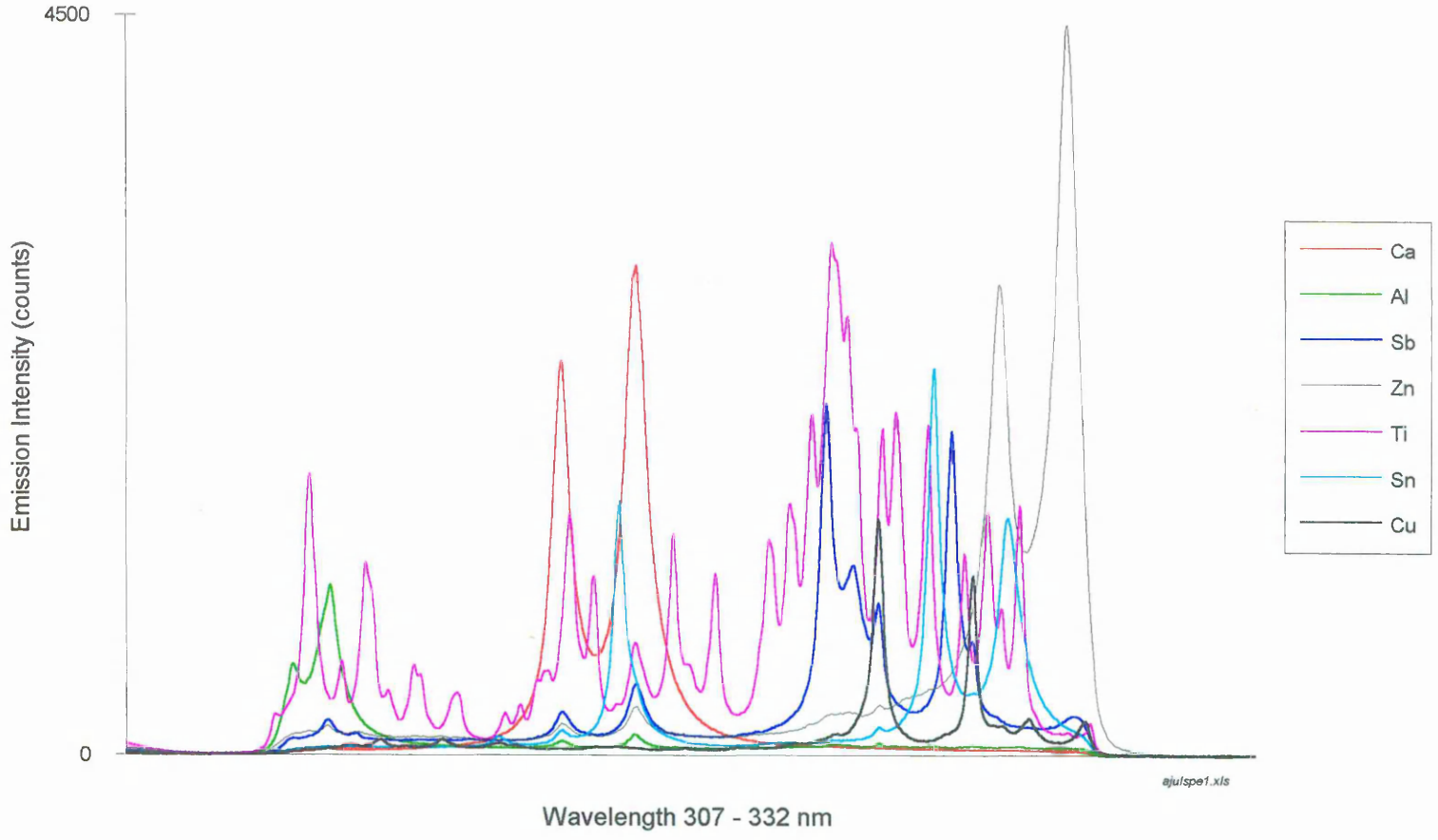

Figure 6 Overlay of the emission spectra for the ablation of the seven materials

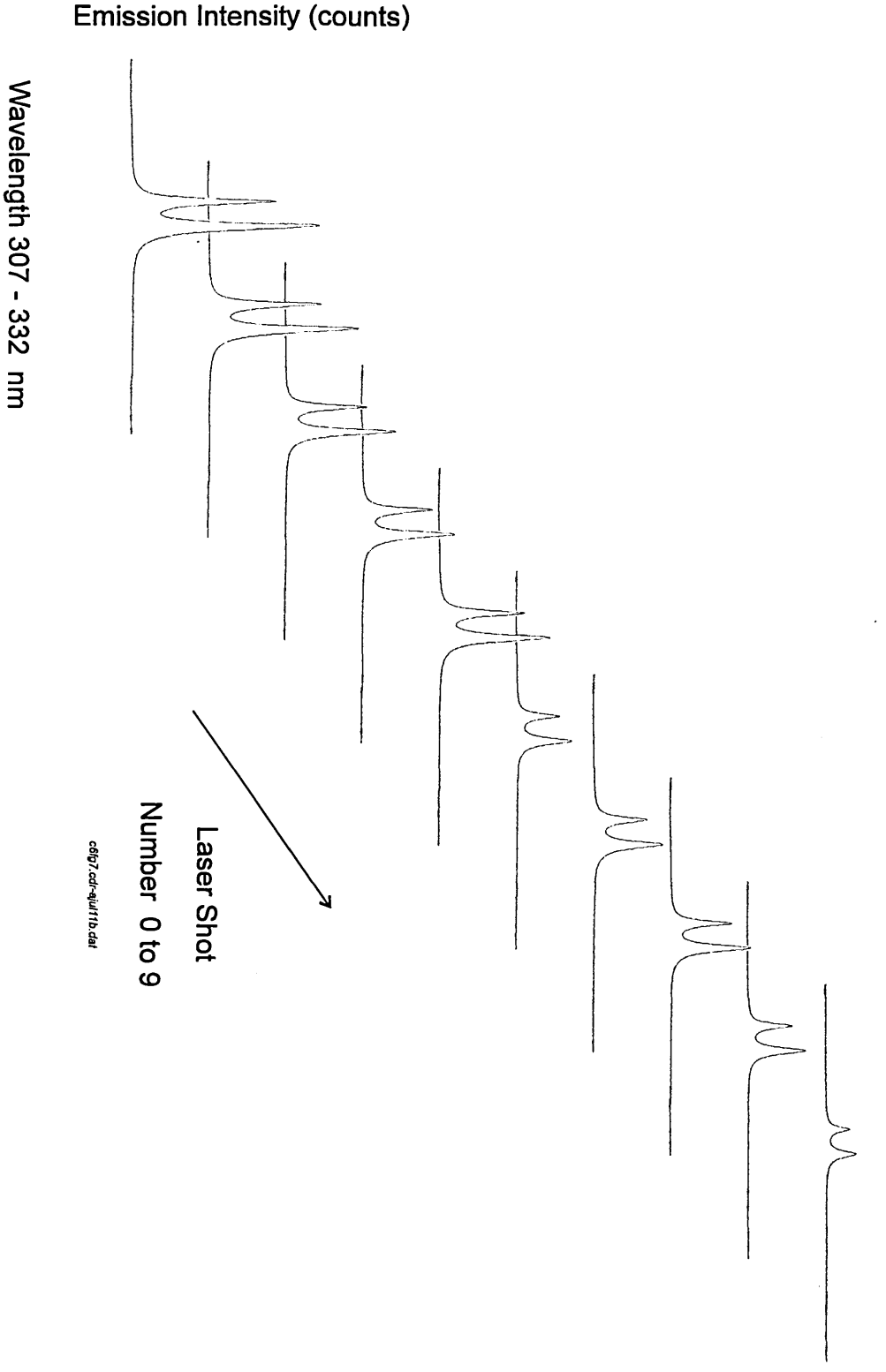

Figure 7 Emission intensity-wavelength-time response for the ablation of calcium carbonate. Each spectrum was produced by a single laser shot at the same sample site.

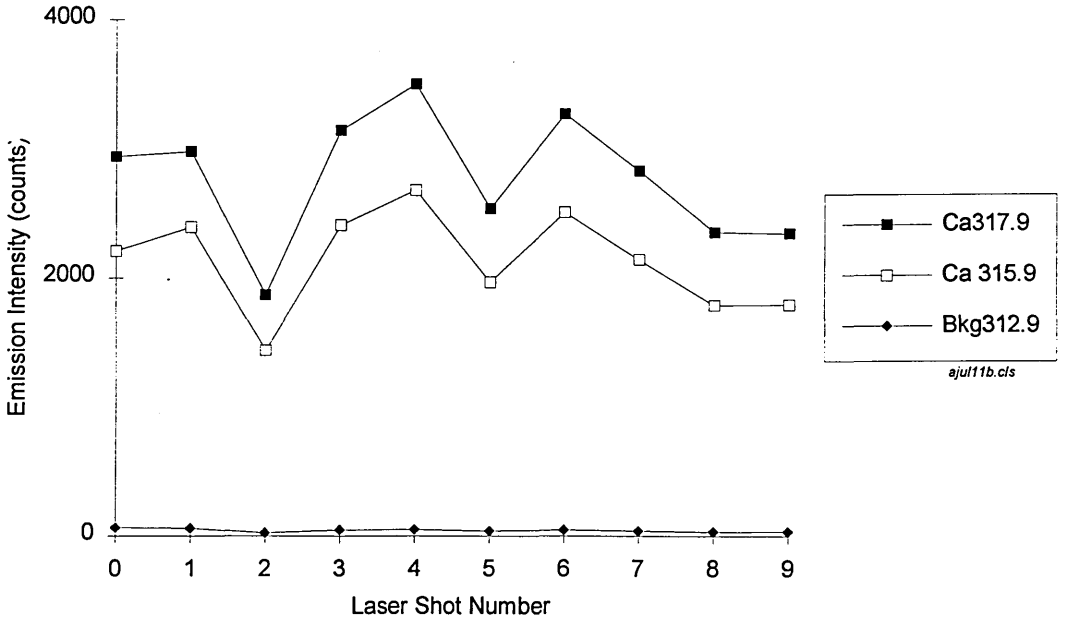

Figure 8 Emission-time response for the ablation of calcium carbonate

The performance of ANNs with either one or two hidden layers and with different number of nodes in the hidden layer(s) was investigated. Artificial neural networks with these different structures were trained with the training file and then tested. Results indicated that for best performance, i.e. least error, the network should have one hidden layer containing 10 neurons. With this structure and after 100,000 iterations, it was possible to discriminate all materials with an accuracy of 100% both in the training and test phases. Typical results for the test mode are shown in Table 5. Performance can be assessed by comparing the output values with the desired values for each material, and by considering the variation of the output code for each material (standard deviation). In each case, the output 0.0 values approximate to 0.0 and the output 1.0 values are very close to 1.0. The highest 0.0 value was 0.0207 and the lowest 1.0 value was 0.9924. This shows that the ANN was 100% successful in discriminating between the materials. The low standard

deviation values that were obtained indicate that the ANN could achieve these results with good precision.

Material	Output Values				
Cu	desired	0.0000000	0.0000000	0.0000000	0.0000000
	mean	0.0001904	0.0007901	0.0002828	0.0096572
	SD	0.0000106	0.0002525	0.0000471	0.0039918
Sn	desired	0.0000000	0.0000000	0.0000000	1.0000000
	mean	0.0004666	0.0000000	0.0010627	0.9957102
	SD	0.0000048	0.0000000	0.0001611	0.0001133
Ti	desired	0.0000000	0.0000000	1.0000000	0.0000000
	mean	0.0003818	0.0206684	0.9955831	0.0072032
	SD	0.0000053	0.0101062	0.0016062	0.0014532
Zn	desired	0.0000000	0.0000000	1.0000000	1.0000000
	mean	0.0023046	0.0000000	0.9970476	0.9985614
	SD	0.0000343	0.0000000	0.0001284	0.0000148
Sb	desired	0.0000000	1.0000000	0.0000000	0.0000000
	mean	0.0002671	0.9923860	0.0010346	0.0000000
	SD	0.0000023	0.0009371	0.0001042	0.0000000
Al	desired	0.0000000	1.0000000	0.0000000	1.0000000
	mean	0.0004447	0.9940660	0.0032040	0.9981207
	SD	0.0000095	0.0014241	0.0009869	0.0010057
Ca	desired	0.0000000	1.0000000	1.0000000	0.0000000
	mean	0.0007854	0.9758306	0.9999750	0.0011966
	SD	0.0000108	0.0184683	0.0000117	0.0001456

SD = standard deviation, n = 10

Table 5 Typical output response from the artificial neural network for the test data

ANNs with more neurons in the hidden layer or with two hidden layers were also found to be successful. It is beneficial, however, to use the successful structure with the smaller number of neurons in the hidden layer. If the structure is over-complex training might not be successful. Using a smaller number of neurons in the hidden layer allows more neurons to be used in the other layers, if required. When fewer than 10 neurons were used in the hidden layer, either successful training was not achieved or performance was not satisfactory (0.0 values not approximating to 0.0, 1.0 values not close to 1.0).

These results indicate that ANNs can be successfully used to discriminate the complex spectra from laser-induced plasma emission spectrometry. This was achieved without the wavelength-calibration of the photodiode array detector, or the identification and assignment of element emission wavelengths. The emission spectra from 7 materials have been discriminated here, and the network can be further trained in the present form to identify a larger number of materials. By increasing the number of output neurones to 5 or 6 then the number of materials in the database could be increased up to 32 or 64, respectively. This qualitative measurement may be useful in the sorting of metals, alloys or plastics containing inorganic additives, provided the ANNs are trained on the spectrum for each material. As the discrimination process is very fast, it should be possible to achieve on-line measurements with identification of the spectrum from each laser shot.

A limitation to the technique is that the ANNs used in this study can only recognise the types of signals that they have been trained with. So, for example, if a sample contained a mixture of titanium and Al, then the ANNs would need to be trained to recognise this mixture. Also there is limited capability towards quantitative measurements. The use of other types of ANN, such as Kohonen networks, could resolve these problems. Kohonen networks

are self-organised and enable training without supervision, i.e. unsupervised networks; the input patterns are presented only, and the network organises, or trains, itself. An advantage of this type of ANN is that there are many more output neurons, e.g. 100, which enable a greater level of description of the input patterns to be achieved, and this may be more suitable to quantitative applications.

6.5 Conclusions and Recommendations For Further Work

Artificial neural networks (ANNs) have been successfully used for pattern recognition of spectra generated by laser-induced plasma emission spectrometry. The technique was applied to 7 materials and it was possible to identify all training and test spectra with an accuracy of 100%. This success rate and the rapid discrimination time indicates that the technique combined with laser-induced plasma emission spectrometry may be useful in on-line industrial situations where, for example, rapid sorting of materials is required.

With further work, the technique could be applied to a wider spectral region, e.g. 100 or 200 nm, that encompasses emission lines for more elements. The wider spectral region could be achieved here by using a lower resolution grating in the spectrometer. The lower resolution would probably lead to many spectral interferences that would interfere with element identification by conventional techniques of wavelength identification. With the ANN technique, spectral interferences would probably not present a problem because the feature extraction program and the ANNs examine the whole wavelength region and not just pre-determined emission lines. The data base could be expanded with further work to include other metals, alloys or plastics containing inorganic additives, and investigate the use of other types of artificial neural networks in quantitative analysis.

6.6 References

1. Harrison G. R., *Wavelength Tables with Intensities in Arc, Spark or Discharge Tube*, M.I.T. Press, Cambridge, Mass., USA, 1969.
2. Chau F. T, Lau K. S., Wong K. H., Mak C. H. and Wong W. K., Laboratory Microcomputer, 1990, **9**, (3), 88-93. A Software Package For Spectrum Processing Of A Laser Induced Plasma Spectrometer.
3. Langsam Y., Tenenbaum A. and Thurm J., Journal of Chemical Information Computer Science, 1980, **20** (4), 230-234. Computer-Aided Spectral Identification Of Laser-Induced Plasma Emission.
4. Eberhart R. C. and Dobbins R. W., in *Neural Network PC Tools*, Eberhart R. C. and Dobbins R. W., Editors, Academic Press, San Diego, USA, 1990, pp 9-34.
5. Saatchi R. and Jervis B. W., Computing Control Engineering Journal, 1991, **2**, 61-68. PC-Based Integrated System Developed To Diagnose Specific Brain Disorders.
6. Sigillito V. G. and Hutton L. V., in *Neural Network PC Tools*, Eberhart R. C. and Dobbins R. W., Editors, Academic Press, San Diego, USA, 1990, pp 235-250.
7. Beale R. and Jackson T., *Neural Computing: An Introduction*, Adam Hilger, Bristol, UK, 1990.
8. Bhagat P., Chemical Engineering Progress, 1990, August, 55-60. An Introduction To Neural Nets.
9. Simpson M., Anderson D. R., McLeod C. W., Cooke M. and Saatchi R,, Analyst, 1993, **118**, 1293-1298. Use Of Pattern Recognition For Signatures Generated By Laser Desorption-Ion Mobility Spectrometry Of Polymeric Materials.

10. Bos M. and Weber H. T., Analytica Chimica Acta, 1991, **247**, 97-105. Comparison Of The Training Of Neural Networks For Quantitative X-ray Fluorescence Spectrometry By A Genetic Algorithm And Backward Error Propagation.
11. Bos A., Bos M. and van der Linden W. E., Analytica Chimica Acta, 1990, **233**, 31-39. Processing Of Signals From An Ion-selective Electrode Array By A Neural Network.
12. Meyer M. and Weigelt T., Analytica Chimica Acta, 1992, **265**, 183-190. Interpretation Of Infrared Spectra By Artificial Neural Networks.
13. Bos M., Bos A. and van der Linden W. E., Analyst, 1993, **118**, 323-328. Data Processing By Neural Networks In Quantitative Chemical Analysis.
14. Hieftje G. M. and Glick M., Applied Spectroscopy, 1991, **45** (10), 1706-1716. Classification Of Alloys With An Artificial Neural Network And Multivariate Calibration Of Glow Discharge Emission Spectra.
15. Minsky M. and Papert S., *Perceptrons*, M.I.T. Press, Cambridge, MA, USA, 1969.
16. Rumelhart D. E. and McClelland J. L., *Parallel Distributed Processing, Explorations in the Microstructure of Cognition, Vol 1: Foundations*, MIT Press, Cambridge, USA, 1986.
17. Eberhart R. C. and Dobbins R. W., in *Neural Network PC Tools*, Eberhart R. C. and Dobbins R. W., Editors, Academic Press, San Diego, USA, 1990, pp 35-58.
18. Personal Communication, Saatchi R., School of Engineering Information Technology, Sheffield Hallam University, Sheffield, UK.

Chapter 7

Conclusions And Recommendations For Future Work

7.0 Conclusions and Future Work

An optical multichannel analyser and a Q-switched Nd:YAG have been successfully configured in an integrated laser-induced plasma emission spectrometry system. The operations of the laser and optical multichannel analyser were synchronised so that the optical multichannel analyser was able to monitor discreetly the laser-induced plasma from each laser shot. Studies of the ablation of copper metal showed that characteristics of the laser-induced plasma were influenced by the operating conditions. Relatively high laser energy produced a plasma that was more intense and longer-lived than that produced by lower energy. Time resolved measurement enabled large improvements in sensitivity to be realised, and precision was improved from 17.1 to 3.8 % relative standard deviation (RSD) by accumulating a relatively large number of laser shots (2100 vs. 30). For the determination of copper in aluminium alloy, the limit of detection was 0.010 % m/m and precision was 3.0 % RSD using an aluminium signal from the alloy matrix was used as internal standard, both comparable to other published data.

The optical multichannel analyser was used separately to monitor an inductively coupled plasma (ICP) emission source. Precision with this more stable source was 0.5 % RSD, indicating that the optical multichannel analyser is capable of achieving good precision. The optical multichannel analyser enabled several emission lines and the spectral background to be monitored simultaneously during a transient signal event produced by sample introduction with flow injection.

Studies showed that the ablation of polymeric materials is different from metals. The rate of material removal was higher for the polymer but the plasma had a shorter lifetime. Operating conditions of relatively low laser energy and focused laser radiation were found to provide improved analytical performance for

antimony, calcium and zinc in poly (vinyl chloride) samples. Selective volatilisation of antimony occurred and the effect was minimised by firing only a small number of laser shots at a sample site. Linear calibration graphs were obtained with limits of detection of 0.09, 0.04 and 0.07 % m/m for antimony, calcium and zinc, respectively, indicating bulk analysis capabilities. Precision was improved from 7.3 to 1.8 for antimony when a carbon signal from the polymer matrix was used as an internal standard. A range of poly (vinyl chloride) samples was successfully monitored for twelve elements (Al, Ba, Ca, Cu, Fe, Mg, Pb, P, Sb, Sn, Ti, Zn), without the need for time-consuming sample digestion, demonstrating a rapid survey analysis capability. Sensitivity and speed of measurement were higher than another direct technique, energy dispersive X-ray fluorescence.

The micro-analysis capability of laser-induced plasma emission spectrometry was successfully applied to the depth profile measurement of coatings on steel substrates. A series of coatings was studied, zinc/nickel alloy, tin and titanium nitride, on steel substrates over a range of coating thickness up to 8.0 μm. Depth profile performance and the shape of the resultant crater were greatly influenced by operating conditions, and it was found that defocused laser light and maximum laser energy provided improved performance and depth resolution. New output parameters were devised, and studies showed a linear relationship between the area under the zinc profile line and coating thickness. Good precision for replicate measurements was obtained with rapid measurement times of 50 s. The performance indicates that laser-induced plasma emission spectrometry can be used for the rapid depth profile measurement of coatings. In addition, the technique was also able to detect a layer of aluminium within a zinc coating, and the technique detected an ultra-thin chromium coating (20 nm). The technique has significant advantages compared to conventional glow discharge-optical emission spectrometry, such

as speed (50 vs. 700 s), smaller size of crater (~1 mm vs. ~10 mm) and non-invasive measurement capabilities, suggesting the technique may be appropriate for industrial application.

A novel technique for the processing of laser-induced plasma emission spectra was developed. Artificial neural networks, a form of artificial intelligence, were applied to the emission spectra of 7 materials. The artificial neural networks were successfully trained and could rapidly differentiate between the spectra with a 100 % success rate. There was, however, limited capability towards quantitative measurements, which might be resolved by the use of other types of artificial neural networks, such as Kohonen networks.

Future work could address a number of issues. A more integrated and versatile laser-induced emission spectrometry system would provide computer control of the laser energy, sample manipulation and fibre optic observation position. These are set manually in this work, which is time-consuming and may lead to loss of precision in the case of laser energy. The positioning of the sample and fibre optic could be achieved by mounting each separately on computer-controlled motorised XYZ stages. Automated sample manipulation would enable the sample to be quickly positioned at different distances from the laser focal point and the fibre to be rapidly aligned to the laser spot. It would enable versatile laser sampling of material, such as allowing a fresh area of sample to be ablated by each laser shot, or a large area of sample to be examined by ablating in a grid pattern. The computer program of the optical multichannel analyser could be modified to provide integrated control of these parameters. The provision of a miniature video camera to monitor the sample position would provide precise ablation of different regions of the sample.

With further work, the effect of operating parameters, such as a buffer gas or the focal length of the focus lens, upon the ablation of polymeric materials and coated substrates could be investigated. Buffer gases that could be studied are argon, helium, neon and nitrogen, and may lead to improvements in analytical performance for the analysis of polymeric materials, and to improvements in depth profile performance for coated samples. Investigation of the use of partial gas pressures could provide further improvements. The depth profile studies could be extended to the measurement of thicker coatings such as 100 μm, the quantification of coating elements, and to the measurement of other coatings such as metallic multi-layers and coating systems with an insulating component, e.g. paints containing metals, titanium nitride on glass or plastic substrates.

Artificial neural networks could be applied to the studies described in this thesis, such as to emission spectra recorded with the optical multichannel analyser from an ICP emission source, to provide enhanced performance in terms of speed of data processing. This might be useful in laboratory-based applications of material quality control, or in on-line applications of ICP emission spectrometry. In metallurgical applications of laser-induced plasma emission spectrometry, artificial neural networks could be applied to the spectra of different alloys in order that alloys could be rapidly sorted by type. For example, aluminium alloys could be sorted by copper content. This could be extended to other alloying elements. In the polymeric materials study, artificial neural networks could be trained to recognise the spectra from polymeric materials containing additives at different concentrations. When trained, the technique could then rapidly differentiate between polymer samples by the additive content of each sample. The rapid data processing capability of artificial neural networks could then exploit the full potential speed of laser-induced plasma emission spectrometry in an on-line implementation of survey analysis. The

laser-induced plasma emission spectrometry system used in these studies has a capability of up to ten laser shots (and associated emission spectra) per second. With appropriate sample manipulation, this could provide a powerful sorting tool for inorganic additives in polymeric materials.

Recent studies[1] have used laser ablation-ion mobility spectrometry (LA-IMS) and artificial neural networks to rapidly differentiate between different types of polymeric materials, for example, between poly (vinyl chloride) and polyethylene. The combination of LA-IMS with simultaneous laser-induced emission spectrochemical measurement would provide a powerful technique to identify polymer type and the inorganic additives present. Artificial neural networks could be used to rapidly process the data from this combined technique.

Reference

1. Simpson M., Anderson D. R., Saatchi R., McLeod C. W. and Cooke M., Analyst, 1993, 118, 1293-1298. The Use Of Pattern Recognition For Signatures Generated By Laser Desorption - Ion Mobility Spectrometry Of Polymeric Materials.

Acknowledgement

I would like to acknowledge and thank several people:

My Supervisors, Cameron McLeod, Reza Saatchi and Trevor Smith for their advice and encouragement. I thank Reza Saatchi also for writing the feature extraction computer program used in the artificial neural network studies.

Staff of Sheffield Hallam University: Brian Didsbury for his help with the design and construction of equipment; Kevin Blake for the scanning electron microscopy examinations; and Mac Jackson for the Talysurf surface analyses.

For supplying samples: Richard Dellar (FMC Corporation (UK) Ltd, Process Additives Division, Manchester) for the polymer samples; Tim English (British Steel Technical, Swinden Laboratories, Rotherham) for the coated zinc/nickel, tin and chromium coated samples; Gavin Williams (Materials Research Institute, Sheffield Hallam University) for the titanium nitride coated sample; and Arne Bengston (Swedish Institute for Metals Research, Stockholm, Sweden) for the zinc coated sample.

Richard Burdett (EG&G, Sorbus House, Wokingham) for helpful discussions about the optical multichannel analyser.

My Friends and Colleagues, in particular Alan Cox and David Mowthorpe, for their support and encouragement.

I am very grateful to the DTI and SERC for funding this research project under the LINK TAPM program, and also to the School of Science, Sheffield Hallam University.

Finally, I must give special thanks to my Family, my wife Alison and son David John, for their patience, help and support while 'Daddy finishes his book'.

Postgraduate Studies

1. Courses, Conferences and Seminars

Courses and conferences

Those attended and participated in during the period of this research are listed below:

Date	*Course / Conference*	*Location*
5/91	Laser Safety Training Course	Loughborough University
9/91	European Materials Research Society, Laser Ablation Summer School	Carcans-Maubuisson, France
10/91	BCR, Community Bureau of Reference Arsenic Speciation Meeting	Brussels, Belgium
3/92	Royal Society of Chemistry Conference	Newcastle University
1/93	European Plasma Winter Conference, paper presented: Survey Analysis of Polymeric Materials Using Laser-Induced Plasma Emission Spectrometry	Granada, Spain
2/93	Fisons VG Elemental, Training Course Laser Ablation - ICP - MS	Winsforth, Cheshire
7/93	Post-CSI Symposium on Analytical Applications of Glow Discharge Sources	York University
9/93	Spectro Analytical ICP Application Seminar	Sheffield Hallam University
5/94	Laser Ablation Workshop, British Geological Survey	Kegworth, Nottinghamshire

Seminars at Sheffield Hallam University:

participation in weekly research group seminars

attendance at School of Science seminars

presentation of papers at seminars of the School of Science, and the School of Engineering Information Technology

Seminars with collaborating establishment:

participation and presentation of papers at 3 monthly progress meetings of Sheffield Hallam University, UMIST, Arun Technology, DTI and SERC, as part of the DTI and SERC LINK TAPM funded project

2. Publications

Anderson D. R., McLeod C. W. and Smith A. T., Journal of Analytical Atomic Spectrometry, 1994, **9**, 67-72. Rapid Survey Analysis of Polymeric Materials Using Laser Induced Plasma Emission Spectrometry.

Anderson D. R., McLeod C. W., Smith A. T., and English T., submitted to Applied Spectroscopy, 7/94. Depth Profile Studies Using Laser-Induced Plasma Emission Spectrometry.

Simpson M., Anderson D. R., Saatchi R., McLeod C. W. and Cooke M., Analyst, 1993, **118**, 1293-1298. The Use Of Pattern Recognition For Signatures Generated By Laser Desorption - Ion Mobility Spectrometry Of Polymeric Materials.

Simpson M., Anderson D. R., McLeod C. W. and Cooke M., Analyst, 1993, **118**, 449-451. Polymer Characterisation Using Laser Desorption - Ion Mobility Spectrometry.

Bibliography

Andrews D. L., *Lasers in Chemistry*, Springer Verlag, London, Second Edition, 1990.

Cremers D. A, and Radziemski L. J., Editors, *Laser-Induced Plasmas and Applications*, Marcel Dekker, New York, 1989.

Eberhart R. C. and Dobbins R. W., *Neural Network PC Tools: A Practical Guide*, Academic Press, San Diego, USA, 1990.

Moenke-Blankenburg L., *Laser Micro Analysis*, Wiley, New York, 1989.

Montaser A. and Golightly D. W., Editors, *Inductively Coupled Plasmas in Analytical Spectrometry*, VCH Publishers, New York, 1987.

Ready J. F., *Effects of High Power Laser Radiation*, Academic Press, New York, 1971.

Slickers K., *The Automatic Atomic Emission Spectroscopy*, Brühl Universitätsdruckerei, Giessen, Germany, Second Edition, 1993.

Appendix 1

Calculations used in the thesis.

1. Calculation of the rate of material removal from the size of the laser crater

- crater dimensions were taken from Talysurf surface measurements of laser-produced craters

calculation of crater volume

assume crater is cylindrical in shape

volume of cylinder = $\pi r^2 h$

where r = radius of crater

h = depth of crater

mass removed per crater

density of material (ρ) = mass / volume

$\therefore$ mass = ρ volume

volume of material removed = $\pi r^2 h$

$\therefore$ mass removed = $\rho \pi r^2 h$ (mg mm^{-2} mm^2 mm)

mass removed = $\rho \pi r^2 h$ (mg)

For poly (vinyl chloride):

crater produced by 10 laser shots

radius of crater = 0.5 mm

depth of crater = 50 μm = 0.05 mm

ρ poly (vinyl chloride) = 1.4 mg mm^{-3}

mass removed (10 laser shots) = $1.4 \pi 0.5^2 0.05$ mg

$\therefore$ rate of mass removal = 5.5 μg per laser shot

For zinc/nickel coating on steel:

crater produced by 200 laser shots

radius of crater = 0.7 mm

depth of crater = 7.4 μm = 0.0074 mm

ρ zinc 7.14 mg mm^{-3}

ρ nickel 8.90 mg mm^{-3}

ρ iron 7.86 mg mm^{-3}

ρ average = 7.97 mg mm^{-3}

mass removed (200 laser shots) = $7.97 \pi 0.7^2 0.0074$

$\therefore$ rate of mass removal = 0.45 μg per laser shot

The mass removed per laser shot was calculated for other materials using the densities below. Density values were taken from CRC Handbook of Chemistry and Physics, 60th Edition, except that for poly (vinyl chloride), which was from the Goodfellows Catalogue (1992).

ρ tin 7.28 mg mm^{-3}

ρ chromium 7.20 mg mm^{-3}

ρ titanium 4.50 mg mm^{-3}

2. Calculation of tin coating thickness from the tin coating weight

- values of coating weight for each sample were provided by the supplier of the samples (British Steel Technical, Swinden Laboratories, Rotherham, UK)

density of material (ρ) = mass / volume

$\therefore$ volume = mass / ρ

volume = length x width x height

where height = coating thickness (T)

$\therefore$ length x width x T = mass / ρ

$\therefore$ T = (mass / ρ) / (length x width)

mass = 10.8 g m^{-2} = 10.8 x 10^{-4} g cm^{-2}

ρ = 7.28 g cm^{-3}

let length and width = 1 cm

$\therefore$ T = (10.8 / 7.28) / (1 x 1)

$= 1.479 \times 10^{-4}$ cm

$\therefore$ coating thickness = 1.479 μm

3. Calculation of the mass of chromium coating removed with the first laser shot

coating thickness of chromium = 0.020 μm (= 20×10^{-6} mm)

assume crater is cylindrical in shape

volume of cylinder = $\pi r^2 h$

where radius of crater (r) = 0.7 mm

h = height = coating thickness = 20×10^{-6} mm

density of material (ρ) = mass / volume

where ρ chromium = 7.20 mg mm^{-3}

$\therefore \rho$ = mass / ($\pi r^2 h$)

$\therefore$ mass = $\rho \pi r^2 h$

$= 7.2 \times 10^{-6} \pi 0.7^2 \ 20 \times 10^{-6}$

$= 221.67 \times 10^{-6}$ mg

= 0.22 μg

$\therefore$ mass detected with first laser shot = 0.22 μg

Appendix 2

A copy of the published paper associated with the work of this thesis is below:

Rapid Survey Analysis of Polymeric Materials by Laser-induced Plasma Emission Spectrometry*

David R. Anderson and Cameron W. McLeod
Division of Chemistry, School of Science, Sheffield Hallam University, Sheffield, UK S1 1WB

Trevor A. Smith
Arun Technology Limited, Unit 16, Southwater Industrial Estate, Station Road, Southwater, Horsham, Sussex, UK RH13 7UD

Laser-induced plasma emission spectrometry has been applied to the analysis of poly(vinyl chloride) materials. Methodologies used to optimize the monitoring of the time-dependent emission from the laser-induced plasma are discussed, and the effects of key parameters, such as laser energy, sample position and repetitive firing at given sites, were examined. Basic performance data are reported for Ca [limit of detection 0.016% m/m and 4.8% relative standard deviation (RSD)] and Sb (limit of detection 0.04% m/m and 4.8% RSD) and the potential use for rapid survey analysis is demonstrated.

Keywords: *Laser-induced plasma emission spectrometry; gated diode array detection; laser ablation; polymer analysis*

Polymeric materials generally contain a wide variety of additives which are used to give specific properties to the material.[1] These include, pigments for colour (*e.g.*, white TiO_2), fillers (*e.g.*, $CaCO_3$), stabilizers (*e.g.*, Zn, Pb and Ba), flame-retarding agents (*e.g.*, Sb, P) and smoke suppressants (*e.g.*, Zn), among others. These inorganic components vary in concentration from trace (μg g^{-1}) to minor (%) levels. Analytical techniques currently in use for such analyses include solution-based atomic spectrometric methods[2,3] and X-ray fluorescence spectrometry.[4] An alternative approach is direct spectrochemical analysis by laser ablation (LA), either by direct spectral measurement of the laser-induced plasma, or by coupling to another analytical technique. For example, LA with inductively coupled plasma (ICP) atomic emission spectrometry has been used for survey analysis of paints and polymers,[5] while ICP mass spectrometry has been applied to polymeric and refractory materials.[6]

Direct spectrochemical measurement of the plasma, laser-induced plasma emission spectrometry (LIPS), enables rapid, *in situ* analysis,[7,8] and is particularly suited to process measurement.[9] The emission signals from the laser-induced plasma are complex and vary greatly with time. Time-resolved measurement is usually essential for the separation of the analyte emission response from the intense plasma background.[10] Basic characterization of the laser-induced plasma and systematic studies concerning the effect of key parameters, such as the wavelength of the laser light and the type and pressure of the buffer gas, have been reported.[11–16] Niemax *et al.*,[16] concluded that a wavelength of 1064 nm was more suitable than 266 nm for analysis of glass and steel matrices. Other workers[13–15] found that a reduced pressure of Ar gas, typically 133.32×10^3 Pa, offered improved analytical performance. For process monitoring situations, where it may not be feasible to achieve partial pressures, atmospheric pressure has been used. Cremers and Archuleta[9] reported the *in situ* measurement of molten steel for five elements (Ni, Cr, Si, Mn and Cu) using a laser wavelength of 1064 nm by LIPS and LA-ICP and concluded that at least semiquantitative analysis was feasible. Lorenzen *et al.*[17] described the *in situ* monitoring of S, Si and Zn in rubber production using an excimer laser operating at 248 nm, and discussed the choice of laser wavelength for this application.

The present study examines the application of LIPS to the rapid survey analysis of poly(vinyl chloride) (PVC) samples, and provides information about the emission characteristics of the laser-induced plasma, in particular the emission–time profiles of analyte and background emission. Basic performance data for the determination of Sb, Ca and P in PVC samples are presented.

Experimental

Instrumentation

A schematic diagram of the LIPS system is shown in Fig. 1, and details of the instrumentation and operating parameters are given in Table 1. The system consisted of a Q-switched Nd:YAG laser with output wavelength of 1064 nm, an optical multi-channel analyser (OMA) that comprised a spectrometer, an intensified photodiode array (PDA) detector, a computerized control system and a master pulse generator. Operation of the laser and the OMA was synchronized electronically using the master pulse generator. This controlled the timings of the laser flash lamp and Q-switched laser firing, and the detector gating and scanning of the detector array. Both the laser flash lamp and the OMA detector were operated at 10 Hz. The laser was fired during alternate flashes of the flash lamp, *i.e.*, at 5 Hz, and the OMA recorded a blank spectrum during the flash lamp cycles when the laser did not fire. Each blank spectrum was automatically subtracted from

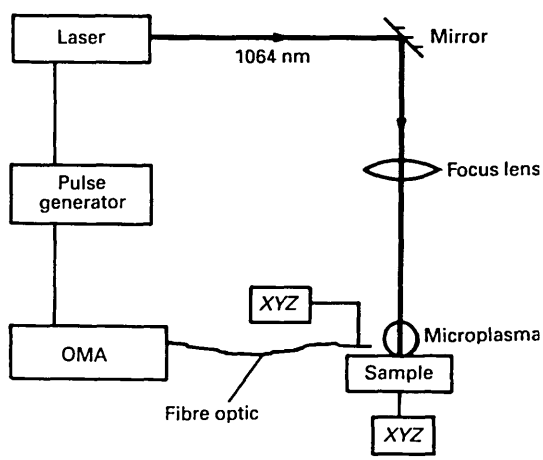

Fig. 1 Schematic diagram of laser and spectrometer system

* Presented in part at the 1993 European Winter Conference on Plasma Spectrochemistry, Granada, Spain. January 10–15, 1993.

Table 1 Instrumentation and parameters used in this study

Laser	Spectra Physics DCR II
Wavelength	1064 nm
Repetition rate	10 Hz
Laser flash lamp energy	40 J
Pulse-width	10 ns
Reflecting mirror	45° (Newport 10 QM 20 HM-15)
Focus lens	500 mm focal length (Newport SBX 040 AR.18)
Ablation gas	Air at room temperature and pressure
Sample position (relative to laser focal point)	−0.5 mm (0.5 mm towards lens)
OMA	EG&G OMA III
Spectrometer	0.28 m Czerny–Turner
Grating	2400 g mm^{-1}
Spectral window	25 nm
Effective resolution	0.20 nm
Detector	Intensified photodiode array
Light collection and transfer	Fibre optic, bundle of 19 × 200 μm UV-grade fused silica
Fibre optic observation position	
From laser focal point	12 mm
Above sample surface	1 mm
Pulse generator	EG&G 1310

Table 2 List of element emission lines for each spectral window monitored in this study

Wavelength range/nm					
237–262		267–292		307–332	
240.549	Cu	279.553	Mg II	308.215	Al I
241.949	Sn	280.199	Pb I	308.802	Ti II
247.857	C I	280.270	Mg II	309.271	Al I
250.200	Zn II	283.306	Pb I	315.887	Ca II
250.911	C II	283.999	Sn I	317.502	Sn I
251.203	C II	285.213	Mg I	317.933	Ca II
251.743	Ti II	286.333	Sn I	322.579	Fe II
252.560	Ti II	286.426	Pb	322.775	Fe II
252.852	Sb I	287.792	Sb I	323.252	Sb I
253.401	P I	—	—	323.452	Ti II
253.565	P I	—	—	323.612	Ti II
254.480	Cu II	—	—	323.904	Ti II
255.328	P I	—	—	324.199	Ti II
255.493	P I	—	—	324.754	Cu I
255.796	Zn II	—	—	326.233	Sn I
256.253	Fe II	—	—	326.751	Sb I
259.806	Sb I	—	—	327.396	Cu I
259.881	Cu II	—	—	328.233	Zn I
261.418	Pb	—	—	328.321	Sn II
				330.259	Zn I

the previous emission spectrum to yield a net signal from the plasma. The run time for 5 laser shots was 1 s.

Laser light was delivered to the sample by a mirror, and a lens was used to focus the light onto the sample surface. The laser-induced plasma was formed at the surface of the sample, and radiation was transmitted to the OMA by a fibre optic cable. The light was dispersed by the grating of the spectrometer and detected by an intensified photodiode array. The detector was time-gated to allow precise control of the integration time.

Various spectral regions could be monitored by setting the grating to the required centre wavelength. This was controlled by the grating-drive mechanism which rotated the grating until the required wavelength window covered the detector elements. Three spectral windows 237–262, 267–292 and 307–332 nm of centre wavelengths 250, 280 and 320 nm, respectively, were used to detect the elements selected (Al, Ba, Ca, Cu, Fe, Mg, Pb, P, Sb, Sn, Ti and Zn). The emission lines monitored are given in Table 2. In addition, two barium lines were utilized (230.423 and 233.527 nm) at centre wavelength 230 nm.

Data Acquisition

The OMA hardware and software allowed versatile collection, storage and manipulation of data. For example, individual scans of the photodiode array, representing separate laser shots, could either be stored in separate memories or accumulated into a single memory. The time-gating capability of the OMA was used in two ways to address the problem of complex, time-dependent emission from the laser-induced plasma. Two data acquisition modes of OMA operation are described below, incremental mode and fixed time mode (FT). An incremental program was used for preliminary studies in which each scan of the array was stored in a separate memory, and the integration window (100 ns) was stepped sequentially through the lifetime of the plasma by the increment time (100 ns). This enabled the spectra to be time-resolved to produce an emission–wavelength–time (E–W–T) profile of emission from the plasma. Examination of the transient signal responses within these profiles enabled suitable values for delay and integration times to be selected for use in an FT program.

The FT data acquisition mode exploited the separation, in time, of the analyte response from the background signal and allowed greater measurement sensitivity to be realized. Here, the start of integration was delayed by a set time, the delay time, to enable rejection of the initial intense background signal, and the integration period captured the analyte emission signal response; typical parameters were delay time 500 ns, and integration time 1 μs.

Two FT programs, FT1 and FT2, were used to acquire the laser generated spectra. Method FT1 consisted of firing 30 laser shots at the same spot, each shot being stored individually, *i.e.*, 1 scan in 30 memories (30 scans total). Method FT2 accumulated five laser shots into one memory at one sample site, and this was repeated seven times in total with a fresh site each time, *i.e.*, 5 scans in 7 memories (35 scans total). The run times for FT1 and FT2 were 6 and 7 s, respectively, with a further 25 s required for sample translation for FT2.

Materials

Poly(vinyl chloride) samples (A–F) were supplied in sheet form by FMC Process Additives (UK). Sample X was industrial grade PVC (Darvic), obtained locally.

Procedure

Samples were analysed as received with no sample preparation. The sample was mounted on an *XYZ* manipulator and a fresh area of material postioned at the laser spot. The manipulator was moved in height (*Z*) until the sample was at the laser focal point, 500 mm from the focusing lens, and then moved 0.5 mm towards the lens. With the laser operating at a suitable flash lamp energy, *e.g.*, 40 J, the acquisition was started. The laser fired under control of the OMA software and the master pulse generator, and the resulting scans were stored on the computer and printed. Separate routines were used off-line to perform individual pixel analyses to give emission–time profiles and statistical information.

Results and Discussion

Preliminary Studies

Previous studies[18] of LIPS with metallurgical samples found that emission signal responses and analytical performance were greatly influenced by the complex, interdependent relationship of several parameters, *e.g.*, laser energy, sample position relative to laser focal point, position of the fibre optic and OMA

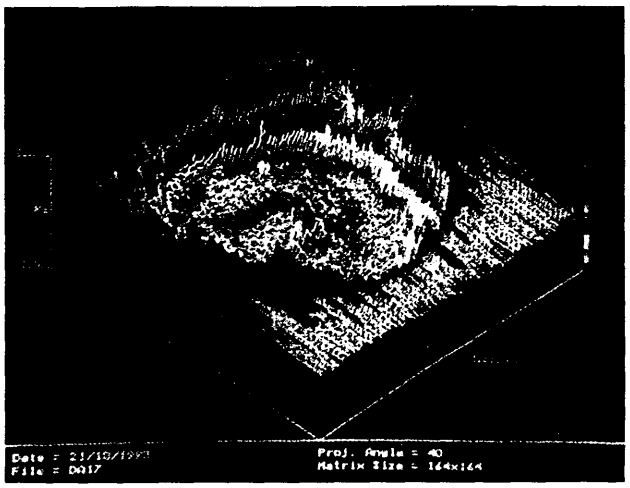

Fig. 2 Talysurf stylus-profile of a crater in PVC (sample X) produced by ten laser shots, laser flash lamp energy 40 J. The profile was recorded by 164 scans in a 1.63 mm square grid

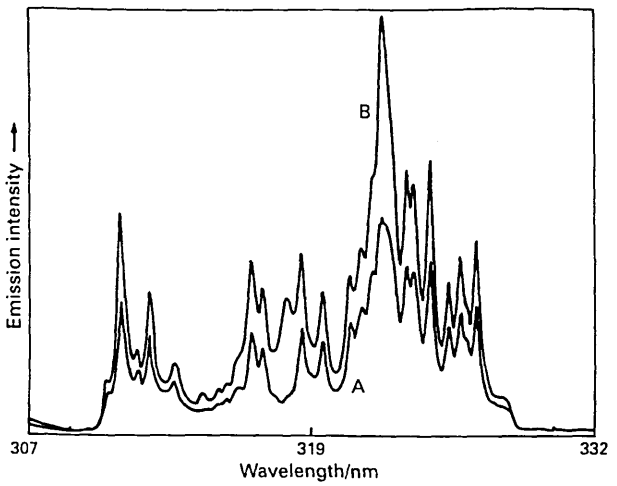

Fig. 3 LIPS spectra for ablation of: A, Ti metal; and B, PVC sample X (laser flash lamp energy 40 J). OMA parameters: delay time, 900 ns; integration time, 100 ns

detector settings. For example, ablation with a relatively high laser energy (flash lamp energy 70 J, irradiance $\approx 3.1 \times 10^{11}$ W cm^{-2}) produced a more intense, longer-lived plasma that required a different fibre optic viewing position and OMA settings for optimal performance compared with ablation with a lower energy (flash lamp energy 40 J, $\approx 8.0 \times 10^{10}$ W cm^{-2}). For this preliminary study with polymeric materials, initial selection of laser lamp energy was made by examining the amount of laser-damage to the sample and the variation in emission intensity produced by different values of laser energy. For optimum LIPS performance, it may be necessary to characterize the experimental parameters listed above for the ablation of polymeric materials and also consider the effects of polymer properties such as transparency and colour upon ablation.

A relatively low laser energy (flash lamp energy 40 J) was chosen, which inflicted minimal laser damage to the sample but produced suitable emission responses. The laser appeared to couple well with coloured, opaque samples. A Talysurf stylus-profile of the crater produced in PVC (sample X) by ten laser shots is depicted in Fig. 2. It shows the round crater to be approximately 1 mm in diameter and 50 μm deep. A darkened region, about 2 mm in diameter, was observed around each crater.

The LA of an opaque polymer was compared with the ablation of metal using conditions previously established for metal samples. Fig. 3 depicts spectra from the ablations of sample X and Ti metal, taken from the respective E–W–T profiles. The spectra are very similar and most emission lines can be identified as Ti, indicating the presence of Ti in the polymer, probably as the pigment titanium dioxide. The spectrum for the polymer is more intense than that for the metal, probably due to a combination of factors such as, greater coupling of the laser and plasma with the polymer, and the lower temperatures needed for volatilization and decomposition of the polymer compared with the metal.

In the case of transparent polymeric samples, no emission signals were obtained when material was ablated with the operating parameters specified under Experimental. Faint tunnelling through the material and ablation of the metal support underneath the sample were observed. This would suggest that a plasma was not induced on the surface of the polymer, and that the laser light was transmitted through the plastic to the metal. The tunnelling was due to the self-focusing of the laser

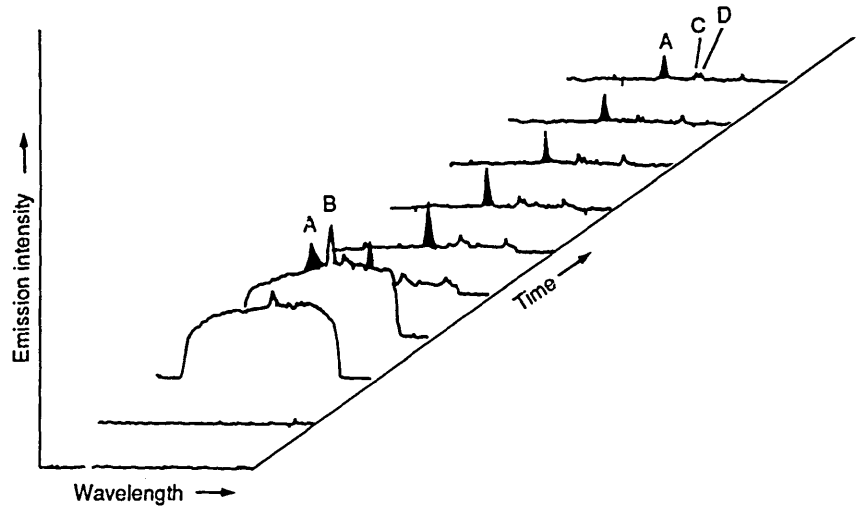

Fig. 4 Emission–wavelength (237–262 nm)–time (0–900 ns) profile for ablation of sample A using the Incremental program, (increment time, 100 ns; integration time, 100 ns): A, carbon I 247.9 nm; and B, carbon II 250.9 and 251.2 nm; C, antimony 252.9; and D, phosphorus 253.4 and 253.5 nm

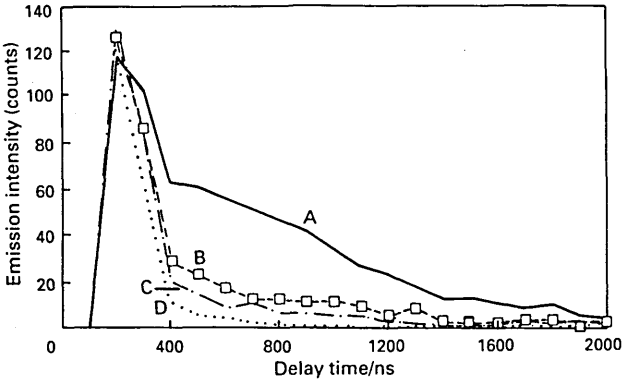

Fig. 5 Emission–time profile for ablation of sample A with the Incremental program, (increment time, 100 ns; integration time, 100 ns): A, carbon I 247.9; B, antimony 252.9; C, phosphorus 253.4; and D, background 245.0 nm

beam within the material, which trapped the light and prevented it from spreading, to produce a waveguide.[19] This was not evident in the opaque samples because the laser light was absorbed, leading to ablation and production of the laser-induced plasma. When the transparent sample was moved away from the laser focus position, *i.e.*, 3 mm away from the lens (+3 mm), emission signals and laser damage on the sample surface were observed. The plasma was induced in the air above the sample surface, and the plasma was responsible for volatilizing sample material and creating the crater. Results indicated that it was feasible to gain elemental composition data from transparent polymer material. These conditions were not adopted for opaque samples because greater damage was inflicted upon these materials without any significant improvement in performance.

An E–W–T profile recorded with the OMA incremental program from the ablation of sample A (Fig. 4) shows the intense background continuum at early times, and the emergence of atom/ion emission at later times. Carbon ion emissions (250.9, 251.2 nm) were evident initially, and carbon atom emissions (247.9 nm) later. The intense background signal and carbon ion emissions reflect the high temperatures of the plasma at early times, but as the plasma expanded and cooled, the background signal decayed rapidly and atomic emission lines for Sb and P became prominent. An E–T profile for selected wavelengths (Fig. 5) shows the responses of C, Sb and P to be indistinguishable from the background up to 400 ns. After this, emission signals for these three elements remain above background up to about 1.5 μs. These observations enable suitable detector settings to be obtained for the FT data acquisition mode; the background signal is reduced significantly, by 500 ns, so selection of a time delay of 500 ns would minimize background contributions and a signal integration of 1 μs would be appropriate for monitoring analyte emission.

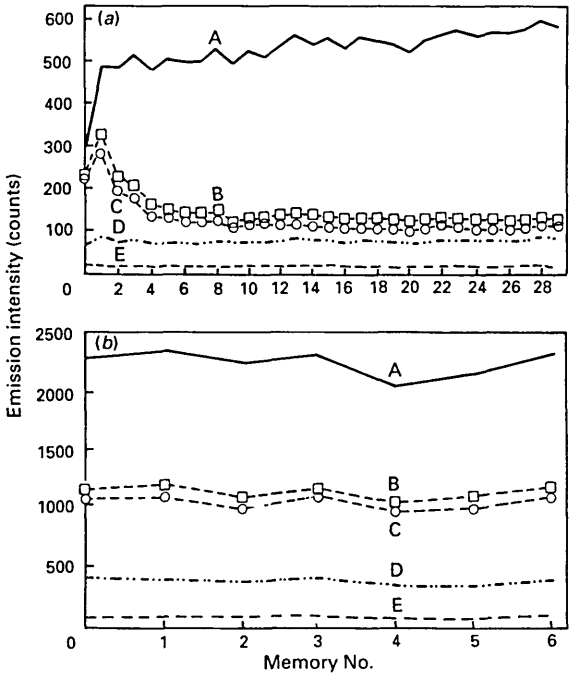

Fig. 6 Emission–time profile for ablation of sample A with FT program (delay time, 500 ns; integration time, 1 μs): (*a*) FT1, 30 shots at same spot; and (*b*) FT2, 5 shots in each memory, 7 memories, fresh site each memory: A, carbon I 247.9; B, antimony 252.9; C, antimony 259.8; D, phosphorus 253.4; and E, background 245.0 nm

Analytical Performance

Full quantitative measurement of inorganic additives in polymeric materials is considered to be difficult because of the absence of suitable certified reference materials (CRMs) necessary to prepare calibration graphs. Quantitative measurements in this work are based on using characterized samples as calibration standards. To obtain analytical performance data, OMA FT programs were devised using the system operating parameters established above. Initial studies used two FT programs, FT1 and FT2, to examine the effect of repetitive firing of the laser on signal response and to test for sample homogeneity, prior to making performance measurements. Results from the ablation of sample A by both methods are shown in Fig. 6 (laser flash lamp energy 40 J, delay time 500 ns, integration time 1 μs). With FT1, the Sb emission responses were not similar throughout the experiment, although the C and P emission signals were reasonably constant. Both Sb lines increased in intensity at first, and then decreased until

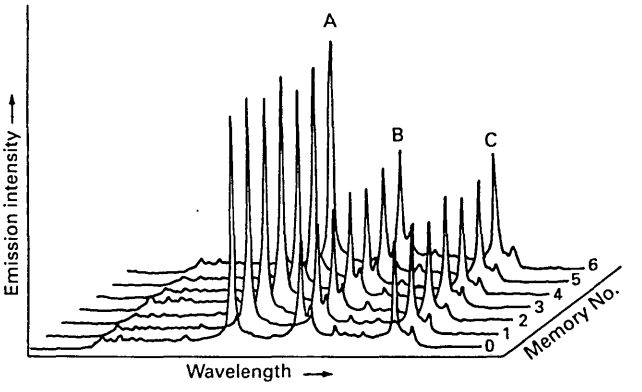

Fig. 7 Emission–wavelength (237–262 nm)–memory number profile for ablation of sample A with FT2, with delay time, 500 ns; integration time, 1 μs, 5 shots in each memory, 7 memories, fresh site each memory: A, carbon I 247.9; B, antimony 252.9; and C, antimony 259.8 nm

Table 3 Comparison of data from fixed time methods FT1 and FT2 for the ablation of sample A

Parameter	Method FT1	Method FT2
No. of shots per site	30	5
RSD C 247.8 nm	10.6	4.8
RSD Sb 252.8 nm	29.7	4.8
RSD P 253.4 nm	6.9	7.0
S/N (Sb 4.9%)	13.4	97
S/N (P 2.6%)	4.5	33
Value of *n* for statistical calculation	30	7

about memory number 9, after which a relatively constant signal response was observed. Emission responses for all elements were fairly constant with FT2 [Fig. 6(*b*)].

The emission response for Sb was not linear with concentration for method FT1, but FT2 did produce a linear response. It would appear that the Sb in the vicinity of the laser spot was selectively volatilized during the first few laser shots, possibly through formation of volatile antimony chloride, leading to a depletion of Sb for the remaining shots. The effect was not due to higher concentration levels of Sb at the surface as similar E–T profiles were obtained from the ablation of material beneath the sample surface. Use of a small number of laser shots, *i.e.*, five on several sites with method FT2, enabled a linear calibration to be produced. Reasonably constant signals for C, Ca and P were obtained by FT1, suggesting that these elements were not selectively volatilized and it was still possible to make representative measurements after firing 30 laser shots at the same site.

The emission responses for C and Sb were more reproducible with method FT2 compared with FT1. An emission–wavelength–memory number profile (Fig. 7) for ablation with FT2 clearly indicates good repeatability for successive laser firings, and results suggest that the sample is relatively homogeneous. Precision [relative standard deviation (RSD)] improved from 10.6 and 29.7 (FT1) to 4.8 and 4.8 (FT2) for C and Sb, respectively, but there was no significant change for phosphorus, RSD 6.9 (Table 3). Using the C signal (247.86 nm) as an internal standard, RSD was further improved to 2.3 and 3.4 for Sb and P, respectively. This approach is only applicable for element emission signals that are within the spectral region 237–262 nm that contains a C emission signal. The signal:noise ratio for C, Sb and P was considerably improved using FT2, due to the accumulation of five laser shots into each OMA memory compared with one shot with FT1.

Using method FT2, linear calibration graphs were generated for Sb (to 4.9% m/m) and Ca (to 6.8% m/m) emissions (Sb 252.8 and 258.8 nm; Ca 315.9 and 317.9 nm) with three data points for each element. The correlation coefficients were

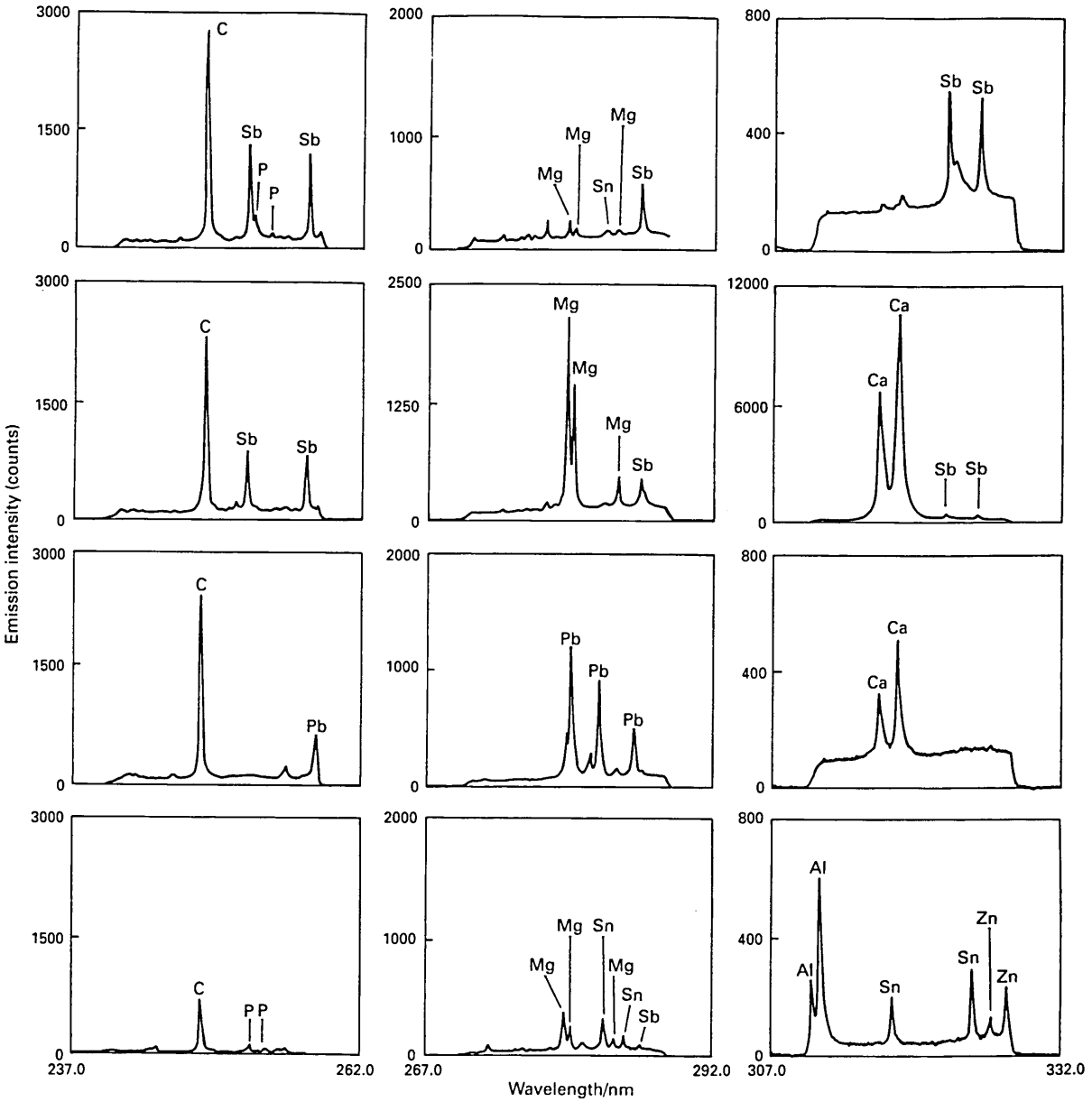

Fig. 8 Laser-induced plasma emission spectra from samples A, B, D and E (from top to bottom). Spectra were recorded with fixed time method FT2, delay time 500 ns, integration time 1 μs, 5 shots in each memory, 7 memories, fresh site each memory. Emission wavelengths are given in Table 2

0.9936 and 0.9999 for Sb 259.8 nm and Ca 317.9 nm, respectively. Limits of detection based on 3σ (measurement of blank PVC sample) were estimated at 0.04 and 0.016% m/m for Sb 252.8 nm and Ca 317.9 nm, respectively. The data are similar to values obtained for elements in steel (Ni, Cr, Si and Mn) by Cremers and Archuleta[9] using LIPS.

Survey Analysis

To demonstrate the rapid analysis capability, a range of PVC samples was examined. (The composition values quoted were supplied by the manufacturer.) Spectra from four samples are shown in Fig. 8 for three spectral regions. Samples A and B are clearly seen to contain Sb as the emission lines for Sb are identified within all three spectral windows for both samples. The greater emission intensity for A compared with B indicates the higher concentration present in A (Sb: A, 4.9% m/m; B, 2.8% m/m). Tin and P are present in sample A (P 2.6% m/m, Sn 0.05% m/m). Calcium emission lines are evident in samples B and D, the greater emission intensity of B indicating the higher concentration present (Ca: B, 6.8% m/m; D, 0.4% m/m). Emission lines of magnesium were observed for all four samples. Barium was detected in samples B (Ba: 0.1% m/m), the Ba emission lines (230.423 and 233.527 nm) are not shown in Fig. 8. Lead (3.0% m/m) is present in sample D, and Al, P, Sn and Zn are evident in E. Samples C and X (not shown) contain Sn and Zn, and Ti and Mg, respectively. These results show that the technique can be used for the rapid analysis of samples of PVC for a range of elements, without the need for time-consuming sample dissolution and possible loss of volatile elements.

Conclusions

Laser-induced plasma emission spectrometry has been applied to the rapid survey analysis of polymeric materials. This study monitored a range of twelve elements (Al, Ba, Ca, Cu, Fe, Mg, Pb, P, Sb, Sn, Ti and Zn), and provided analytical data for key elements (Sb and Ca). Quantitative measurement was limited by the availability of characterized samples. To address this problem, it is proposed to prepare a series of samples, covering a wide range of concentration levels for selected elements, which will enable additional calibrations and further quantitative measurements to be made.

The speed of analysis, compactness of instrumentation and simplicity of operation suggest that the technique has the potential for compositional monitoring of polymeric materials in industrial processes, such as manufacture and recycling.

We would like to thank Richard Dellar (FMC Corporation, Manchester, UK M17 1WT) for providing samples. We are grateful to Richard Burdett (EG&G, Sorbus House, Wokingham, UK) for valuable assistance in configuring the OMA system. We thank Mike Simpson for helpful discussions and Mac Jackson (School of Engineering) for the talysurf analysis. The authors thank the DTI and SERC for funding this project under the LINK TAPM scheme.

References

1 *Plastic Additives Handbook,* eds. Gächter and Muller, Hanser, 1983.
2 Wong, K. L., *Anal. Chem.,* 1981, **53,** 2148.
3 DiPasquale, G., and Casetta, B., *At. Spectrosc.,* 1984, **5,** 209.
4 Warren, P. L., *Anal. Proc.,* 1990, **27,** 186.
5 Booth, P. K., and McLeod, C. W., *Mikrochim. Acta,* 1989, **3,** 283.
6 Marshall, J., Franks, J., Abell, I., and Tye, C. *J. Anal. At. Spectrom.,* 1991, **6,** 145.
7 Moenke-Blankenburg, L., *Laser Micro Analysis,* Wiley, 1989.
8 *Laser-induced Plasmas and Applications* eds. Cremers, D. A., and Radziemski, L. J., Marcel Dekker, New York, 1989.
9 Cremers, D. A., Archuleta, F. L., and Dilworth, H.C., *Proceedings of the 5th Process Tech. Conf. on Meas. and Control Instrum. in the Iron and Steel Industry,* April 14–17, 1985, pp. 157–162. Iron and Steel Society, Warrendale, PA, USA.
10 Cremers, D. A., and Radziemski, L. J., in *Applications of Laser Spectroscopy,* eds. Cremers, D. A., and Radziemski, L. J., Marcel Dekker, New York, 1986, ch. 5, pp. 380–395.
11 Niemax, K., Leis, F., Sdorra, W., and Ko, J. B., *Mikrochim. Acta,* 1989, **2,** 185.
12 Niemax, K., Ko, J. B., and Sdorra, W., *Fresnius' Z. Anal. Chem.,* 1989, **335,** 648.
13 Niemax, K., and Sdorra, W., *Mikrochim. Acta,* 1992, **107,** 319.
14 Iida, Y., *Anal. Sci,* 1991, **7,** 61.
15 Kuzuya, M., and Mikami, O., *J. Anal. At. Spectrom.,* 1992, **7,** 493.
16 Niemax, K., Sdorra, W., and Brust, J., *Mikrochim. Acta,* 1992, **108,** 1.
17 Lorenzen, C. J., Carlhoff, C., Hahn, U., and Jogwich, M., *J. Anal. At. Spectrom.,* 1992, **7,** 1029.
18 Anderson, D. R., and McLeod, C. W., unpublished work.
19 Ready, J. F., *Effects of High Power Laser Radiation,* Academic Press, New York, 1971.

Paper 3/02845C
Received May 19, 1993
Accepted November 8, 1993